جمهورية العراق
وزارة التعليم العالي والبحث العلمي
جامعة بابل
كلية هندسة المواد
قسم هندسة البوليمر والصناعات البتروكيمياوية

تشخيص وتحليل الفشل للأوعية المركبة الطبقية المصنعة بواسطة عملية لف الخيوط

أطروحة مقدمة الى

عمادة كلية هندسة المواد /جامعة بابل وهي جزء من

متطلبات نيل درجة فلسفة الدكتوراه في هندسة

المواد/البوليمر

من قبل

علا عبد الحسين كاظم

بكالريوس هندسة المواد/البوليمر 2013
ماجستير في هندسة المواد/البوليمر 2016

بأشراف

أ.د. نجم عبد الأمير سعيد

2022 م 1443 هـ

Republic of Iraq

Ministry of Higher Education and Scientific Research

University of Babylon

College of Materials Engineering

Department Engineering of Polymer and Petrochemical Industries

Characterization and Failure Analysis of Laminated Composite Vessels Manufactured Using Filament Wounding Process

A dissertation

Submitted to the Council of the College of Materials Engineering/ University of Babylon in Partial Fulfillment of the Requirements for the Degree of Doctorate of Philosophy in Materials Engineering/ Polymer

By

Ola Abdul Hussain Kadhum

B.Sc. Materials Engineering/Polymer 2013

M.Sc. Materials Engineering/Polymer 2016

Supervised by

Prof. Najim Abdul Ameer Saad (Ph.D.)

2022 A.D **1443 A.H**

Abstract

Composite pressure vessels are very important in applications that requires high lightness such as aerospace, constructions, automotive, energy gas saving and liquid energy saving systems that suffer from leakage and explosion especially when metal pressure vessels are used.

Ruptured of the pressure vessel can be extremely dangerous if the cracks are not well detected in early stage, this work proposes early failure analysis identification techniques for pressure vessels using measurements of ultrasonic wave velocity, X-ray CT scan examination and finite element method.

First, filament winding machine has been designed and manufactured capable of winding with different angle orientations of three types of fibers with 75% wt. to reinforce epoxy matrix are carbon fibers, Kevlar fibers and E- glass fibers with different winding angle orientations $[\pm 45°]_3$, $[\pm 55°]_3$, $[\pm 65°]_3$ and $[\pm 75°]_3$ as well as three symmetrical composite laminates have symmetrical sequence $[\pm 45^{\circ}, \pm 55^{\circ}, \pm 65^{\circ}, \pm 75^{\circ}]_s$ being exposed to internal pressure loads for identifying their pressure strength and failure modes.

Mechanical performances like ring stiffness and hardness were used to study the effect of fiber reinforcements, orientations angles and symmetrical ply sequence effects.

Numerical models have been built to simulate the pressure vessels in automobile applications and specified the weak areas that exhibited failure where the Von-Misses failure criteria has been used to evaluate the capacity of the pressure vessels to withstand high pressure 25 MPa; this can be achieved by building a model based on Finite elements analysis using ACP ANSYS workbench 17.

Failure detection results showed the affectivity and the usability of ultrasonic wave velocity technique in detect the crack place for different material types and sizes while the X-ray CT scan has ability to detect the defects type, direction and dimension in addition to clarifying the fibers winding properties.

The obtained internal pressure test results show a strong influence of type of used reinforcing fibers, winding orientations and ply sequence on the pressure vessel strength where the maximum pressure recorded up to 10 MPa for CF/epoxy laminates which show no failure. KF/epoxy and GF/epoxy exhibit failure where the SEM revealed the dominant failure mode of pressure vessels was cohesive failure.

The internal pressure and hoop stress performance have showed the best results are for CF/epoxy with [±55°$_3$] angle orientation, the rate of improvement for burst pressure and hoop stress comparing with epoxy [150%, 1331%], respectively and [150%, 1043.5%] for symmetrical CF/epoxy.

The results of mechanical behavior clarified improvement when reinforcing epoxy with fibers, the best results are for CF/epoxy with winding angle [±45°$_3$] where the rate of improvement for hardness comparing with epoxy [58.3%]. On other hand. GF/epoxy with winding angle [±55°$_3$] shows the highest improvement ring stiffness comparing with epoxy [1768.3%]. The symmetrical ply sequence also show improvement in mechanical properties where Symmetrical GF/epoxy shows the highest improvement in ring stiffness comparing with epoxy [4071.4%].

The numerical simulation was also used to predict the composite pressure vessels behavior using Von-Mises criteria where the best results were for CF/epoxy with winding angle [±55°$_3$] where the rate of decreasing in deformation comparing with epoxy [94.76%] von-Mises stress comparing with epoxy [54.6%], and von-Mises strain comparing with epoxy [94.8%]. Symmetrical laminates also showed improvement where the maximum reduction rate was for symmetrical CF/epoxy in deformation comparing with epoxy [89%], von-Mises stress comparing with epoxy [25.2%], and von-Mises strain comparing with epoxy [94.3%].

List of Contents

Item	Title	Page
	Abstract	I
	List of Contents	III
	List of Figures	IX
	List of Tables	XVI
	List of Symbols	XVII
	List of Abbreviations	XVIII
Chapter One: Introduction		1-9
1.1	General Introduction:	1
1.2	Composite Pressure Vessel Applications	2
1.3	Failure Accidents	4
1.4	Detection of Failure in Pressure Vessels	6
1.5	Aims and Objectives	8
1.5	Thesis Layout	9
Chapter Two: Theoretical Part and Literature Review		10-60
2.1	Introduction	10
2.2	Pressure Vessel	10
2.3	Classification of Pressure Vessels	11
2.3.1	Shape of Vessel	11
2.3.1.1	Spherical Pressure Vessel	11
2.3.1.2	Cylindrical Pressure Vessels	12
2.3.2	Wall Thickness	12
2.3.2.1	Stresses in Thin Walled Cylinders	13
2.3.2.1.1	Hoop Stresses	13
2.3.2.1.2	Axial Stresses	15

2.3.3	End Constructions	16
2.4	Structural Composite	18
2.5	Modeling of Structures Composed of Composites	18
2.5.1	The Microscopic Level	19
2.5.2	The Macroscopic Level	20
2.5.3	The structural Level	21
2.6	Laminar Composites	22
2.6.1	Laminate configuration types	22
2.6.1.1	Symmetric laminates	22
2.6.1.2	Anti-symmetric laminates	22
2.6.1.3	Unsymmetrical laminates	24
2.6.2	Laminates and Laminate Notations	24
2.6.2.1	Unidirectional Laminates	24
2.6.2.2	Angle-Ply Laminates	25
2.6.2.3	Cross-Ply Laminates	25
2.6.2.4	Balanced Laminates	25
2.6.2.5	Quasi-Isotropic Laminates	25
2.7	Fabrication Processes	27
2.7.1	Filament Winding	27
2.8	Constituent Materials	28
2.8.1	Reinforcements	28
2.8.2	Resin System	30
2.7	Winding Methods	30
2.7.1	Winding Patterns	31
2.7.1.1	Hoop Winding	31
2.7.1.2	Helical Winding	31
2.7.1.3	Polar Winding	31

2.10	Failure	33
2.10.1	Failure of Composite Materials	33
2.10.2	Categories of Failures	33
2.10.3	Failure Modes	34
2.10.3.1.	Fiber Buckling	34
2.10.3.2.	Fiber Breakage	34
2.10.3.3.	Matrix cracking	34
2.10.3.3.	Delamination	35
2.11	Failure of Pressure Vessels	37
2.12	Allowable Stresses Unidirectional Laminates	38
2.13	Failure Mechanism	39
2.14	Failure Theories	40
2.14.1	Maximum Shear Stress Theory (Tresca)	40
2.14.2	The Coulomb Yield Criterion	41
2.14.3	Maximum Distortion Energy	42
2.14.4	Maximum Stress and Strain Criteria	43
2.14.5	Approximation Strength Criteria	44
2.15	Destructive and Nondestructive Test	46
2.15.1	Visual testing (VT)	47
2.15.2	X-Ray Radiography and Computed Tomography	48
2.15.3	Ultrasonic Microscopy	49
2.15.4	Thermography	50
2.15.5	Acoustic Emission	51
2.16	Literature Review	53
2.17	Concluding remarks	59
Chapter Three: Modeling and Numerical Simulation		61-79
3.1	Numerical Procedure Flow Chart	61

3.2	Finite Element Analysis Procedure	63
3.3	Simulation Modelling	64
3.3.1	Analysis of a Composite Shell Model	65
3.3.2	Analysis of the End Cups Model	76
3.3.3	Static Structural Model	78
3.4.3.1	Connect the Cylinder with the Cups	78
3.4.3.2	Boundary Conditions	79
Chapter Four: Experimental Work		80-99
4.1	Introduction	80
4.2	Materials and its Characterization	81
4.2.1	Resin System	81
4.2.2	Reinforcements	82
4.3	Filament Winding Machine	82
4.3.1	Mechanical Part	84
4.3.2	The Electronic Part	85
4.3.3	The Programming Part	86
4.4	Specimen Manufacturing	87
4.4.1	Procedure	87
4.4.2	Specimens	89
4.5	Epoxy Tube Manufacturing	90
4.6	Experimental Tests	91
4.6.1	Density Test	91
4.6.2	Burst Pressure Test Setup	91
4.6.2.1	Test Setup	91
4.6.2.2	Test Cups Design	92
4.6.2.3	Test Procedure	94

4.6.2.4	Hoop Stress Calculations	94
4.7	Thermal Behavior	95
4.7.1	Differential Scanning Calorimetry Test	95
4.8	Mechanical Tests	95
4.8.1	Hardness	95
4.8.2	Ring Stiffness Test	95
4.9	Failure Detection Tests	96
4.9.1	Ultrasound Waves Velocity Test	96
4.9.2	X-ray Computed Tomography	98
4.10	Microstructural Properties	99
4.10.1	Digital Microscope	99
4.10.2	SEM Test	99
Chapter Five: Results and Discussion		100-174
5.1	Introduction	100
5.2	Characterization of Materials	101
5.2.1	Differential Scanning Calorimeter	101
5.3	Density Test	105
5.4	Internal Pressure Test	106
5.4.1	Effect of Winding Angle Configuration	106
5.4.2	Effect of the Type of Reinforcing Fiber	107
5.4.3	Effect of Ply Sequences	107
5.5	Hoop Stress Studies	109
5.5.1	Effect of Winding Angle Configuration	109
5.5.2	Effect of the Type of Reinforcing Fiber	110
5.5.3	Effect of Ply Sequences	110
5.6	Leaks Analysis of Pressure Vessels	111

5.6.1	Analysis of Epoxy Tube	111
5.6.2	Analysis of Fiber Composite Laminates Tubes	112
5.7	Microstructural Results	113
5.8	Mechanical Behavior	131
5.8.4	Hardness Results	131
5.8.5	Ring Stiffness	132
5.8.5.1	Effect of Reinforcing Fiber Types	133
5.8.5.2	Effect of Fiber Orientation	133
5.8.5.3	Effect of Symmetry	134
5.9	Failure Detection Tests	135
5.9.1	Ultrasonic Wave Velocity	135
5.9.2	X-Ray CT Scan	145
5.10	Numerical Simulation Results	151
5.10.1	Total Deformation Distribution	151
5.10.1.1	Effect of Type of Reinforcing Fibers	152
5.10.1.2	Effect of Winding Angle	152
5.10.1.3	Effect of Ply Sequences	156
5.10.2	Equivalent Von-Mises Stress	158
5.10.2.1	Effect of Type of Reinforcing Fibers	159
5.10.2.2	Effect of Winding Angle	160
5.10.2.3	Effect of Ply Sequences	164
5.10.3	Equivalent Elastic Strain	166
5.10.3.1	Effect of Type of Reinforcing Fibers	166
5.10.3.2	Effect of Winding Angle	167
5.10.3.3	Effect of Ply Sequences	171
Chapter Six: Conclusions and Recommendations		175-177

6.1	Conclusions	175
6.2	Recommendations	177
References		178-188

List of Figures

No.	Subject	Page
1.1	Examples of pressure vessels for storing CNG and CH_2	2
1.2	Modified Van Hool a330 FC bus, powered by hydrogen fuel cell.	3
1.3	A glimpse of the aftermath of the 1919 failure of 5-story-high tank that unleashed 12,000 tons of molasses on Boston's North End. (Photograph by Leslie Jones, Boston Herald. With permission.)	5
1.4	Water heater explosion at Avon High School	6
1.5	An air receiver tank explosion	6
2.1	The spherical pressure vessel	11
2.2	A cylindrical pressure vessel	12
2.3	Free-body diagram of a cylinder carrying internal pressure showing hoop stress. (a) Short section of a cylinder showing internal pressure acting radially on the inside wall. (b) Axial view of a half-section of the wall of a pressurized cylinder. (c) Side view of a half-section of a pressurized cylinder showing the wall dimensions.	14
2.4	Free-body diagram of a cylinder carrying internal pressure showing longitudinal stress: a) internal forces in the walls of pressure vessel. B) Internal pressure acting in all directions on walls of a cylinder and cross-sectional area of cylinder wall.	15
2.5	Hoop and axial stresses in thin walled cylinder	16
2.6	Open end cylinder	17
2.7	Closed end cylinder	17
2.8	Laminated plates- level of modeling	18
2.9	Principle axes of a lamina	21
2.10	Angle-ply layer of a filament-wound shell	23
2.11	Filament-wound cylinders with various numbers nT of T -segments: nT = 2 (a), 4 (b), 8 (c), and 16 (d).	24

2.12	Lay-ups schematics for laminar composites Unidirectional , b) Cross-ply, c) Angle-ply, and d) Multidirectional	26
2.13	Schematic presentation of the filament winding technology	28
2.14	Comparing carbon fiber size with human hair size	29
2.15	Schematic diagram of the various filament winding machines and patterns	32
2.16	Typical failure modes in fiber reinforced composites	35
2.17	Main failure modes in fiber reinforced composite laminates	36
2.18	Illustration of micro-buckling failure mode	36
2.19	Rupture in a pressure vessel due to excessive internal pressure	37
2.20	The failure mode of a composite pressure vessel	38
2.21	The failure process in composite laminate	39
2.22	The yield direction under a compressive stress σ_1 for a material obeying the coulomb criterion	42
2.23	Definition of the octahedral shear stress	42
2.24	Failure surface corresponding to maximum stress criterion	43
2.25	Typical shapes of the curves corresponding to the second-order polynomials	45
2.26	Failure surface in the stress space	45
2.27	Various optical aids used in visual inspection. (a) Mirror on stem (b) Hand magnifying glass (c) Illuminated magnifier (d) Inspection glass (e) Borescope.	47
2.28	Principle of a helical CT scanning system	48
2.29	Ultrasonic microscopy testing	50
2.30	Pulsed thermography schematic showing how defects lead to a distortion of the heat flow through a component	51
2.31	A basic overview of an acoustic emission set-up	52
3.1	Flowchart of procedure of analysis of closed cylindrical pressure vessels	61
3.2	Steps in Ansys PrePost Modeling	63
3.3	The general Pre- and post-processing workflow for finite element modeling and material analysis	64
3.4	The modeling system	64
3.5	ACP components	65
3.6	The Laminator program.	66
3.7	Cylinder geometry	68

3.8	Meshing of the cylinder.	68
3.9	Fabric properties of carbon fibers.	70
3.10	Polar properties of the fiber	71
3.11	Stackup of ±55° ply	71
3.12	Stackup polar properties of ±55° ply	72
3.13	Rosettes dialog	72
3.14	The reference direction of shell element (rosettes)	73
3.15	Oriented element set properties	73
3.16	Object tree of a layup definition of 3-layers composite laminates	74
3.17	The Object tree of a layup definition of the symmetrical laminates	74
3.18	The ±45° orientation of fibers within one ply	75
3.19	Mechanical model components	76
3.20	End cups geometry	77
3.21	End cups mesh	77
3.22	Bonding of the cylinder with the cups	78
3.23	Boundary condition of the cylinder	79

4.1	The Flowchart of Experimental Tests	80
4.2	The machine construction and elements	83
4.3	The electronic elements	85
4.4	The programing elements	86
4.5	The main interface of the device program	87
4.6	Winding process	88
4.7	CF/epoxy laminates unit cells: (a) 45°, (b) 55°, (c) 65°, (d) 75°	89
4.8	A) Manufactured Epoxy Tube, B)Top View of the Manufactured Epoxy Tube	90
4.9	Hydrostatic Pressure Tester	92
4.10	A and B: represent cups of the Qulitest apparatus, C and D: represent the designed end cups.	93
4.11	Ring stiffness test rig	96
4.12	A): longitudinal ultrasound wave direction, B) Shear ultrasound wave direction.	98
4.13	Medical X-ray CT scan.	99
5.1	Thermal History Behavior of epoxy	101

5.2	Thermal History Behavior of GF/epoxy	103
5.3	Thermal History Behavior of CF/epoxy	103
5.4	Thermal History Behavior of KF/epoxy	104
5.5	Density of epoxy CF/epoxy, KF/epoxy and GF/epoxy laminates	105
5.6	The effect of winding angle configuration on burst pressure test	106
5.7	The effect of ply sequence on burst pressure test	108
5.8	Hoop stress performance of epoxy, CF/epoxy, KF/epoxy and GF/epoxy	109
5.9	Hoop stress of symmetrical laminates	110
5.10	Failure of epoxy tube, a) before burst pressure test, b) after burst pressure test.	111
5.11	Water leakage of GF/epoxy	112
5.12	Water leakage of $[\pm 45°_3]$ KF/epoxy laminate. A) Experimental water leakage during the experimental test, B) digital microscope for the leakage area.	114
5.13	Scanning electron microscopy of $[\pm 45°_3]$ Kevlar fiber composite laminate.	115
5.14	Water leakage of $[\pm 55°_3]$ KF/epoxy laminate: A) Experimental water leakage during the experimental test, B) Digital microscope for the leakage area.	116
5.15	Scanning electron microscopy of $[\pm 55°_3]$ KF/epoxy laminate	117
5.16	Failure of $[\pm 65°_3]$ KF/epoxy laminate tube: A): Experimental water leakage during the experimental test, B): Digital microscope for the leakage area.	118
5.17	Scanning electron microscopy of $[\pm 65°_3]$ KF/epoxy laminate	119
5.18	Failure of $[\pm 75°_3]$ KF/epoxy laminate: A) Experimental water leakage during the experimental test, B) Digital microscope for the leakage area.	120
5.19	Scanning electron microscopy of $[\pm 75°_3]$ KF/epoxy laminate	122
5.20	Figure 5.20: failure of symmetrical KF/epoxy laminate tube: A) Experimental water leakage during the experimental test, B) Digital microscope for the leakage area.	123

5.21	SEM of symmetrical KF/epoxy laminate.	124
5.22	Figure 5.22: water leakage of $[\pm 55°_3]$GF/epoxy laminate tube: A) Experimental water leakage during the experimental test, B) Digital microscope for the leakage area.	125
5.23	Scanning electron microscopy of $[\pm 55°_3]$ GF/Epoxy laminate.	126
5.24	Figure 5.24: Failure of $[\pm 65°_3]$GF/epoxy laminate tube. A) Experimental water leakage during the experimental test, B) Digital microscope for the leakage area.	127
5.25	Scanning electron microscopy of $[\pm 65°_3]$ GF/epoxy laminate.	128
5.26	Failure of $[\pm 75°_3]$ GF/epoxy laminate tube. A) Experimental water leakage during the experimental test, B) Digital microscope for the leakage area.	129
5.27	Scanning electron microscopy of $[\pm 75°_3]$ GF/epoxy laminate	130
5.28	Hardness of CF/epoxy, KF/epoxy and GF/epoxy laminates	131
5.29	Hardness of symmetrical CF/epoxy, KF/epoxy and GF/epoxy laminates.	132
5.30	Ring stiffness of epoxy, CF/epoxy, KF/epoxy and GF/epoxy laminates.	132
5.31	Ring stiffness of epoxy and symmetrical CF/epoxy, KF/epoxy and GF/epoxy laminates.	134
5.32	Variation of longitudinal velocity of epoxy, $[\pm 45°_3]$, $[\pm 55°_3]$, $[\pm 65°_3]$ and $[\pm 75°_3]$ CF/epoxy laminates before burst pressure.	136
5.33	Variation of longitudinal velocity of epoxy, $[\pm 45°_3]$, $[\pm 55°_3]$, $[\pm 65°_3]$ and $[\pm 75°_3]$ CF/epoxy laminates after burst pressure	136
5.34	Variation of shear velocity of epoxy, $[\pm 45°_3]$, $[\pm 55°_3]$, $[\pm 65°_3]$ and $[\pm 75°_3]$ CF/epoxy laminates before burst pressure	137
5.35	Variation of shear velocity of epoxy, $[\pm 45°_3]$, $[\pm 55°_3]$, $[\pm 65°_3]$ and $[\pm 75°_3]$ CF/epoxy laminates after burst pressure	137
5.36	Variation of longitudinal velocity of epoxy, $[\pm 45°_3]$, $[\pm 55°_3]$, $[\pm 65°_3]$ and $[\pm 75°_3]$ KF/epoxy before burst pressure.	138
5.37	Variation of longitudinal velocity of epoxy, $[\pm 45°_3]$, $[\pm 55°_3]$, $[\pm 65°_3]$ and $[\pm 75°_3]$ KF/epoxy laminates after burst pressure.	138

5.38	Variation of shear velocity of epoxy, $[\pm 45°_3]$, $[\pm 55°_3]$, $[\pm 65°_3]$ and $[\pm 75°_3]$ KF/epoxy laminates before burst pressure.	139
5.39	Variation of shear velocity of epoxy, $[\pm 45°_3]$, $[\pm 55°_3]$, $[\pm 65°_3]$ and $[\pm 75°_3]$ KF/epoxy laminates after burst pressure	139
5.40	Variation of longitudinal velocity of epoxy, $[\pm 45°_3]$, $[\pm 55°_3]$, $[\pm 65°_3]$ and $[\pm 75°_3]$ GF/epoxy laminates before burst pressure	140
5.41	Variation of longitudinal velocity of epoxy, $[\pm 45°_3]$, $[\pm 55°_3]$, $[\pm 65°_3]$ and $[\pm 75°_3]$ GF/epoxy laminates after burst pressure.	140
5.42	Variation of shear velocity of epoxy, $[\pm 45°_3]$, $[\pm 55°_3]$, $[\pm 65°_3]$ and $[\pm 75°_3]$ GF/epoxy laminates before burst pressure	141
5.43	Variation of shear velocity of epoxy, $[\pm 45°_3]$, $[\pm 55°_3]$, $[\pm 65°_3]$ and $[\pm 75°_3]$ GF/epoxy laminates after burst pressure.	141
5.44	Variation of longitudinal velocity of symmetrical composite laminate before burst pressure	142
5.45	Variation of longitudinal velocity of symmetrical composite laminate after burst pressure.	142
5.46	Variation of longitudinal velocity of symmetrical composite laminate before burst pressure	143
5.47	Variation of longitudinal velocity of symmetrical composite laminate after burst pressure.	143
5.48	X-ray CT scan of epoxy tube.	145
5.49	X-ray CT of GF/epoxy laminate. A): $[\pm 45°_3]$, B): $[\pm 55°_3]$, C): $[\pm 65°_3]$ and D): $[\pm 75°_3]$	146
5.50	X-ray CT of CF/epoxy laminate. A): $[\pm 45°_3]$, B): $[\pm 55°_3]$, C): $[\pm 65°_3]$ and D): $[\pm 75°_3]$	148
5.51	X-ray CT of A): $[\pm 45°_3]$, B): $[\pm 55°_3]$ KF/epoxy laminate	149
5.52	X-ray CT of A): $[\pm 65°_3]$, B): $[\pm 75°_3]$ KF/epoxy laminate.	150
5.53	Total deformation of epoxy, CF/epoxy, KF/epoxy and GF/epoxy laminates.	151
5.54	Total deformation of epoxy.	152
5.55	Total deformation of CF/epoxy laminate: A) [±45°], B) [±55°].	153
5.56	Total deformation of KF/epoxy laminate: A) [±45°], B) [±55°], C)[±65°], D)[±75°] .	154
5.57	Total deformation of GF/epoxy laminate: A) [±45°], B) [±55°],	155

	C)[±65°], D)[±75°] .	
5.58	Total deformation of symmetrical composite laminates	156
5.59	Total deformation of A: Symmetrical CF/epoxy laminate, B: Symmetrical KF/epoxy laminate and C: Symmetrical GF/epoxy laminate.	157
5.60	Von-Misses stresses epoxy, CF/epoxy, KF/epoxy and GF/epoxy laminates.	158
5.61	Von-Misses stress of epoxy	160
5.62	The maximum Von-Mises stress of CF/epoxy laminates A) $[\pm 45°]_3$, B) $[\pm 55°]_3$, C) [±65°], D) [±75°].	161
5.63	Von-Mises stress of KF/epoxy laminates A) $[\pm 45°]_3$, B) $[\pm 55°]_3$, C) [±65°], D) [±75°].	162
5.64	Von-Mises stress of GF/epoxy laminates A) $[\pm 45°]_3$, B) $[\pm 55°]_3$ C) [±65°], D) [±75°].	163
5.65	Von-Mises stress of epoxy and symmetric sequence laminates	164
5.66	The Von-Mises stress of A: Symmetrical CF/epoxy laminate, B: Symmetrical KF/epoxy and C: Symmetrical GF/epoxy.	165
5.67	Von-Misses strain of epoxy, CF/epoxy laminates, KF/epoxy and GF/epoxy.	166
5.68	Maximum Von-Mises strain of epoxy	167
5.69	Maximum Von-mises strain of CF/epoxy laminates A) $[\pm 45°]_3$, B) $[\pm 55°]_3$, C) [±65°], D) [±75°].	168
5.70	Maximum Von-Mises strain of KF/epoxy laminates A) $[\pm 45°]_3$, B) $[\pm 55°]_3$.	169
5.71	The maximum Von-Mises strain of glass GF/epoxy laminates A) $[\pm 45°]_3$, B) $[\pm 55°]_3$.	170
5.72	Maximum Von-misses strain of epoxy and symmetrical composite laminates.	171
5.73	Maximum Von-Mises strain of symmetrical laminates A) CF/epoxy, B) KF/epoxy, C) GF/epoxy.	172

List of Tables		
No.	**Subject**	**page**
1.1	Causes and methods of detection of service failure in pressure vessels	7
2.1	Burst pressure for the filament-wound fiberglass pressure vessels	38
2.2	Types of Failure Analysis Criterion	40
3.1	Properties of Carbon fiber composite lamina.	67
3.2	Properties of Kevlar fiber composite lamina.	67
3.3	Properties of E-glass fiber composite lamina.	67
3.4	The total number of nodes and elements of CF/epoxy, KF/epoxy and GF/epoxy laminates.	69
3.5	The total number of nodes and elements of symmetrical CF/epoxy, KF/epoxy and GF/epoxy laminates.	70
4.1	Mechanical properties of the resin system employed	81
4.2	Mechanical properties of the reinforcements employed.	82
5.1	DSC data of epoxy and CF/epoxy, KF/epoxy and CF/epoxy	104
5.2	Data of Total deformation, Von misses stress and Von misses strain of epoxy and CF/epoxy, KF/epoxy and GF/epoxy laminates	173
5.3	Data of Total deformation, Von misses elastic stress and Von misses elastic strain of symmetrical composite laminates.	174

List of Symbols

English Symbols

Symbol	***Description***	***Unit***
t	Wall thickness	mm
R^m	Mean Radius of vessel	mm
D^m	Mean Diameter of vessel	mm
E	Modulus of Elasticity	GPa

	or Young's Modulus	
L	length	mm
p	pressure	N/m^2
A_w	Area of the wall	
V	internal volume	m^3
W	weight	N
w	width	mm
R	Radius	mm
D	diameter	mm
A_p	Projected area	m^2
F_R	Resistance force	MPa
A	Area	m^2
ΔH_m	enthalpy	J
D_o	Outer radius	mm

Greek Symbols

Symbol	***Description***	***Unit***
σ_L	Longitudinal stress	MPa
σ_h	hoop stress	MPa
τ_{max}	Maximum shear stress	MPa
τ_f	Shear stress at failure	MPa
θ	Angle	degree
λ	Wave Length	A^o
ρ_f	Density of Object in Fluid.	g/cm^3
ρ_o	Density of Object in Air.	g/cm^3
σ	Stress	MPa

σ_m	Mean Stress	MPa
λ	mass fraction	m
υ	Poisson's Ratio	--
T_d	Temperature of degradation	C^0
T_g	Glass transition temperature	C^0
NWP	Nominal Working Pressure	MPa

List of Abbreviations

Symbol	***Description***
ASTM	American Society for Testing and Materials Specifications
ACP	Ansys Composite PrepPost
AP	Analysis Ply
BP	Burst pressure
CF	Carbon Fiber
CFRP	Carbon-Fiber Reinforced Polymer
CFRE	Carbon Fiber Reinforced Epoxy
CT	Computed tomography
CNG	Compressed Natural Gas
DSC	Differential Scanning Calorimetry
FEM	Finite-Element Method
FRP	Fiber Reinforced Polymer
GFRP	Glass Fiber Reinforced Polymer
GF	Glass Fiber
MP	Modeling Ply
NDT	nondestructive test

NDE	Nondestructive evaluation
OES	Oriented Element Sets
PP	Production Ply
RTM	Resin Transfer Molding
SEM	Scanning Electron Microscopy
US	Ultrasonic
VT	Visual testing
XCT	X-ray computed tomography

بِسْمِ ٱللَّهِ ٱلرَّحْمَٰنِ ٱلرَّحِيمِ

{ يَا أَيُّهَا الَّذِينَ آمَنُوا إِذَا قِيلَ لَكُمْ تَفَسَّحُوا فِي الْمَجَالِسِ فَافْسَحُوا يَفْسَحِ اللَّهُ لَكُمْ وَإِذَا قِيلَ انشُزُوا فَانشُزُوا يَرْفَعِ اللَّهُ الَّذِينَ آمَنُوا مِنكُمْ وَالَّذِينَ أُوتُوا الْعِلْمَ دَرَجَاتٍ وَاللَّهُ بِمَا تَعْمَلُونَ خَبِيرٌ }

صَدَقَ اللهُ العَليُ العَظيم

{ المجادلة من الآية: 11}

Acknowledgments

*Praise to our almighty **Allah**, the most merciful and gracious for enabling me to complete this thesis. The grateful thanks to the Prophet of Mercy **Mohammad** and his viticulturist **Ahl-Albait (Allah peace upon them).***

*I would like to express my deepest thanks and sincere gratitude to my supervisor **Prof. Dr. Najim A. Saad** for his active, valuable supervision and his assistance, guidance, encouragement and help throughout the steps of this work.*

*I would like to thank the Head of Department of **Materials engineering college in Babylon University**. Sincere thanks are also expressed to the staff of the material engineering college.*

*Special thanks for **Eng. Ahmed Alwash and Haider Hadi** for their efforts in constructing the filament wound machine.*

*I would like to thank all persons who stood beside me and offered their support in one way or another and all my friends for their assistance. Special thanks for **Sura Kamil** and **Adwaa Mohammed,** I also wish to convey my utmost appreciation and thanks to my Family for their love, help, supports and extraordinary patience during the years of my study.*

Ola A. Kadhum

2022

Dedication

I Would Like to Dedicate This Thesis to All for Their

Support and Encouragement

Whom I Love Most in All My Life

My Kindest Mother and My Family

My Husband and his Family

My son "Ali"

The soul of my friend "Ola Ali"

And to All People I Love.

Ola

الخلاصة

اوعية الضغط المركبة مهمة جدا خفيفة الوزن مهمة جدا في التطبيقات التي تتطلب خفة وزن عالية مثل تطبيقات الفضاء والانشائات والسيارات وانظمة توفير الطاقة الغازية وانظمة توفير الطاقة السائلة التي تعاني من التسرب والانفجار خاصة عندما يتم استخدام اوعية ضغط معدنية.

يمكن ان يكون تمزق الوعاء شديد الخطورة اذا لم يتم اكتشاف الشقوق في مرحلة مبكرة, يقترح هذا العمل تحديد الفشل المبكر لأوعية الضغط باستخدام قياس سرعة الموجات الفوق الصوتية وفحص الاشعة السينية المقطعية و تحليل العناصر المحددة. في البداية يتم تصميم وتصنيع جهاز لف الخيوط قادر على لف الالياف بزوايا مختلفة لثلاث أنواع من الياف بنسبة وزنية 75% لتقوية أرضية الايبوكسي وهي الياف الكاربون والياف الكفلر والياف الزجاج باتجاهات مختلفة لزوايا اللف وهي $[\pm 45°_3]$, $[\pm 55°_3]$, $[\pm 65°_3]$ و $[\pm 75°_3]$ بالاضافة الى ثلاث مركبات طبقية متناظرة بتسلسل متناظر $[[\pm 45°][\pm 55°][\pm 65°][\pm 75°]]_s$ والتي يتم تعريضها الى احمال ضغط داخلي لتحديد قوة الضغط وانماط الفشل الاداء الميكانيكي الميكانيكية مثل الجسائة الحلقية والصلادة تم استخدامها لدراسة تاثير تقوية الالياف و زوايا التوجيه وتسلسل الطبقات.

تم بناء نماذج عددية لمحاكاة أوعية الضغط في تطبيقات المركبات وتحديد المناطق الضعيفة التي أظهرت فشلًا حيث تم استخدام معيار للفشل فون مايسس تم استخدامه لتقييم قدرة اوعية الضغط على تحمل قيم ضغط مرتفع 25 ميجاباسكال حيث يمكن تحقيق ذلك من خلال بناء نموذج يعتمد على تحليل العناصر المحددة باستخدام ACP ANSYS workbench 17.

أظهرت نتائج الكشف عن الفشل مدى فاعلية وإمكانية استخدام تقنية سرعة الموجات فوق الصوتية في الكشف عن مكان الشق لأنواع وأحجام المواد المختلفة ، في حين أن الأشعة المقطعية لديها القدرة على الكشف عن العيوب من النوع والاتجاه والأبعاد بالإضافة إلى توضيح خصائص لف الألياف.

كما اظهرت نتائج اختبارات الضغط الداخلي التي تم الحصول عليها تاثيرا قويا لنوع الياف التقوية المستخدمة واتجاهات اللف و تسلسل الطبقات على قوة وعاء الضغط حيث تم تسجيل اقصى ضغط اعلى من 10 ميجاباسكال لمركبات الكاربون الطبقية والتي لم تظهر اي فشل.مركبات الكفلر والزجاج اظهرت فشلا حيث كشفت نتائج المجهر الالكتروني الماسح ان وضع الفشل السائد لاوعية الضغط كان فشلا متماسكا.

اداء الضغط الداخلي والاجهاد المحيطي اظهرت افضل النتائج هي لمركب الياف كاربون /ايبوكسي مع اتجاه زاوية $[\pm 55°_3]$ حيث ان اعلى اجهاد محيطي هو لمركبات الياف كاربون /ايبوكسي ومعدل التحسن

لضغط الانفجار وإلاجهاد المحيطي مقارنة مع الايبوكسي [150٪ ، 1331٪] على التوالي و[150٪ ، 1043.5٪] لمركب الياف الكاربون / الايبوكسي المتناظر.

أوضحت نتائج السلوك الميكانيكي تحسناً عند التقوية بالألياف ، وأفضل النتائج هي لمركب الياف الكاربون / ايبوكسي بزاوية لف [$_3$45°±] حيث معدل التحسن للصلادة مقارنة مع الايبوكسي [58.3٪]. من ناحية أخرى ، اظهر مركب الياف زجاج/ ايبوكسي بزاوية لف [$_3$55°±] أعلى تحسن للجساءة الحلقية مقارنة مع الايبوكسي [1768.3٪]. كما اظهرت الطبقات المتناظرة تحسنًا في الخواص الميكانيكية حيث اظهر مركب الياف الزجاج / ايبوكسي المتناظر أعلى تحسن في الجسائة الحلقية [4071.4٪].

تُستخدم المحاكاة العددية أيضًا للتنبؤ بسلوك اوعية الضغط المركبة باستخدام معيار فون مايسس حيث أفضل النتائج كانت لمركب الياف الكاربون/ ايبوكسي بزاوية لف [$_3$55°±] حيث ان معدل التناقص في التشوه مقارنة مع الايبوكسي [94.76٪] , إجهاد فون مايسس مقارنة مع الايبوكسي [54.6٪] ، وانفعال فون مايسس مقارنة مع الايبوكسي [94.8٪].المركبات الطبقية المتناظرة أيضًا اظهرت تحسنًا حيث اعلى انخفاض كان لمركب الياف الكاربون / الإيبوكسي المتناظر في التشوه مقارنة مع الايبوكسي [89٪] ، إجهاد فون مايسس مقارنة مع الايبوكسي [25.2٪] ، وانفعال فون مايسس مقارنة مع الايبوكسي [94.3٪].

CHAPTER ONE

Introduction

CHAPTER TWO

Theoretical Part and Literature Review

CHAPTER THREE

Modeling and Numerical Simulation

CHAPTER FOUR

Experimental Work

CHAPTER FIVE

Results and Discussion

CHAPTER SIX

Conclusions and Recommendations

References

Chapter One

Introduction

1.1. General Introduction:

Pressure vessels are one of the main equipment those widely used in industrial facilities. The pressure vessels defined as cylindrical or spherical vessels those designed to store or hold pressurized liquids, gases or fluids with a differential pressure between inside and outside. Usually, the inner pressure is higher than the external pressure, except in some cases [1].

Pressure vessels are created by filament winding for a long period. Although they seem to be easy structures, pressure vessels are one of the most difficult to design. Filament-wound composite pressure vessels have found widespread use not only for military use however conjointly for civilian applications [2].

New possibilities to improve the performance of pressure vessels were offered in the middle of 20^{th} century and were associated with the development of composite materials and filament winding technology [3].
According to unique capabilities of composite pressure vessels, especially significant weight saving and special application various research and studies were done on this kind of pressure vessels[4].

The high stiffness-to weight ratio combined with corrosion resistance and thermal performance provide a material that outperforms other more traditional homogeneous materials such as steel or aluminum.[5]. Also having a multilayer or orthotropic structure, composite pressure vessels could withstand higher operating pressure and temperature making it the best replacement for isotropic pressure vessels [6].

The production process for filament-wound composites has the potential to introduce variety of processing defects like foreign inclusions, Fiber misalignment can occur when fibers are laid up and fibers misalignment in the same layers or between layers. These defects can lead to delamination either during production or in service. Several techniques have been proposed to investigate these defects, possibly produced after damage caused in composite materials[7].

1.2. Composite Pressure Vessel Applications

Today composite pressure vessels are used in many fields, such as: the car industry, the aerospace industry, rescue services, etc. The use of hydrogen to feed fuel cells and for combustion in conventional engines requires a safe and expensive fuelling method. Storing hydrogen in pressure vessels of the CH_2 (compressed hydrogen) type has become the predominant technology, especially in cars. The weight of the vessel itself should be low enough in order for the latter to be installed in a car without the necessity to reduce the boot space. For this reason, wholly composite vessels (Figure 1.1) must be installed [8].

Figure 1.1 Examples of pressure vessels for storing CNG and CH_2 [8]

Composite pressure vessels offer a significant reduction of weight can be reached with composite pressure vessel reinforced with glass, carbon or organic fibers whose specific strength (strength to density ratio) is much higher than that of metal alloys traditionally used to fabricate pressure vessels. Also metals generally require several machining operations to obtain the final product[9].

Due to global industrialization and population growth the consumption of fossil fuel has been rising at an increasing rate since the 19th century. As the demand for petroleum-based products increases then so does the fuel price. Most industry sectors, and in particular the automotive industry, are seeking an alternative energy to reduce the dependence on fossil fuels. As a renewable and "environmental friendly" fuel, hydrogen gas generated using a hydrogen fuel cell is being evaluated as an alternative fuel for road vehicles. At the moment, field testing of hydrogen-powered vehicles is in progress.
For example, Figure 1.2 shows a commercial bus that has been modified to run on hydrogen [10].

Figure 1.2: Modified Van Hool a330 FC bus, powered by hydrogen fuel cell.[10]

There are many ways to store hydrogen fuel on road vehicles, compressing the hydrogen gas and then storing it within a pressure vessel is one of the efficient storage methods in terms of energy density. Natural gas cylinders have been used in automobiles for many years, However, the main difference between storing natural gas and hydrogen gas is that hydrogen needs to be stored at much higher pressure in order to increase the energy density; the storage vessels for natural gas and hydrogen gas are typically designed for the pressure capacity of 25 MPa and 70 MPa, respectively. [11]

Methane stored is stored and distributed in hard containers at a pressure of 20–25 MPa (2900–3600 psi), usually in cylindrical or spherical shapes at high pressure can be used in place of gasoline (petrol), diesel fuel, and propane/LPG. CNG combustion produces fewer undesirable gases than the fuels mentioned earlier. It is safer than other fuels in the event of a spill, because natural gas is lighter than air and disperses quickly when released. CNG may be found above oil deposits, or may be collected from landfills or wastewater treatment plants where it is known as biogas.[12]

1.3. Failure Accidents:

Failures can be immediate and catastrophic due to high energy loads, such as impact. In many cases, the overall strength is not compromised, as long as a significant number of carrier fibers are functional. The damage in composite laminates determines the life of the primary carrying structure. The extent of damage consists of damage in the inside layer of the lamina, such as fiber breakage, fiber separation, or matrix cracking. Also, delamination between the layers are created. The formed defect may or not affect already existing structure damage [13]

Some of the problem associated with filament winding of cases are the need for metallic inserts, the degradation of mechanical properties at elevated temperatures, resin failure due to excessive strain concentration in filament-

wound resin structures, and abrasion damage to filaments during winding process [14]

Any pressure vessel accident, like any boiler accident, is dangerous. Most of the time a pressure vessel contains gas and liquid, which are harmful when explosion occurs.[15]

Most pressure accidents can be lumped into two categories: equipment (engineering) and operator (user) errors. Engineering causes result from poor design of controls and safety, material strength, material compatibility, or faulty component production. User, technician, or operator errors are from faulty assembly and installation, poor maintenance, or poor operating practices such as failure to follow established procedures, use of wrong materials, and misuse of equipment. It is also imperative to use pressure regulators, compatible materials (fitting, gauges, etc.), safe assembly of a system that utilizes a pressure vessel, and proper use of equipment. Also, be extremely careful with low pressure=high volume; for instance, do not mix oil and oxygen. [15]

Pressure vessels have given way or exploded in some rather dramatic fashions. The most notorious explosions are shown from figure 1.3 to figure 1.5 [16].

Figure 1.3: A glimpse of the aftermath of the 1919 failure of 5-story-high tank that unleashed 12,000 tons of molasses on Boston's North End. (Photograph by Leslie Jones, Boston Herald. With permission.) [16]

Figure 1.4 Water heater explosion at Avon High School.[16]

Figure 1.5: An air receiver tank explosion. [16]

1.4. Detection of Failure in Pressure Vessels

Possible types of defect or problem in composite pressure vessel include matrix cracking, fiber breakage, delamination between plies, and de-bonding between linear and composite over warp. Monitoring the structural integrity of filament-wound composite structures can help prevent catastrophic failures and prolong their service life. [17]

If a pressure vessel leaks, it could poison or suffocate those in close proximity to it. It is not uncommon for fires or explosion to occur during operation. If a vessel ruptures, the event can be even more catastrophic, resulting in considerable damage to life and property. Any pressure vessel

accident, like any boiler accident, is dangerous. Most of the time a pressure vessel contains gas and liquid, which are harmful when explosion occurs.[18]

There is a certain amount of statistical information available on the failure of pressure system components. Information on pressure vessel failure is given by Phillips and Warwick. It classifies failures as catastrophic or potentially dangerous. The former are disruptions of the vessel which require major repair or scrapping; the latter are defects which might deteriorate under the working conditions and which require remedial action. For all the service failures the causes were classified. The results are shown in Table 1.1 [19].

Table 1.1 Causes and methods of detection of service failure in pressure vessels [19]

	No. of cases	*Percentage of total cases*
Causes of failures:		
Cracks	118	89.3
Maloperation	8	6.1
Pre-existing from manufacture	3	2.3
Corrosion	2	1.5
Creep	1	0.8
	132	100.0
Causes of cracks:		
Fatigue	47	35.6
Corrosion	24	18.2
Pre-existing from manufacture	10	7.6
Miscellaneous	2	1.5
Not ascertained	35	26.5
	118	89.4
Method of detection:		
Visual examination	75	56.9
Leakage	38	28.8
Non-destructive testing	10	7.5
Hydraulic tests	2	1.5
Catastrophic failure	7	5.3
	132	100.0

The vast majority of failures, some 89.3%, were due to cracks. The causes of cracks were therefore analysed separately as shown in the table 1.1. The table also gives the methods by which the failures were detected.

1.5. Aim and Objectives

1.5.1. Aim: The aim of this work includes:

- Design and construct a filament winding machine to produce filament wound pressure vessels.
- Detection and prediction of failure of filament wound pressure vessels accompanying with exposing to internal pressure loads using nondestructive techniques.

1.5.2. Objectives

In order to achieve previous aims, the following activities will be carried out**:**

1- Design and construct a filament winding machine to produce filament wound pressure vessels.

2- Using three different fibers (carbon fibers, Kevlar fibers and glass fibers) to reinforce the epoxy matrix.

3- Using four different winding angles$[\pm 45°_3]$, $[\pm 55°_3]$, $[\pm 65°_3]$ and $[\pm 75°_3]$ as well as symmetrical laminates$[[\pm 45°]\ [\pm 55°][\pm 65°]\ [\pm 75°]]_s$.

4- Evaluate the manufacturing pressure vessels by using two failure detection techniques (ultrasonic wave velocity and X-ray CT scan) before the internal pressure test.

5- Applied internal pressure load to evaluate the effect of

- Type of reinforcing fibers.
- Winding angle configurations
- Symmetrical ply sequences.

6- Study the internal pressure performance and hoop stress behavior.

7- Evaluate the composite pressure vessels by ultrasonic wave velocity and X-ray CT scan techniques after the internal pressure test.

8- Studying the numerical simulation of pressure vessel using Von-Mises failure criteria that gives indication of pressure vessel's performance and

strength ability under high pressure 25 MPa through building a model based on FEM- ACP ANSYS workbench 17.

1.4 Thesis Layout

This thesis includes sis chapters, as follows:

Chapter One: Is an introduction about pressure vessels, their applications and detection of failures.

Chapter Two: This chapter will provide a detailed on general structure and classifications of pressure vessels, their important properties and failure detection and criteria, composite laminates, structure and its configuration types, manufacturing process as well as literatures review.

Chapter Three: discusses the numerical analysis, which involves design of the pressure vessel with different materials used and winding angles.

Chapter Four: Introduces the experimental work, which describes the used materials, procedure of sample processing according to ASTM standards and test equipment selected.

Chapter Five: covers the results and discussion of the experimental work and numerical simulation.

Chapter Six: Summarizes the conclusions and give some suggestions for future work.

Additionally, references as well as Arabic abstract are included.

Chapter Two

Theoretical Part and Literature Review

2.1. Introduction:

Developments in pressure vessels during the nineteenth and early twentieth centuries were accompanied by all-too-frequent terrible pressure vessel explosions. Tragic accidents led to the development of basic standards for manufacturing and operation of pressure vessels. Further advances in metallurgy, welding technology and non-destructive testing helped, but an actual understanding of the science and mechanics of pressure vessel failure did not finally arrive until late twentieth century. Even in the twenty-first century, the catastrophic failure of pressure vessel that pressure vessels remain hazardous unless carefully designed, operated and inspected [20]

2.2. Pressure Vessel

A pressure vessel is defined as a container with a pressure differential between outside and the inside. The inside pressure is usually higher than the outside, except for some isolated situation. Pressure vessels also have a combination of high-pressure together with high temperature, and in the some flammable fluids or highly radio-active materials. Because of such hazards it is imperative that the design be such that no leakage can occur. It should be borne in mind that the rupture of a pressure vessel has a potential to cause extensive physical injury and property damage. [14]

2.3. Classification of Pressure Vessels

Pressure vessels can be classified in many ways according to:

2.3.1 Shape of Vessel

Pressure vessels are usually spherical or cylindrical, with domed ends. The cylindrical vessels are generally preferred, since they present simpler manufacturing problems and make better use of the available space. Boiler drums, heat exchangers, chemical reactors, and so on, are generally cylindrical. [14]

2.3.1.1 Spherical Pressure Vessel

A sphere is a very strong structure and it's preferred for storage of high pressure fluids. A spherical pressure vessel has approximately twice the strength of a cylindrical pressure vessel with the same wall thickness. The distribution of stresses on the sphere's surfaces, both internally and externally are equal. Spheres however, are much more costly to manufacture than cylindrical vessels. [21] A spherical pressure vessel is shown in Figure 2.1.

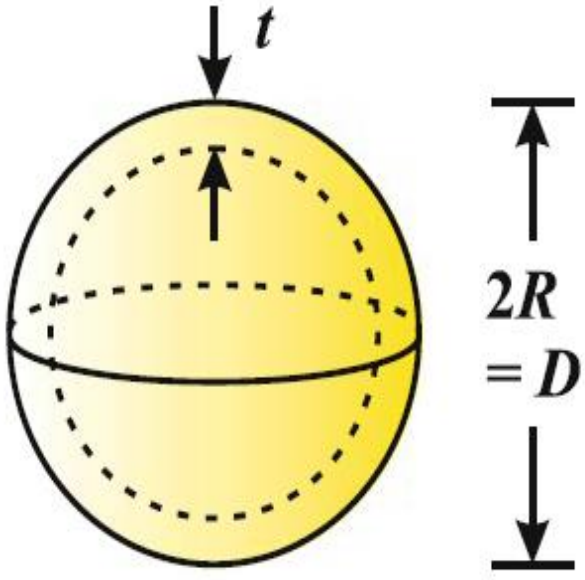

Figure 2.1 : The spherical pressure vessel [22]

2.3.1.2 Cylindrical Pressure Vessels:

A horizontally supported cylindrical pressure vessel with a hemispherical head is shown in Figure 2.2. [14].

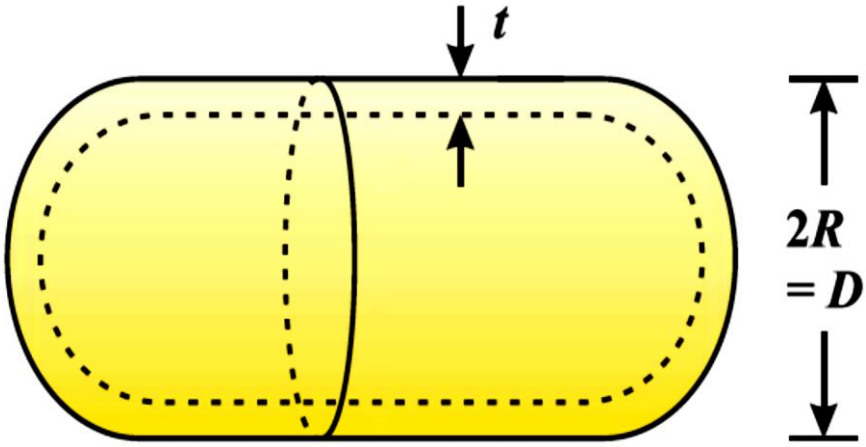

Figure 2.2: A cylindrical pressure vessel [22]

2.3.2 Wall Thickness:

The pressure vessel can be classified according to wall thickness into:

- Thin-walled cylinder
- Thick-walled cylinder

The distinction between the two types of vessels is based on the nature of the circumferential (also known as hoop) stress distribution over the thickness of the vessel. If the variation of this stress is such that it may be assumed approximately constant, the vessel is referred to as thin-walled. If not, it is known as thick walled.[23]

The pressure vessel is considered to be thin if

$$R_m/t \geq 10 \quad \ldots\ldots\ldots\ldots\ldots (2.1)$$

Where t is the wall thickness of the vessel. Because the diameter is twice the radius, the criterion for a vessel to be considered thin walled is also written as

$$D_m/t \geq 20 \quad \ldots\ldots\ldots\ldots\ldots (2.2)$$

Obviously, if the vessel does not satisfy the criteria listed in eqs. (2.1) and (2.2) it's considered to be thick walled.[24].

2.3.2.1 Stresses in Thin Walled Cylinders

Thin-walled tubes exposed to pressure generally develop two types of relevant stresses in the walls. [25]

2.3.2.1.1 Hoop Stresses

In which a ring around the cylinder is analyzed to determine the stress tending to pull the ring apart work in the tangential direction perpendicular to the length of the cylinder. [25]

As shown in Figure 2.3. The internal pressure pushes outward evenly all around the ring. The ring must develop a tensile stress in a direction tangential to the circumference of the ring to resist the tendency of the pressure to burst the ring. The magnitude of the stress can be determined by using half of the ring as a free body, as shown in Figure 2.3 (b). The resultant of the forces due to the internal pressure must be determined in the horizontal direction and balanced with the forces in the walls of the ring. The resultant force is the product of the pressure and the projected area of the ring. [26]

For a ring with a mean diameter D_m and a length L,

F_R= pA_p=p (D_m L) …… (2.3)

The tensile stress in the wall of the cylinder is equal to the resisting force divided by the cross-sectional area of the wall. Again assuming that the wall is thin, the wall area is[24]

A_w = 2t L …… (2.4)

Then the stress is

$$\sigma = \frac{F_R}{A_w} = \frac{F_R}{2tL} \quad \ldots\ldots\ldots\ldots \quad (2.5)$$

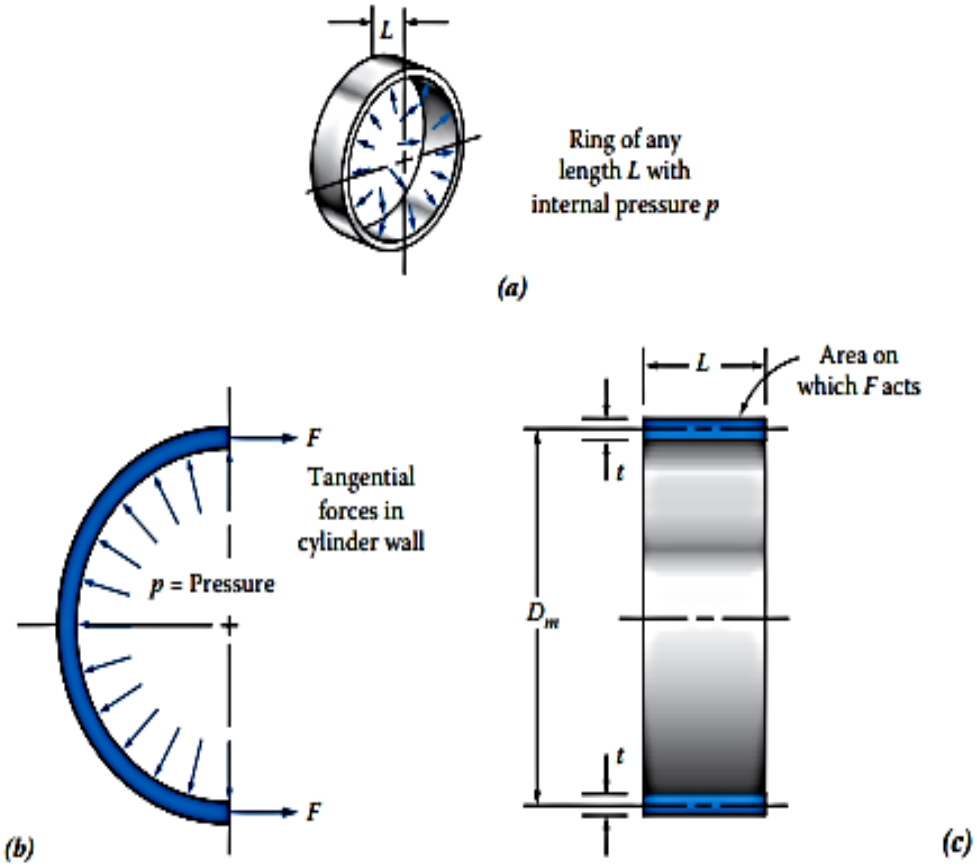

Figure 2.3: Free-body diagram of a cylinder carrying internal pressure showing hoop stress. (a) Short section of a cylinder showing internal pressure acting radially on the inside wall. (b) Axial view of a half-section of the wall of a pressurized cylinder. (c) Side view of a half-section of a pressurized cylinder showing the wall dimensions. [24]**.**

Combining Equations (2.4) and (2.5) gives

➪ **Hoop Stress in a Thin-Walled Cylinder**

$$\sigma = \frac{F_R}{A_w} = \frac{pD_m}{2t} \quad \ldots\ldots\ldots\ldots\ldots (2.6)$$

This is the equation for the hoop stress in a thin cylinder subjected to internal pressure. Notice that the magnitude of the hoop stress is twice that of the longitudinal stress. [24]

2.3.2.1.2 Axial Stresses

Is the tendency for the internal pressure to pull the cylinder apart in a direction parallel to its axis [25]

Figure 2.4 shows a part of a cylinder, which is subjected to an internal pressure, cut perpendicular to its axis to create a free body. Assuming that the end of the cylinder is closed, the pressure acting on the circular area of the end would produce a resultant force of [24]

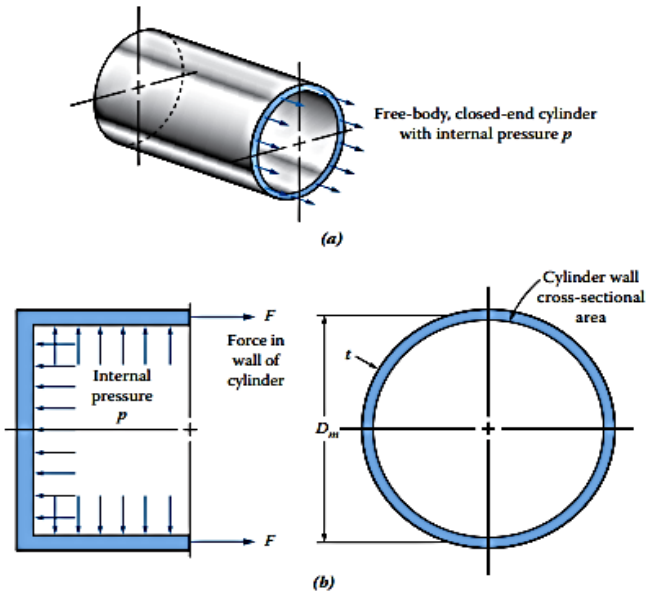

Figure 2.4: free-body diagram of a cylinder carrying internal pressure showing longitudinal stress: a) internal forces in the walls of pressure vessel. B) Internal pressure acting in all directions on walls of a cylinder and cross-sectional area of cylinder wall. [24]**.**

F_R= pA=p ($\frac{л\ D^2 m}{4}$) …… (2.7)

This force must be resisted by the force in the walls of the cylinder, which, in turn, creates a tensile stress in the walls. The stress is

σ =$\frac{F_R}{A_w}$ …… (2.8)

Assuming that the walls are thin, as we did for spheres,

A_w=л D_m t …… (2.9)

Where t is the wall thickness. Now combining Equations (2.7) through (2.9),

⇨ Longitudinal Stress in a Thin-Walled Cylinder

$$\sigma = \frac{F_R}{A_w} \frac{p(\pi D_m^2/4)}{\pi D_m t} = \frac{pDm}{4t} \quad \ldots\ldots\ldots\ldots\ldots (2.10)$$

This is the stress in the wall of the cylinder in a direction parallel to the axis, called the longitudinal stress. [24]

So that the formulas defining hoop and axial stresses in a cylinder are in Equation (1) and (2).

$\boldsymbol{PD/2t} = \sigma_1$ …… (2.6)

$\boldsymbol{PD/4t} = \sigma_2$ …… (2.10)

Figure 2.5 represented both hoop and axial stresses are acting on thin walled cylinder

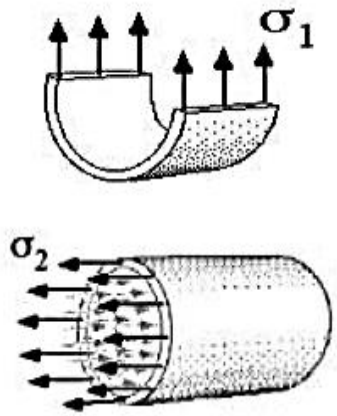

Figure 2.5: Hoop and axial stresses in thin walled cylinder.[25]

2.3.3 End Constructions:

- Open-ended vessels, namely cylinders, cylinders liners and so on in which there is no axial component of wall stress. A simple cylinder with a piston is an open ended cylinder, an open ended cylinder is subjected to radial and hoop stresses [22] as shown in figure 2.6.
- Closed-ended vessels as shown in figure 2.7 with various types of ends, namely, flat end, hemispherical, semi-ellipsoidal, or dish end in which

an axial stress must exist to equilibrate the fluid pressure.[27]. A closed end cylinder, such as a tank, is also subjected to longitudinal stress in addition to the hoop and radial stresses. [22]

Open cylinders are typified by interference-fitted bushes as shown in figure 2.6, in which there are no longitudinal pressures and so no axial stresses. [22]

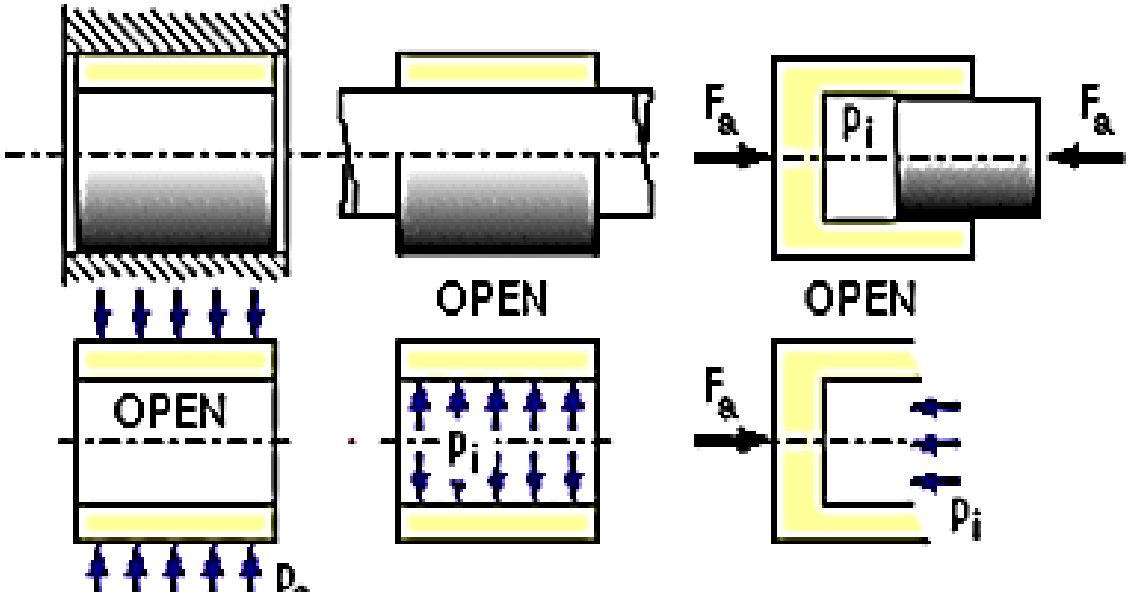

Figure 2.6: Open end cylinder. [28]

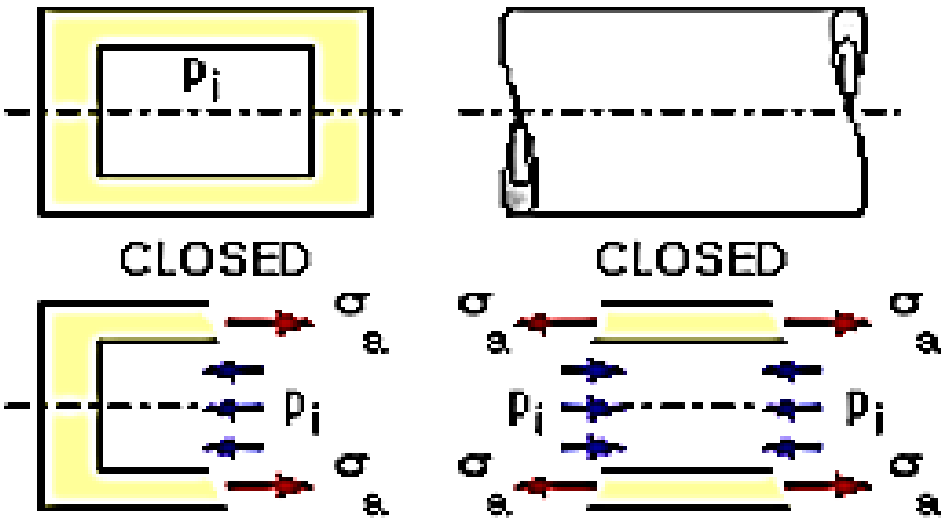

Figure 2.7: Closed end cylinder.[28]

2.4. Structural Composite

A Structural composite is a multilayered and normally low density composite used in applications requiring structural integrity, ordinarily high compressive, and tensional strengths and stiffness's. The properties of these composite depend not only on the properties of the constituent materials, but also on the geometrical design of the structural elements. Laminar composites and sandwich panels are two of the most common structural composites. [4]

2.5 Modeling of Structures Composed of Composites

Composite materials consist of two or more constituents and the modeling, analysis and design of structures composed of composites are different from conventional materials such as steel. For example, a laminated structure there are two levels of modeling (Figure 2.8).[29]

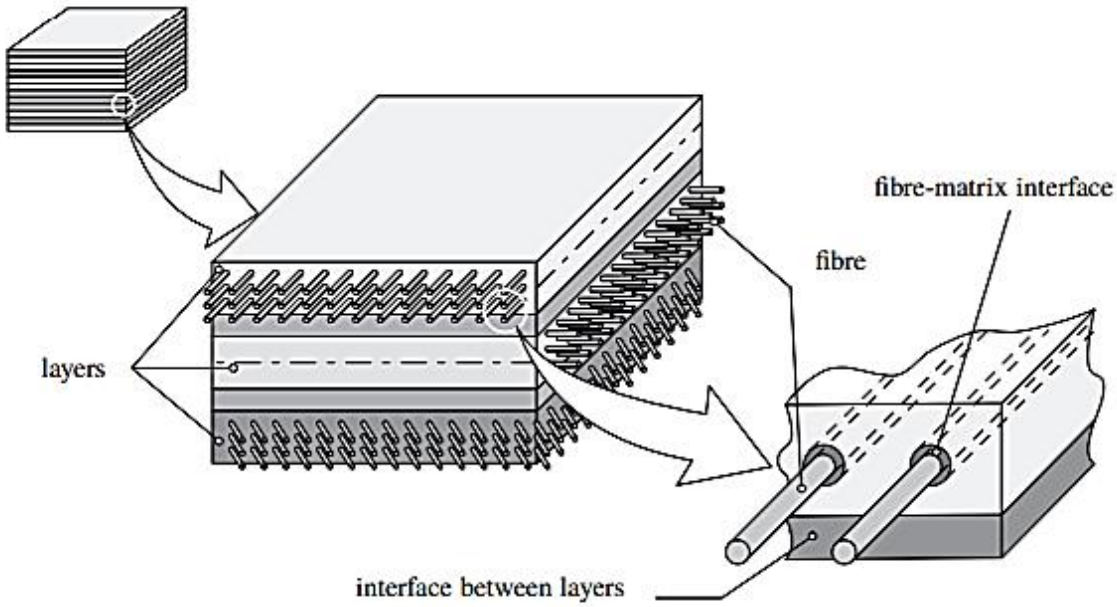

Figure 2.8: Laminated plates- level of modeling. [29]

At the micro-mechanical level the average properties of a single reinforced layer (a lamina or a ply) have to be determined from the individual properties of the constituents, the fibers and matrix, and may be the fiber-matrix interface. The average characteristics include the elastic moduli, the thermal and moisture expansion coefficients, etc. [29].

A laminate is a stack of laminae. Each layer of fiber reinforcement can have various orientation and in principle each layer can be made of different materials. Knowing the macro-mechanics of a lamina, one develops the macro-mechanics of the laminate. Averaged stiffness, flexibility, strength, etc. can be determined for the whole laminate. The structure and orientation of the laminae in prescribed sequences to a laminate lead to significant advantages of composite materials when compared to a conventional monolithic material. In general, the mechanical response of laminates is anisotropic. [30]

The last step is the modeling on the structure level and to analyze the global behavior of a structure made of composite material. By adapting the classical tools of structural analysis on anisotropic elastic structure elements the analysis of simple structures as beams or plates may be achieved by analytical methods, but for more general boundary conditions and/or loading and for complex structures, numerical methods are used. Summarizing the different size scales of mechanical modeling structure elements composed of fiber reinforced composites it must be noted that, independent of the different possibilities to formulate beam, plate or shell theories, three modeling levels must be considered [31]

2.5.1 The Microscopic Level:

Where the average mechanical characteristics of a lamina have to be estimated from the known characteristics of the fibers and the matrix material taking into account the fiber volume fraction and the fiber packing arrangement. The micro-mechanical modeling leads to a correlation between constituent properties and average composite properties. In general, simple mixture rules are used in engineering applications. If possible, the average material characteristics of a lamina should be verified experimentally. On the micro-mechanical level a lamina is considered as a quasi-homogeneous orthotropic material. [30]

The micro-mechanics of a lamina does not consider the internal structure of the constituent elements, but recognizes the heterogeneity of the ply. The micromechanics is based on some simplifying approximations. These concern the fiber geometry and packing arrangement, so that the constituent characteristics together with the volume fractions of the constituents yield the average characteristics of the lamina. Note that the averaged properties are derived by considering the lamina to be quasi-homogeneous. [31]

2.5.2 The Macroscopic Level:

Where the effective (average) material characteristics of a laminate as shown in figure 2.9 have to be estimated from the average characteristics of a set of laminae taking into account their stacking sequence. The macro-mechanical modeling leads to a correlation between the known average laminae properties and effective laminate properties. On the macro-mechanical level a laminate is considered generally as an equivalent single layer element with a quasi-homogeneous, anisotropic material behavior.[32]

At the macro-mechanical level, only the averaged properties of a lamina are considered and the microstructure of the lamina is ignored. The properties along and perpendicular to the fiber direction, these are the principal directions of a lamina, are recognized and the so-called on-axis stress-strain relations for a unidirectional lamina can be developed. Loads may be applied not only on-axis but also off-axis and the relationships for stiffness and flexibility, for thermal and moisture expansion coefficients and the strength of an angle ply can be determined. [32] [31]

Following are the basic assumptions used in deriving the constitutive relations.

- The composite material is assumed to behave in a linear (elastic) manner. That is, Hooke's law as well as the principal of superposition are valid. [33]

- At the lamina level, the composite material is assumed to be homogenous and orthotropic. Hence the material has two planes of symmetry, one coinciding with fiber direction and the other perpendicular to the fiber direction. [33]
- The state of stress in a lamina is predominantly plane stress.[33]

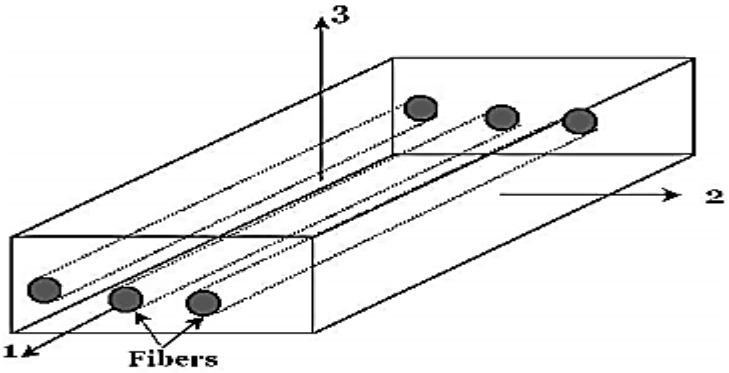

Figure 2.9: Principle axes of a lamina. [33]

2.5.3 The Structural Level

Where the mechanical response of structural members like beams, plates, shells etc. have to be analyzed taking into account possibilities to formulate structural theories of different order. In the recent years in the focus of the researchers is an additional level - the nanoscale level. [30]

There are two reasons for this new direction:

• Composites reinforced by nanoparticles and

• Nano-size structures.

The last step is the modelling on the structure level and to analyze the global behavior of a structure made of composite material. By adapting the classical tools of structural analysis on anisotropic elastic structure elements the analysis of simple structures as beams or plates may be achieved by analytical methods, but for more general boundary conditions and/or loading and for complex structures, numerical methods are used. [30] [31]

2.6. Laminar Composites

A Laminar composite is composed of two dimensional sheets or panels (plies or lamina) bonded to one another. Each ply has a preferred high strength direction, Such as is found in continues and aligned fiber reinforced polymers. A multilayered structure such as this is termed a laminate. Laminate properties depend on several factors. Including how the high-strength direction varies from layer to layer. In this regard, there are four classes of laminar composite: unidirectional, cross-ply, angle-ply, and multidirectional. [34]

2.6.1. Laminate Configuration Types

There are an infinite number of laminate configurations that can be constructed depending on the ply elastic properties, ply thickness, ply angle, ply type, stacking sequence, number of plies, etc. However, the laminate configurations can be classified in one of the three main types: symmetric, anti-symmetric and un-symmetric.

2.6.1.1. Symmetric Laminates

A laminate is said to be symmetric when the plies in the upper half of the laminate (for ordinate $z > 0$) are identical, in terms of ply properties, ply angle, ply thickness and ply position relative to the mid-plane, to the plies in the lower half of the laminate (for ordinate $z < 0$). An example of a symmetric laminate is $[0°, 45°, –45°, 90°]_s$, where the subscript s indicates the laminate is symmetric and only the first half of the stacking sequence is shown. The full form is [0°, 45°, –45°, 90°, 90°, –45°, 45°, 0°]. [35]

2.6.1.2. Anti-Symmetric Laminates:

A laminate is said to be anti-symmetric when for a given ply configuration (that is a ply with certain elastic properties and thickness) in the lower half of a laminate there is an identical ply configuration in the upper half of the laminate, but with an alternating ply angle. In composite technology, an

antisymmetric $\pm\varphi$ angle-ply laminate is usually fabricated by a continuous filament winding process. [36]

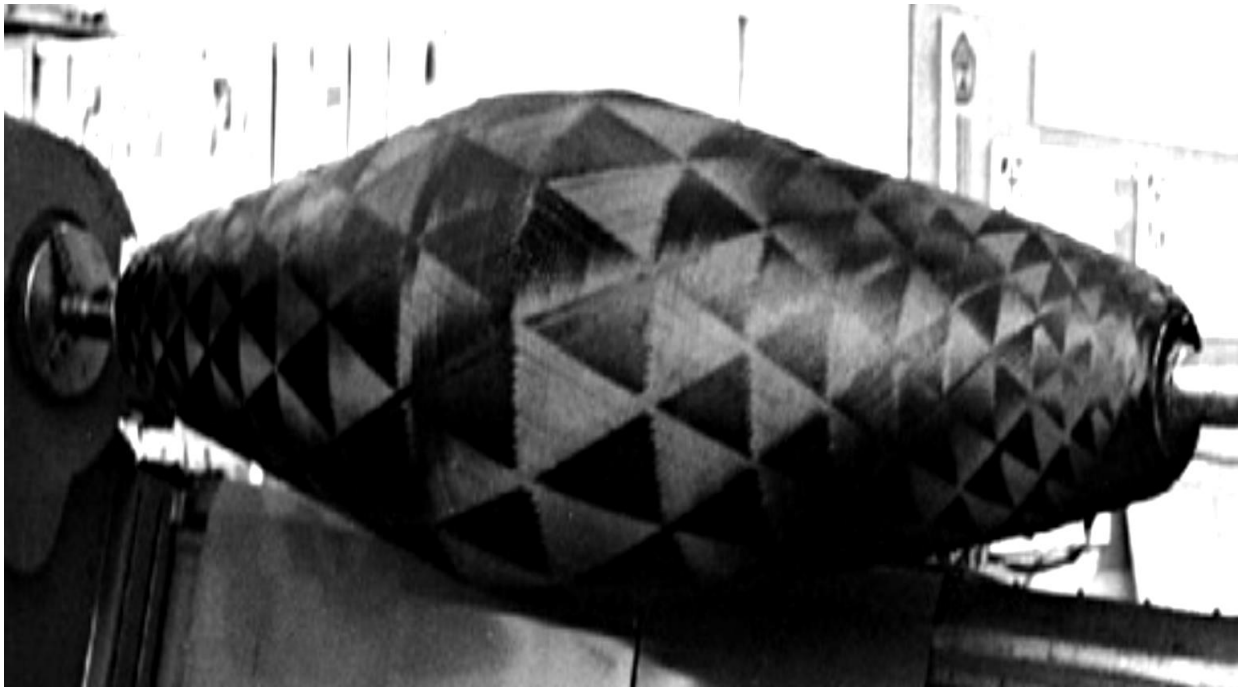

Figure 2.10: Angle-ply layer of a filament-wound shell. [37]

As can be seen in this figure 2.10, the angle-ply layer is composed from two plies with $+\varphi$ and $-\varphi$ orientation of the fibers and these plies are interlaced in the process of filament winding. As a result, the structure of the layer is characterized by the distinctive regular mosaic pattern consisting of triangular-shaped, repeating in chess-board fashion, two-ply segments (T -segments) with alternating $\pm\varphi$ and $\mp\varphi$ reinforcement. The T -segments are arranged in regular geometric pattern around the circumference and along the axis forming the so-called cross-over circles. [37]

Depending on the parameters of the winding process, various numbers nT of T –segments located along the circumference can be obtained. For a cylindrical shell, the structures corresponding to nT = 2, 4, 8, and 16 are shown in Figure 2.11. [38]

Figure 2.11: Filament-wound cylinders with various numbers *nT* of *T* -segments: *nT* = 2 (a), 4 (b), 8 (c), and 16 (d). [38]

2.6.1.3. Unsymmetrical Laminates:

The third category of laminate types is the unsymmetrical laminate. A laminate type which is neither symmetric nor antisymmetric is classified as an unsymmetrical laminate. Unsymmetrical laminates are made from multioriented plies. Note that in the case of an unsymmetrical laminate, the plies do not have to be of the same thickness. [36]

2.6.2. Laminates and Laminate Notations

There are a number of standard laminate types and notations that are important:

2.6.2.1. Unidirectional Laminates

In a unidirectional laminate, all of the plies are oriented in the zero-degree or 90-degree direction. An example is the four-ply thick zero-degree laminate

[0°, 0°, 0°, 0°]. Note that this is the same as a single ply or lamina, only thicker, as a result of multiple layers. [35]

2.6.2.2. Angle-Ply Laminates

Angle-ply laminates have an arbitrary number of layers (n). Each ply has the same thickness and is the same material. In an angle-ply laminate, all of the plies follow a sequence of +θ/–θ. An example is a $[30°/–30°]_4$ laminate with a stacking sequence of [30°, –30°, 30°, –30°, 30°, –30°, 30°, –30°]. The subscript 4 indicates that the pattern is repeated four times. [39].

2.6.2.3. Cross-Ply Laminates

In a cross-ply laminate, the plies are stacked in alternating layers of zero-degree and 90-degree. An example is $[0°, 90°]_2$, where the subscript 2 indicates that the pattern repeats twice [0°, 90°, 0°, 90°]. Symmetric Laminates. In a symmetric laminate, the ply fiber orientation is symmetrical about the centerline of the laminate. [39].

2.6.2.4. Balanced Laminates

In a balanced laminate, for every ply of + θ orientation, there is an identical ply of the same material and thickness of –θ orientation. An example of a balanced laminate is [0°, 30°, –30°, 30°, –30°, 0°]. This laminate is balanced but is not symmetric. However, it could be made symmetric by reordering the stacking order to [0°, 30°, –30°, –30°, 30°, 0°].[40]

2.6.2.5. Quasi-Isotropic Laminates

A quasi-isotropic laminate is made up of three or more plies of identical materials and thicknesses with equal angles between each ply and the next. If the total number of plies is n, the angle between plies is p/n. Quasi-isotropic laminates usually exhibit isotropic elastic behavior in the xy plane. An example of a balanced and symmetric quasi-isotropic laminate is [0°, 90°, 45°, –45°, –45°, 45°, 90°, 0°]. This laminate has two 0° plies, two 90° plies, two 45° plies, and two –45° plies. [35]

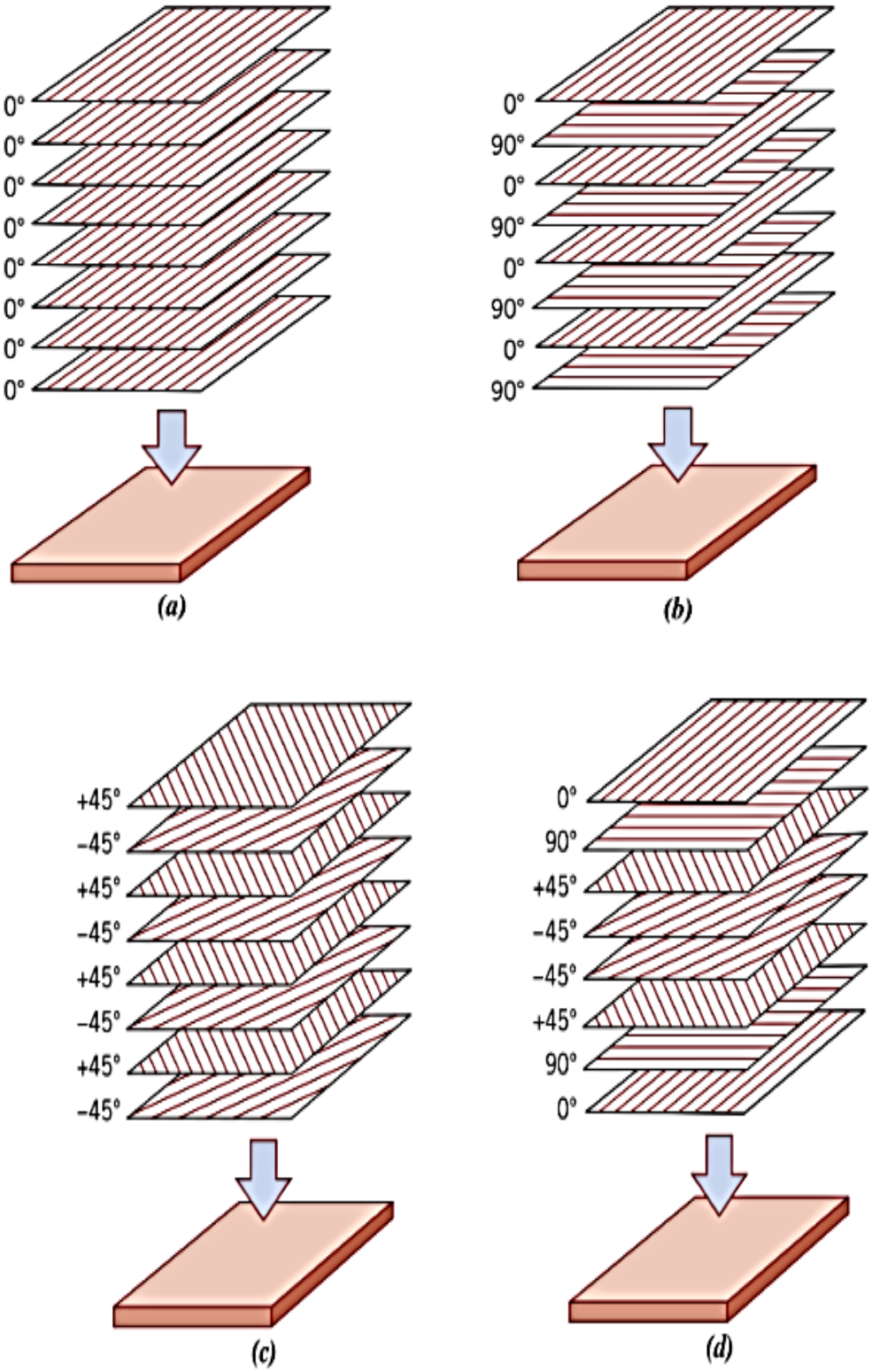

Figure 2.12: Lay-ups schematics for laminar composites

a) Unidirectional , b) Cross-ply, c) Angle-ply, and d) Multidirectional [34]

2.7. Fabrication Processes

Selection of composite fabrication process has emerged as one of the paramount challenges in the field of composite materials. The manufacturing technique for composite laminates depends on many factors such as the characteristics of matrix and reinforcement (fiber/matrix type, fiber content, fiber orientation, fiber length, etc.), geometry of the products (shape, size, etc.), and its end use. Different fabrication techniques for FRP laminate composites such as Hand Lay-up Process, Filament Winding Process, Compression Molding Process, Vacuum Bagging Process, Autoclave Molding, Resin Transfer Molding (RTM) Process and Pultrusion Process. [41]

2.7.1. Filament Winding

Filament winding is one of the oldest manufacturing methods for structural composites. Wet winding has the advantage of using the raw materials, fiber and resin, in its direct form without intermediate processing steps. The manufacturing speed measured in mass per time is among the highest in comparison to other methods. In sum, this contributes to relatively low manufacturing costs for filament wound composite parts compared to other methods and explains its continued importance. [42]

Filament winding is a process where composite parts are manufactured by winding of continuous fibers on a rotating mandrel in specific orientations. For high volume production of symmetrical composite parts, filament winding process is the most economical way. This process is primarily used for hollow, generally circular, or oval sectioned components, such as pipes and tanks. [41]

In the wet-winding procedure, the fibers as shown in figure 2.13 pass through a heated resin bath before reaching the feed head and are then deposited onto the mandrel. In this situation, rollers are used to remove excess resin, to force remaining resin into the fibers and flatten the tows. A variation

to this is the controlled wet procedure, in which resin is metered onto the fiber. In the case of pre-preg winding, the resin bath and rollers are not required, the pre-impregnated fiber being fed directly into the feed head from the spools, then laid onto the mandrel. For pre-preg winding, the mandrel is generally heated to promote resin tack and flow. The fully wound part is then cured either at room temperature in an oven or in an autoclave, depending on the resin system. [43] [41]

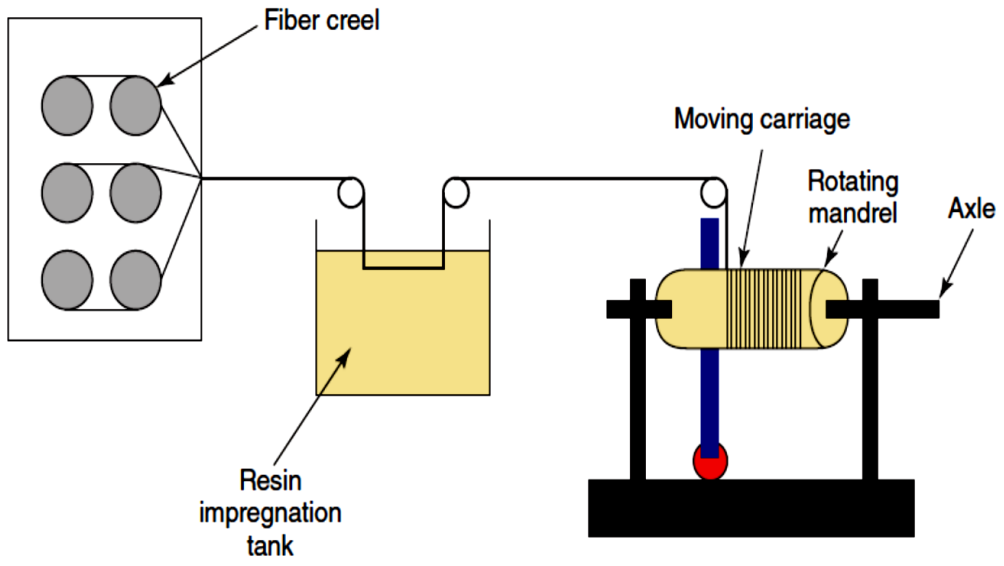

Figure 2.13 :Schematic presentation of the filament winding technology [41]

2.8. Constituent Materials

2.8.1. Reinforcements

Glass, carbon and aramid fibers are the most widely used reinforcement types in filament winding applications. The filament winding technique has many applications, including the civil, military and aerospace industries. Hence, cheap fibers with inferior properties, as well as very expensive fiber types with superior properties, are used.[44]

Glass roving reinforcements are most widely used in filament winding applications. Glass fibers have types like ‘A’, ‘C’, ‘D’, ‘E’, ‘R’, ‘S’, ‘S2’, ‘E-

CR' and 'AR'. Generally, E and S2 type of glass rovings are commonly used in filament winding applications. [45].

Carbon and aramid fibers can also be used in filament winding applications. Both aramid and carbon fibers have better mechanical properties than any kind of glass fibers. Additionally, carbon and aramid fibers both have better thermal properties. Aramid fibers are generally used in products which may be subjected to impact loading. A disadvantage of aramid fibers is the ease of moisture absorption, which has a negative effect on the structural performance of the material. Both carbon and aramid fibers have applications in the aerospace and defense industry. Both types of fibers are more expensive than E-glass. [44]

A carbon fiber is a long, thin strand of material about 0.0002-0.0004 in (0.005-0.010 mm) in diameter and composed mostly of carbon atoms as shown in figure 2.14. Carbon fibers are classified by the tensile modulus of the fiber. The English unit of measurement is pounds of force per square inch of cross-sectional area, or psi. Carbon fibers classified as "low modulus" have a tensile modulus below 34.8 million psi (240 GPa). [46]

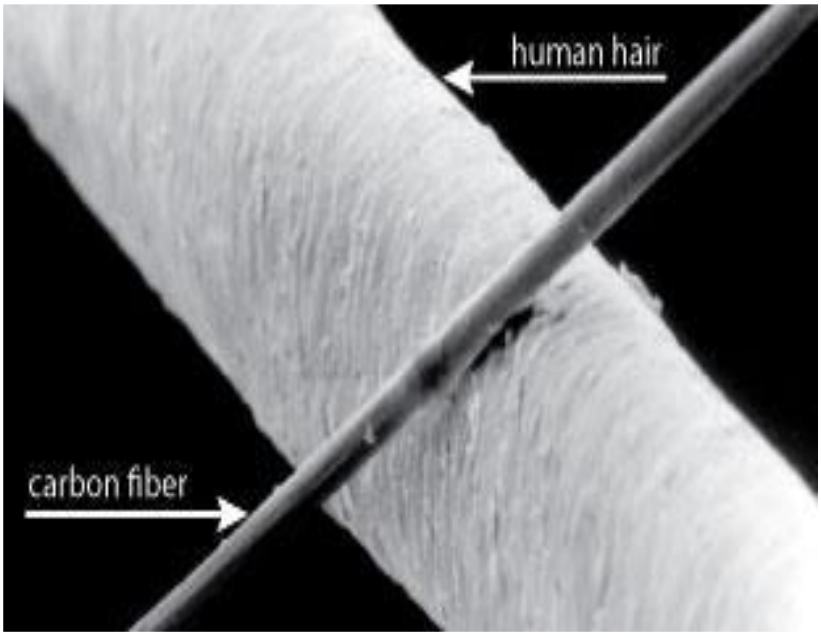

Figure 2.14: Comparing carbon fiber size with human hair size [46]

2.8.2. Resin system

As in other composite part production techniques, a resin system is used in filament winding: this resin system is called the matrix material after curing. The purpose of the resin system is virtually identical to the one used in other composite parts produced by different techniques. The characteristics of the resin system are: [44]

• They hold the fibers together and so help to distribute the load evenly

• They protect the fibers from abrasion during winding and from abrasion and corrosion after curing

• They provide interlaminar shear strength

• They help to control the chemical and electrical properties of the composite part as matrix systems, both thermosets and thermoplastics can be used in the filament winding process. [44]

Most standard composite resins (epoxy, polyester, phenolic, some imides, silicone, and thermoplastics) can be used for filament winding provided that certain specific requirements are met. Polyesters and epoxies are the most common. [47]

Viscosity and pot life are two of the main factors in selecting a resin for wet winding. Low viscosity, generally around 2000 centipoise, is desirable to help wet the fibers, spread the band, and lower the friction over the guides during the winding process. Pot life is primarily a function of the time it takes for winding the part; larger and thicker parts require a longer pot life than smaller and thinner parts. [32]

2.9. Winding Methods

There are three main variants of the filament winding process:

(1) wet winding, in which the dry reinforcement is impregnated with a liquid resin just prior to winding; (2) wet-rolled prepreg winding, in which the dry reinforcement is impregnated with the liquid resin and then rewound prior to

filament winding; and (3) towpreg winding, in which a commercially impregnated tow is purchased from a material supplier. [35].

2.9.1. Winding Patterns

2.9.1.1. Hoop Winding:

The simplest is hoop winding, which comprises a mandrel rotating continuously about its longitudinal axis while the fiber feed carriage advances one fiber bandwidth after each mandrel axis of rotation. Consequently, fibers are deposited almost normal to the longitudinal axis as shown in figure 2.15. [43]

2.9.1.2. Helical Winding:

Helical winding, which is most commonly used, is achieved when the mandrel rotates continuously about a horizontal axis while the fiber feed carriage traverses back and forth. In helical winding (Figure 2.15) the mandrel rotates more or less continuously, while the feed carriage traverses back and forth at a speed regulated to generate the desired helical angle. Winding angles ranging between 25-80° can be achieved with this method [47].

2.9.1.3. Polar Winding:

Polar winding is a special case of helical winding in which the filament path can be described by the intersection of a plane passed through the part Figure 2.15. The mandrel for polar winding is supported on only one end, permitting the filaments to cover the other end completely in a continuous path. The fiber delivery system can be stationary or movable [47].

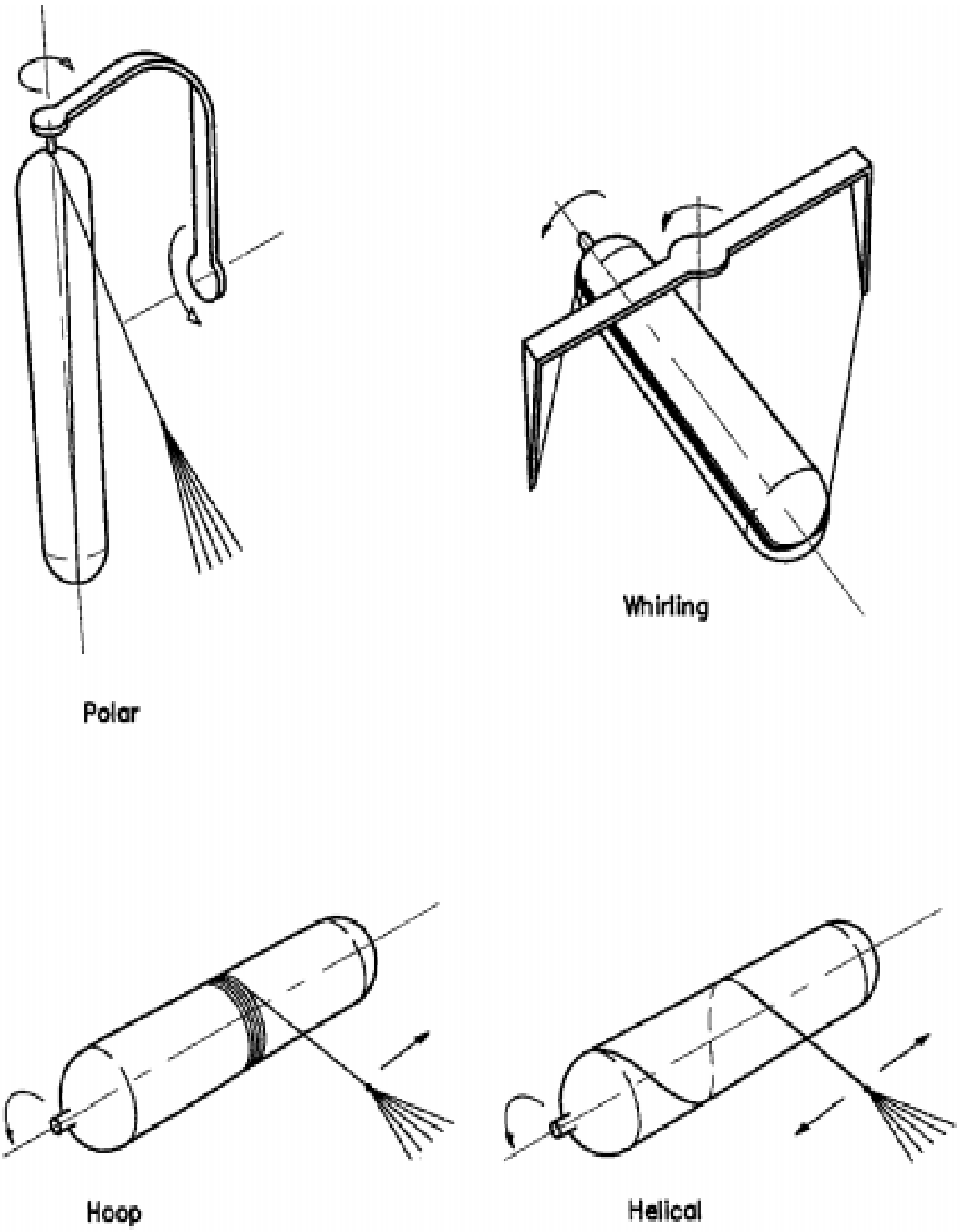

Figure 2.15: Schematic diagram of the various filament winding machines and patterns [43]**.**

2.10. Failure:

Failure of a structure is an event, the transition from a normal working state, where the structure meets its intended requirements, to a failed state, where it does not meet its requirements. Failure of any structure cannot be predicted exactly, deterministically but it can only be characterized by the stochastic properties of the structure and the actions the structure is subjected to. [48]

2.10.1. Failure of Composite Materials

The failure of composites has been investigated extensively from the micromechanical and macromechanical points of view. On the micromechanical scale, failure mechanisms and processes vary widely with type of loading and are intimately related to the properties of the constituent phases, i.e., matrix, reinforcement, and interface-interphase. Failure predictions based on micromechanics, even when they are accurate with regard to failure initiation at critical points, are only approximate with regard to global failure of a lamina and failure progression to ultimate failure of a multi-directional laminate. For these reasons a macromechanical approach to failure analysis is preferred [49].

2.10.2. Categories of Failures

1. Material-Improper selection of material; defects in material.
2. Design-Incorrect design data; inaccurate or incorrect design methods; inadequate shop testing.
3. Fabrication-Poor quality control; improper or insufficient fabrication procedures including welding; heat treatment or forming methods.
4. Service-Change of service condition by the user; inexperienced operations or maintenance personnel and upset conditions [39].

2.10.3 Failure Modes

Typical failure modes for fiber-reinforced composites can be seen in Figure 2.21 and are:

2.10.2.1. Fiber Buckling

Fiber buckling is characterized by a reduction of compressive stiffness and strength of the laminate. The onset and magnitude of the fiber buckling and the compressive property loss is dictated by the properties of the fibers and matrix. Fiber buckling is shown in figure 2.21 [39].

2.10.2.2. Fiber Breakage

Fiber breakage as shown in figure 2.16 occurs when fibers break, making them unable to carry tensile loads. When fibers are surrounded by a matrix, the matrix works as a bridge across the broken fiber transmitting the load. This is called fiber bridging. The failure (separation) of a fiber-reinforced composite ultimately comes from breakage of fibers. When plies of unidirectional fibers are stacked in a laminate, the stress on fibers is enhanced in the vicinity of ply cracks in the adjacent plies, causing a narrow distribution of fiber failure sites [50].

2.10.2.3. Matrix Cracking

Matrix cracking in itself is not normally a reason for ultimate laminate failure. However, matrix cracks may cause other harmful effects. Among those effects are normally moisture absorption, stiffness reduction dominated by the matrix, and it may provoke delamination. Matrix cracking is shown in figure 2.16 [51].

2.10.3.4 Delamination:

The separation of two adjacent plies in composite laminates, represents one of the most critical failure modes in composite laminates shown in figure 2.16. In fact, it is an essential issue in the evaluation of composite laminates for durability and damage tolerance. Thus, broken fibers, delaminated regions, cracks in the matrix material, as well as holes, foreign inclusions and small voids constitute material and structural imperfections that can exist in composite structures[52].

Figure 2.17 and figure 2.18 represent some experimental failure modes.

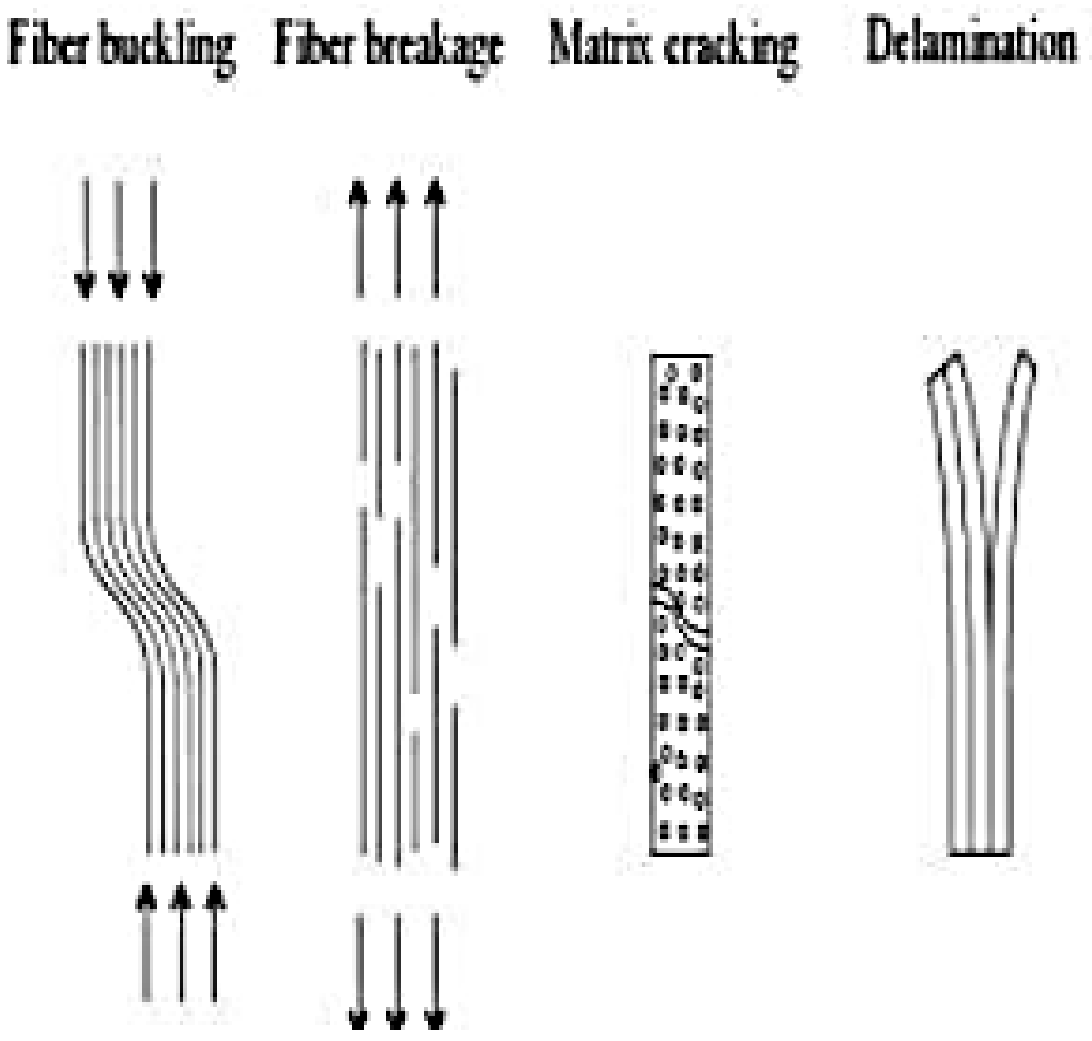

Figure 2.16: Typical failure modes in fiber reinforced composites. [25]

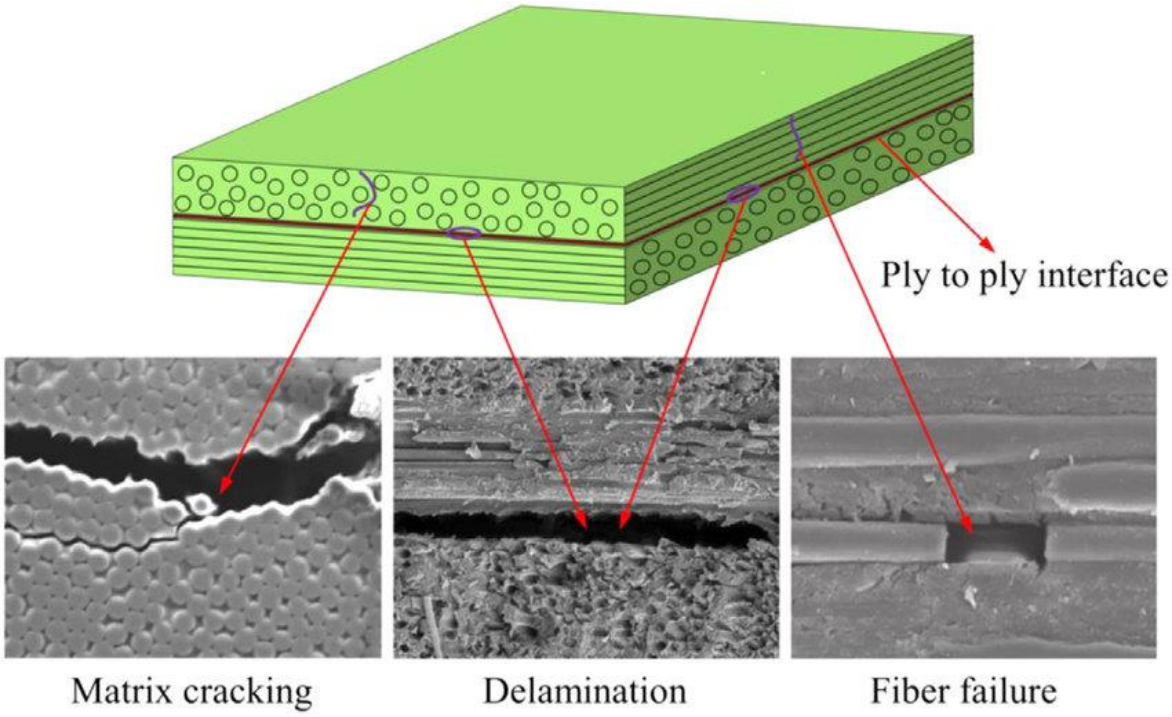

Figure 2.17: Main failure modes in fiber reinforced composite laminates.[53]

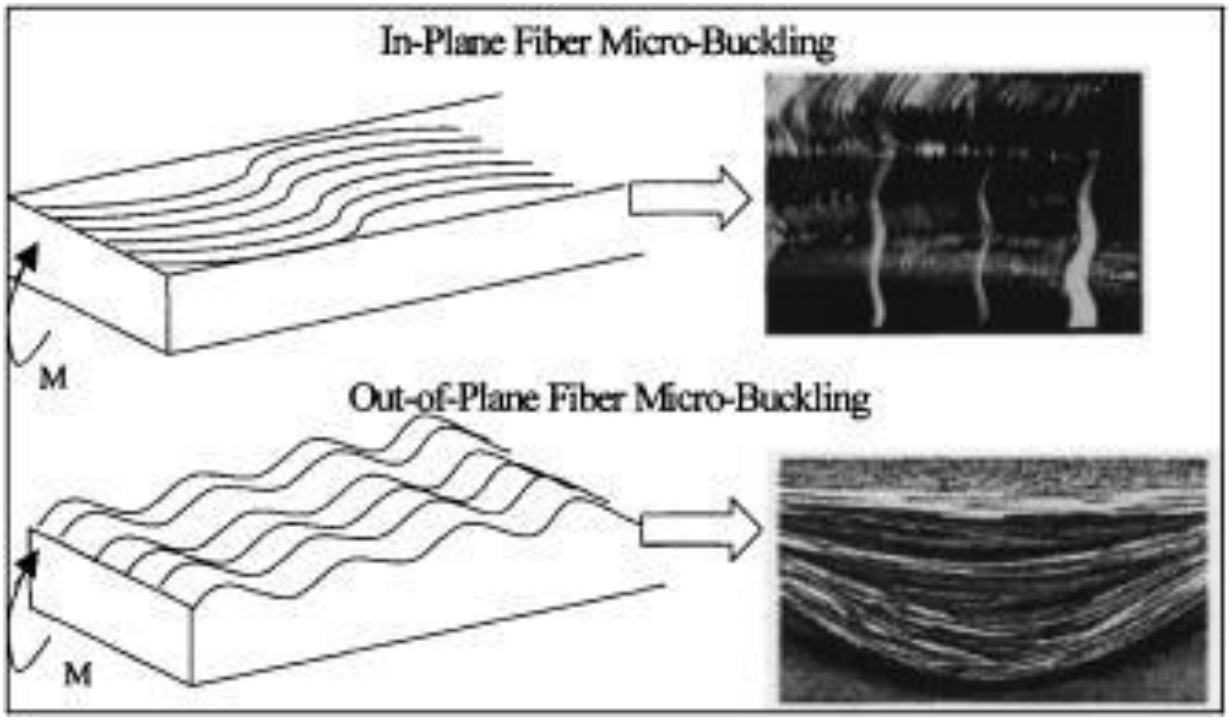

Figure 2.18: Illustration of micro-buckling failure mode.[54]

2.11 Failure of Pressure Vessels

Pressure vessels are used for various industrial applications. To ensure safe operation of pressure vessels, it is important to know its burst pressure. Burst pressure is the pressure at which vessel burst/crack and internal fluid leaks. For light weight application pressure vessel are made of composite material. Payload performance /speed /operating range depends up on weight. Use of composites for pressure vessels improves performance and also offer significant amount of material savings. Stacking sequence is very crucial to strength of composite pressure vessels. [55]

In design of pressure vessels two modes of failure needs to be considered; plastic deformation of the vessel walls and fracture. When internal pressure of the vessel increases, depending on amount of pressure, four states is possible to happen in sequence, elastic, yield, plastic deformation and fracture. When plastic deformation occurs, deformation will be permanent and load capacity of the vessels increases. By increasing the pressure, at certain value, load capacity rise, so, as a result, rapid reduction in wall thickness and burst will happen as shown in figure 2.19. [56]

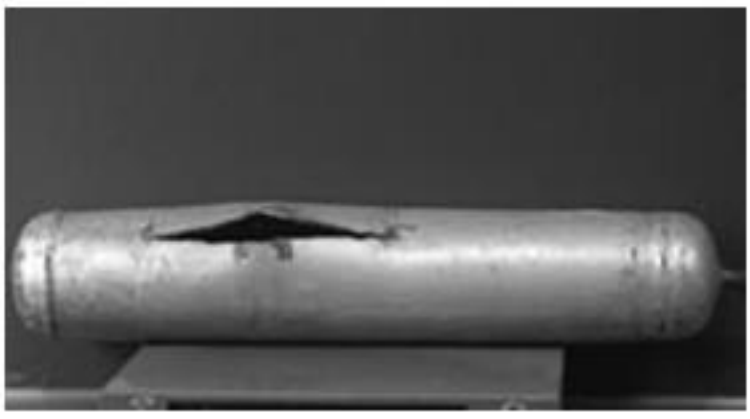

Figure 2.19: Rupture in a pressure vessel due to excessive internal pressure [56]

The pressure level in which the pressure vessel will burst is defined as the burst pressure. In another word, burst in vessel happens when undergoes plastic wall collapse due to the internal pressure, which leads to rupture and total failure. Accurate predicting of the burst pressure may result in saving of the material and lowering the production cost without sacrificing the design safety. [55] [56]

2.12 Allowable Stresses Unidirectional Laminates

Unidirectional fibrous composite ply can experience two modes of failure associated with

• Fiber failure, and

• Cracks in the matrix [38]

Table 2.1: Burst pressure for the filament-wound fiberglass pressure vessels. [38]

Diameter of the vessel (mm)	Layer thickness (mm)		Calculated burst pressure (MPa)	Number of tested vessels	Experimental burst pressure	
	h_1	h_2			Mean value (MPa)	Variation coefficient (%)
200	0.62	0.60	10	5	9.9	6.8
200	0.92	0.93	15	5	13.9	3.3

Figure 2.20: The failure mode of a composite pressure vessel. [38]

2.13. Failure Mechanism

In a laminated composite at locations where failure is initiated, stiffness is reduced and the surrounding material must carry the service loads. Because the fibers are the supported material in the composite, when they fail the structure is consequently endangered. [57]

Failures occur in stages, where one case of damage can lead to a series of failures in the material, as shown in the stress-deformation curve, shown in Figure 2.21 [13].

Each point in Figure 2.21 displays a basic failure within a singular layer of the composite laminate panel. As a result of the layer failures, the final state is the total failure of the composite laminate. This figure implies that the failure in the layer is almost sudden. Nevertheless, in reality, failure is progressive, since the present mechanisms, such as matrix cracking, occur gradually, rather than all at once [13].

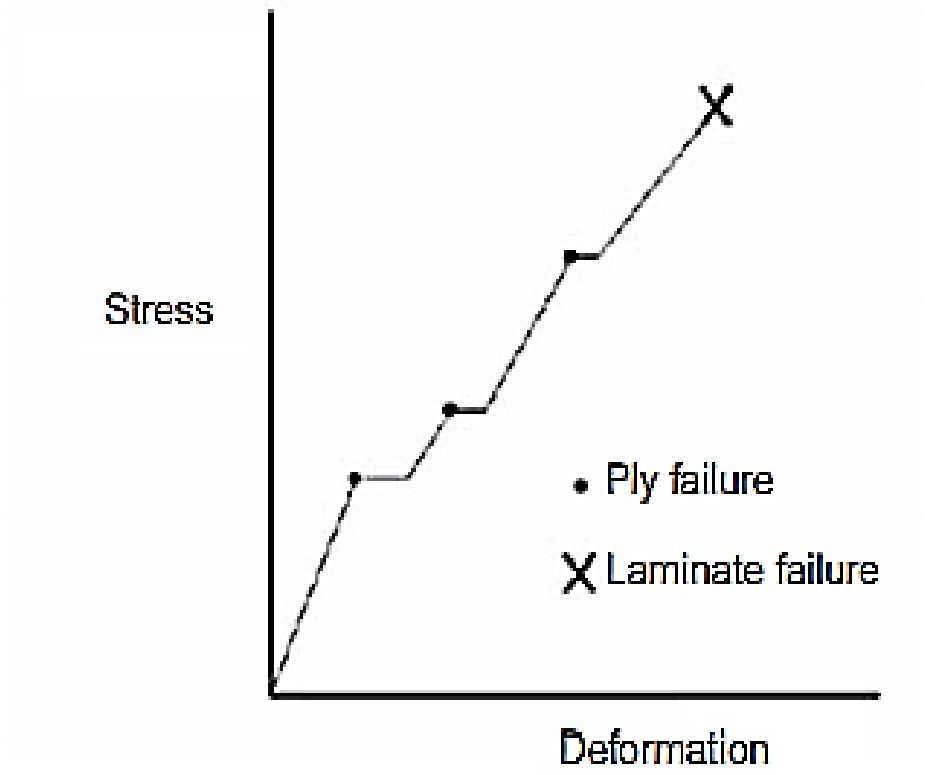

Figure 2.21: The failure process in composite laminate [13].

2.14. Failure Theories

Precise analyzing the strength of composite layers requires employing failure criteria. Different types of failure analyses can be used for evaluating the strength of composites laminae. However, there are 2 categories in general, which are the independent criterion and interactive criterion. The differences between both types are shown in Table 2.2 below. [6]

Table 2.2: Types of Failure Analysis Criterion [6]

Criteria	**Description**
Independent	The application of such method to detect failure is simple and significant but it lacks of stress interactions detection between each lamina. Examples of independent criteria are the maximum stress and strain failure criterion. [6]
Interactive	The stress interactions in lamina failure mechanism are included, enabling failure predictions on the lamination plies of an orthotropic structure. However, parameters and properties must be clearly and accurately input. Examples of interactive criteria are Tsai-Wu failure criterion, Tsai-Hill failure criterion, Hoffman failure criterion. [6]

2.14.1. Maximum Shear Stress Theory (Tresca)

Failure occurs when the maximum shear stress at an arbitrary point in a stressed body is equal to the maximum shear stress at failure (rupture or yield) in a uniaxial tensile test. [58]

$$\tau_{max}=\frac{\sigma_1-\sigma_3}{2}=\tau_{max_{tensile}}=\frac{\tau_{f_{tensile}}}{2} \quad \ldots\ldots\ldots\ldots\ldots (2.29)$$

$$\sigma_1-\sigma_3=\tau_{f_{tensile}} \quad \ldots\ldots\ldots\ldots\ldots (2.30)$$

2.14.2. The Coulomb Yield Criterion

The Tresca yield criterion assumes that the critical shear stress is independent of the normal pressure on the plane on which yield is occurring. Although this assumption is valid for metals, it is more appropriate in polymers to consider the possible applicability of the Coulomb yield criterion, which states that the critical shear stress for yielding to occur in any plane varies linearly with the stress normal to this plane, i.e. [59]

$\tau = \tau_c - \mu\sigma_N$ …… (2.31)

The Coulomb criterion was originally conceived for the failure of soils and c was termed the 'cohesion' and the coefficient of internal friction. For a compressive stress, σ_N has a negative sign so that the critical shear stress for yielding to occur on any plane increases linearly with the pressure applied normal to this plane. The Coulomb criterion is often written as stress, N has a negative sign so that the critical shear stress for yielding to occur on any plane increases linearly with the pressure applied normal to this plane. The Coulomb criterion is often written as [60]

$\tau = \tau_c$ –tan Øσ_N …… (2.32)

Where μ has been written as tan Ø for reasons that will now become apparent. Consider uniaxial compression under a compressive stress σ_1 where yield occurs on a plane whose normal makes an angle Θ with the direction of σı (Figure 2.22). The shear stress is $\tau_1 = \sigma \sin \Theta \cos \Theta$ and the normal stress is $\sigma_N = -\sigma_1 \cos^2 \Theta$. Yield occurs when [59]

$\sigma_1 \sin \Theta \cos \Theta = \tau_c + \sigma_1 \tan \varnothing \cos^2 \Theta$ ……(2.33)

i.e. when

$\sigma_1 \cos \theta \sin \Theta - \tan \varnothing \cos^2 \Theta = \tau_c$ …… (2.34)

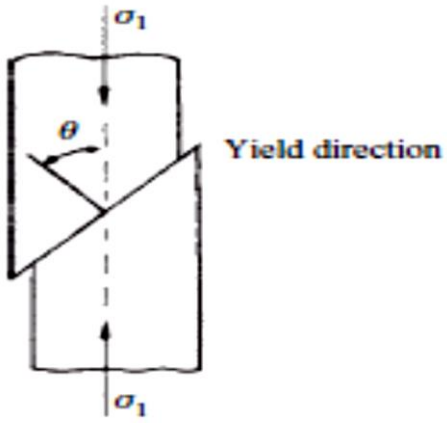

Figure 2.22: The yield direction under a compressive stress σ_1 for a material obeying the coulomb criterion. [60]

2.14.3. Maximum Distortion Energy

(or maximum octahedral shear stress) theory (von Mises): Failure occurs when the maximum distortion energy (or maximum octahedral shear stress) at an arbitrary point in a stressed medium reaches the value equivalent to the maximum distortion energy (or maximum octahedral shear stress) at failure (yield) in simple tension [58]

$$\sigma_1^2 + \sigma_2^2 + \sigma_3^2 - (\sigma_1\sigma_2 + \sigma_2\sigma_3 + \sigma_3\sigma_1) = 2\sigma_{f\,\text{tensile}}^2 \ldots\ldots\ldots (2.35)$$

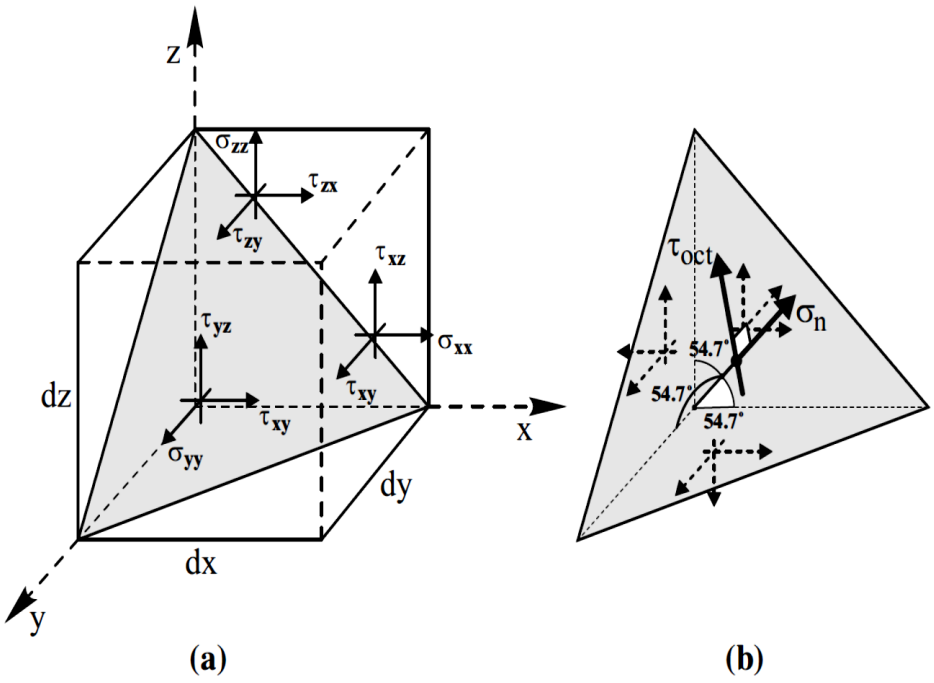

Figure 2.23: Definition of the octahedral shear stress. [58]

2.14.4. Maximum Stress and Strain Criteria

These criteria belong to a structural type and are based on the assumption that there can exist three possible modes of failure caused by stressesσ_1,σ_2 and τ_{12} or strainsε_1,ε_2 andγ_{12}, when they reach the corresponding ultimate values.

The maximum stress criterion can be presented in the form of the following inequalities[37]

$$\sigma_1 \leq \overline{\sigma_1^+}, \sigma_2 \leq \overline{\sigma_2^+} \quad \text{if} \quad \sigma_1>0 \quad \sigma_2>0$$
$$|\sigma_1| \leq \overline{\sigma_1^-}, |\sigma_2| \leq \overline{\sigma_2^-} \quad \text{If} \quad \sigma_1<0 \quad \sigma_2<0 \quad \ldots\ldots\ldots (2.36)$$
$$|\tau_{12}| \leq \overline{\tau_{12}}$$

It should be noted here and subsequently that all the ultimate stresses σ and τ including compressive strength values are taken as positive quantities. The failure surface corresponding to the criterion in Eqs. 2.36 is shown in Fig. 2.24. As can be seen, according to this criterion failure is associated with independently acting stresses, and any possible stress interaction is ignored. It can be expected that the maximum stress criterion describes adequately the behavior of those materials in which stressesσ_1,σ_2 and τ_{12} are taken by different structural elements. [37]

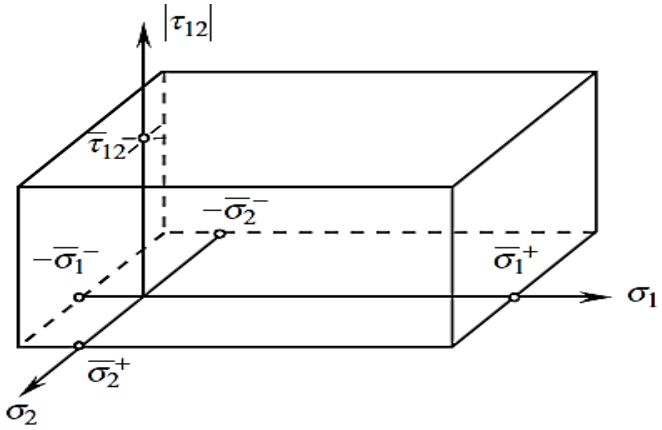

Figure 2.24: Failure surface corresponding to maximum stress criterion. [37]

2.14.5. Approximation Strength Criteria

Failure theories of a lamina are based on strength properties. This topic is called the macro-mechanics of a single layer or a lamina. A laminate is a stack of laminae. Each layer of fiber reinforcement can have various orientation and in principle each layer can be made of different materials. Knowing the macro-mechanics of a lamina, one develops the macro-mechanics of the laminate. Average stiffness, flexibility, strength, etc. can be determined for the whole laminate.[30]

In contrast to structural strength criteria, approximation criteria do not indicate the mode of failure and are constructed by approximation of available experimental results with some appropriate function depending on stresses σ_1,σ_2 and τ_{12}. The simplest and the most widely used criterion is a second-order polynomial approximation, typical forms of which are presented in Figure 2.25, in the stress space shown in Figure 2.26, the polynomial criterion corresponding to Figure 2.25 can be written as[37]

$$F(\sigma_1, \sigma_2, \tau_{12}) = R_{11}\,\sigma_1^2 + R_{22}\,\sigma_2^2 + S_{12}\,\tau_{12}^2 = 1 \ldots\ldots\ldots \quad (2.37)$$

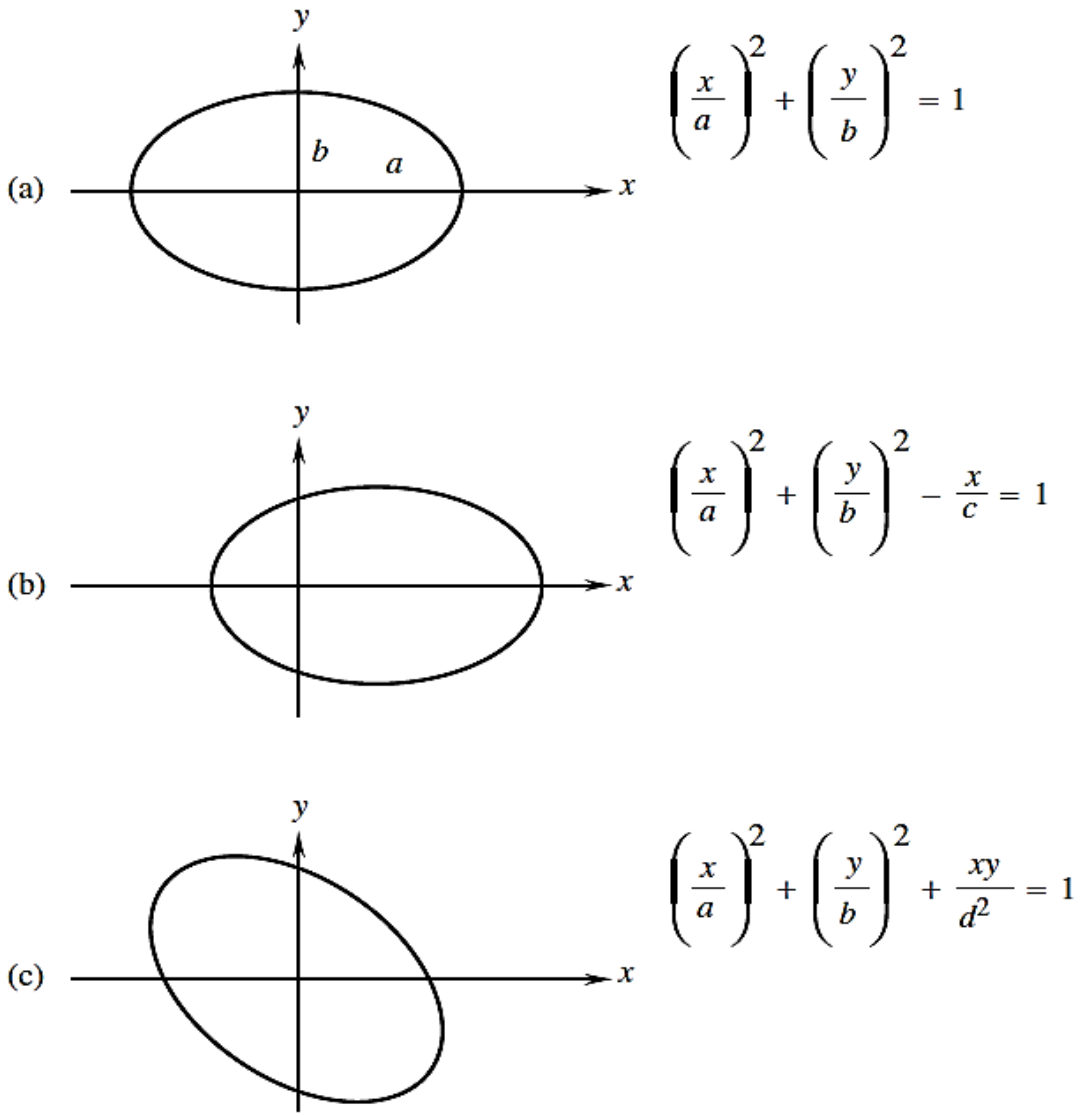

Figure 2.25: Typical shapes of the curves corresponding to the second-order polynomials.[37]

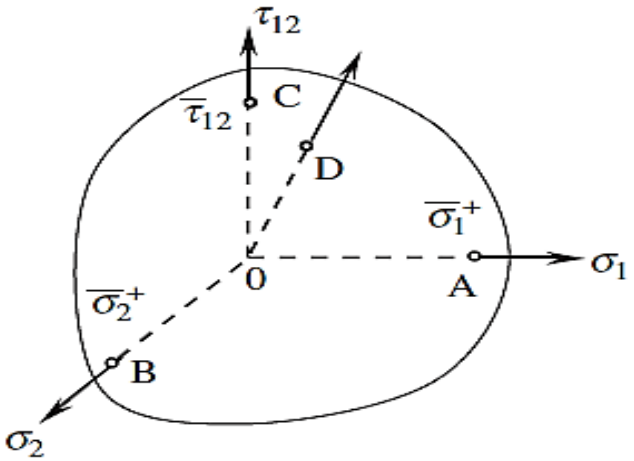

Figure 2.26: Failure surface in the stress space. [37]

2.15. Nondestructive Test

The evaluation of the structural condition of pressure vessels is carried out through Non-Destructive Testing (NDT). Nondestructive testing (NDT) or Nondestructive evaluation (NDE) refers to techniques, which are used to detect, locate and assess defects or flaws in materials or structures or fabricated components without affecting in any way their continued usefulness or serviceability. It is evident that techniques to detect critical flaws before they have grown unacceptably large are of vital importance in the industry for in-service inspection, quality control and failure analysis. [61]

For the purposes of these notes, NDT methods may be divided into conventional and nonconventional. To the first group belong commonly used methods like visual or optical inspection, liquid penetrant testing, magnetic particle testing, eddy current testing, radiographic testing and ultrasonic testing. The second group includes those NDT methods used only for specialized applications like neutron radiography, acoustic emission, infrared testing, microwave techniques, leak testing, holography etc.[62]

It must also be remembered that none of these methods provide solutions to all possible problems, i.e. they are not optional alternatives but rather complementary to each other. The basic principles, typical applications, advantages and limitations of the conventional methods will now be briefly described. [63].

Nevertheless, tests such as ultrasound, industrial radiography and electromagnetic particles, among others, are active methods that require the Unlike the aforementioned methods, acoustic emission (AE) is a passive one, in which discontinuities in the material release energy as the structural components are subjected to load or stress. Then, the energy released travels through the material as sound waves that spread cylindrically, and a transducer receives and converts it to a voltage signal for it to be processed as data of acoustic or microseismic activity.[64]

2.15.1. Visual Testing (VT)

Often overlooked in listings of NDT methods, visual inspection is one of the most common and powerful means of non-destructive testing. Visual testing requires adequate illumination of the test surface and proper eye-sight of the tester. It is also a fact that all defects found by other NDT methods ultimately must be substantiated by visual testing. Figure 2.27 shows a portable light, a mirror on stem, a 2X or 4X hand lens, one illuminated magnifier with magnification 5X or 10X. For internal inspection, light lens systems such as borescopes allow remote surfaces to be examined. [65]

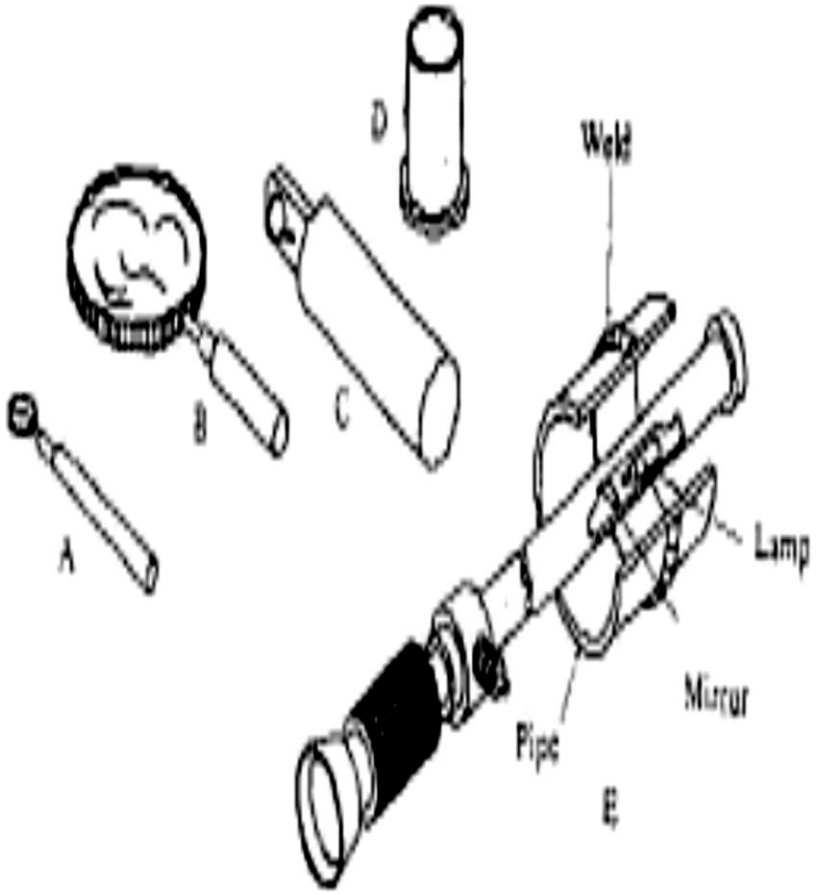

Figure 2.27: Various optical aids used in visual inspection. (a) Mirror on stem (b) Hand magnifying glass (c) Illuminated magnifier (d) Inspection glass (e) Borescope. [65]

2.15.2. X-Ray Radiography and Computed Tomography

Radiography involves penetrating the object with short wavelength electromagnetic radiation. The amount of radiation that passes through the object is captured by a detector. The absorption is a function of density and thickness of the material. Cavities and discontinuities lead to a detectable variation in absorption. CT scanning is used to generate an exact three-dimensional cross sectional image of the entire part.[61][32]

Typical defects that can be detected using this technique are delamination, undulations, porosities, fiber cracks or impact damages. Three-dimensional volume is reconstructed by using radiographic images of different perspectives. Figure 2.28 represents the principle of CT scanning [61]

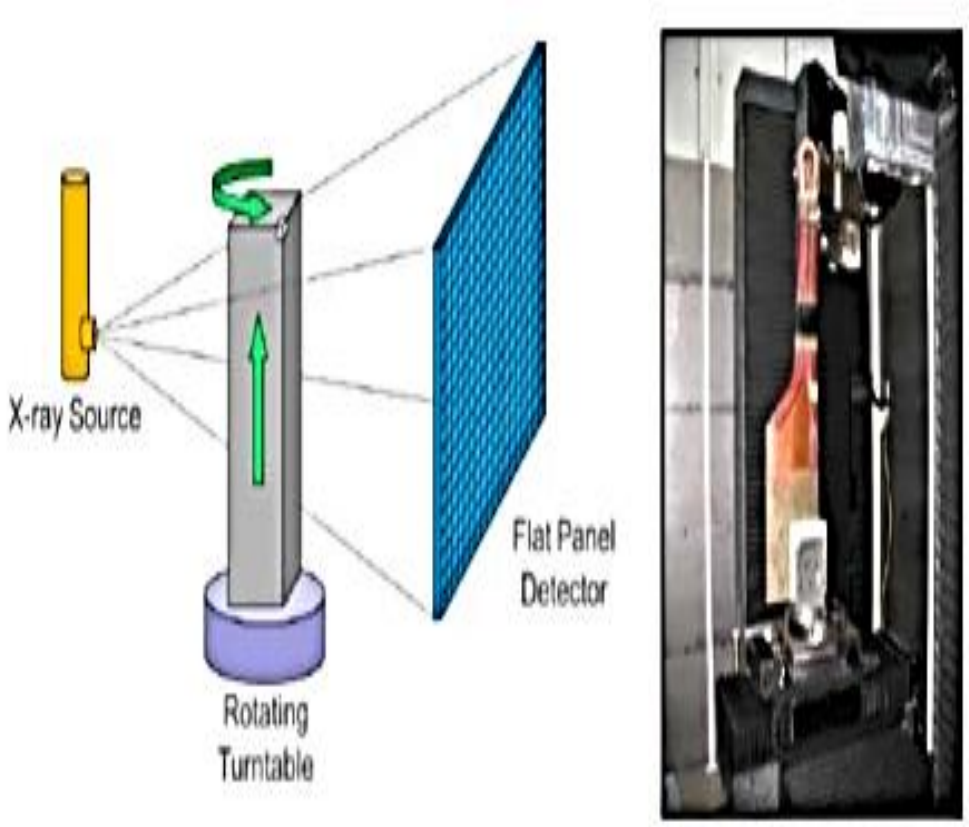

Figure 2.28: Principle of a helical CT scanning system. [61]

Cracks that are parallel to the radiation beam and cracks smaller than the resolution are difficult to spot. As a rule of thumb, the defects must be at least 2% in size of the thickness of the material so that it can be effectively detected. This method is used on wide variety of products such as forgings, castings and weldments. [65]

The main disadvantages of XCT are; limitations in spatial and temporal resolution and the lack of contrast between phases in the scanned specimen having similar attenuation coefficients e.g. carbon fiber and polymer matrix in a composite. The spatial resolution is determined by the detector resolution and the distance between the sample and the source. Often, the highest resolution is obtained at the expense of a small sample size or a small scanning area, and one needs to adopt a compromise between sample size and resolution. This represents one of the main limitations when using current generation of X-ray CT systems to study composite materials. [66].

2.15.3. Ultrasonic Microscopy

Ultrasonic testing as shown in figure 2.29 is used to detect size porosity, measure dimensions, or determine some properties of materials, in which high frequency (0.5-50 MHz) sonic waves are transmitted through the test material (specimen) and the measurement of the amplitude, frequency, or time of arrival of the returned echoes. Generally, ultrasonic test set-up consists of a pulser/receiver, a transducer and a display device. The pulser generates high voltage electrical pulses and drives the transducer, and the transducer converts the electrical pulses into high frequency vibration or ultrasound. The ultrasonic energy is introduced into the specimen and propagates through the materials in the form of ultrasonic waves. [46]

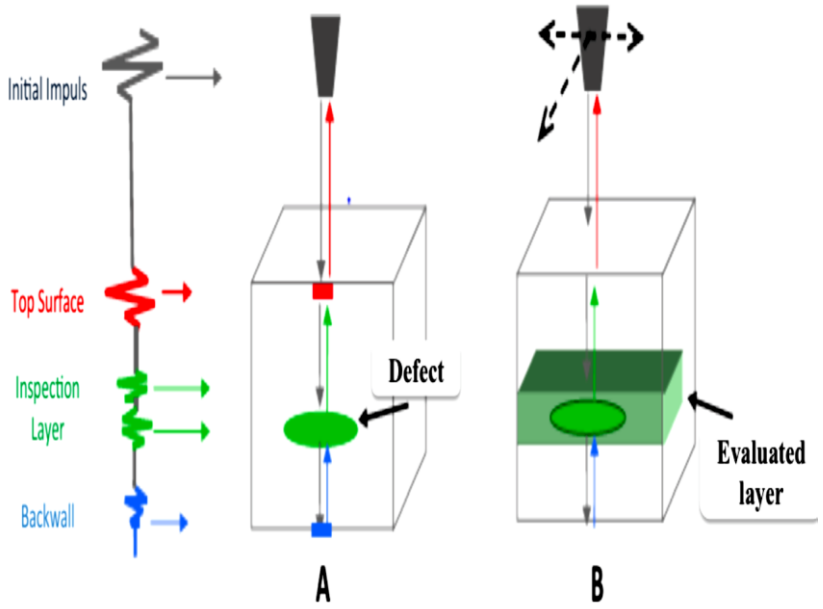

Figure 2.29: Ultrasonic microscopy testing [46]

Ultrasonic are the obvious advantages, namely: (1) Ultrasonic directivity is good, it can form a narrow beam. (2) A wavelength, small defects can also be a good reflection. (3) The distance resolution and the resolution of the defects are well. Because of crack is one of the most dangerous defects by ultrasonic testing can greatly improve the defect detection rate, and to ensure product quality. [27].

2.15.4. Thermography

Thermography testing makes use of infrared (IR) imaging to detect defects within the component. An IR camera records spatial and temporal distribution of the surface temperature after the component has been heated. Defects disturb the heat flow and hence can be detected. Thermal NDT methods generally use active thermography. Here, heat waves are sent using an external or internal source. This allows measurement of depth, thickness, and size of internal flaws. Furthermore, Pulse and Lock-In Thermography are in use for NDT applications globally for flaw imaging. Figure 2.30 represents the principle of IR imaging technique [61]

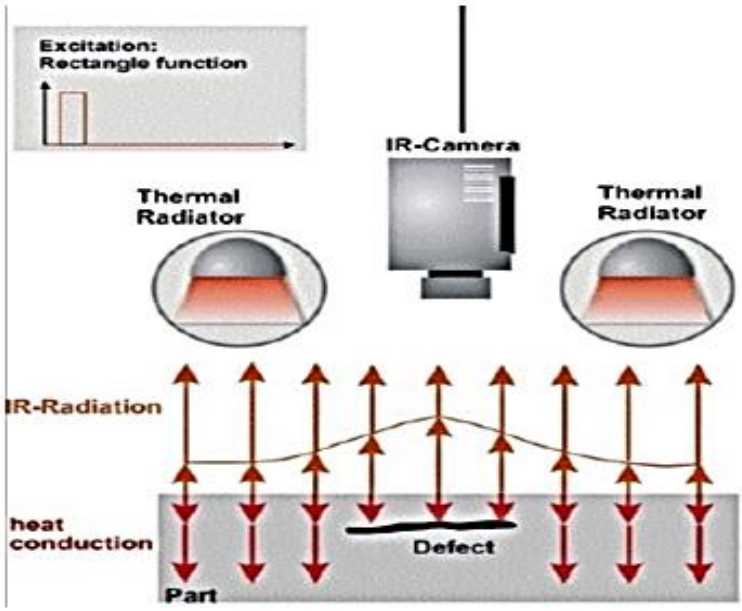

Figure 2.30 : Pulsed thermography schematic showing how defects lead to a distortion of the heat flow through a component.[61].

2.15.5. Acoustic Emission

Acoustic emission (AE) as shown in figure 2.31 is a nondestructive monitoring method which takes advantage of the elastic energy after crack propagation events .The micro-motion of the tip of the crack excites elastic waves which are acquired by sensors on the surface of the material. The number of recorded signals during loading is connected to the number of active sources within the material [67]

Additionally, the signals depend on their source, and specifically the intensity and the mode of fracture. Therefore, the number of recorded hits and key waveform features like amplitude, energy and frequency carry information from the damage mode and the fracture process. In general, tensile mode of failure generally develops before shear; therefore, the characterization of cracks as to their mode provides a warning before failure. [68]

The received wave depends on the motion of the crack tip, as well as on the orientation of the crack relatively to the receivers and the distance between the cracking source and the sensor. When a cracking event occurs, all possible wave modes (longitudinal, transverse and Rayleigh if the crack is surface breaking) are excited. [69]

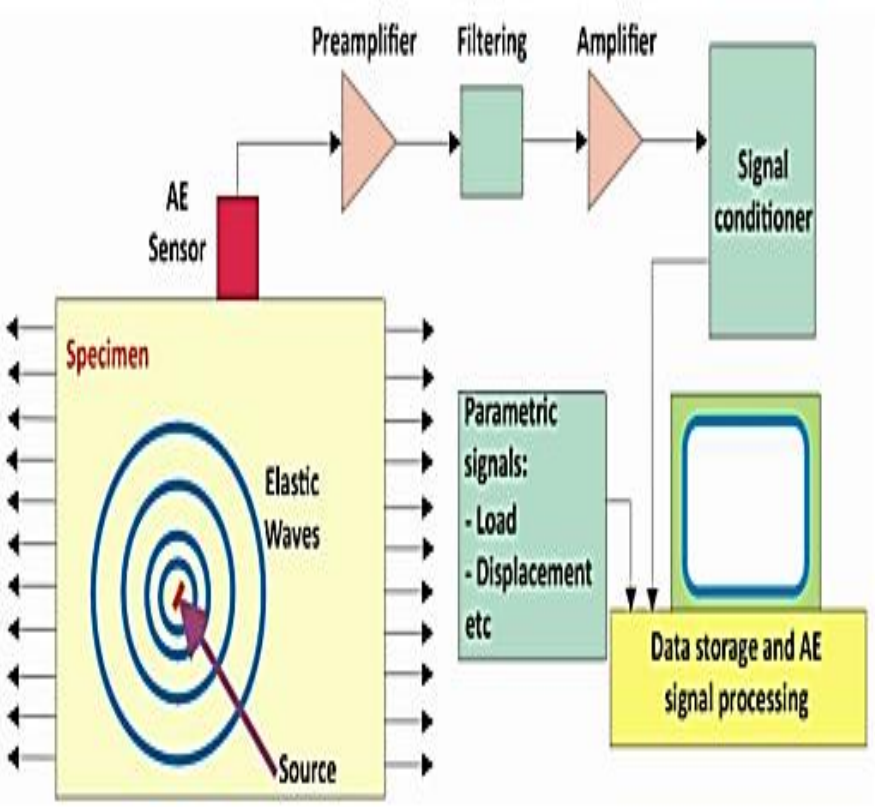

Figure 2.31: A basic overview of an acoustic emission set-up [70]

The acoustic signals in this method are developed by damages inside the component. The stress inside the component finds when different degrees of divergent forces from the stress waves are generated inside the sample. AE method have therefore the ability to find the defects in such an early stage so they not are enough crucial for reduce mechanical properties in a serious way. The piezoelectric sensor is very sensitive to signals and can thus receive these divergent forces early in the damage initiator process. [61]

2.16. Literature Review:

In 2005, Karpuz, Pınar et al. [11], determined the mechanical characteristics of the filament wound composite tubes working under internal pressure loads. The tested tubes were manufactured by wet filament winding method, employing two different fiber types carbon fibers and glass fibers, and five different winding angle configurations (25°, 45°, 54.8°, 65° and 90°) .The internal pressure test results revealed that the carbon fiber reinforced composite tubes exhibited a better burst performance compared to the glass fiber reinforced tubes, and the maximum burst performance is achieved at $[54.8°_3]$.

In 2007, F.H. Abdalla et al. [71] designed and developed 2-axis filament winding machine for the fabrication of pipes and round shape specimens, it provided a capability for producing pipe specimens with an internal diameter up to 100 mm and lengths up to 1000 mm. The range of the winding angle, or the fiber orientation angle, starts from 20° to 90° depending on the mandrel diameter used. A control unit was used to control the whole process and achieve regular winding and good surface finish.

In 2011, Theodoros Hasiotis et, al [72] used ultrasonic C-scan techniques for estimation defects of carbon/epoxy system and glass/polyester system. Several artificial defects were embedded into the test plates, varying in shape, magnitude and through thickness position. The technique capable of accurately defining the position and shape of the however, was less accurate for the size of the defects. In the case of the GFRP specimens, the present method led only to a rough estimation of the position and the shape of the defects.

In 2011, Niranjan Kumar [73] analyzed the effect of number of shells on the maximum value of hoop stress on multilayered pressure vessel. It was found that the Maximum hoop stress at the innermost surface decreases due to

multilayering where hoop stress decreases with increase in number of layers, but decrease in hoop stress is more effective up to n=3.

In 2012, AD Mutasher et al. [74], designed and fabricated a small-scale automated filament winding machine where the fiber is impregnated with resin and wrapped on a cylindrical shape mandrel. The machine generates helical winding patterns with various angles. Testing of the prototype shows that it is capable of producing winding angles in the range from 40° to 80° degrees.

In 2013, S Sulaimana et, al. [75] investigated the effects of winding angle of aluminum pressure vessel overwrapping by Carbon/Epoxy fiber reinforced polymer (CFRP). The Laminate were oriented asymmetrically for [0°,0°]s ,[15°,-15°]s,[30°,-30°]s ,[45°,-45°]s ,[55°,-55°]s, [60°,-60°]s ,[75°,-75°]s,[90°,-90°]s orientations. An exact elastic solution along with the Tsai-Wu, Tsai-Hill and maximum stress failure criteria were employed for analyzing data. Investigations exposed that the optimum winding angle happens at 55° winding angle. Results were compared with the experimental ones and there was a good agreement between them.

In 2013, Rayapuri Ashok et, al. [76] built a finite element model of CFRP composite pressure vessel having four layers using finite element software ANSYS 11. The burst pressures for various fiber orientations [+25°/-25°] s, [+35°/-35°] s, [+45°/-45°] s, [+55°/-55°] s, [+65°/-65°] s, and [+75°/-75°] s are predicted using the Tsai-Wu failure criteria. The ±45° fiber orientation angle is obtained as the optimum fiber orientation angle for the composite pressure vessel subjected to high internal pressure loading.

In 2014, José Humberto S. Almeida Jr et al.[77], presents a damage model based on progressive failure analysis to evaluate the mechanical response of composite tubes subjected to hydrostatic internal pressure load. Composite tubes wound at ±55° have the highest burst pressure and radial deformation resistances, and the addition of a hoop layer harmed the

mechanical performance of the tube. The shear stresses increase up to winding angle of ±55°, decreasing for higher angles, where transverse stresses dominate the failure mode.

In 2014, Joon-Seok Park et al. [78], investigated the pipe stiffness (PS) of glass fiber reinforced polymer plastic (GFRP) flexible pipes buried underground with (length 300mm, Diameter 300 mm and thickness 9mm). Pipe stiffness of GFRP flexible pipe is investigated by the parallel plate loading test, The results of pipe stiffness of the GFRP flexible pipe found that GFRP pipe was 718.4 (kN/m^2).

In 2014, Ahmed Arabi Hassen et, al [79] presented work concerns identifying various defects in glass fiber/polypropylene composites by medical X-ray (X-CT) after artificial defects were embedded. Fiber orientation and misalignment were successfully identified using X-CT technique. However, was not able to delamination, porosity and couldn't identify objects with relatively close material densities.

In 2014, J. H. S. Almeida Júnior et, al [80] studied the burst pressure and mechanical behavior of filament wound composite pipes manufactured with different winding angles, from ±35° to ±75°. The mechanical properties were obtained based on finite element method (FEM). In all failure criteria used like Maximum stress , maximum strain, Tsai-Wu and Tsai-Hill, the winding angle of $[90/\pm 50_8/90]$ was found as optimum for the cylinder studied, which was 22% and 172% higher than the $[90/\pm 35_8/90]$ and $[90/\pm 75_8/90]$, by the Tsai-Wu failure criteria.

In 2015, HAWA A et, al [81] investigated the effects of low velocity impact loading on the pressure bearing capacity of the E-glass/epoxy composite pipes. The pipes were produced by the filament winding technique with $(\pm 55°)_3$ winding angles. The specimens were impacted and subjected to burst pressure. The results indicate that for impacted samples, the burst strength of the pipes decreases with increase in energy levels during impact

loading. During the burst tests, several damage types named leakage and eruption were observed.

In 2015, Shildip D. Urade, [82] studied the effect of Multilayer on pressure vessel under high pressure condition. The stress analysis of multi-layer pressure vessel was subjected to internal pressure the hoop stresses for 1, 2 & 3-layer pressure vessel is calculated theoretically. The modeling of pressure vessel is carried out in ANSYS Workbench where stress analysis is carried out. From calculations it is observed that as the numbers of layers increases, the hoop stresses decreases. It is concluded that the multi-layering of pressure vessel is effective up to only 3-layers.

In 2015, B. G. Sumana et, al. [83] investigated the numerical residual stresses induced between the layers of fiber metal laminate (FML) cylinder (glass/epoxy reinforced aluminum laminates) under buckling hydrostatic loading with various fiber orientations such as 0/90˚, 60/30˚, ±45˚ and ±55˚ and different FRP thickness of 1, 2, and 3 mm. The results show that magnitude of residual stresses between the layers decreased along the thickness from outer layer towards the inner layer in sine wave form. The maximum residual Von-Mises stress was at inner aluminum layer while the maximum residual radial stress was at the outermost layer of FML cylinder due to the inward pressure.

In 2015, Srebrenkoska V et al. [84], investigated the hoop tensile properties of continuous fiber reinforced composites pipes of glass fiber and epoxy resin by filament winding method with three different winding angle configurations (10°, 45° and 90°) were tested and the hoop tensile strengths and modulus of elasticity were determined. The results showed that, mechanical properties of composites were depended from winding angles. The optimal values for the hoop tensile strength are obtained for the samples winded with 45° winding angle.

In 2016, G Suresh et, al [85], studied the stiffness of E-glass fiber reinforced with a mixture of vinyl ester (VER) and polyurethane (PU) prepolymer test (with 300 mm diameter) was continued till the internal diameter of the sample subjected to 30% of deflection. It was observed that during the stiffness test, all the PU-loaded VER specimens have regained its original shape and size. While VER glass fiber composite pipes (0% PU) exhibited crazing, wall delamination, and rupture on compression.

In 2016, Ahmed W. Abdel-Ghany et al [86] predicted the failure of four layered FW composite made of E-glass/epoxy, carbon/epoxy and aramid/epoxy composites subjected to internal pressure using the last ply failure technique using ANSYS Composite PrepPost (version 15). The lowest burst pressure was recorded to be at 0° winding angle. The burst pressure at the optimum winding angle $[\pm 55°]_2$ for the three materials. The burst Pressure for Carbon/epoxy is about three times that for E-glass/epoxy. The burst pressure for$[\pm 0°]_2$ comparing the three composites is almost the same. For $[\pm 90°]_2$carbon/epoxy and aramid/epoxy results to about double the burst pressure for E-glass/epoxy.

In 2016, Yan Ma, et al. [87] studied the failure behavior and mechanical properties of unidirectional (UD) prepreg carbon fiber reinforced epoxy resin (CF/Epoxy) laminates were investigated through tensile tests in this study. The physicochemical parameters such as interfacial properties and Mode II interlaminar fracture toughness were measured through a SEM technique. The results showed that the CF/Epoxy laminates with stronger interface but lower Mode II interlaminalr fracture toughness mostly showed splitting fracture mode (69%) in matrix fracture mode (Cohesive failure).

In 2018, Tamer A. Sebaey et al. [88], investigated the GFRP pipe that designed with four different winding angles have been tested under internal pressure with winding angles of$[\pm 45°_3]$, $[\pm 55°_3]$, $[\pm 63°_3]$, and [±63/ ±45/

±55], the maximum failure pressure was that for the pipes with $\pm 55°_3$ winding angles. All specimens failed in the same way of initial leakage governed by matrix cracking. For impact test the combined orientations [±63/ ±45/ ±55] show higher resistance than the other composites.

In 2019, Roberto José de Medeiros, et al. [89] fabricated an epoxy-based vinyl ester resin laminate reinforced with hybrid fabric consisting of carbon and Kevlar fibers subjected to uniaxial tensile tests in order to determine its mechanical properties and damage mechanism. The micrographic analysis of the final damage showed characteristics such as fiber fracture, adhesive fracture (fiber/matrix debonding), Kevlar fiber fraying, in addition to the cohesive fracture in the matrix, for all the test specimens analyzed.

In 2020, Özkan ÖZBEK et al. [90]designed and constructed a 2- axis filament winding machine for the fabrication of different types of fiber reinforced composite pipes. The machine is capable of producing specimens in different design parameters such as dimensions up to 750 mm length and 250 mm diameter, different winding angles for hoop, helical and polar winding types for different winding angles, fiber reinforcements and cross sections.

In 2021, Mateusz Gargol, et al. [91] studied the synthesis and thermal properties of epoxy resin composites incorporating waste fibers of hemp. The commercial epoxy resins Epidian® 5 and triethylenetetramine (TETA) were applied as crosslinking agents for the synthesis of polymeric materials. The DSC curves analysis revealed that T_g of epoxy were 84.1°C. Up to a temperature of 230 °C, all the composites were thermally stable. The addition of an ecological filler in the form of fibers positively influences the thermal resistance of composites. The DSC curves for the obtained samples showed a similar trajectory and one endothermic signal corresponds to the thermal degradation of the samples.

2.17 Concluding Remarks

The literature review referred to number aspects of study the performance of pressure vessel and study its manufacturing, their mechanical, thermal, microstructural properties, processing parameters; effect of winding angle, type of reinforcements, number of layers, etc. the previous literature can be divided into groups:

1- Some researchers have put detailed information about designing and manufacturing of a filament wound machine to fabricate a filament wound pressure vessel with different processing dimension.

2- There are numerous theoretical studies focused on studying the design of pressure vessel and its mechanical properties for internal pressure applications.

3- Some of literatures studied the effect of different processing parameters on mechanical properties of pressure vessel and these studies weren't concern the failure surface properties.

4- Most of microstructural tests were done for tensile failure of different composite laminate failed by tensile tests and neglect other failure tests especially failure by internal pressure.

5- Another group focused on comparing the simulation of carbon fibers reinforced plastic and glass fibers reinforced plastic by different failure theories not predicting of failure behavior.

In current study, it's focused on detection and characterization of failure modes of pressure vessels accompanying exposing to internal pressure that fabricated by filament winding technique from different materials, processing parameters and detection techniques to evaluate the capability and testability of these techniques and detect the place and different failure modes.

Also through this study has been used numerical simulation for the pressure vessel using Von-Mises failure criteria to give information about the pressure vessel strength capability and performance of different types of composite pressure vessels to withstand high pressure.

Mechanical tests have been carried out to examine strength properties of these light weight pressure vessels like ring stiffness and hardness.

Chapter Three

Modeling and Numerical Simulation

3.1 Numerical Procedure Flow Chart

The following flow chart figure 3.1 represents the steps of numerical part which were used to determine the deformation, stress, and strain of closed composite cylinders for automobile applications.

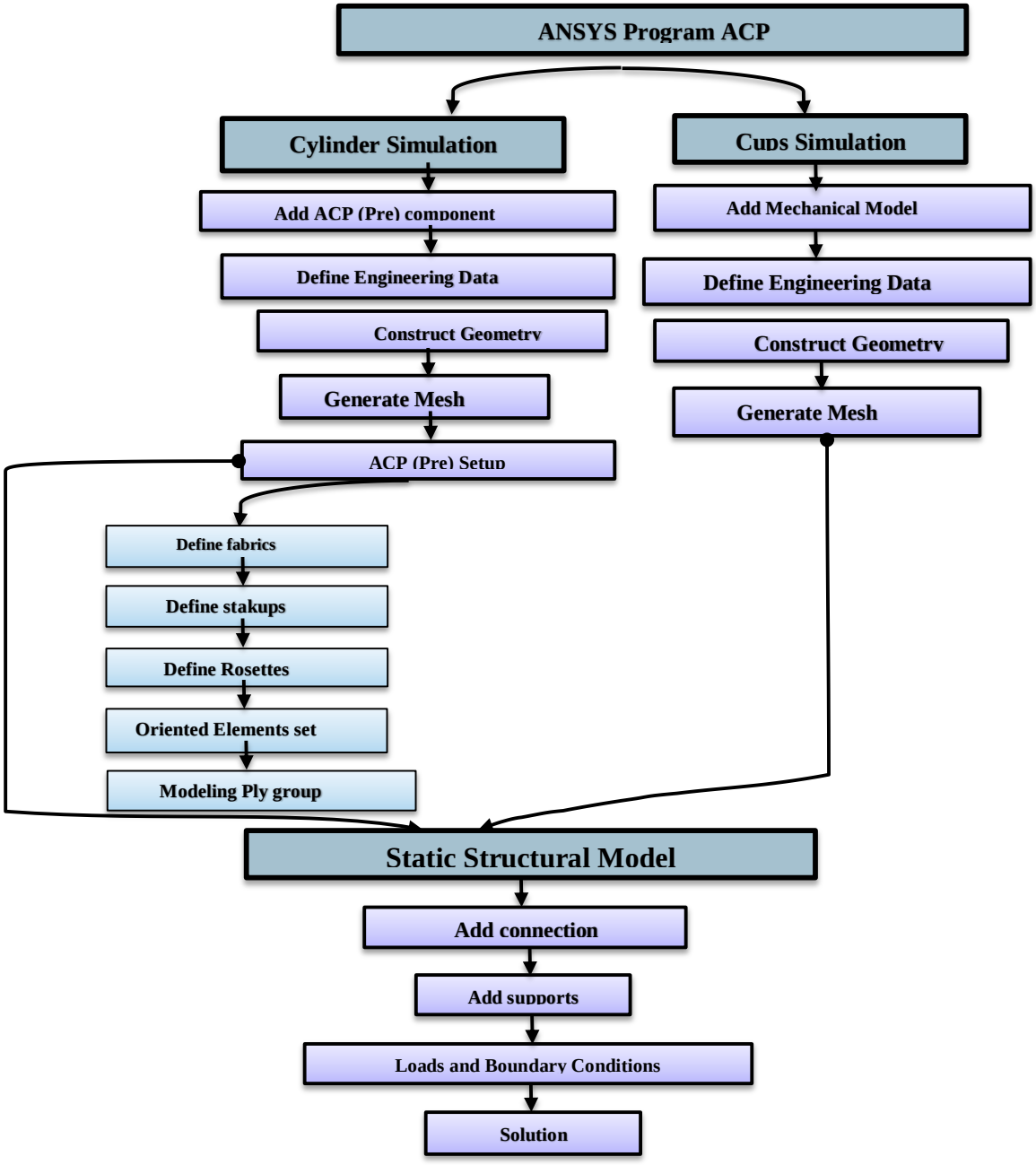

Figure 3.1: Flowchart of procedure of analysis of closed cylindrical pressure vessels.

3.2 Introduction

Engineering layered composites involves complex definitions that include numerous layers, materials, thicknesses and orientations. The engineering challenge is to predict how well the finished product will perform under real-world working conditions. This involves considering stresses and deformations as well as a range of failure criteria. ANSYS Composite Prep Post provides all necessary functionalities for the analysis of layered composite structures. ANSYS Composite Prep Post (ACP) is an add-in to ANSYS Workbench and is integrated with the standard analysis features. The entire workflow for composite structure can be completed from design to final information production as a result. [92]

The Finite Element Method is a powerful tool to analyze components made of fiber reinforced materials. FEA software mostly uses two dimensional elements with layer capabilities to simulate fiber reinforced composite materials. These elements require average material properties of fiber and matrix material, such as average Young's modulus, shear modulus and Poisson's ratio. [93]

Finite Element Algorithms has become a very powerful tool in order to analyze and solve a wide range of engineering problems. Well developed, user friendly, well supported, flexible and multi-field computer codes become a commercial field of engineering tools. One of the challenging and most popular commercial all-purpose program used in Finite Element Modeling is the commercial FEA software "ANSYS".[93]

Analyzing the composite plate experimentally is expensive and for this reason layered composite is modelled utilizing ANSYS ACP, which stands for ANSYS Pre/Post Processor, one of the modeling modules in ANSYS. Using ACP different layered laminate, can be modelled as per the requirement for application. Ansys PrePost packages have a dedicated pre-processor,

solver and post-processor as shown in Figure 3.2 that gives graphical pictures of the structure before and after loading process. [94]

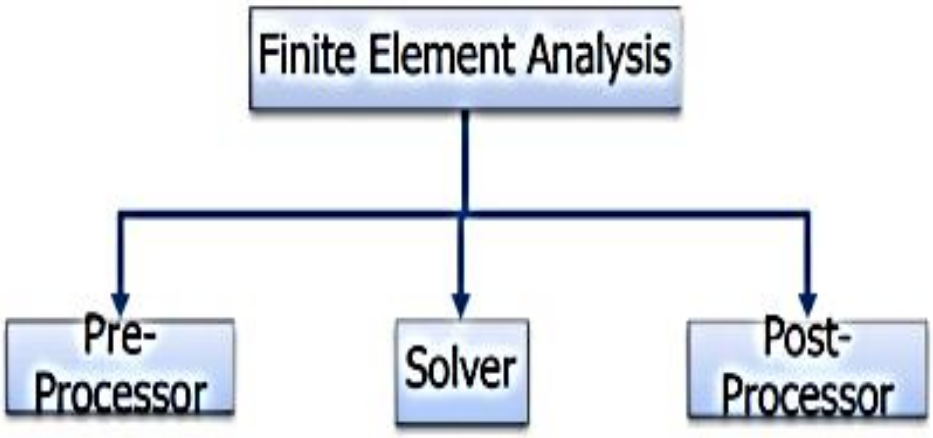

Figure 3.2: Steps in Ansys PrePost Modeling [94]

3.3 Finite Element Analysis procedure

Finite element procedure is divided into three steps: Pre-Processing, Solution, and Post-Processing as shown in figure 3.3 Finite element Analysis is carried out using ANSYS 17.0. Each of the samples is analyzed under the effect of internal pressure. [92]

• **Pre-Processing**- In this step of the analysis, Material properties are entered in pre-processing. Model is created, Mesh and Element type are defined. [92]

• **Solution**: - In this step, boundary conditions in terms of pressure loads, supports are given and the solution is obtained [92]

• **Post-Processing**: - In this step, results are viewed and required results are evaluated and studied. [92]

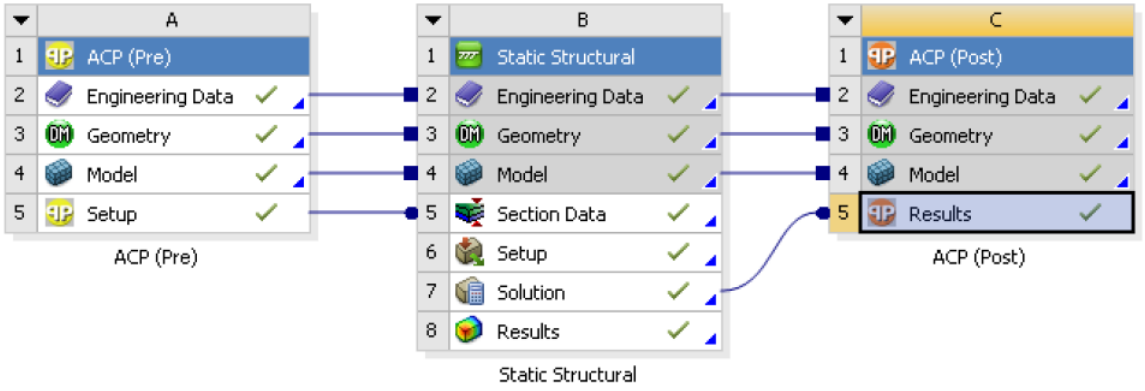

Figure 3.3: The general Pre- and post-processing workflow for finite element modeling and material analysis. [92]

3.4 Simulation Modelling

The process of simulations of composite laminates is very important part, software Ansys workbench 17.0 is used to perform the analysis, the cylinders have to be closed by end cups that modelled by Mechanical Model. The schematic view of the setup simulation done using ACP (Pre) and mechanical model is shown in figure 3.4.

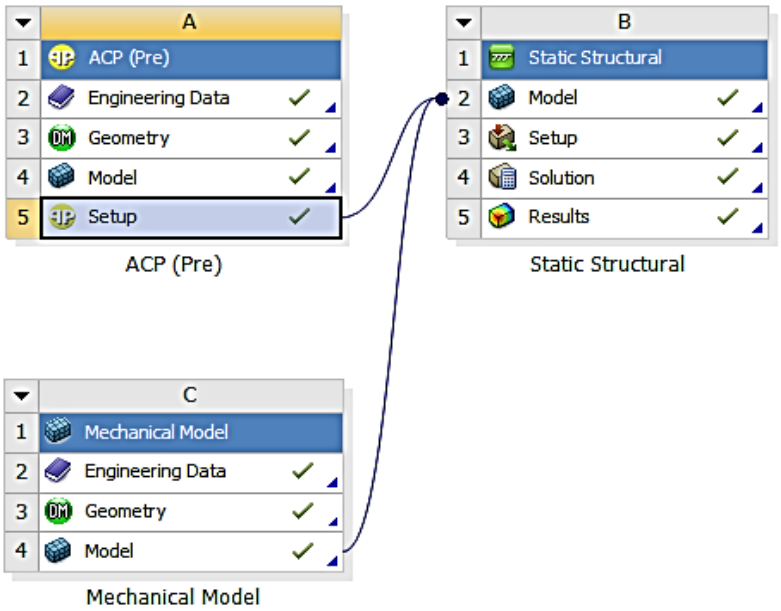

Figure 3.4: The modeling system.

3.4.1 Analysis of a Composite Shell Model

This section outlines the generic build-up of a composite cylinders shell model by Pre-processing

- **Add ACP (Pre) component to the project**

The components ACP (Pre) is available in the Toolbox menu as shown in figure 3.5.

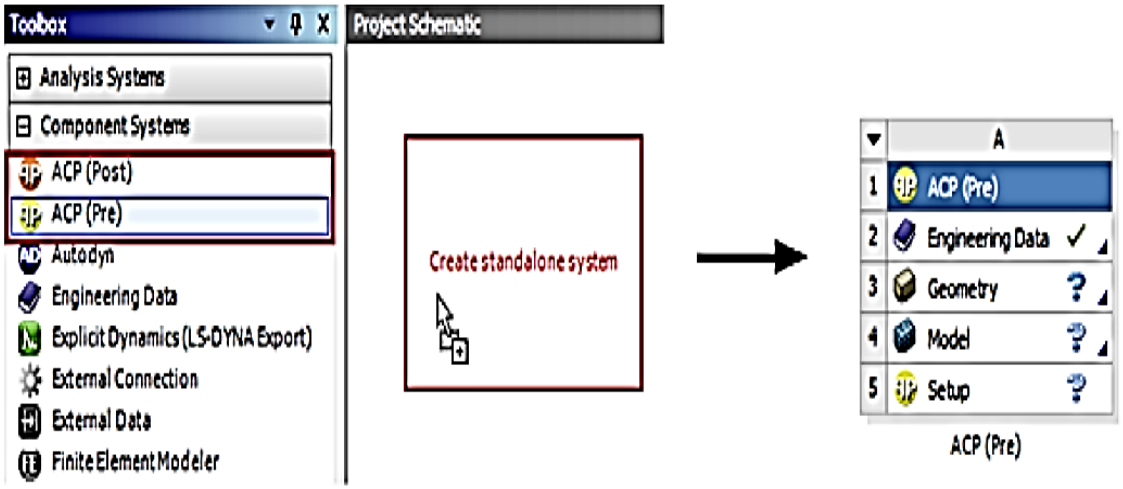

Figure 3.5: ACP components

- **Define Engineering Data**

The material properties of CF/epoxy, KF/epoxy and GF/epoxy laminates estimated through The Laminator program are incorporated in the finite element analysis so that the finite element software simulate the behavior of the shell structure under burst pressure loads. The laminator software is used to calculate the properties of the composite laminates by input the properties of individual fibers and matrix. The Laminator is an engineering program written that analyzes laminated composite plates according to classical laminated plate theory. Input consists of ply material properties, material strengths, ply fiber orientation and stacking sequence, mechanical loads and/or strains, and temperature and moisture loads. Output consists of apparent laminate material properties, ply stiffness and

compliance matrices, laminate "ABD" matrices, laminate loads and mid-plane strains, ply stresses and strains in global and material axes, and load factors for ply failure based on Maximum Stress, Maximum Strain, Tsai-Hill, Hoffman, and Tsai-Wu failure theories. A micromechanics calculator is also included for estimating lamina properties for given fiber and matrix properties. [95]. Figure 3.6 represents the properties of CF/epoxy calculated by The Laminator program.

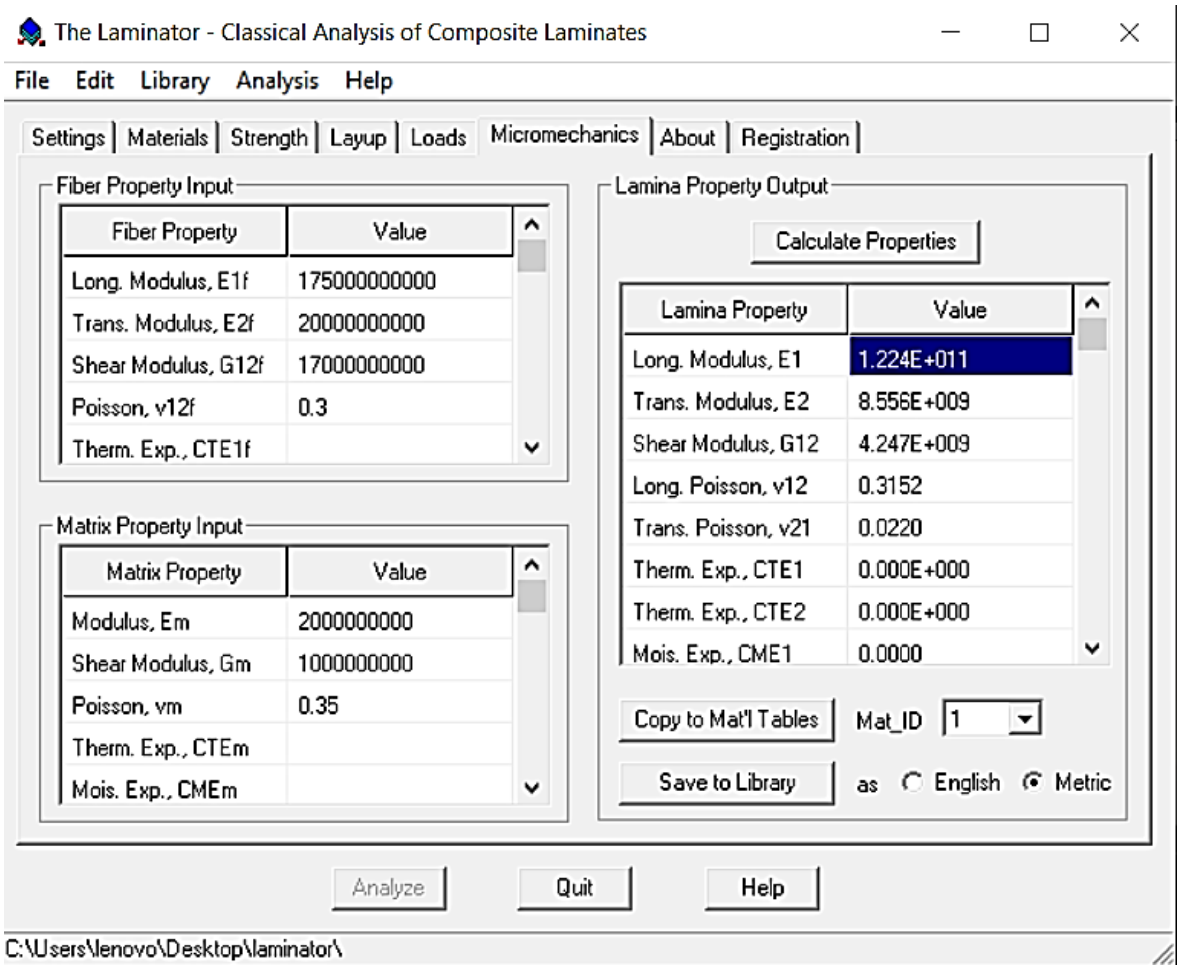

Figure 3.6: The Laminator program.

The extracted properties are entered in the ANSYS 17.0 PrePost. Properties of CF/epoxy, KF/epoxy and GF/epoxy are shown in table 3.1, 3.2 and 3.3.

Table 3.1: Properties of Carbon fiber composite lamina.

Property	**Carbon Fiber/Epoxy**
Young's Modulus	Ex (GPa) 122.4
Ey = Ez (GPa)	8.5
Poisson's Ratio	Vxy = Vxz 0.31
Poisson's Ratio	Vyz 0.02
Shear Modulus	Gxy = Gxz (GPa) 4.2
Gyz (GPa)	3.8
Tensile Strength	Xt (MPa) 2785
Yt = Zt (MPa)	43.78

Table 3.2: Properties of Kevlar fiber composite lamina.

Property	**Kevlar Fiber/Epoxy**
Young's Modulus	Ex (GPa) 59
Ey = Ez (GPa)	6.08
Poisson's Ratio	Vxy = Vxz 0.4
Poisson's Ratio	Vyz 0.04
Shear Modulus	Gxy = Gxz (GPa) 1.8
Gyz (GPa)	1.4
Tensile Strength	Xt (MPa) 1880
Yt = Zt (MPa)	43.46

Table 3.3: Properties of E-glass fiber composite lamina.

Property	**E-Glass Fiber/Epoxy**
Young's Modulus	Ex (GPa) 27.4
Ey = Ez (GPa)	4.9
Poisson's Ratio	Vxy = Vxz 0.29
Poisson's Ratio	Vyz 0.05
Shear Modulus	Gxy = Gxz (GPa) 2.25
Gyz (GPa)	1.8
Tensile Strength	Xt (MPa) 597
Yt = Zt (MPa)	42.7

- **Construct Geometry**

For building a cylindrical pressure vessel, the cylinders with dimensions (inner radius is 50 mm , the thickness 2 mm, length of all cylinders are 300 mm) have been drawn as shown in figure 3.7.

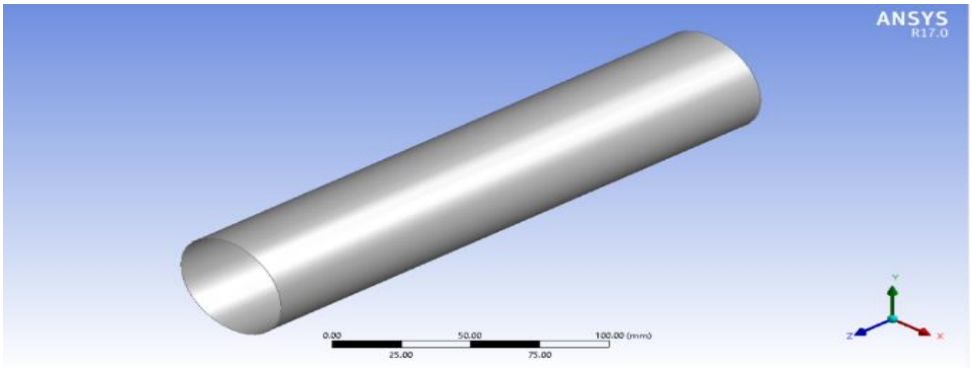

Figure 3.7: Cylinder geometry.

- **Generate Mesh**

Meshing is one of the important aspects in engineering simulation. The meshing setting and pattern are shown in Figure 3.6.

Mesh resolution is a substantial aspect when discretizing scoped body; the higher the mesh resolution the more precious results are obtained. On the other hand, the higher the mesh resolution, the higher the simulation time consumed. Reasonable meshing resolution is adopted to obtain results with acceptable deviation and proper solving time[96]. The total number of nodes and elements of CF/epoxy, KF/epoxy and GF/epoxy laminates are illustrated in table 3.8.

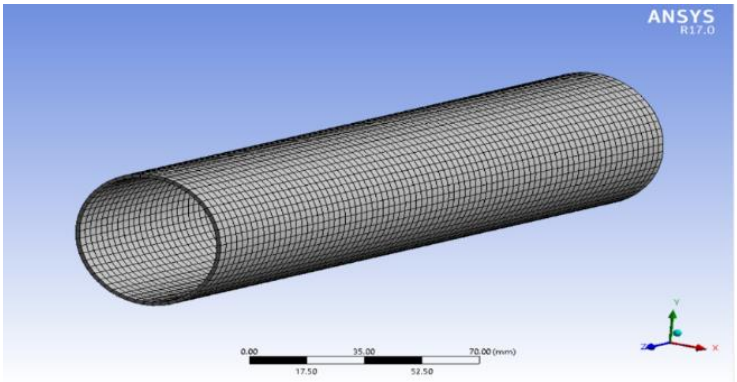

Figure 3.8: Meshing of the cylinder.

Table 3.4: The total number of nodes and elements of CF/epoxy, KF/epoxy and GF/epoxy laminates.

Name of composite laminate	Number of Nodes	Number of Elements
Epoxy	5330	2694
$\pm 45°_3$ CF/epoxy laminate	30507	5791
$\pm 55°_3$ CF/epoxy laminate	30507	5791
$\pm 65°_3$ CF/epoxy laminate	30507	5791
$\pm 75°_3$ CF/epoxy laminate	30507	5791
$\pm 45°_3$ KF/epoxy laminate	30507	5791
$\pm 55°_3$ KF/epoxy laminate	30507	5791
$\pm 65°_3$ KF/epoxy laminate	30507	5791
$\pm 75°_3$ KF/epoxy laminate	30507	5791
$\pm 45°_3$ GF/epoxy laminate	30575	5858
$\pm 55°_3$ GF/epoxy laminate	30507	5791
$\pm 65°_3$ GF/epoxy laminate	30507	5791
$\pm 75°_3$ GF/epoxy laminate	30507	5791

Table 3.5: The total number of nodes and elements of symmetrical CF/epoxy, KF/epoxy and GF/epoxy laminates.

Name of composite laminate	Number of Nodes	Number of Elements
Symmetrical CF/epoxy	30507	5791
Symmetrical KF/epoxy	49543	8126
Symmetrical GF/epoxy	30507	5791

- **ACP (Pre) setup**:
  - ❖ Define Fabrics: where the fiber materials can be associated with a ply of a set thickness. The Fabric property dialog is shown in the figure 3.9.

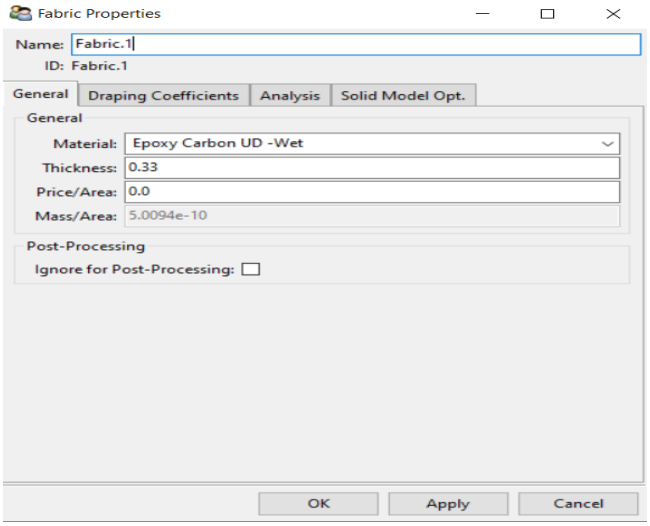

Figure 3.9: Fabric properties of carbon fibers.

The Polar Properties (Classical Laminate Theory) of the Fabric can be plotted as graphical information as shown in figure 3.10.

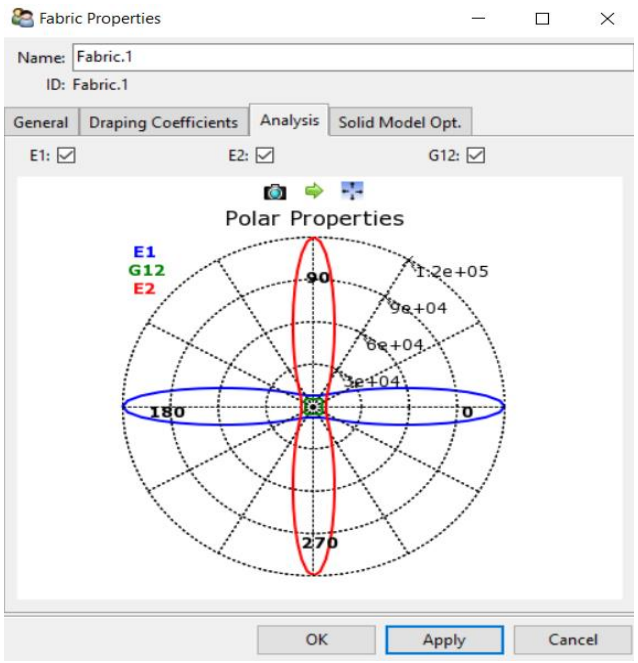

Figure 3.10: Polar properties of the fiber.

- Define Stackups: stackups used to combine fabrics into a non-crimp fabric, such as a [+55, -55,] combinations. From a production point of view, it is considered as one ply which is applied on the form. For the analysis, all plies forming the stackup are considered.

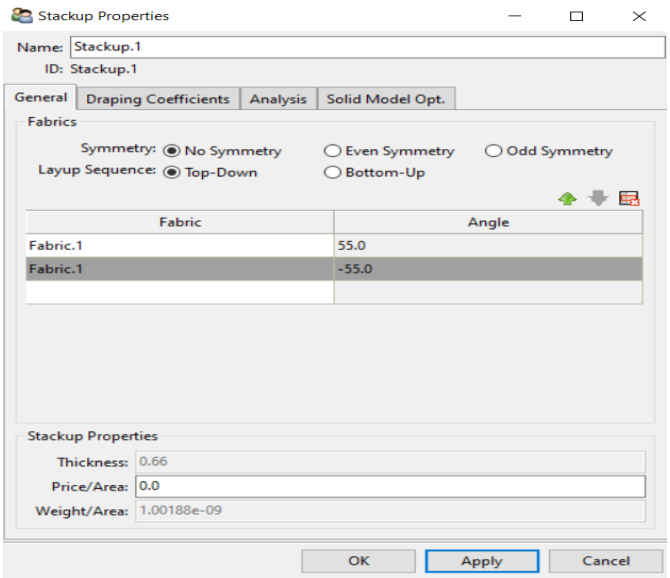

Figure 3.11: Stackup of ±55° ply.

The Fabric and its orientation along with the polar properties which define the in-plane properties of the composite are defined as shown in Figure 3.12.

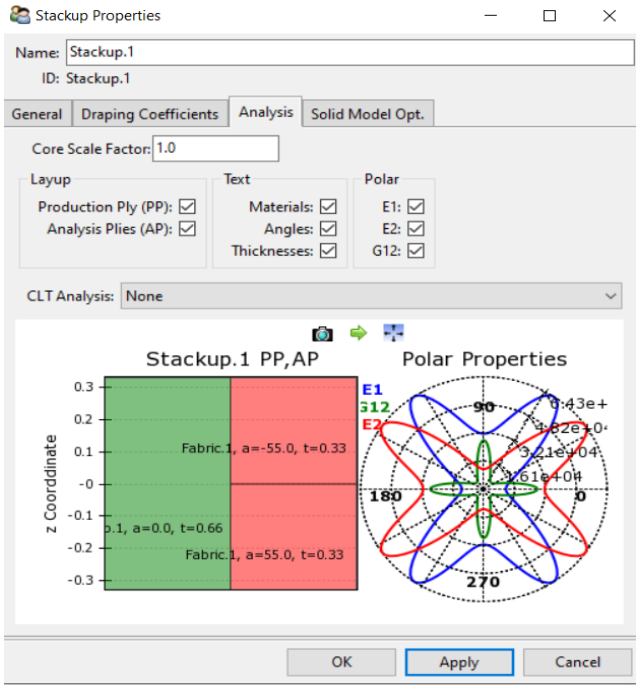

Figure 3.12: Stackup polar properties of ±55° ply.

❖ Define Rosettes

Rosettes are coordinate systems that used to set the reference direction of Oriented Element Sets. In other words, Rosettes define the 0° direction for the composite layup. The rosettes properties dialog shown in figure 3.13.

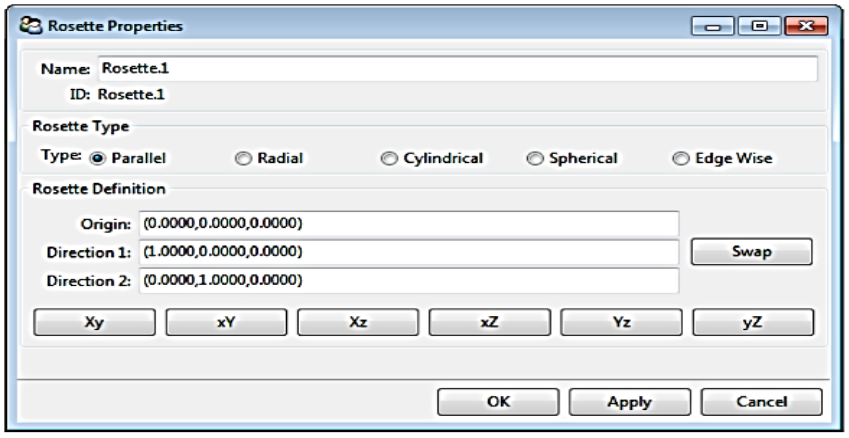

Figure 3.13: Rosettes dialog.

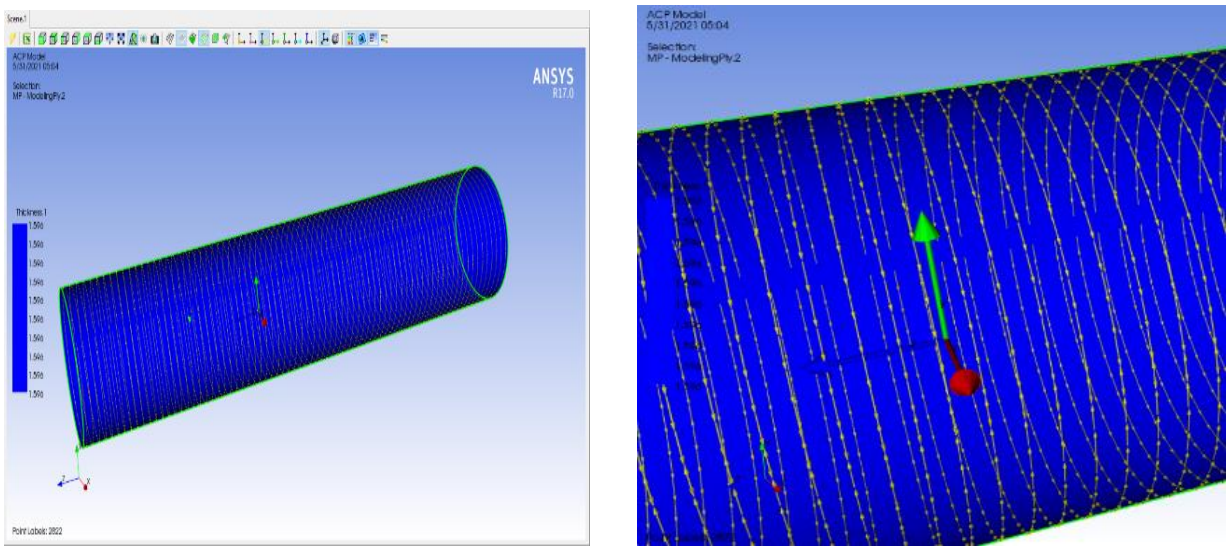

Figure 3.14: The reference direction of shell element (rosettes).

❖ Oriented Element Sets (OES)

The orientation direction of an Element Set is responsible for setting the stacking direction of the associated layup. Oriented element set properties shown in figure 3.15.

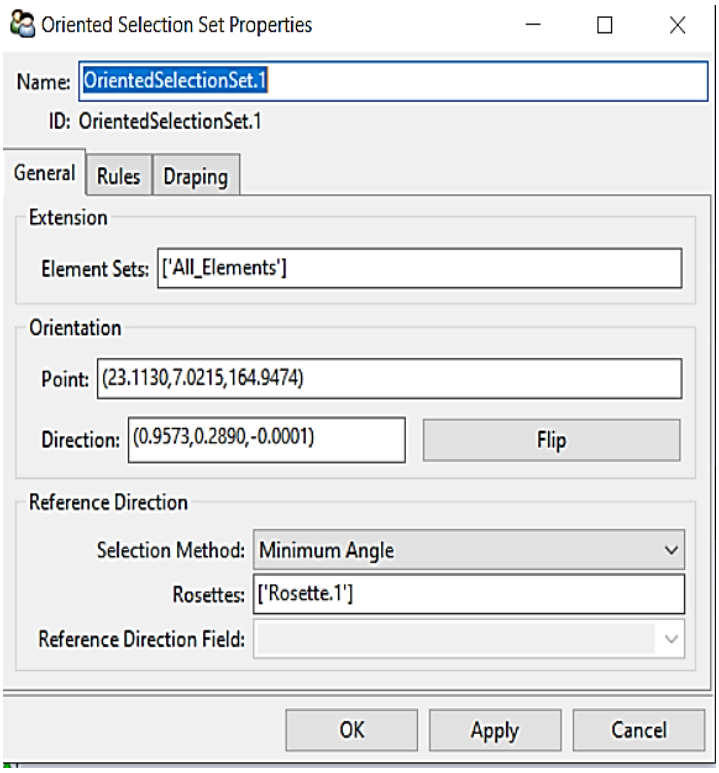

Figure 3.15: Oriented element set properties.

❖ Modeling Ply group

In Modeling Ply Group, it's necessary to define the desired composite lay-up. The ply definition can be organized into Ply Groups as shown in figure 3.16 and 3.17. The lay-up can be tailored by specifying the orientation, layering, and geometrical rules, for each ply by:

- Modeling Ply (MP) where the ACP lay-up is defined at this level.
- Production Ply (PP): the no. of Layers option is defined at this level.
- Analysis Ply (AP): analysis plies describe the plies used in the section definition for the ANSYS solver.

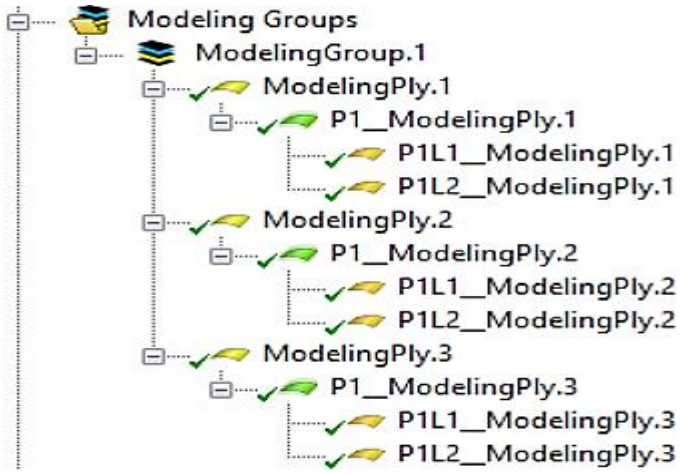

Figure 3.16: Object tree of a layup definition of 3-layers composite laminates

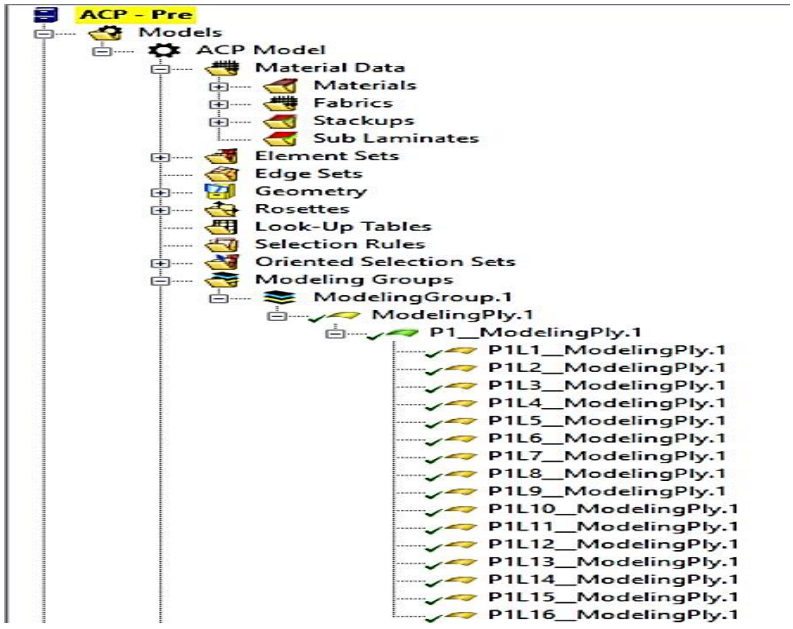

Figure 3.17: The Object tree of a layup definition of the symmetrical laminates.

Figures 3.18 represents the angle direction ±45° within one ply.

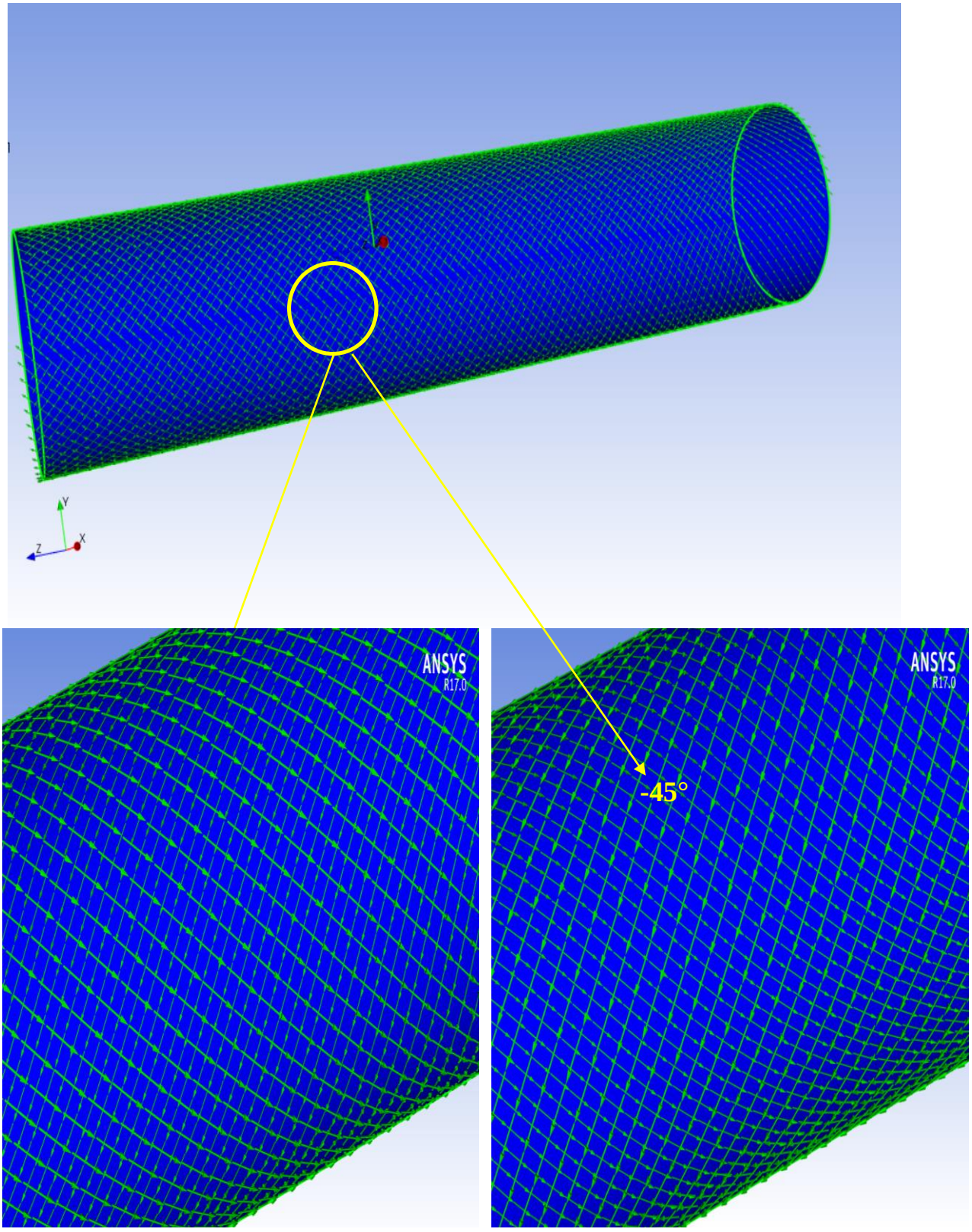

Figure 3.18: The ±45° orientation of fibers within one ply.

3.4.2 Analysis of the End Cups Model

The pressure vessel was modelled in such way that the both ends are closed. This can be done by modeling the end cups by Mechanical Model, this section outlines the simulation of the end cups by Mechanical Model.

3.4.2.1 Add Mechanical Model component to the project

The components Mechanical Model is available in the Toolbox menu as shown in figure 3.19.

Figure 3.19: Mechanical model components.

3.4.2.2 Define Engineering Data

The stainless steel cups properties are enters in the engineering data to simulate the actual behavior of the end cups model.

3.4.2.3 Construct a Geometry

the geometry of the end cups have the dimensions (radius 65 mm , the thickness 15 mm, length of all cups are 50 mm) have been drawn as shown in figure 3.20.

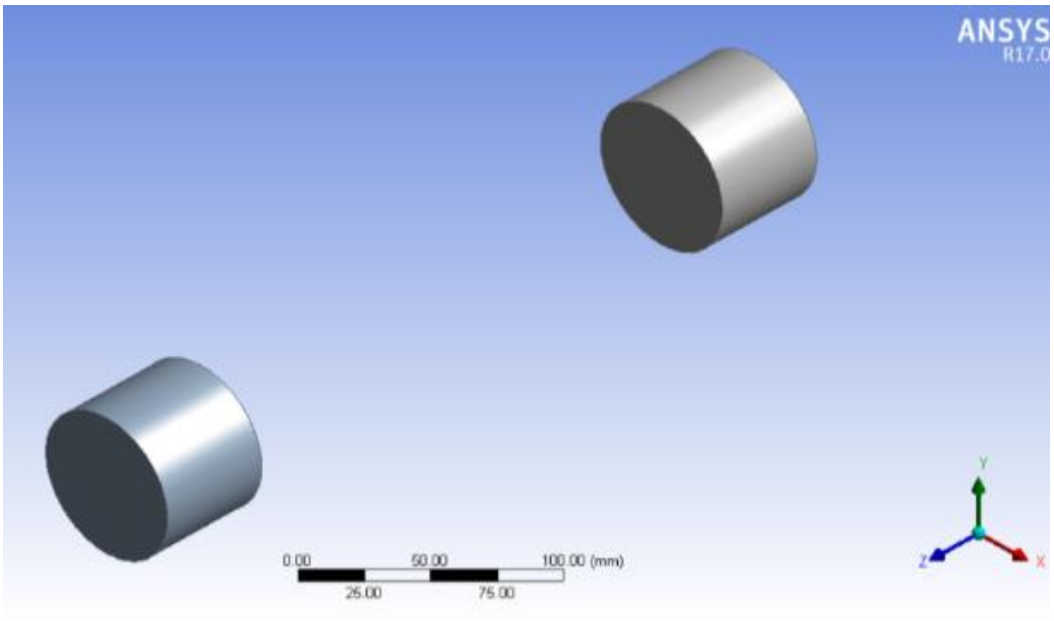

Figure 3.20: End cups geometry.

3.4.2.4 Generate Mesh

Meshing is an integral part of the computer-aided engineering simulation process. The mesh influences the accuracy, convergence and speed of the solution[113]. The meshing of the geometry of cups is shown in figure 3.21.

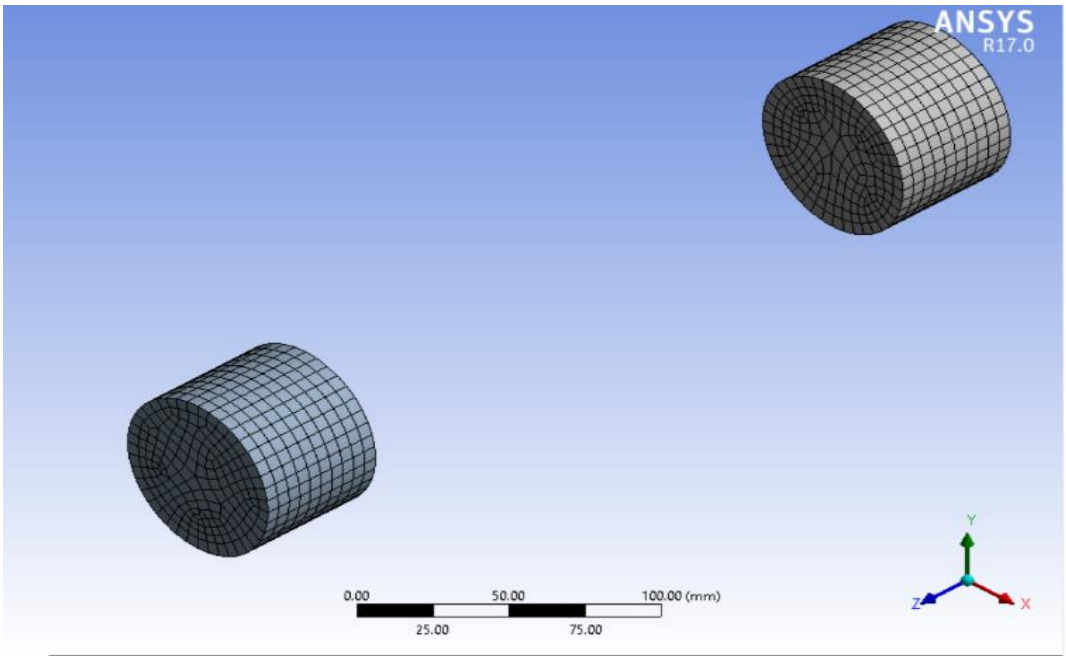

Figure 3.21: End cups mesh.

After all the required pre-processing steps and mechanical model steps are done, the data from the ANSYS-ACP Pre and the mechanical model are exported to another analysis system, "ANSYS Static Structural", to assign internal pressure load to the model. Where, predefined boundary conditions are applied to generate solution values like equivalent stress, equivalent strain and total deformation.

3.4.3 Static Structural Model

It consist of:

3.4.3.1 Connect the Cylinder with the Cups

After transfers the data of the layered cylinder and cups to static structural model, connecting the bodies by adding two bonding acting between each end of the cylinder with each cup as shown in figure 3.22.

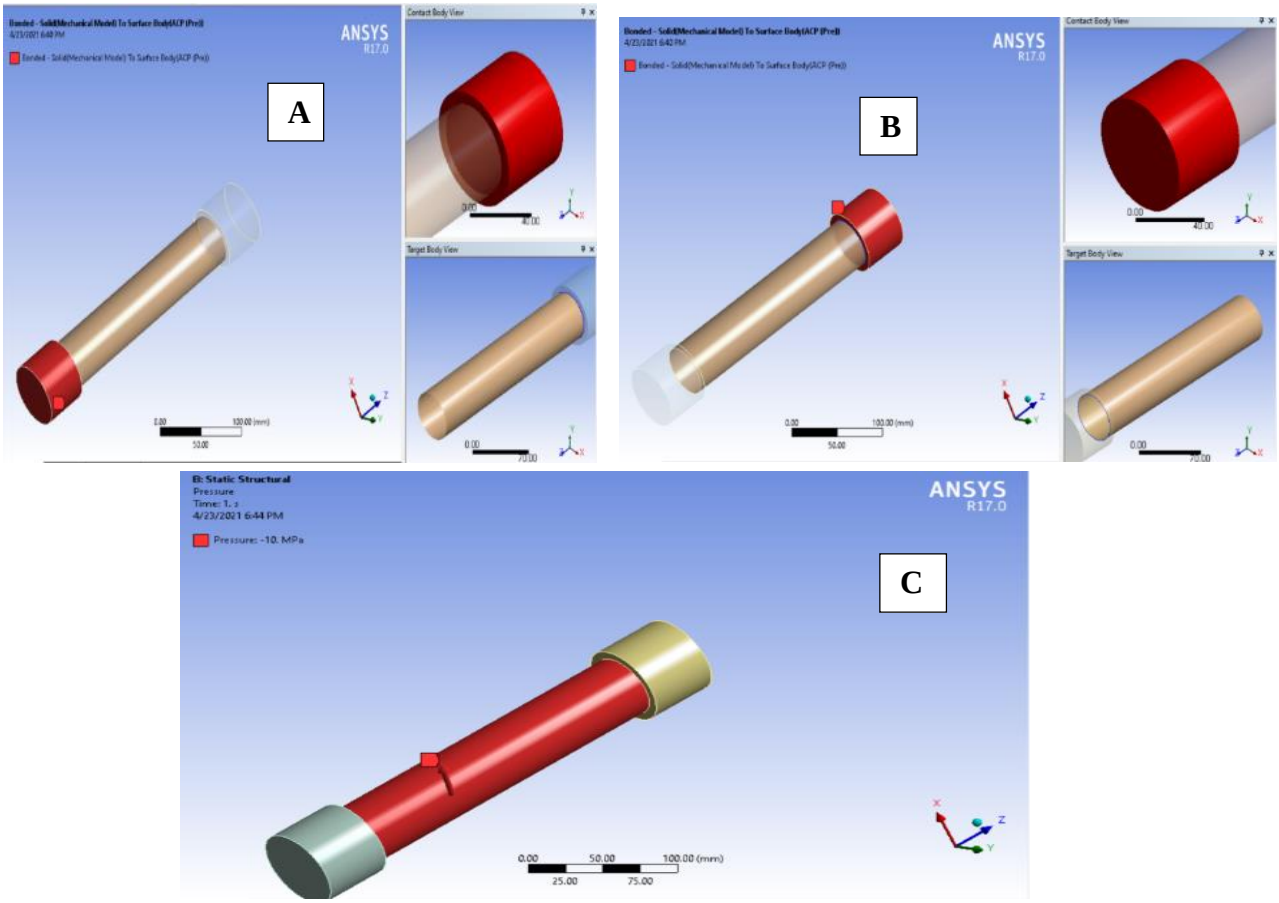

Figure 3.22: Bonding of the cylinder with the cups.

3.4.3.2 Boundary Conditions

The load boundary condition can be applied, where both ends of the pressure vessel was given as cylindrical supports. Pressure load of magnitude 25 MPa was applied on the inner surface of the pressure vessel to meet gas storage requirements in automobile applications. The schematic view of loads is shown in figure 3.23.

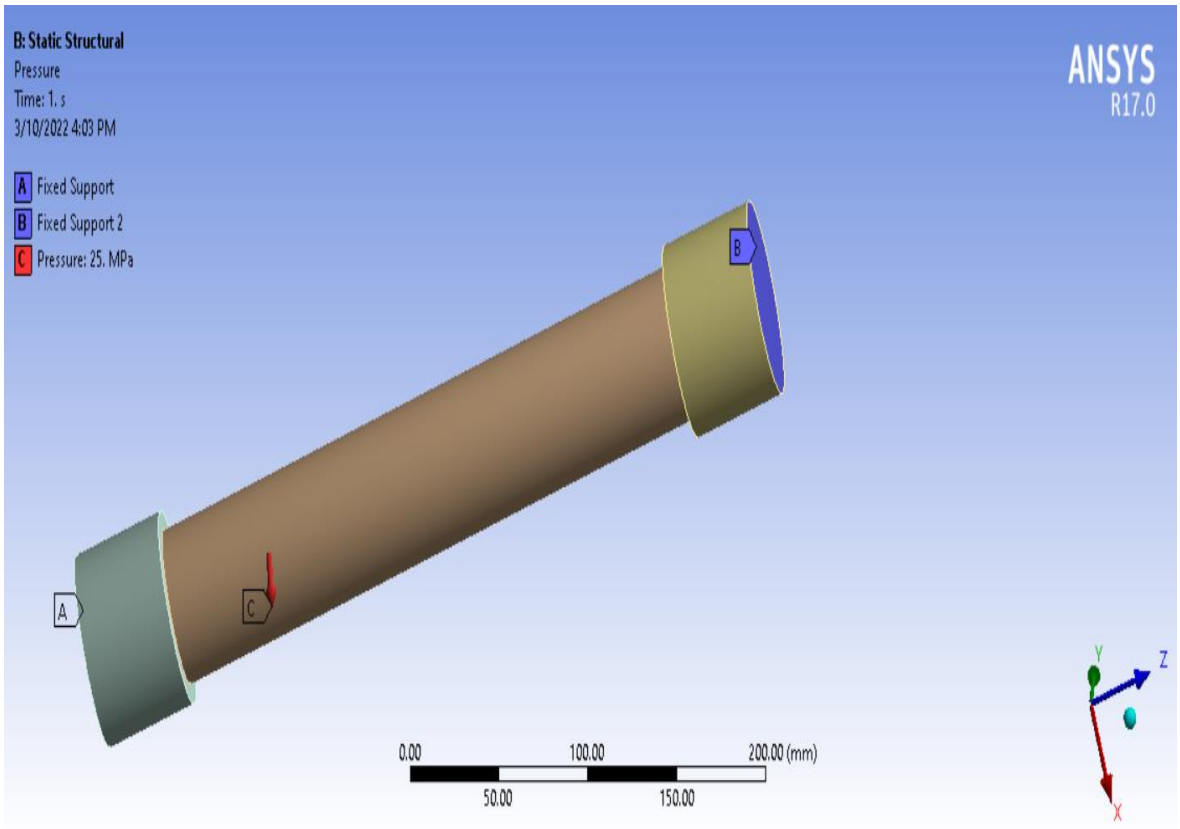

Figure 3.23: Boundary condition of the cylinder.

Chapter Four

Experimental Work

4.1. Introduction:

This chapter covers the experimental works that carried out; the methodology that was used starting from materials specification, sample preparation, instrument instruction and the test samples and testing procedure in detail. Research plan was carried out is shown in figure 4.1.

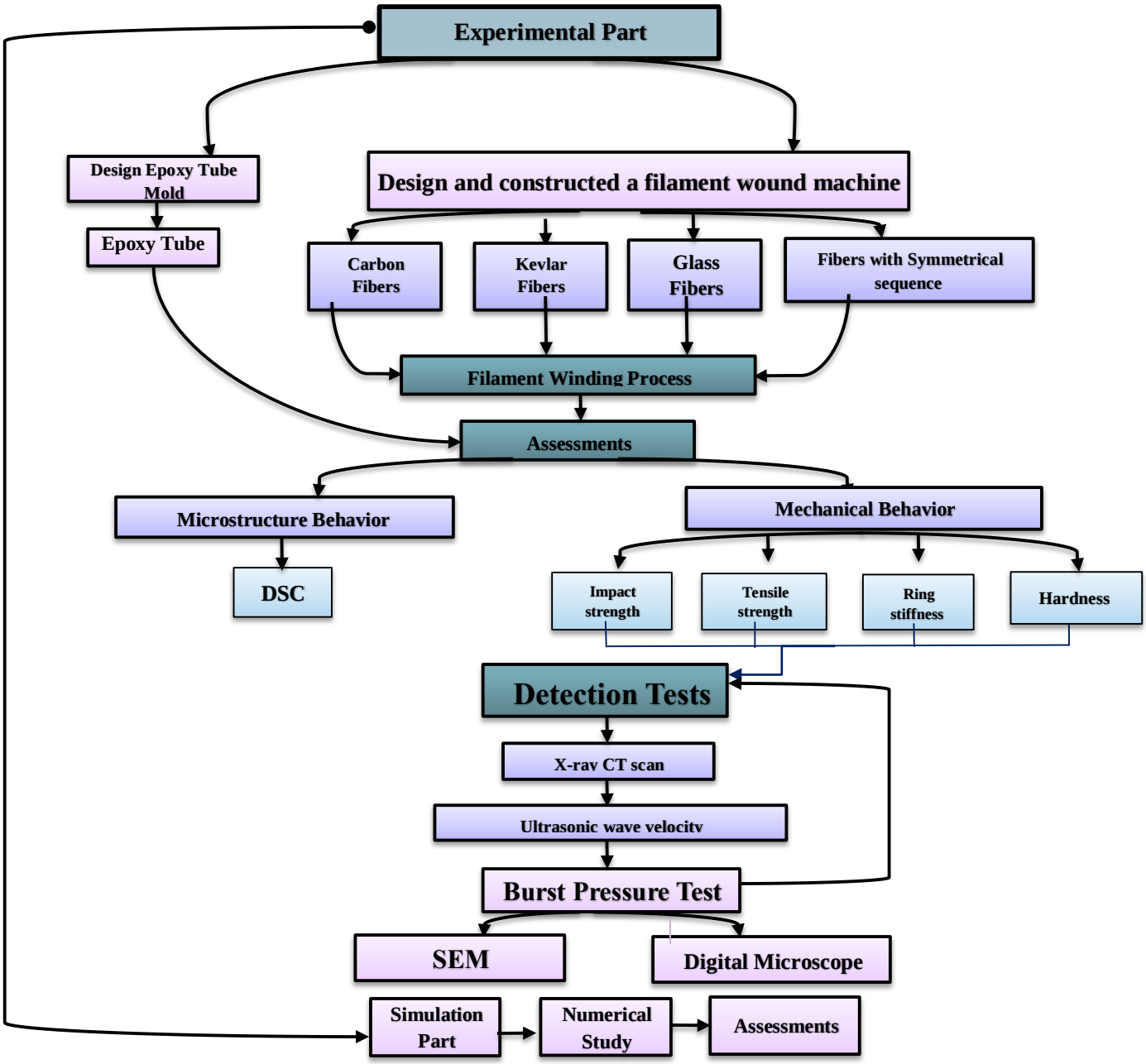

Figure 4.1: The Flowchart of Experimental Tests.

4.2 Materials and its Characterization:

Test tubes are manufactured using an epoxy resin system with three different fiber types. The properties of the resin system and the reinforcements employed in are as follows:

4.2.1 Resin System

The resin system employed in the fabrication of the tubes is SIKADUR 52 LP (IN) [98] characterized by its low viscosity that suitable for filament winding process (80 parts by weight, Hardener 20 parts by weight). The system is characterized by its good mechanical and good adhesion properties. The system are given in Table 4.1.

Table 4.1 Mechanical properties of the resin system employed[98]**.**

Property	**Unit**	**SIKADUR 52 LP RESIN SYSTEM**
Max. Tensile Strength	(MPa)	50
Elongation At Break	(%)	1.9
Elastic Modulus	(MPa)	2000
Tensile Elongation (%)	-	1.9
density	g/cm^3	1.1
Viscosity	mPas at +30 °C	~250
Pot life for 1 Kg at 30 °C	min	~50
Bond strength	MPa	~ 7.5
Shear Modulus	MPa	1000
Poisson ratio	-	0.35

4.2.2 Reinforcements

The reinforcements employed in the fabrication of the composite laminates are E-glass fiber Roving continuous product of Hebei Yuniu Fiberglass manufacturing Co., Ltd, haxcore carbon fiber yarn, continuous product of Suzhou Haxcore Material Technology Co., Ltd. and Kevlar fiber from Hitex® insulation & composites.

The properties of the reinforcements are given in Table 4.2.

Table 4.2 Mechanical properties of the reinforcements employed.

Property	Unit	E-glass fiber	Carbon Fiber	Kevlar Fiber
density	g/cm^3	2.4	1.79	1.44
Max. Tensile Strength	(MPa)	1000	4000	2900
Elastic Modulus (E1)	(MPa)	46000	175000	90000
Elastic Modulus (E2)	(MPa)	10000	20000	12000
Shear modulus	(MPa)	5000	15000	2600
Poisson ratio	-	0.25	0.3	0.44

4.3 Filament Winding machine

In order to manufacture fibrous composite laminates tubes a filament winding machine was designed .The design of filament winding machine was based on the three main parts which are mechanical part, electronic part and software part. The 2-axes movements for automated machine are linear for filament delivery and rotation for filament winding units. The three parts are combined to instruct and initiate the automated the industrial control using portable computer.

Winding diameter of the machine is 50 mm and the winding length is 300 mm. The system is capable of utilizing winding angles from 0° to 90°. The winding speed of the system ranged from 50 to 80 rpm.

The filament winding machine is shown in Figure 4.2

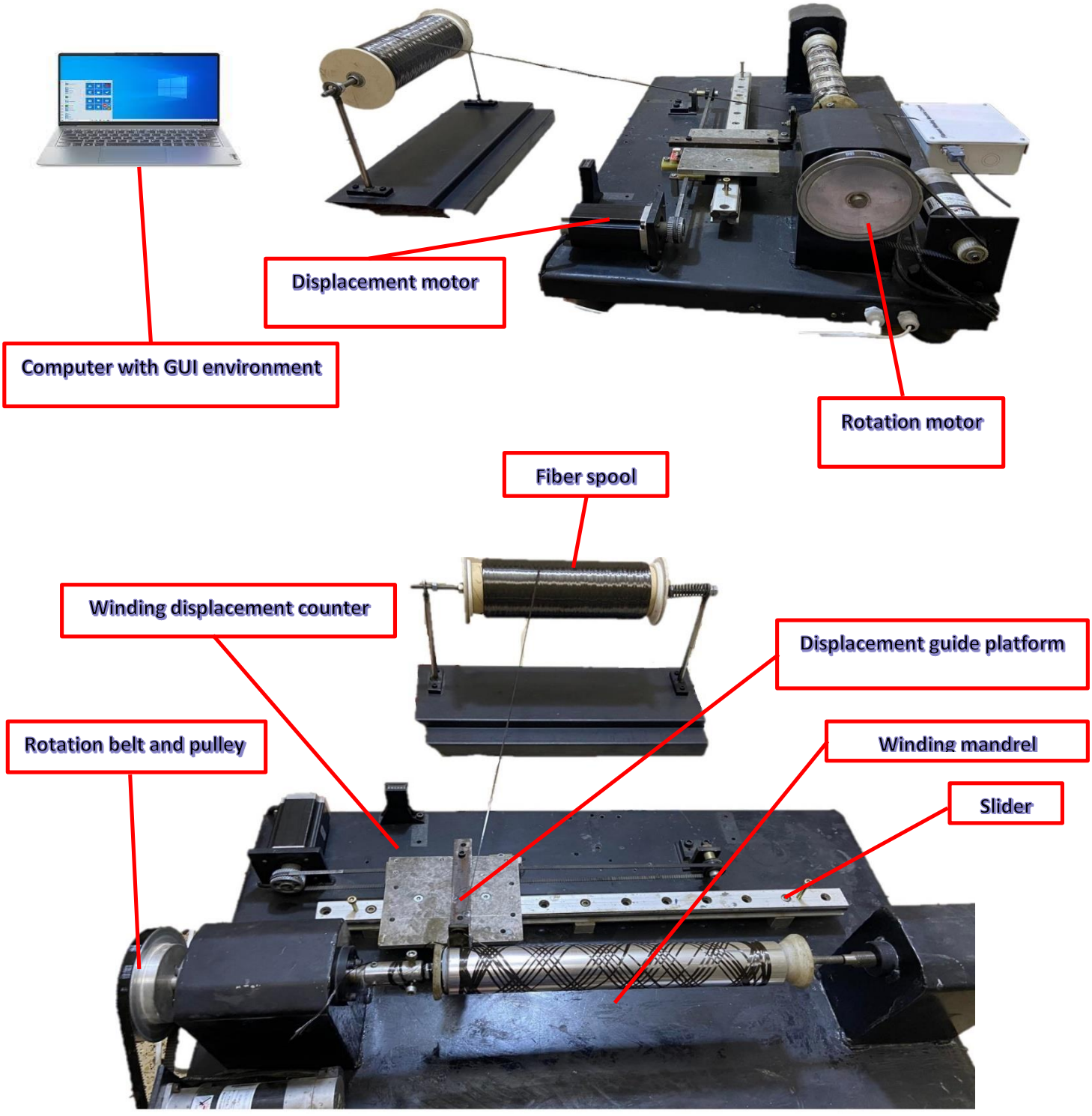

Figure 4.2: The machine construction and elements.

4.3.1 Mechanical Part

The mechanical part of the machine consists of the five basic parts which are main structure:

- Linear axis (x axis)
- Rotation axis (a axis)
- Control drives
- Distance sensors
- Resin bath

Linear axis (x axis) with maximum movement length 35 cm provide linear movement results from turning the circular motion from a stepper motor (3 N·m torque) installed with a gear wheel of diameter 30 mm and time belt (3 mm step), when the wagon is moving linearly on the sliding rail result in generation of rotation of the stepper motor and determines the starting and ending distance. A limiter has been installed on both sides in addition to a counter to calculate the number fiber strokes. The movement speed can be changed from the control program

The rotation axis (a axis) used for circular movement with maximum speed of 150 revolutions per minute .This movement can be produced from a servo motor with a torque of 4 N·m on which a gear is fixed (30 teeth).

The fixed base contains two sliders (Ballburn), on which a pivot is fixed for rotations where the sample reel fixed on it, on the second end there is the movable holder to hold the sample reel.

4.3.2 The Electronic part

Both drivers controlled by ESP32 microcontroller to obtain the required winding motion consequently**. ESP32** (shown in figure 4.3) is a series of low-cost, low-power system on a chip microcontrollers with integrated Wi-Fi and dual-mode Bluetooth.

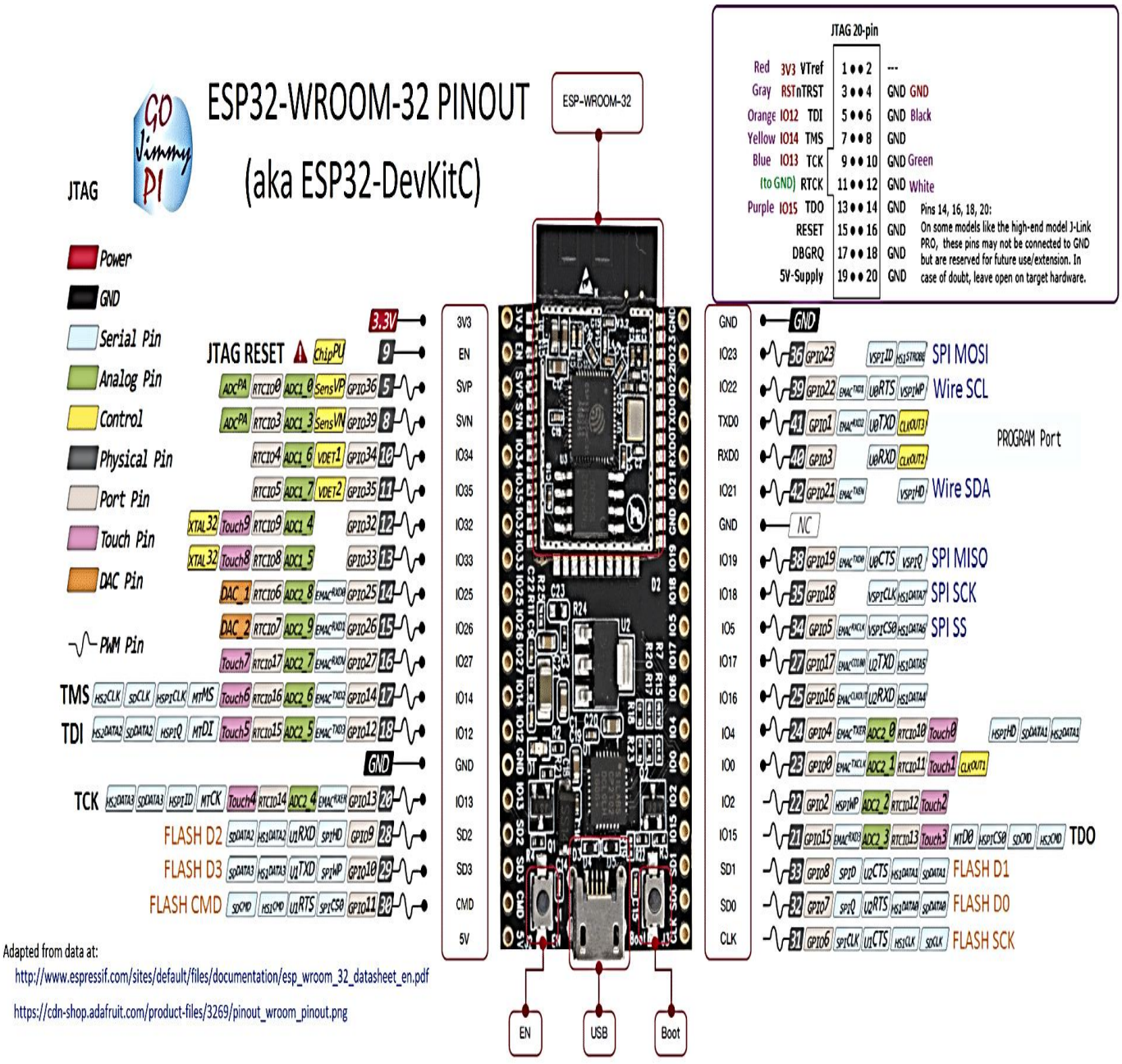

Figure 4.3: The electronic elements

4.3.3 The Programming part

The system configuration including sample length, sample diameter, winding angle, fiber width is set through GUI that operated in Linux OS which installed on raspberry pi4 board as shown in figure 4.4.

Raspberry Pi 4 Model B is the latest product in the popular Raspberry Pi range of computers. It offers ground-breaking increases in processor speed, multimedia performance, memory, and connectivity.

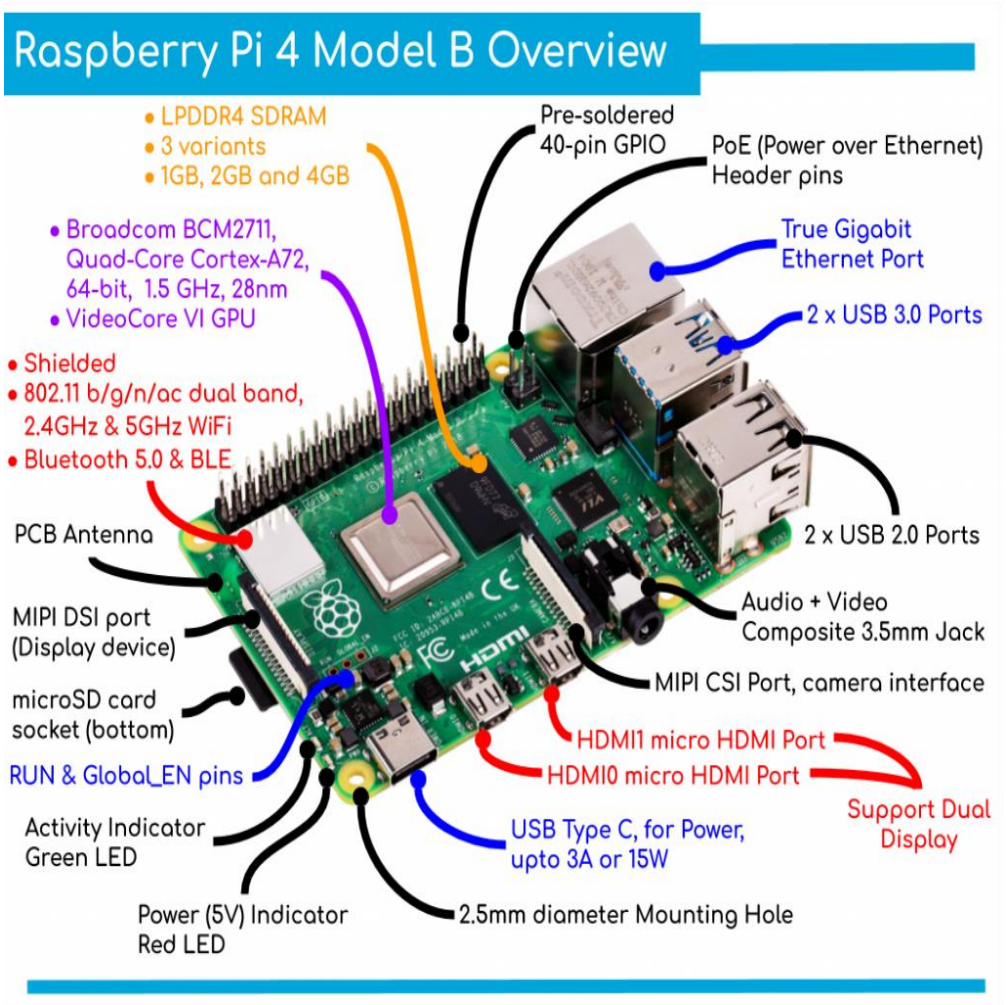

Figure 4.4: The programing elements

In this device, automation (control of the device by a computer program) was adopted to control the winding mechanism, enter of variables and display results. When click on the program icon, the window shown in (Figure 4.5). The input data are the sample length (mm), required mandrel position and the required orientation angle of the winding. After selecting both the distance and the winding angle, when click on the (apply) button then (start) then fibers being wound on the mandrel.

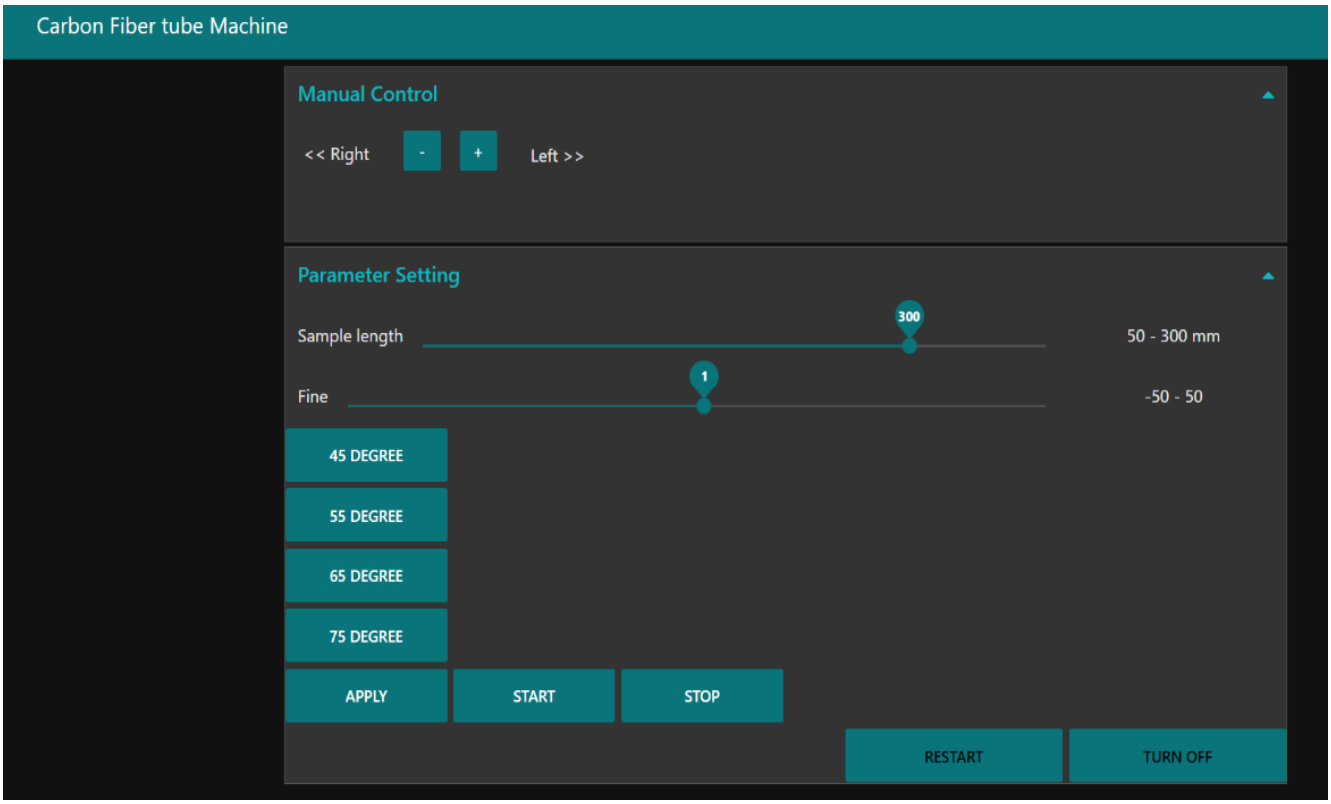

Figure 4.4: The main interface of the device program.

4.4 Specimen Manufacturing

The composite tubes that were employed in internal pressure tests were manufactured utilizing the filament winding technique.

4.4.1 Procedure

The employment of the filament winding technique in a manufacturing process required five main stages:

- **Preparation:**

The filament winding machine and the mandrel were prepared. Fibers were placed on the spools of the winding machine, and the mandrel was placed on the spindle of the machine. Nylon film was wrapped on to the mandrel to obtain smooth surface inside the specimens.

- **Winding:**

Fibers were wound onto the mandrel at pre-designated angles and in patterns. Generally, in this part of the process, commercially available computer codes were used to obtain the desired accuracy.

The prepared resin was deposited into the resin bath tank and the fibers impregnated in a bath with resin as they were wound onto the mandrel as shown in figure 4.6.

Figure 4.6: Winding process.

- **Curing:**

After the winding is completed, the part with the mandrel is left at room temperature for 24 h for curing.

- **Mandrel removal:**

After the curing process is completed, the mandrel is removed and the composite hollow tubes are handled.

- **Cutting**

Once the tubes are manufactured and cured, they are then cut into the desired length by means of mechanical cutting

4.4.2 Specimens

Specimens of CF/epoxy, KF/epoxy and GF/epoxy laminates with four different winding angles were employed as shown in figure 4.6. The test specimens that were manufactured with diameter 50 mm, length 300 mm and the thickness ranged from 0.8 to 2 mm. Specimens of CF/epoxy with different winding angles were employed; $[\pm 45°]_3, [\pm 55°_3], [\pm 65°_3]$ and $[\pm 75°_3]$ as shown in figure 4.7.

Figure 4.7: CF/epoxy laminates unit cells: (a) 45°, (b) 55°, (c) 65°, (d) 75°.

4.5 Epoxy Tube Manufacturing:

In order to apply internal pressure and study the burst pressure bahavior of epoxy matrix, a hollow cylinder of epoxy have been manufactured. The epoxy resin (with 80 parts by weight and Hardener 20 parts by weight) are mixed togather and pured in a hollow alaminum cylinder (with inetrnal diameter 50 mm) and left for curing. The hollow alamnium cylinder then removed to extract the hollow epoxy cylinder that closed from one end.

In order to close the second cylinder side, the mixure of the same resin and the hardner were pured into a cupic molds and left for curing. After curing the cupic cup was extracted.

The last step was gluing the cubic part with the hollow epoxy cylinder with the same resin mixture. Drilling processes are applied to make the hose's hole to enable applying the internal pressure.The epoxy tube cylinder with the end cups were shown in figure 4.8.

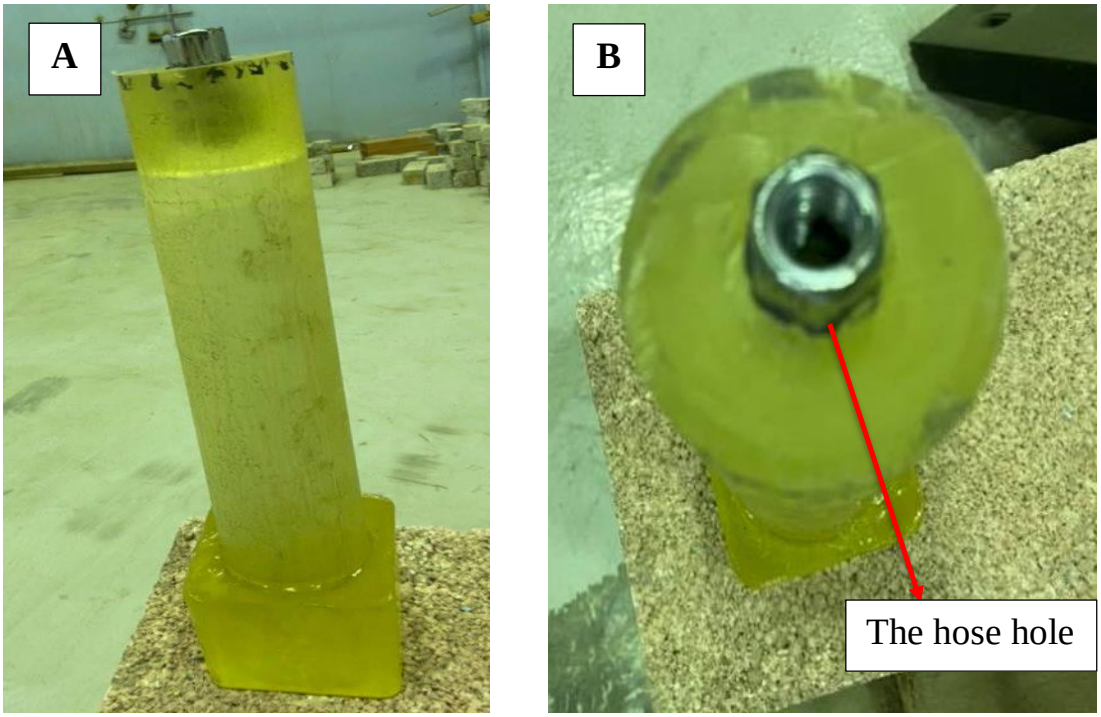

Figure 4.8: A) Manufactured Epoxy Tube, B)Top View of the Manufactured Epoxy Tube

4.6 Experimental tests

4.6.1 Density Test:

The density of the laminate can be done according to the ASTM D-792 using (Matsu Haku HIGH Precision DENSITY TESTER Type GP-120S, with digital accuracy= ±0.0001 g/cm^3 according to Archimedes' principle. The weight of each specimen was measured in air then placed in a distilled water for 2 minutes to remove the air bubbles. Subsequently, the weight was measured with distilled water. The difference between the two measured values gives the weight loss in water by Archimedes' principle.

.The density measured according to Archimedes' law, with the following formula [99]:

$$\rho_o = [W_a / (W_a - W_f)] * \rho_f \quad \ldots\ldots\ldots\ldots\ldots\ldots (4.1)$$

ρ_o: Density of object.

ρ_f: Density of fluid.

W_f: Weight of the object in fluid.

W_a: Weight of object in air.

4.6.2 Burst Pressure Test Setup

Internal pressure tests were performed according to ASTM D-1599 14e^1 [100] standard. The setup was composed of pressurizing system, test cups, and pressure recording units.

4.6.2.1 Test Setup

The internal pressure was applied by Hydrostatic Pressure Tester for Plastic Pipes provided by Qulitest. The QT-HPT Series was designed to determine the resistance of pipes by covers the determination of the time-to-failure of both thermoplastic and reinforced thermosetting/ resin under constant internal pressure.

For testing either thermoplastic or reinforced thermosetting resin pipes, pressure can be applied up to a maximum of 10 MPa. The test tank was made of stainless steel, equipped with a heat-protection layer that was 100 mm thick, and opens via air cylinder, which makes these testers very easy and safe to operate. The system recorded the change in internal pressure with time during the test, until the specimen failed, and so the bursting pressure. The pressure test system is given in Figure 4.9. This test was being done in National Center for Construction Laboratories/Baghdad.

Figure 4.9: Hydrostatic Pressure Tester

4.6.2.2 Machine Cups Design

For the application of internal pressure efficiently, the specimen should be closed properly. The cups should be strong enough to avoid leakage of test fluids, fracture or slip of the specimen at the matching region. The Qulitest apparatus offers different end cups with different diameters (50 mm, 62.5mm, 300 mm) for internal pressure testing but the manufactured specimens have different diameter ranging from 50.8 to 59 mm so it's necessary to manufacture end cups for each tube with analogous shape resemble to the original cups design that closed the tubes at both ends as shown in figure 4.10 it should be mentioned that one cup was drilled to make a hole allow to connect the pressure hose and the other end was closed.

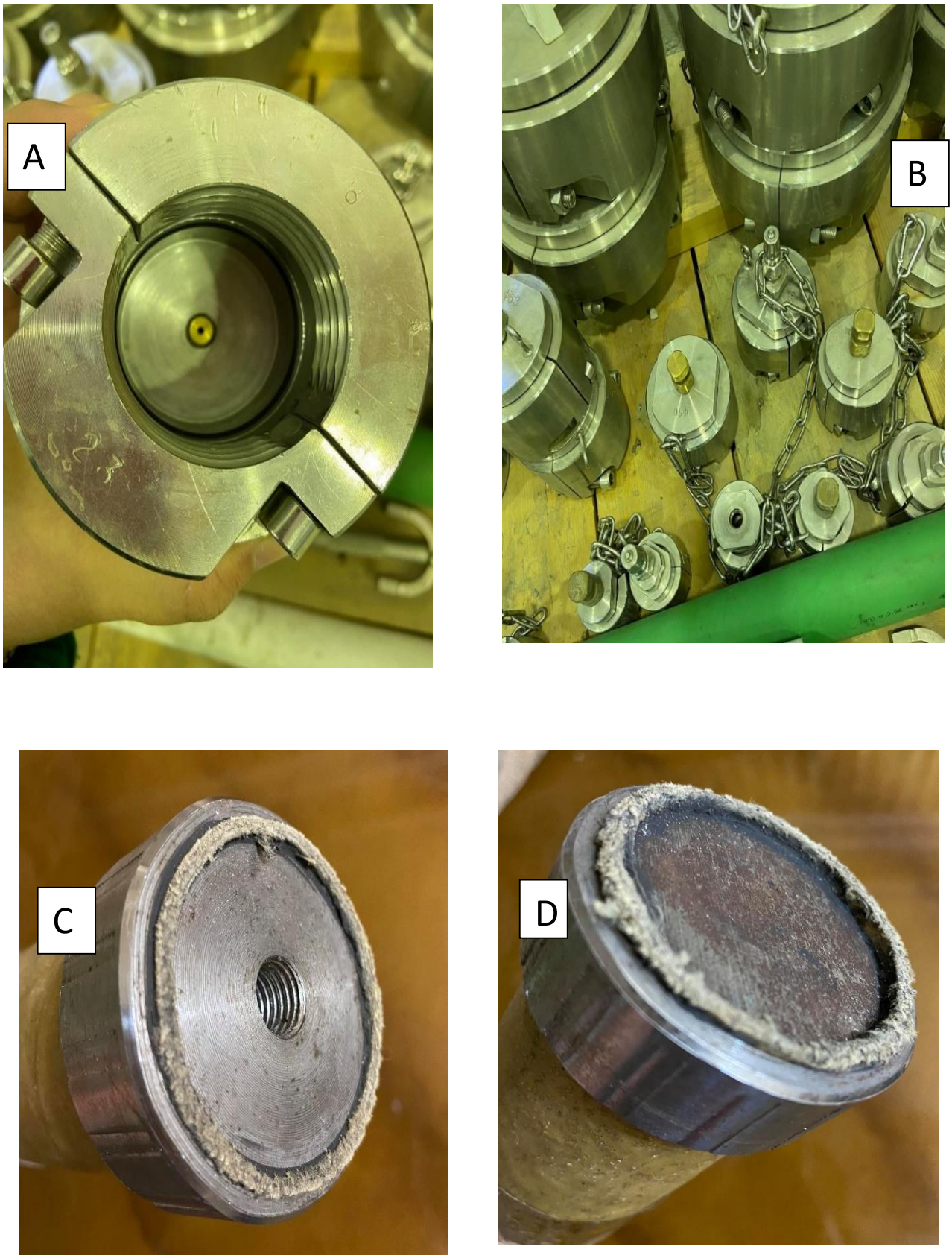

Figure 4.10: A and B: represent cups of the Qulitest apparatus.

C and D: represent the designed end cups.

4.6.2.3 Test procedure:

The internal pressure test experimentation was carried out in the following sequence:

- The tubes were fabricated by wet filament winding method and cut into desired length and the end cups closed by means of air compressor.
- The tube was filled completely with water.
- The tube was attached to the hydraulic pressure system assuring no air was entrapped.
- The test tube was fixed from both sides.
- Pressure was applied and increased uniformly and continuously, until the tube failed. When the test ended, the pressure dropped to zero.
- Using the necessary formulations, the pressure data was evaluated to obtain the mechanical characteristics

4.6.2.4 Hoop Stress Calculations

The hoop stresses that were formed in the tubes were calculated according to the ASTM D-1599 14e¹ standard using equation[100]:

$$\sigma_H = \frac{P\ D_m}{2t} \qquad \text{..... (2.6)}$$

Where

σ_H= hoop stress, MPa, P = internal pressure, MPa

D_m= mean diameter $(d_o - t)$, mm.

t = wall thickness, mm.

4.7 Thermal behavior:

4.7.1.1 Differential Scanning Calorimetry Test

The test was carried out in accordance with ASTM D3418-03 using the SH1MADZ-4 DSC-60 apparatus, which was located in the laboratories of the department of polymer engineering and petrochemical industries/college of Materials Engineering at Babylon. Pure epoxy, CF/epoxy, KF/epoxy and GF/epoxy were evaluated in powder form and a heating rate of 10 C/min with a heating range of 25 to 300 °C.

4.8 Mechanical tests:

4.8.1.1 Hardness Test:

Indentation resistance of the materials is very important property and it can be obtained by Hardness test. Hardness of polymeric material is generally measured by two types of durometer type A and Shore D. This test was achieved according to ASTM methods D-2240[101]. The hardness tool includes a needle positioned in a position perpendicular to the sample and the value should be read (0.5 min). Averages of five reading have was taken at different points to get best accuracy.

4.8.2 Ring Stiffness Test:

The external loading characteristic of epoxy, CF/epoxy, KF/epoxy and GF/epoxy laminates was carried out using parallel plate loading fixture (Figure 4.14) according to the BS 5480:1990 [102]. This test is primarily meant to find out the pipe's stiffness. To continue the test, the specimen was placed between the two parallel plates in a (Bongshin model WDW-SE) instrument. Cross-head speed of 10 mm/min was maintained throughout the test. Then, test was continued till the internal diameter of the sample subjected to 3% and 15% of deflection. The ring stiffness was determined using the formula [102]

$$S_o = \left[0.0186 + \frac{0.025\,\bar{\delta}}{D_m}\right]\frac{\bar{F}}{l\bar{\delta}} \qquad \text{(eq. 4.4)}$$

Where

$\bar{\delta}$: is the average value in (m) of the three deflection measurements.

D_m: is the mean diameter in (m) of the tube, e.g.

$$D_m = D_i + e$$

Where

D_i : is the internal diameter (in m) of the tube.

e: is the minimum wall thickness (in m) of the tube;

$\bar{F}$: is the average value (in N) of the three levels of the force used.

l: is the mean length (in m) of the test piece.

The ring stiffness was being achieved in laboratory of Materials Engineering Faculty/ Babylon University.

Figure 4.14: Ring stiffness test rig.

4.9 Failure Detection Tests

4.9.1 Ultrasound Waves Velocity Test

Ultrasound Waves test can provide valuable information about the internal structure. The devise consist of sensors that converts electrical energy into mechanical vibrations and thus into sound waves through a piezoelectric phenomenon, one of which is called a transmitter that is used to convert

electrical energy into energy acoustic mechanical energy and sending it through the material and another one called the receiver, which re-converts the sound energy into electrical energy again after its penetration or reflection from the material.

The ultrasonic pulse velocity test use the frequency 26 kHz, high energy ultrasonic wave to investigate the general structure of the composite. Ultrasound test achieved by placing sensors on both sides of the samples with two position a) vertically b) horizontally as shown in Figure 4.15.

Special oil was placed between the transmitter and receiver power generator and the surface of the sample to reduce friction and improve the transmission and reception of ultrasound without waste of energy.

The velocity was obtained based on the basic theory of ultrasonic velocity measurement by measuring the transit time from the emitting transducer to the receiving transducer. So that, the velocity was obtained determining the propagation length and the transit time in Equation (4.6) [103]

$$v = L / \Delta t \quad \ldots\ldots\ldots\ldots\ldots\ldots \quad (4.5)$$

Where: v is the ultrasonic velocity. L is the propagation length of the ultrasonic wave between the emitting transducer and the receiving transducer. Δt is the transit time.

The ultrasound wave velocity test was being achieved in laboratory of Materials Engineering Faculty/ Babylon University.

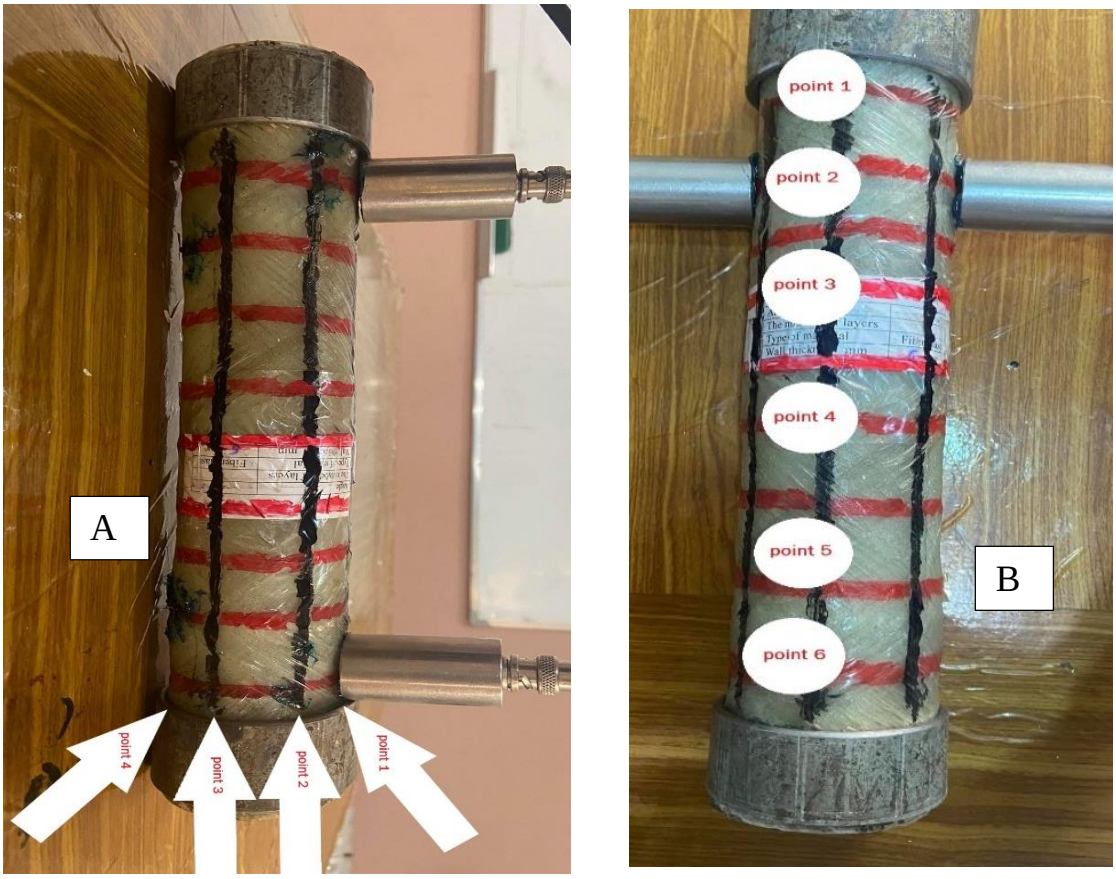

Figure 4.15: A): longitudinal ultrasound wave direction,

B) Shear ultrasound wave direction.

4.9.2 X-ray computed tomography

X-ray CT scan can be used for 3-D image to detect fiber orientation, misalignment, defects, de-bonding, voids, delamination and inclusions, also this technique determines mass distribution and accurately measure and display internal structural configurations. CT images analyzed in similar way to optical scans. The limited resolution of medical CT scan affects the detectability of the composite laminates internal structure.

A medical SIEMENS (SOMATOM Definition AS) machine (figure 4.16) was utilize to perform CT scans where the source and detector rotate around the stationary cylindrical sample was used to scan the panel in a helical mode. The STRATON tube offers a spectrum of selectable tube voltages from 70 kV up to 140 kV. The images scanned with energy of 80 kV, eff. MAs. from 70 to 35 and scan time 12.5 s.

Figure 4.16: Medical X-ray CT scan.

4.10 Microstructural Properties

4.10.1 Digital Microscope

1600X Digital Microscope USB is a high-resolution electron microscope that can be widely used for inspection of cracks and estimation of the crack width since digital microscope uses a digital camera instead of an eyepiece. A digital microscope uses optics and a digital camera to output captured images to a computer monitor. Adopts High Density resolution 0.3M pixels which provides a perfect and super clear view to observe. This test was being achieved in laboratory of Materials Engineering Faculty/ Babylon University.

4.10.2 SEM Test:

SEM and element analysis with TESCAN Mira3 was used to provide microscopes with first class detectors also used to show the structural cracks of composite laminates samples based on the technology of synthetic crystals, Tescan detectors provide very fast and efficient solutions that enhance high imaging quality. The specimens were initially prepared by cutting the fractured sample into a rectangular block and then sputter coating with a thin layer of gold using a sputter-coating unit. SEM test were being done in laboratory of Polymer Engineering Department, Amir Kabir University.

Chapter Five

Results and Discussion

5.1. Introduction:

This chapter covers the detailed experimental and numerical discussion results where different pressure vessel manufactured by filament winding technique are reinforced with 75% wt. of carbon fibers , Kevlar fibers and glass fibers with four different winding angles [±45°₃], [±55°₃], [±65°₃] and [±75°₃] are subjected to internal pressure to evaluate their burst pressure behavior. The burst pressure behavior test studied the effect of fiber reinforcements on its burst strength behavior, also studied the effect of winding angle configurations and the effect of symmetrical stacking sequence.

Failure detection tests include ultrasound wave velocity and X-ray CT scan were employed for detection of their behavior and crack existence. In addition, the mechanical results such as tensile, elastic modulus, impact strength, and hardness were discussed in this chapter.

FEA Analysis studies achieved with ANSYS workbench 17-ACP includes numerical results of total deformation, the Von-Mises stress and the Von- Mises strain and comparing them with their yield point to estimate the composite strength and their failure behavior at 25 MPa.

5.2 Characterization of Materials:

5.2.1. Differential scanning calorimeter (DSC):

The glass transition temperatures (T_g) of epoxy and CF/epoxy, KF/epoxy and GF/epoxy laminates were characterized by differential scanning calorimeter (DSC).

DSC was used to show the effect of reinforcing fibers; carbon fibers, Kevlar fibers and glass fibers on the thermal properties of reference material (epoxy). Figure 5.1 explains the thermal behavior of the epoxy, where the T_g appears at 80.78 ºC which approximately agreed with Mateusz Gargol [91]and T_d at 308.13 ºC.

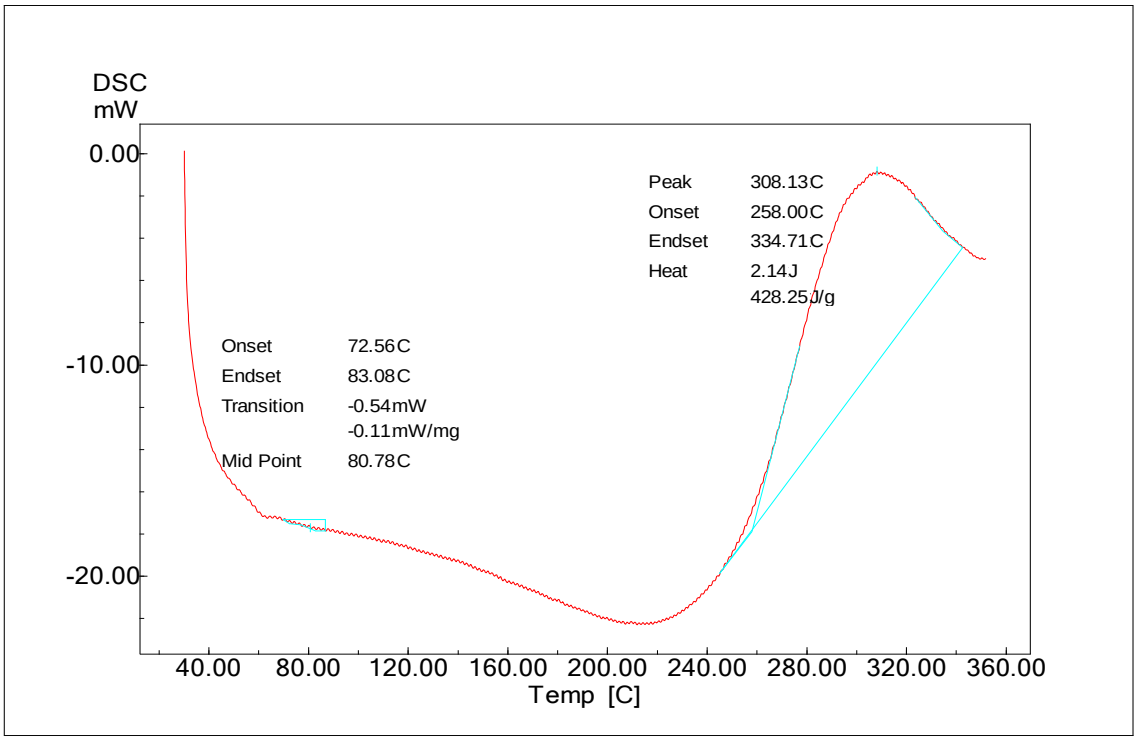

Figure 5.1: Thermal History Behavior of epoxy.

DSC analyses indicate that T_g of the composite laminates increases when reinforcing with fibers .It is observed from figures 5.2 and 5.3 where the T_g of pure epoxy increases from 80.78 ºC to 87.61 ºC when reinforcing with CF while KF show the highest increment in T_g from 80.78 ºC to 89.02 ºC since KF is organic material and have high active surface more than CF and GF and form a strong bond between fibers and the epoxy matrix that increasing the T_g.

T_g Decreases from 80.78 ºC to 78.26 ºC when reinforcing with glass fiber as shown in figure 5.2 since poor adhesion between GF and polymeric matrix leading to multisource of firing leads to lowering T_g.

Also DSC curves show decreasing in viscosity due to crosslinking till degradation T_d, where $T_d$of epoxy appeared at 308.13 ºC and decreased for CF /epoxy and KF/epoxy where KF/epoxy higher decreasing to 266.36 ºC since KF have melting temperature lower than CF and GF.

Thermal properties of GF /epoxy laminate show increasing in T_d to 311.83 ºC this can be attributed to the oxidize nature of glass fibers and the high melting temperature of glass fibers.

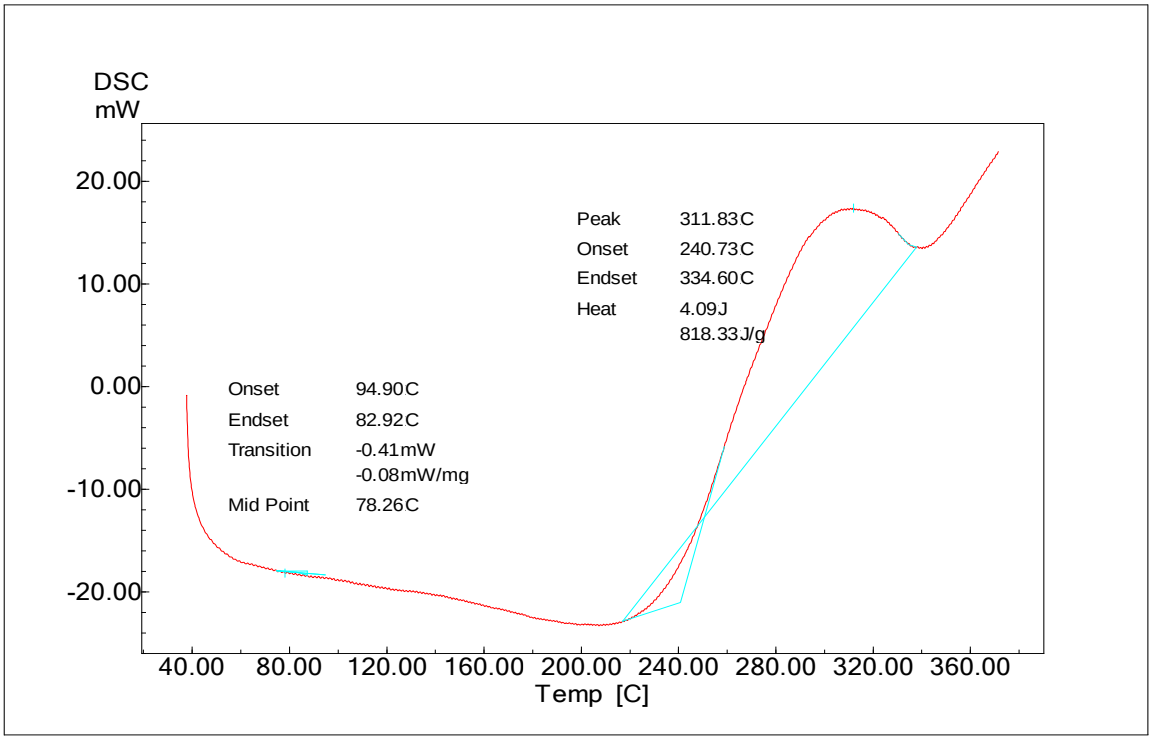

Figure 5.2: Thermal History Behavior of GF/epoxy.

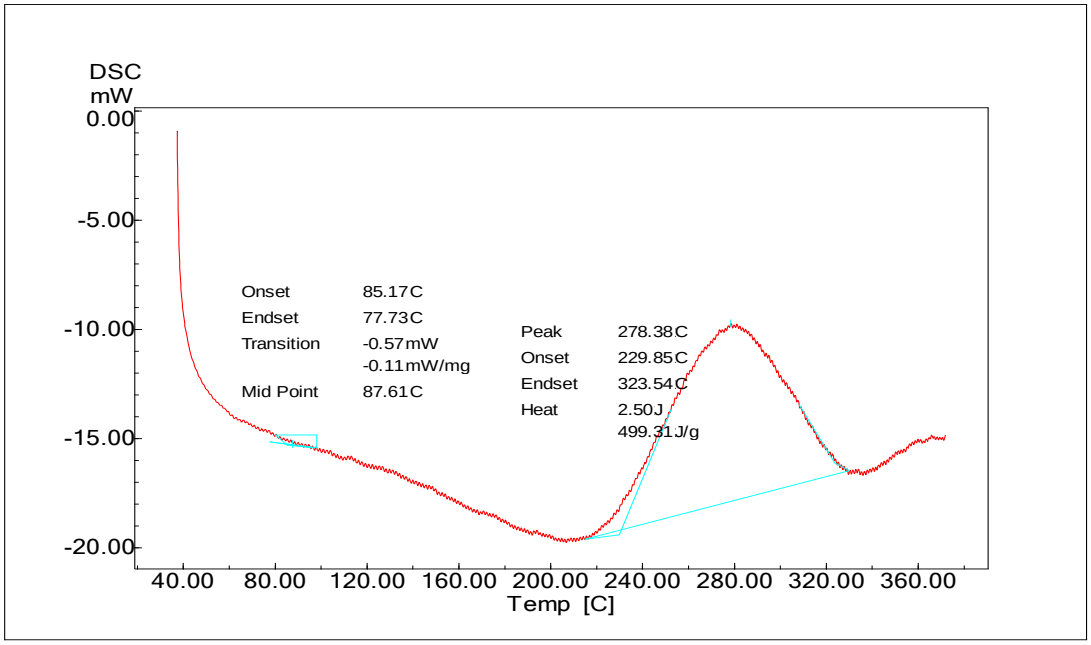

Figure 5.3: Thermal History Behavior of CF/epoxy.

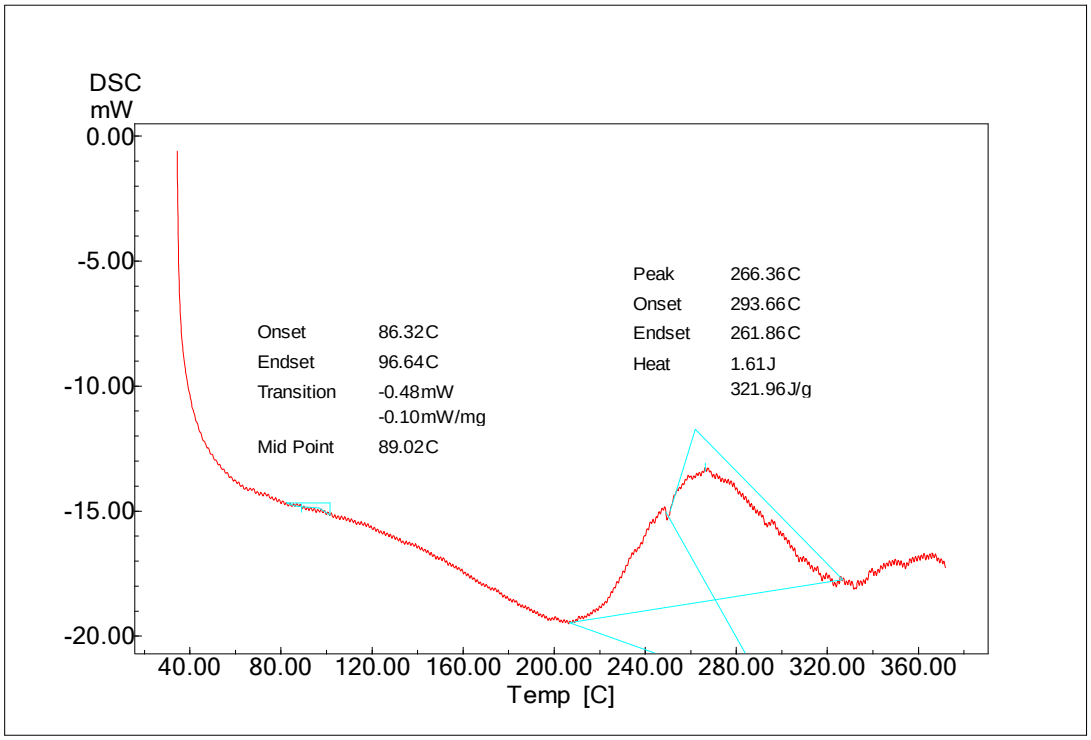

Figure 5.4: Thermal History Behavior of KF/epoxy.

The values of T_g and T_d of CF/epoxy, KF/epoxy and CF/epoxy are shown in Table 5.1

Table 5.1: DSC data of epoxy and CF/epoxy, KF/epoxy and CF/epoxy.

Property	Epoxy	CF/ epoxy laminate	KF/ epoxy laminate	GF/ epoxy laminate
T_g °C	80.78	87.61	89.02	78.26
T_d °C	308.13	278.38	266.36	311.83

5.3 Density Test:

Figure 5.5 illustrates the density of epoxy, CF/epoxy, KF/epoxy and GF/epoxy laminates. The density of epoxy increased when reinforcing with fibers. Increasing in the density of composite laminates could be attributed to the high densities of the reinforcing fibers compared with the density of the epoxy.

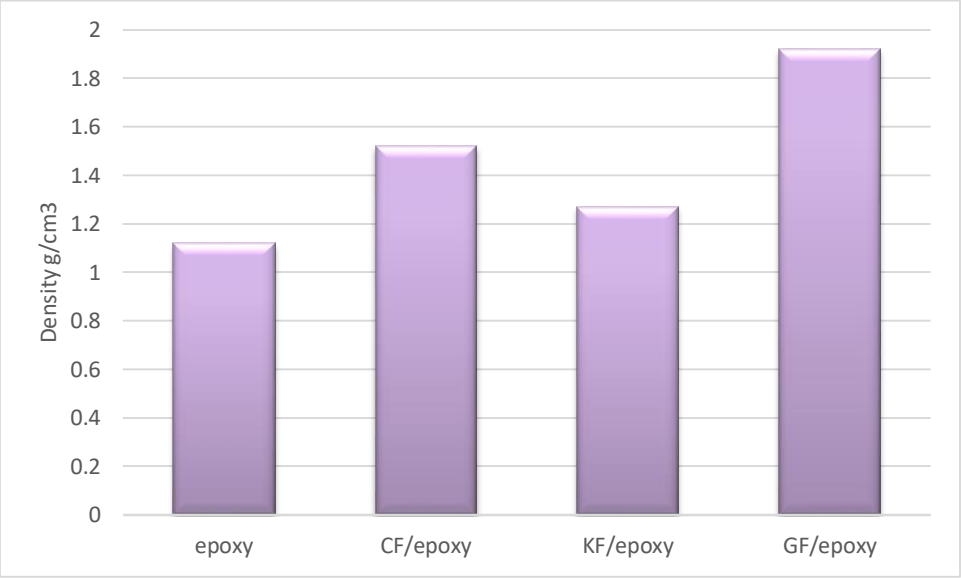

Figure 5.5: Density of epoxy CF/epoxy, KF/epoxy and GF/epoxy laminates

The density of the composite laminates mainly depends upon the type of reinforcing fibers. It can be seen that the GF/epoxy laminates have the highest density among the composite laminates this is can be attributed to the higher density of the glass fibers (2.4 g/cm^3) compared with the density of the carbon fibers (1.79 g/cm^3) and the Kevlar fibers (1.44 g/cm^3), also it's noted that KF/epoxy laminates have the least value of density.

5.4 Internal Pressure Behavior

In order to determine the burst pressure behavior of the epoxy and composite laminates; CF/epoxy, KF/epoxy and GF/epoxy with different angle orientations were subjected to internal pressure load. The results discussion involve three section: the effect of type of reinforcing fibers, effect of winding angle and the effect of symmetrical stacking sequence on their burst pressure behavior.

5.4.1 Effect of Winding Angle Configuration

The effect of winding angle on the burst pressure for the epoxy and CF/epoxy, KF/epoxy and GF/epoxy laminates is shown in figure 5.6 which represents the effect of winding angle configurations on burst pressure performance epoxy and CF/epoxy, KF/epoxy and GF/epoxy laminates.

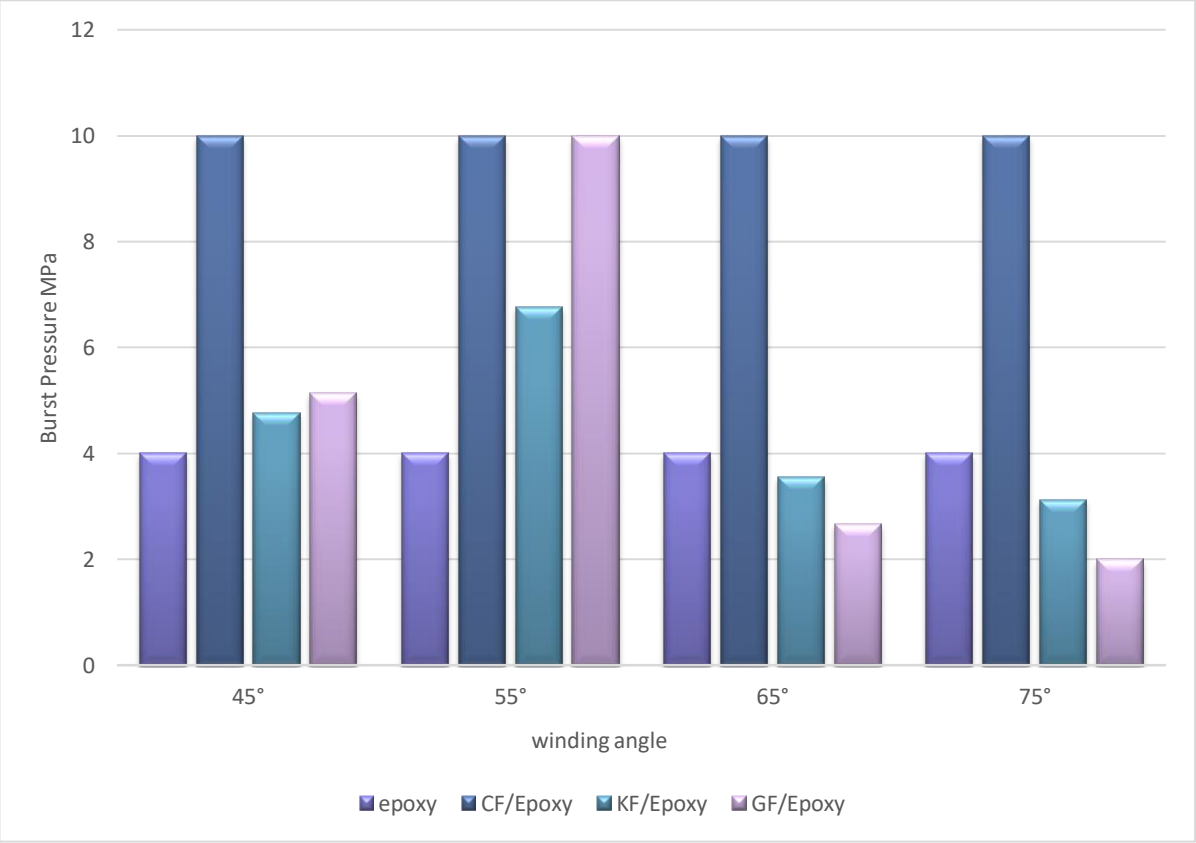

Figure 5.6: The effect of winding angle configuration on burst pressure test.

It can be observed that the burst pressure performance higher for laminates with [±45°₃] and [±55°₃] winding angle configuration, where the maximum burst pressure is for winding angle configuration [±55°₃] for all fiber laminate types, although most of studies report that [±55°₃] angle is the optimum, because the interlaced fibers are in equilibrium which provide a twice hoop stress the axial one. For larger winding configurations than [±55°₃], the burst pressure performance decreases to lower values, this can be explained by the resistance of the composite tube to axial load decreases. Considering this, [±55°] being the best winding configuration.

Larger winding angles decreases to values lower than epoxy tube due to large wall thickness of the epoxy that effect on the burst pressure performance.

5.4.2 Effect of the Type of Reinforcing Fiber

Fiber type is another production parameter has affected the burst performance. By examining the figure 5.6 it can be seen that CF/epoxy laminates show the best burst performance exceeding 10 MPa which show no failure compared to the KF/epoxy and GF/epoxy laminates. This is an expected result considering that carbon fibers are much stronger and stiffer than Kevlar fibers and glass fibers.

It can be shown that the epoxy internal pressure performance has best improvement of epoxy by 150% when reinforcing with CF/epoxy with [±55°₃] angle orientation

5.4.3 Effect of Ply Sequences:

Different laminates with symmetrical sequences are used to find out the effect of symmetry ply sequence on the burst pressure performance. Figure 5.7 represents the effect of symmetrical sequence on the burst pressure.

It has been established that the symmetrical ply sequence improves the value of burst pressure strength where the burst pressure of the composite tubes increases with the symmetrical ply sequence as shown in figure 5.7 since the symmetrical sequence eliminate shear coupling as well as supply a uniform stress distributed and that lead to stabilizing the stress and high strength composite.

It can be seen that the CF/epoxy has the highest burst pressure performance exceeds 10 MPa, this attribute to the high strength and stiffness of carbon fibers. Also GF/epoxy show the same results exceeds 10 MPa because of the high wall thickness of the symmetrical GF/epoxy raise the burst pressure performance.

KF show the lowest burst pressure value about 6 MPa, however reinforcing with symmetrical sequence raise the burst pressure behavior of the epoxy by 150% when reinforcing with CF and GF, 50% when reinforcing with KF.

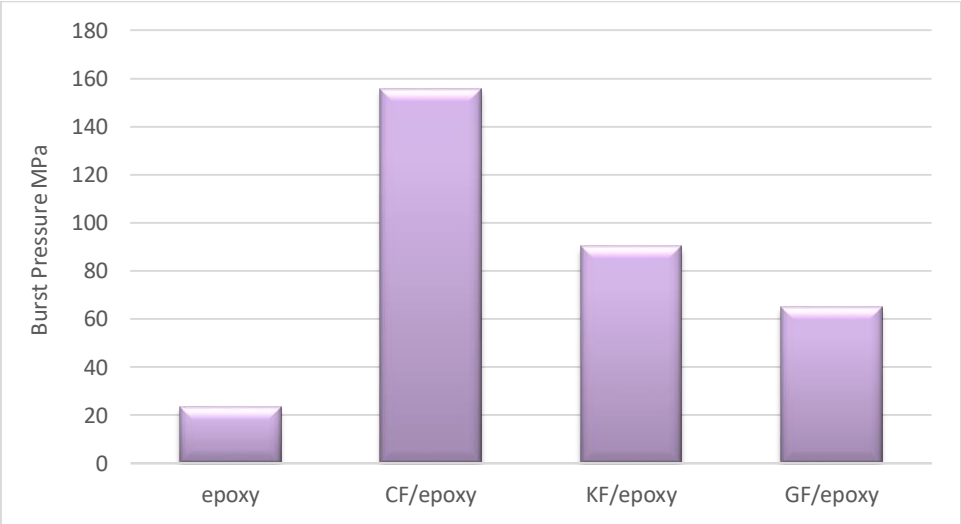

Figure 5.7: The effect of ply sequence on burst pressure test.

5.5 Hoop Stress Behavior

The results are shown in Figure 5.8 which illustrate the hoop stress values of composite laminates as calculated in (eq. 4.2), hoop stress performance have been discussed into three sections; the effect of type of reinforcing fibers and effect of winding angle and the effect of symmetrical stacking sequence.

5.5.1 Effect of Winding Angle Configuration

Hoop stresses are affected by winding angles orientations as shown in figure 5.8 where the hoop stress for composite laminates with winding angles orientations [±55°$_3$] have the best hoop stress performance. The higher Hoop stresses can be explained by higher hoop resistance generated to resist the bursting effect that results from the application of pressure since the direct correlation between hoop stress and pressure. For winding orientations larger than [±55°$_3$], the hoop stresses tending to decrease because of decreasing in hoop resistances with lowering of pressure that the material can withstands.

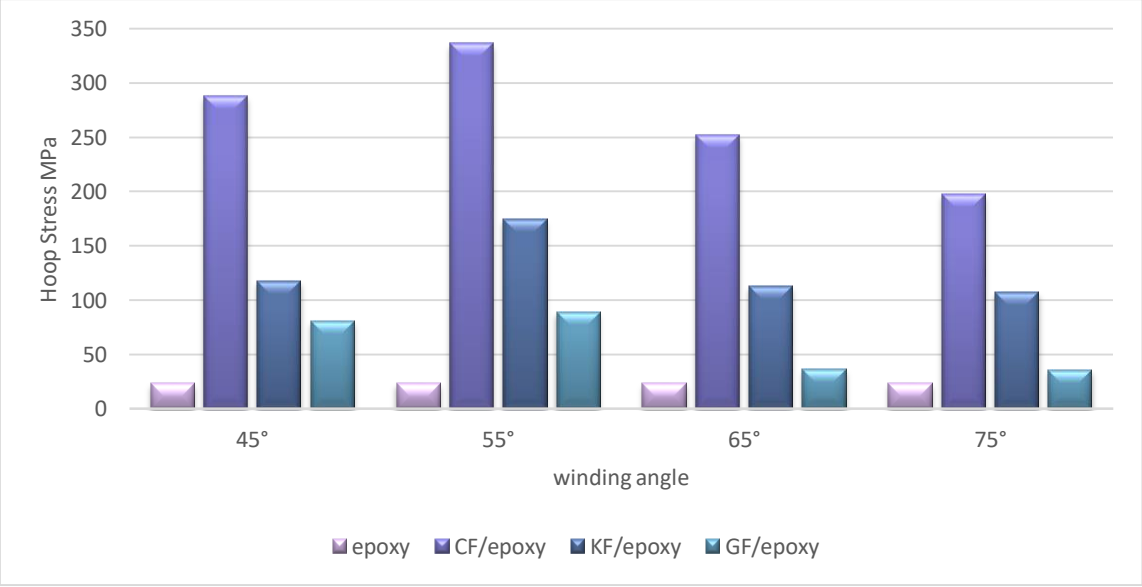

Figure 5.8: Hoop stress performance of epoxy, CF/epoxy, KF/epoxy and GF/epoxy.

5.5.2 Effect of the Type of Reinforcing Fiber

The effect of reinforcing fibers on hoop stress of different composite laminates is shown in figure 5.8 where the CF/epoxy laminates have the highest hoop stress compared to the KF/epoxy and GF/epoxy laminates, this can be explained by the high strength of these fibers making them withstand the growing in the applied pressure which increasing the hoop stress.

Hoop stress of the epoxy improved when reinforcing with fibers by 1331% with CF/epoxy with [±55°₃] angle orientation.

5.5.3 Effect of Ply Sequence:

As mentioned above, the hoop stress increases with increasing pressure and effected by type of material, the effect of symmetrical sequence on the burst pressure performance is shown in figure 5.9.

CF/epoxy laminate has the highest hoop stress value while GF/epoxy laminate show the lowest hoop stress value. However, epoxy hoop stress improved by 559.7% when reinforcing with CF, 321.2% when reinforcing with KF, 176.7% when reinforcing with GF.

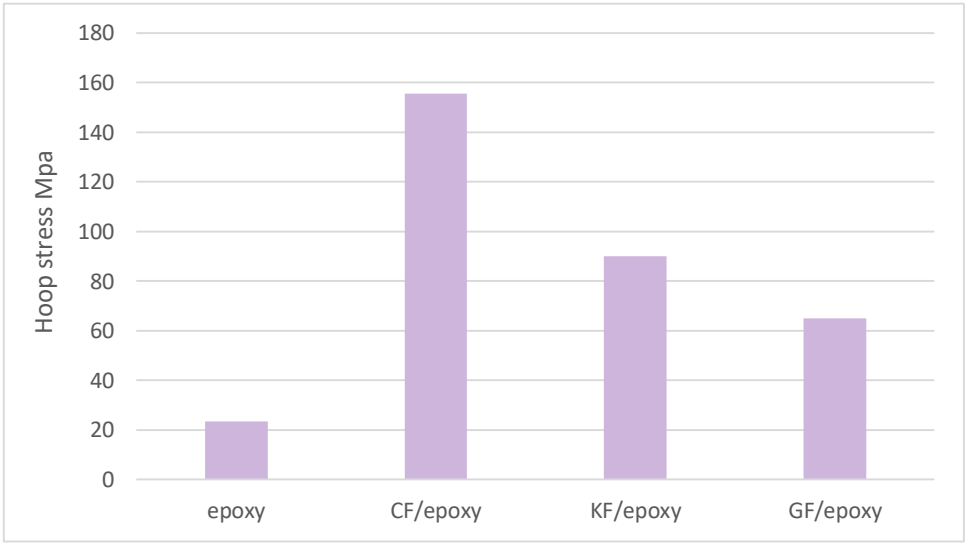

Figure 5.9: Hoop stress of symmetrical laminates.

5.6 Leaks Analysis of Pressure Vessels:

5.6.1 Analysis of Epoxy Tube:

During the burst pressure test, the epoxy tube experienced loading and bursting under internal pressure and starts losing its structural integrity leading to sudden failure through breaking, the propagating crack runs swiftly along the tube as shown in figure 5.10.

Sharp fracture could be due to the nature of epoxy that's behave as brittle material which experience a sudden rapid fracture under 4 MPa where exhibits brittle failure or no plastic deformation. Brittle fracture is not prefers in pressure vessels because of the fast vessels failure and may lead to sudden accidents; this is not preferred failure especially when the tube vessel used to transfer gas.

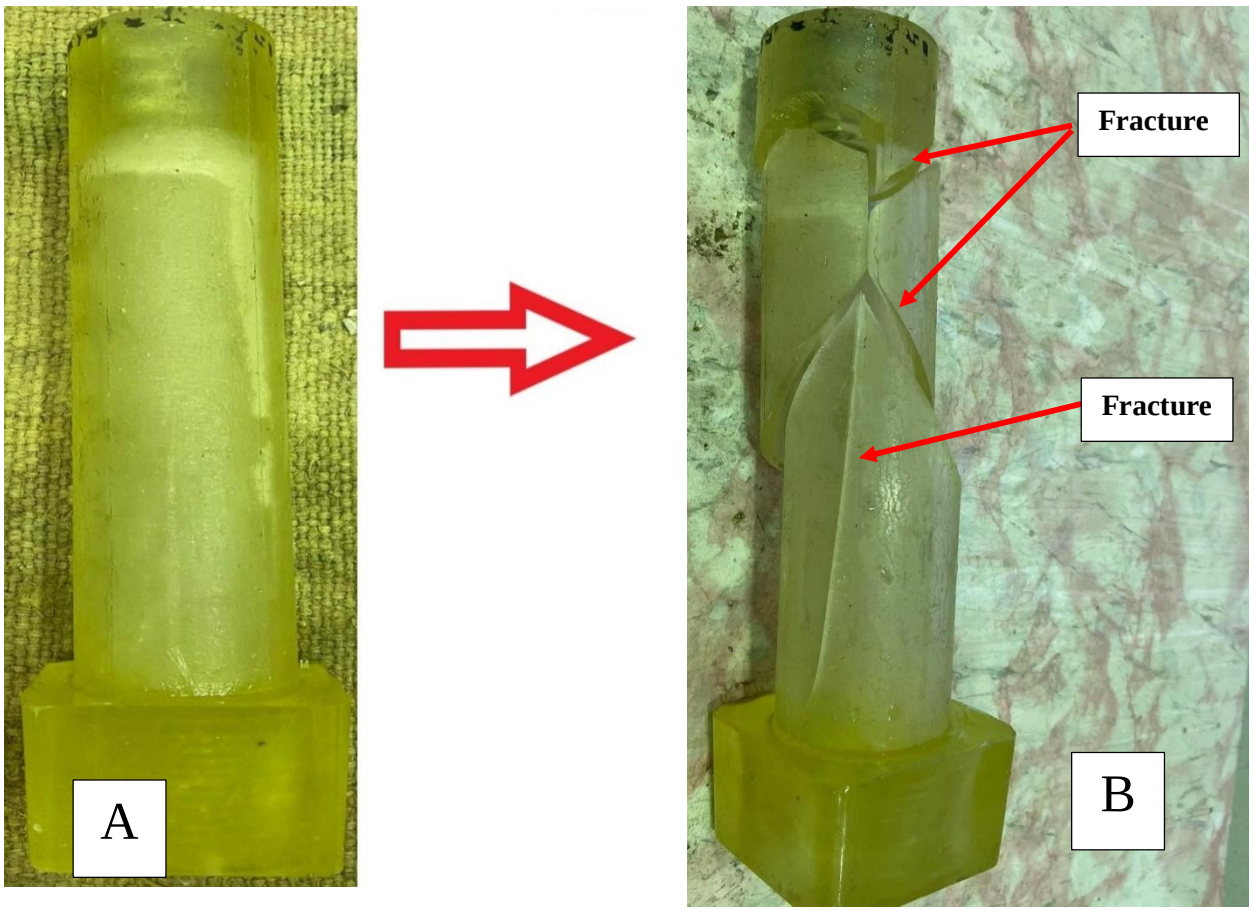

Figure 5.10: Failure of epoxy tube, a) before burst pressure test, b) after burst pressure test.

5.6.2 Analysis of Fiber Composite laminates Tubes:

Since the composite laminates consist of multiple layers, which develop a higher hoop stress in the internal surface than the external one. This leads to conception that the fracture would start in the inner layer, because this layer is the first layer to exceed the strength limit and decreasing the structure capacity to stand loads. [104]

Increasing the internal pressure load gradually increases the number of cracks leading to water leakage on the sample surface.

During the burst pressure test, all the pipes failed with a water leakage (these results agreed with Hawa [105] indicating matrix cracking or fiber matrix interface de-bonding started at the inner surface of pipe and propagated through the outer surface as shown in figure 5.11.

Figure 5.11: Water leakage of GF/epoxy.

5.7 Microstructural Results:

After the burst pressure test, the pipes were examined by naked eye, and there was no cracking, whitening or delamination in the composite laminates except for the $[\pm 75°_3]$ Kevlar fiber composite laminates as will show later.

SEM and digital microscope techniques were utilized to discover damage formation and progression of composite laminates pipes. Typical SEM images of fracture surfaces' in micro scale after burst pressure test are represented where the micrographic analysis of the final damage shows characteristics such as fiber fracture, adhesive fracture (fiber/matrix debonding), Kevlar fiber fraying, in addition to the cohesive fracture in the matrix, for all the test specimens analyzed. The most common failure mode presents as cohesive failure.

Figure 5.12 represents the water leakage during experimental burst pressure test and the digital microscope for the leakage area of the $[\pm 45°_3]$ KF/epoxy laminate where it show that the average width of the crack is 0.05 mm and the crack parallel to the winding area.

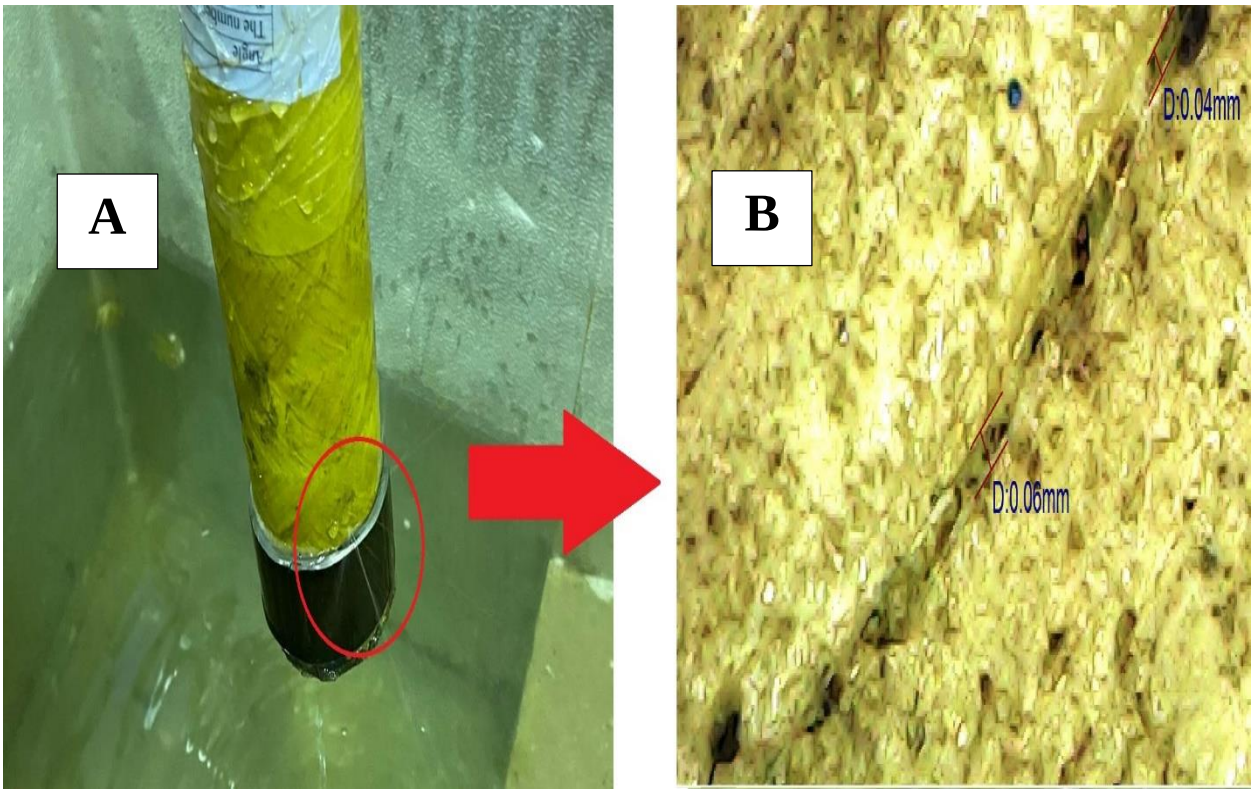

Figure 5.12: Water leakage of $[\pm 45°_3]$ KF/epoxy laminate.
A) Experimental water leakage during the experimental test, B) digital microscope for the leakage area.

By examining the crack under SEM as in figure 5.13 that shows details of the fracture mechanism of the $[\pm 45°_3]$ KF/epoxy laminate, from figure 5.13 (a) it can be seen that Kevlar fiber fraying occurs as the composite laminate tube results from exposing to high pressure loads.

However, a cohesive failure also occurs resulting from fracture of the bonding of fiber/matrix interface where occurs when a layer of adhesive remain in both surfaces. It also can be seen that the spread of same in the warp, causing fraying of Kevlar fiber, being evidenced by the appearance of the Kevlar fibers, as shown in Figure 5.13 (c and d). The same type of damage suffered in Kevlar fibers was also detected in the work developed by Roberto [89]

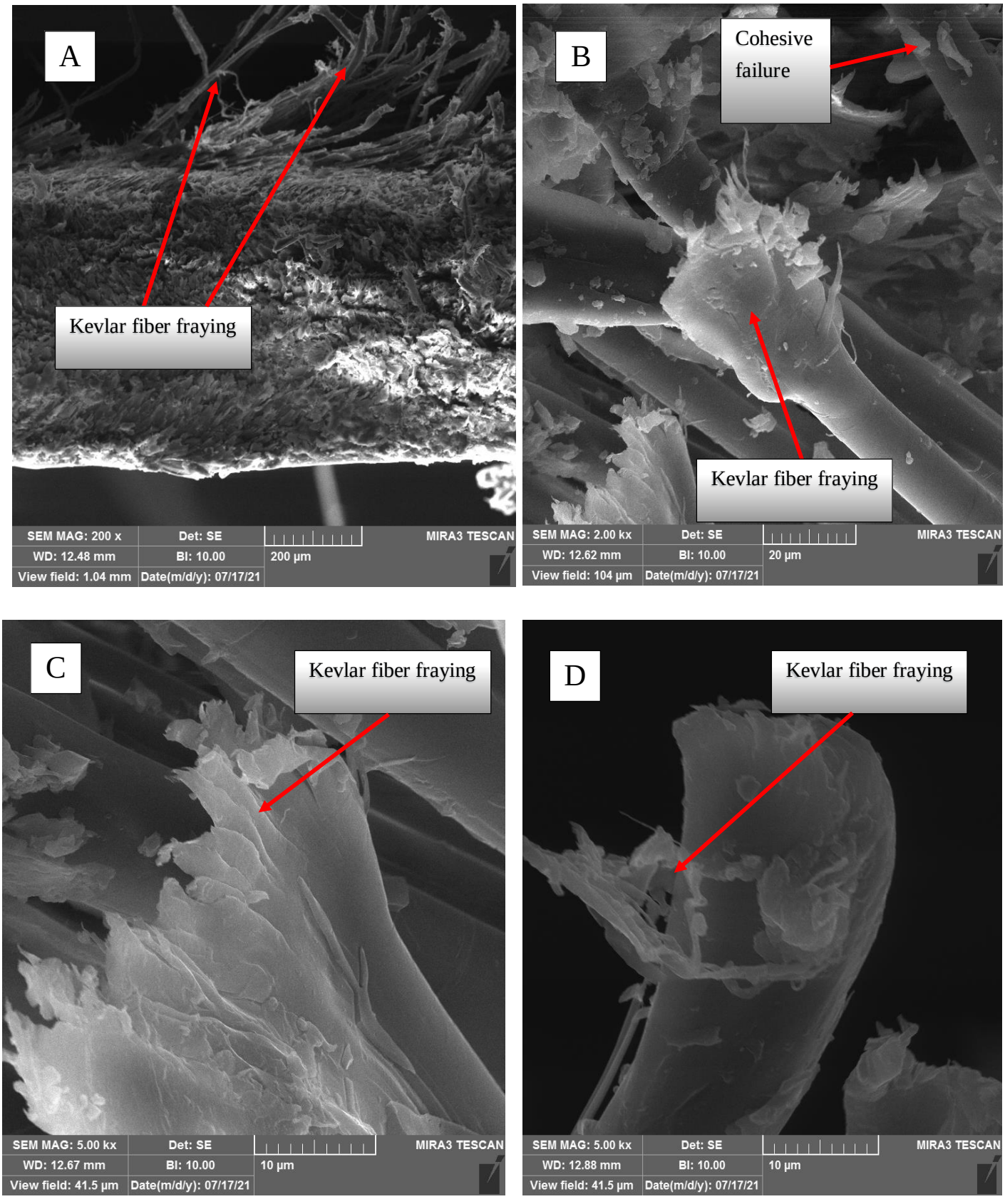

Figure 5.13: Scanning electron microscopy of $[\pm 45°_3]$ Kevlar fiber composite laminate.

Figure 5.14 represents the water leakage during experimental burst pressure test and the digital microscope for the leakage area of $[\pm 55°_3]$ KF/epoxy laminate where it show that the average diameter of the crack is 0.036 mm runs along the winding area.

It can been mentioned that the $[\pm 55°_3]$ KF/epoxy has the minimum crack width.

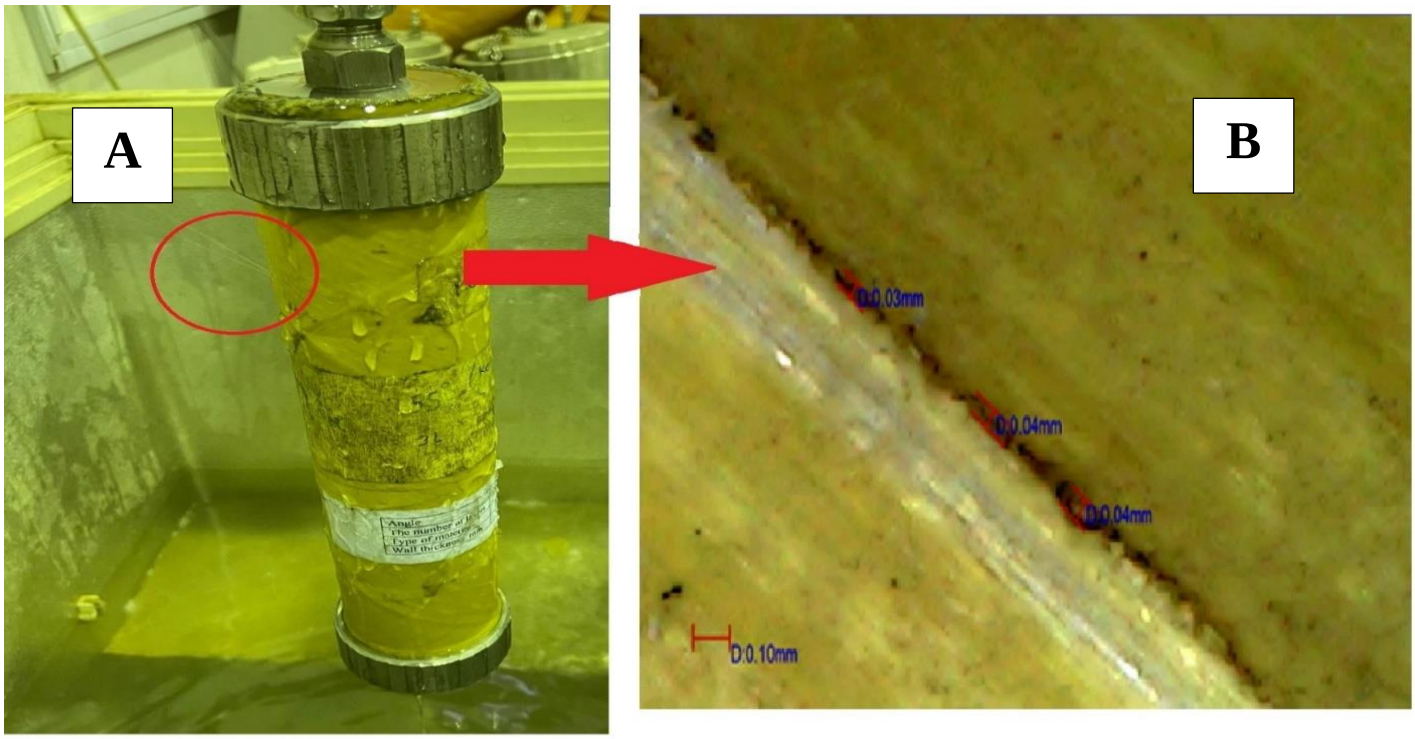

Figure 5.14: Water leakage of $[\pm 55°_3]$ KF/epoxy laminate:
A) Experimental water leakage during the experimental test,
B) Digital microscope for the leakage area.

By examining the crack under SEM, Figure 5.15 shows the SEM images of the $[\pm 55°_3]$ KF/epoxy laminate after burst pressure test. There were distinct failure modes that were detected named; delamination, fiber debonding and cohesive failure. These modes were observed while the internal pressure was increased.

Figure (5.15 a) shows a SEM image of a delamination area that propagates along the fiber/matrix interface. The cause for the delamination

damage is majorly due to internal pressure exceeds the interlaminar strength of the laminate.

Figure 5.15 (b and c) shows cohesive failure of the interface occurs due to propagating pressure load exceed the fiber/matrix bond strength.

On the other hand, the debonding as in figure (5.15 d) that occurs between fiber/matrix interfaces caused by the development of stress concentration which causes further de-bonding under pressure loading.

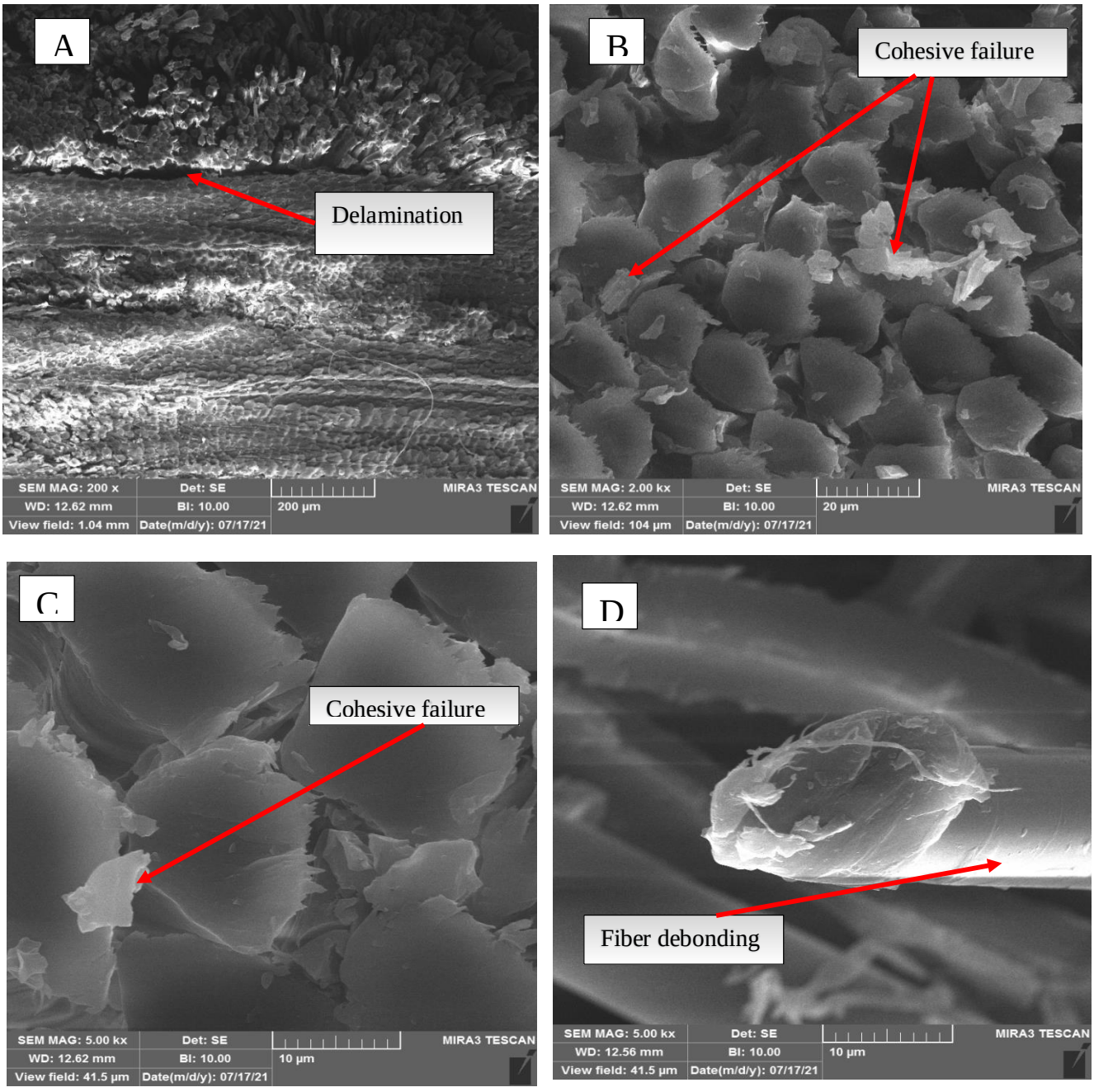

Figure 5.15: Scanning electron microscopy of $[\pm 55°_3]$ KF/epoxy laminate.

Figure 5.16 represents the water leakage during experimental burst pressure test and the digital microscope for the leakage area where it show that the average diameter of the crack is 0.05 mm runs along the winding area.

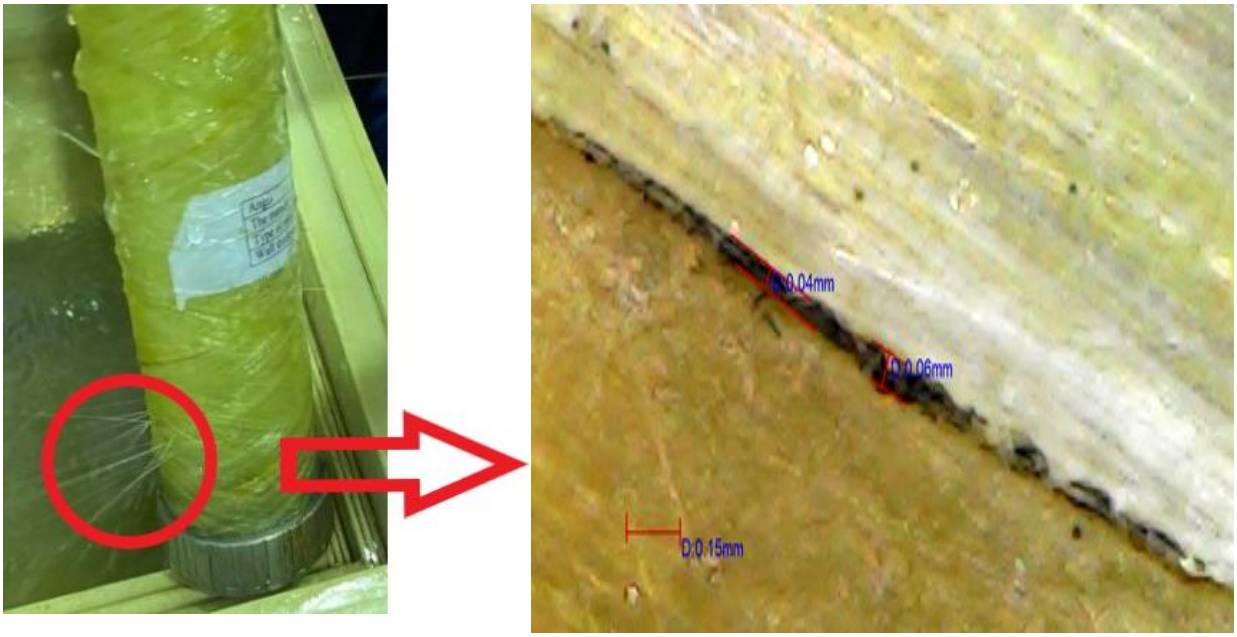

Figure 5.16: Failure of $[\pm 65°_3]$ KF/epoxy laminate tube:

A) Experimental water leakage during the experimental test,

B) Digital microscope for the leakage area.

Figure 5.17 represents the scanning electron microscope of $[\pm 65°_3]$ KF/epoxy laminate which show different failure modes like fiber pullout, fiber fraying, delamination and fiber debonding.

From figure 5.17 (a) it can be seen that delamination as well as Kevlar fiber pullout occurs as the composite laminate exposed to high pressure load.

Furthermore, it is also seen the cohesive failure in the fiber/matrix interface as in Figure 5.17 (b).

It is also can be seen the fraying of Kevlar fiber being evidenced by the appearance of the Kevlar fiber, as shown in Figure 5.17 (c and d).

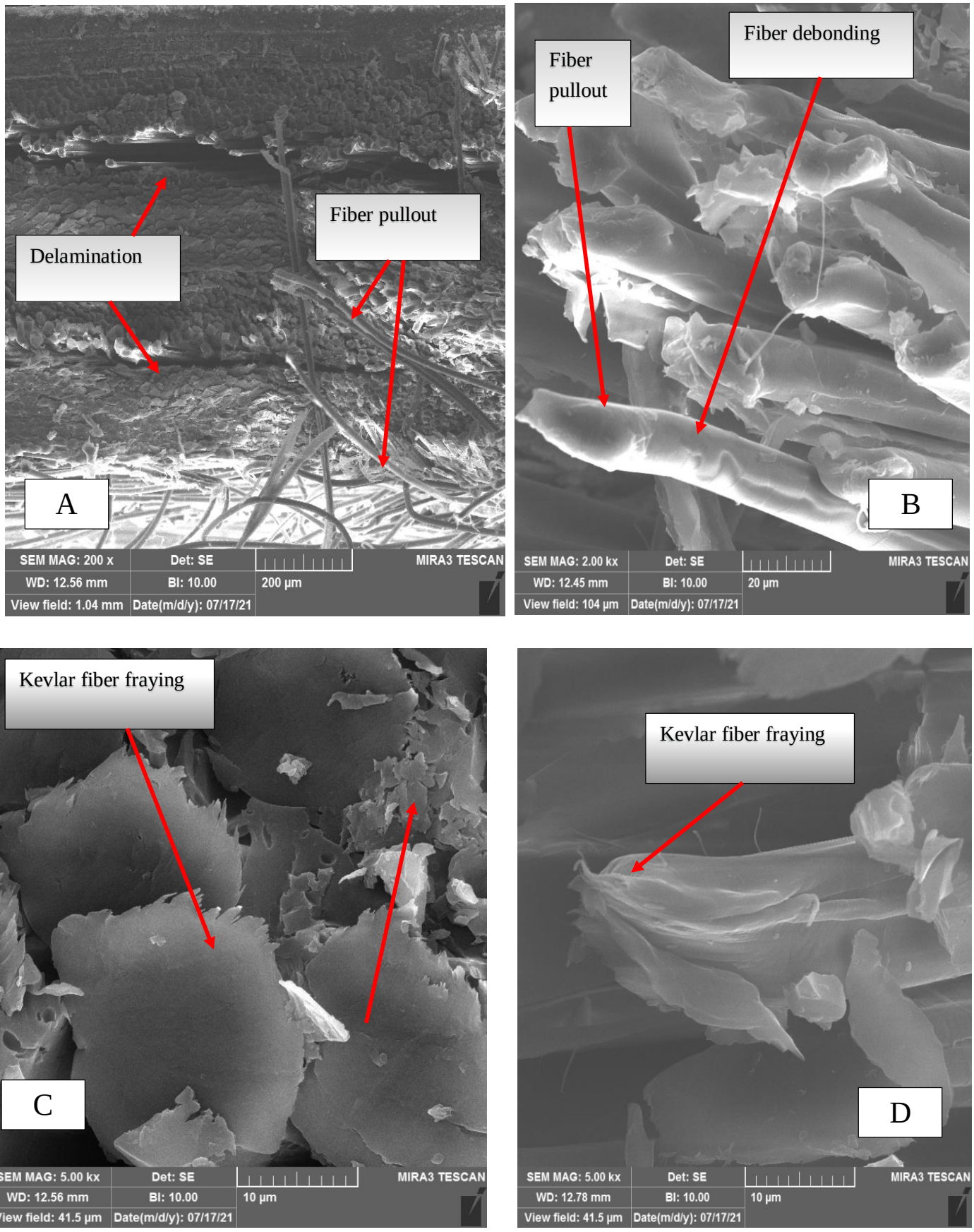

5.17: Scanning electron microscopy of $[\pm 65°_3]$ KF/epoxy laminate

From figure 5.18 which represents the water leakage during experimental burst pressure test and the digital microscope for the leakage area that can be seen the Kevlar fiber composite laminate with winding angle $[\pm 75°_3]$has the largest crack diameter that is 0.26 mm.

Figure 5.18: Failure of $[\pm 75°_3]$ KF/epoxy laminate:

A) Experimental water leakage during the experimental test,

B) Digital microscope for the leakage area.

The leakage and fracture strengths are affected considerably with winding angles. Figure 5.18, it is observed that matrix cracks run parallel to the fiber direction $75°$ of the KF/epoxy laminates, eventually leading to leakage failure where the crack is propagated along the winding direction.

Figure 5.19 represents the SEM of $[\pm 75°_3]$ KF/epoxy laminate which show different failure modes like fiber pullout, cohesive failure, fiber fraying, fiber debonding and fiber splitting.

From figure (5. 19 a) It can be seen that large number of Kevlar fiber pullout occurs as the composite laminate exposed to high internal pressure load.

From figure 5. 19 (b and c) show a combination of cohesive failure that appears as matrix fragments adhere to the fibers. Also can be seen the fraying of Kevlar fiber being evidenced by the appearance of the Kevlar fiber, as shown in Figure 5. 19 (c)

When stress further increased, obvious splitting and fibrillation of the Kevlar fibers was observed, suggesting that adhesive wear took place at the burst pressure moment and this splitting and fibrillation are likely due to the high pressure that caused high frictional work and led to high temperature at the frictional interface as shown in figure 5.19 (d)

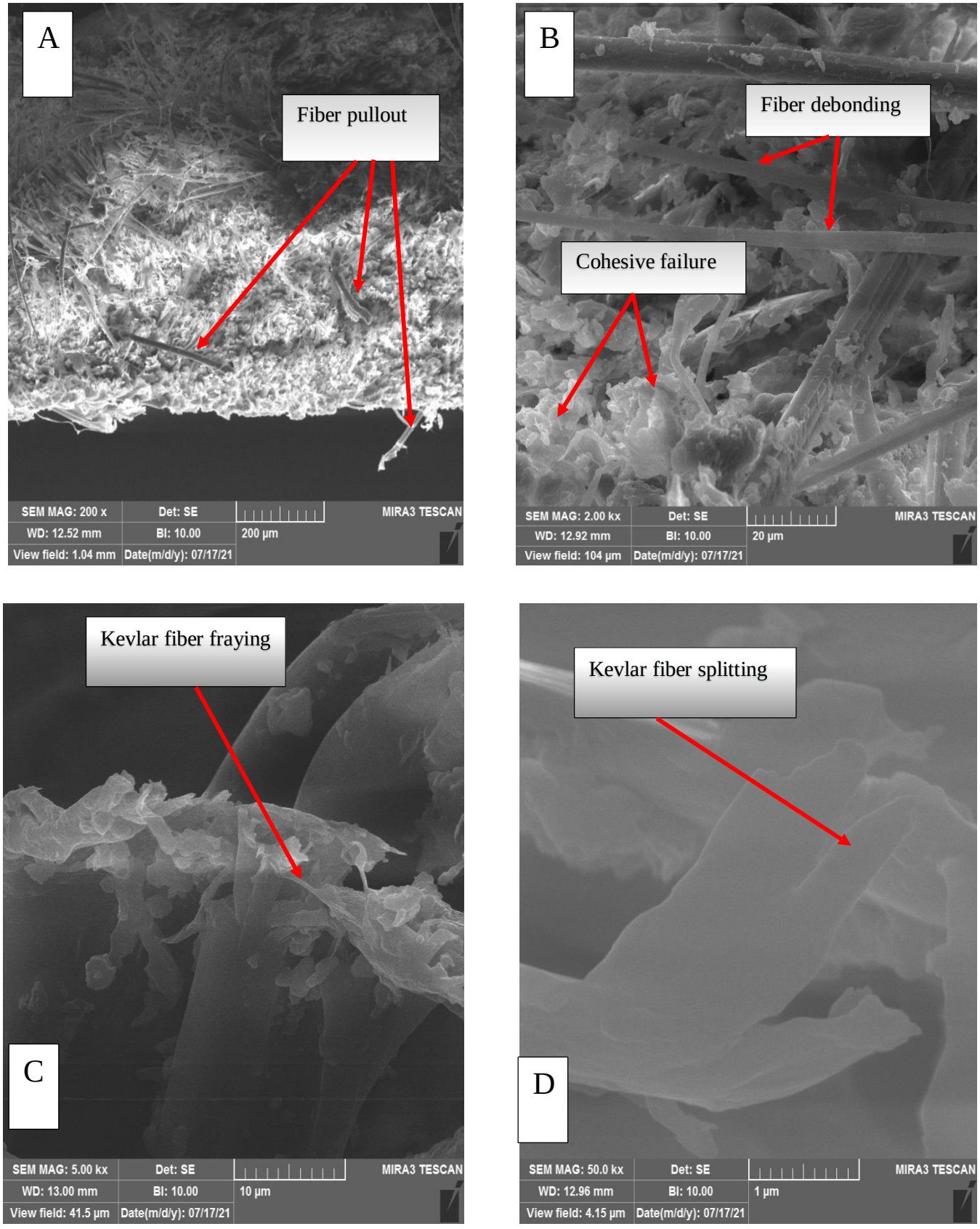

Figure 5.19: Scanning electron microscopy of $[\pm 75°_3]$ KF/epoxy laminate.

Figure 5.20 represents the water leakage during experimental burst pressure test of the symmetrical KF/epoxy laminate and the digital microscope for the leakage area where it show that the average diameter of the crack is 0.038 mm and the crack parallel to the winding area.

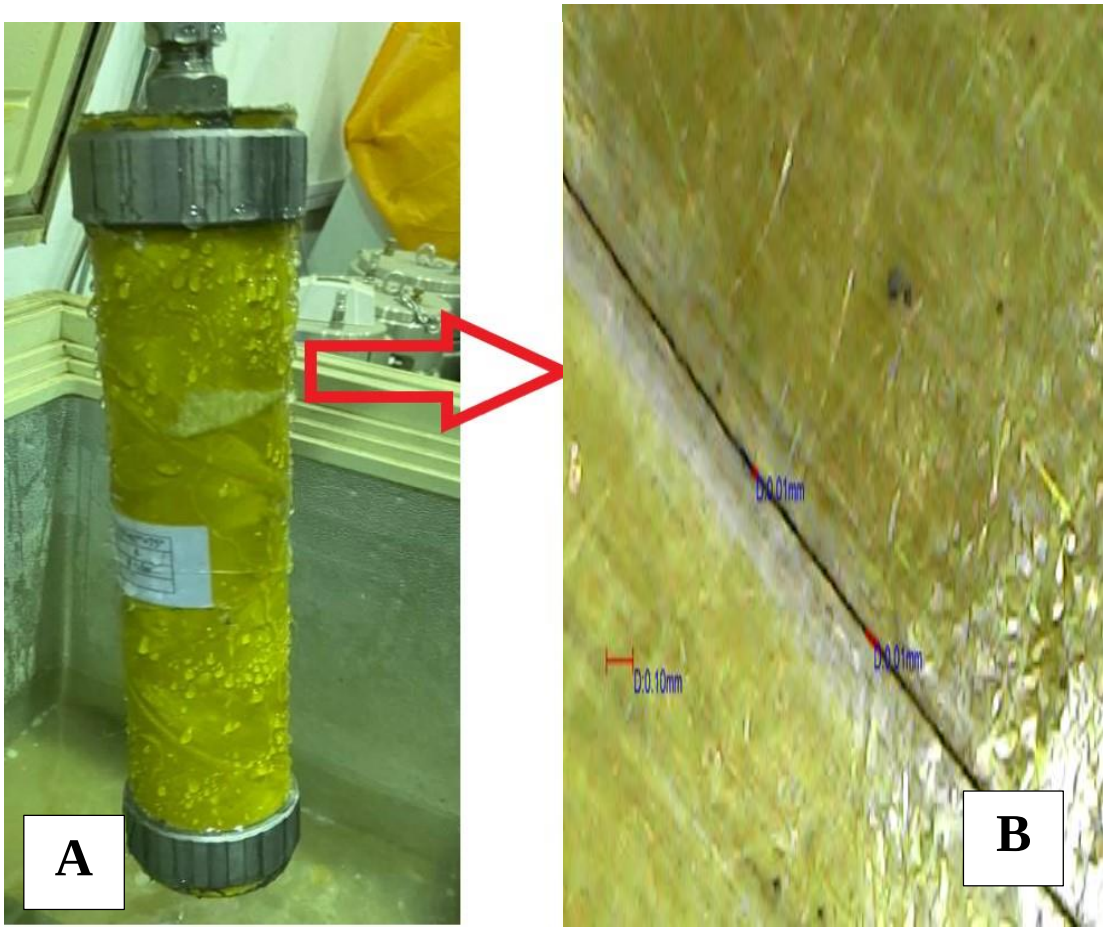

Figure 5.20: failure of symmetrical KF/epoxy laminate tube:

A) Experimental water leakage during the experimental test,

B) Digital microscope for the leakage area.

SEM micrographs of the symmetrical KF/epoxy laminates as shown in figure 5.21 that have several combination of failure modes such as fiber pullout, delamination, cohesive failure and some voids.

Figure (5.21 a) shows the delamination generated in the fiber/matrix interface.

Also interfacial crack propagation that can avoid the force to be transferred in a properly way, generating a matrix debonding, which finally

pull out Kevlar fibers in addition to some pulled-out fibers from epoxy matrix, fiber pullout represented by the formation of holes (empty spaces) in the laminate during loading condition as shown in Figure (5.21 b).

The Figure (5.21 c and d) show the predominant failure mode is the cohesive failure occurs when a layer of adhesive remains on fiber surfaces.

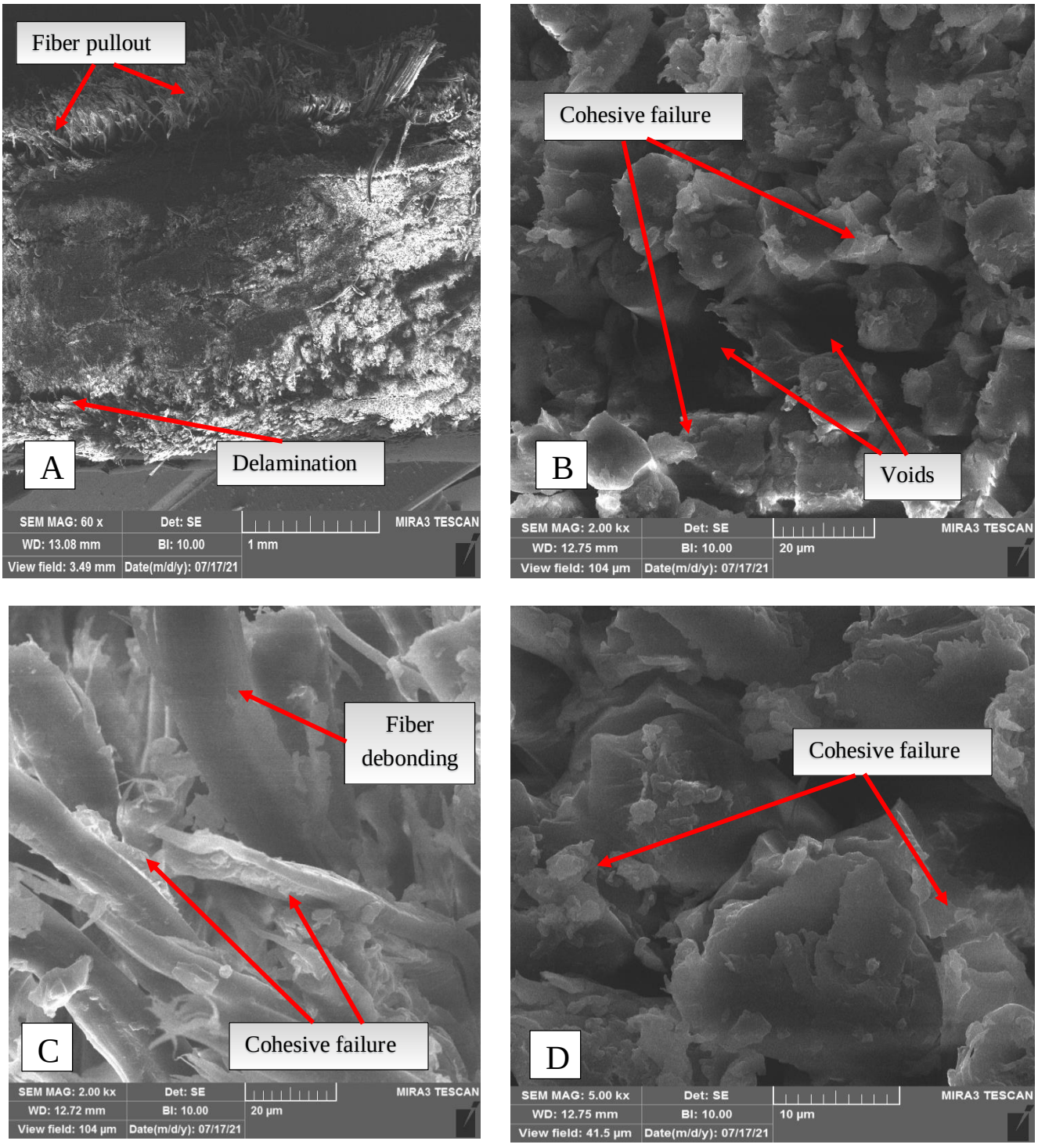

5.21: SEM of symmetrical KF/epoxy laminate.

Figure 5.22 represents the water leakage $[\pm 55°_3]$GF/epoxy during experimental burst pressure test and the digital microscope for the leakage area where it show that the average diameter of the crack is 0.055 mm.

It can be seen that $[\pm 55°_3]$GF/epoxy has the smallest crack diameter of glass reinforced laminates.

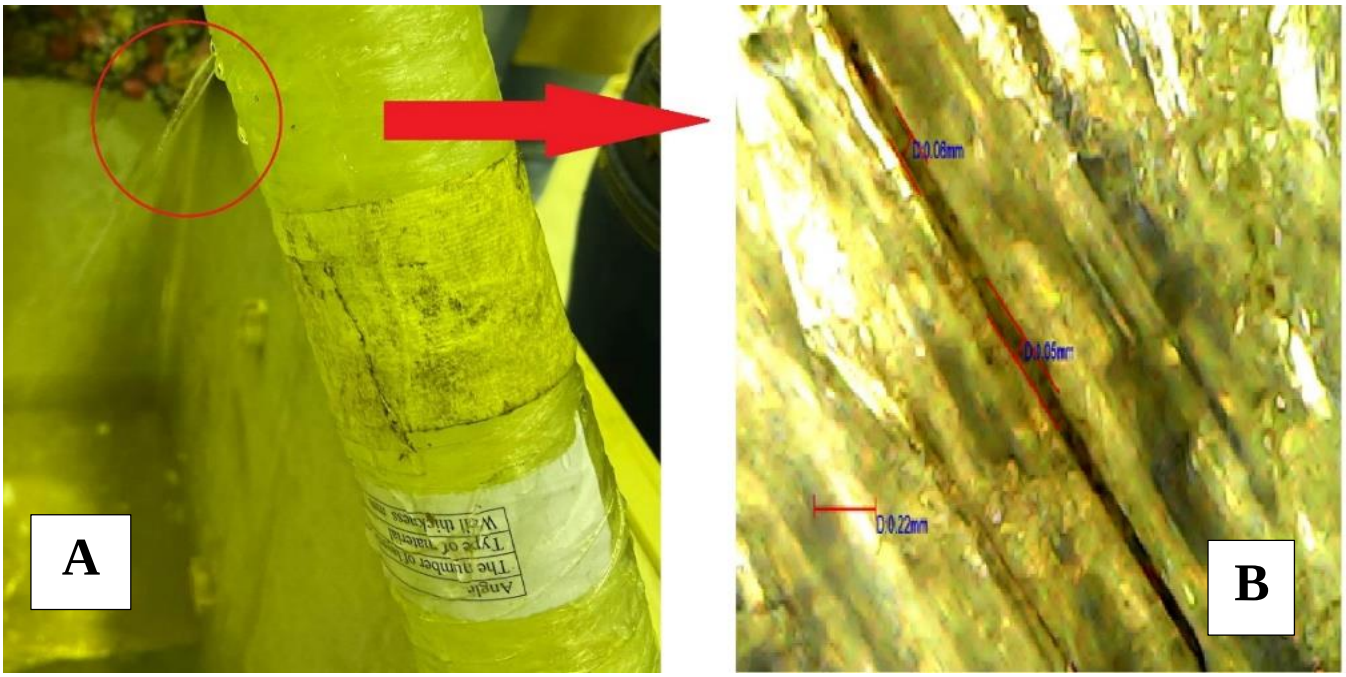

Figure 5.22: water leakage of $[\pm 55°_3]$GF/epoxy laminate tube:
A) Experimental water leakage during the experimental test,
B) Digital microscope for the leakage area.

Figure 5.23 represents the scanning electron microscope of $[\pm 55°_3]$ GF/epoxy laminate which show deferent failure modes like fiber pullout, cohesive failure, delamination and fiber breakage.

From figure 5. 23 (a) It can be seen that delamination extend along the laminate interface.From figure 5. 23 (b and c) show a combination of cohesive failure that appears as matrix fragments adhere to the fibers. It can be also seen from figure 5. 23 (b and c), that large number of glass fiber breakage occurred at stresses exceeding the strength of the weakest fiber in addition to the brittleness of the glass fibers.

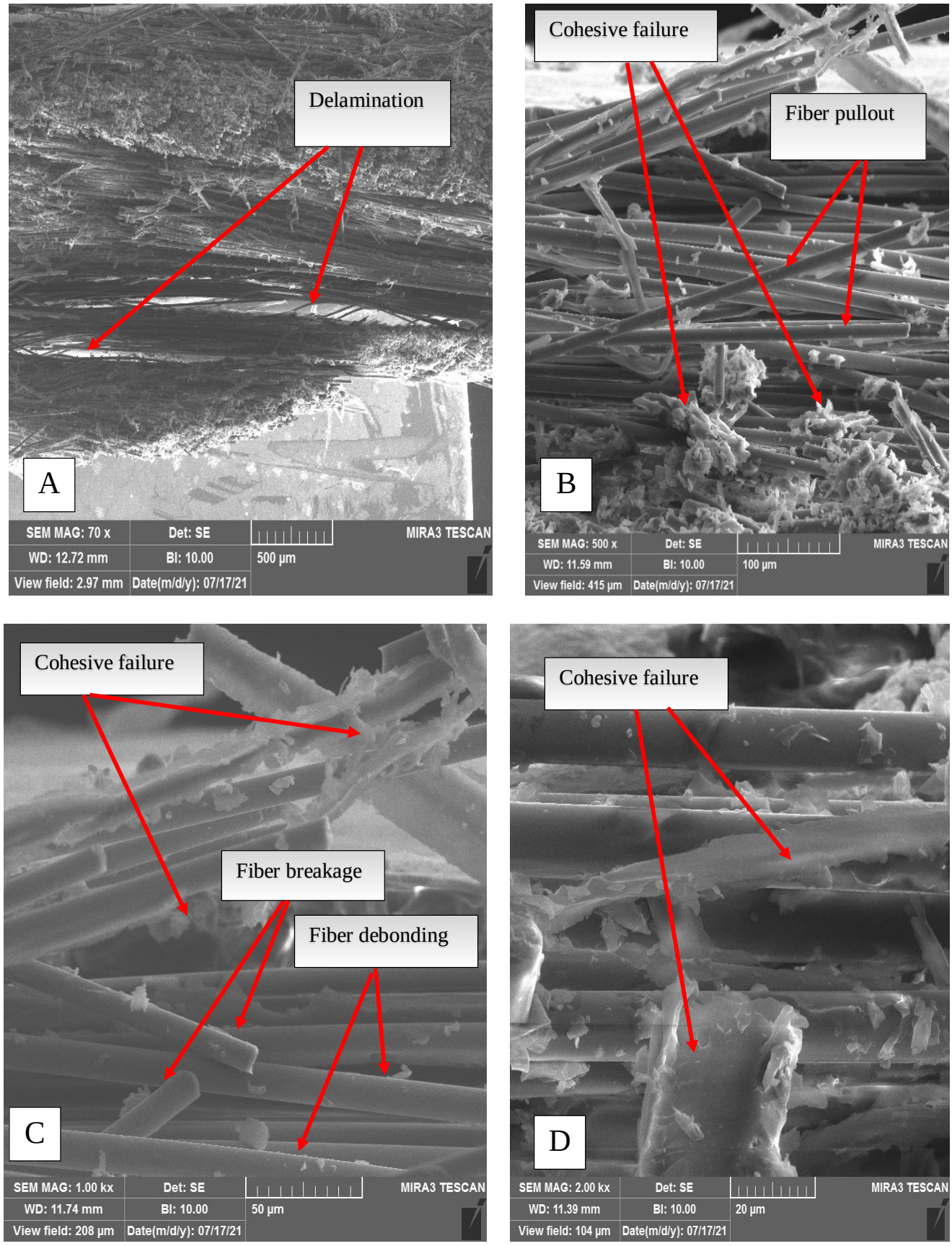

Figure 5.23: Scanning electron microscopy of $[\pm 55°_3]$ GF/Epoxy laminate.

Figure 5.24 represents the water leakage during experimental burst pressure test and the digital microscope for the leakage area where it show a considerable large crack with average diameter of 0.155 mm.

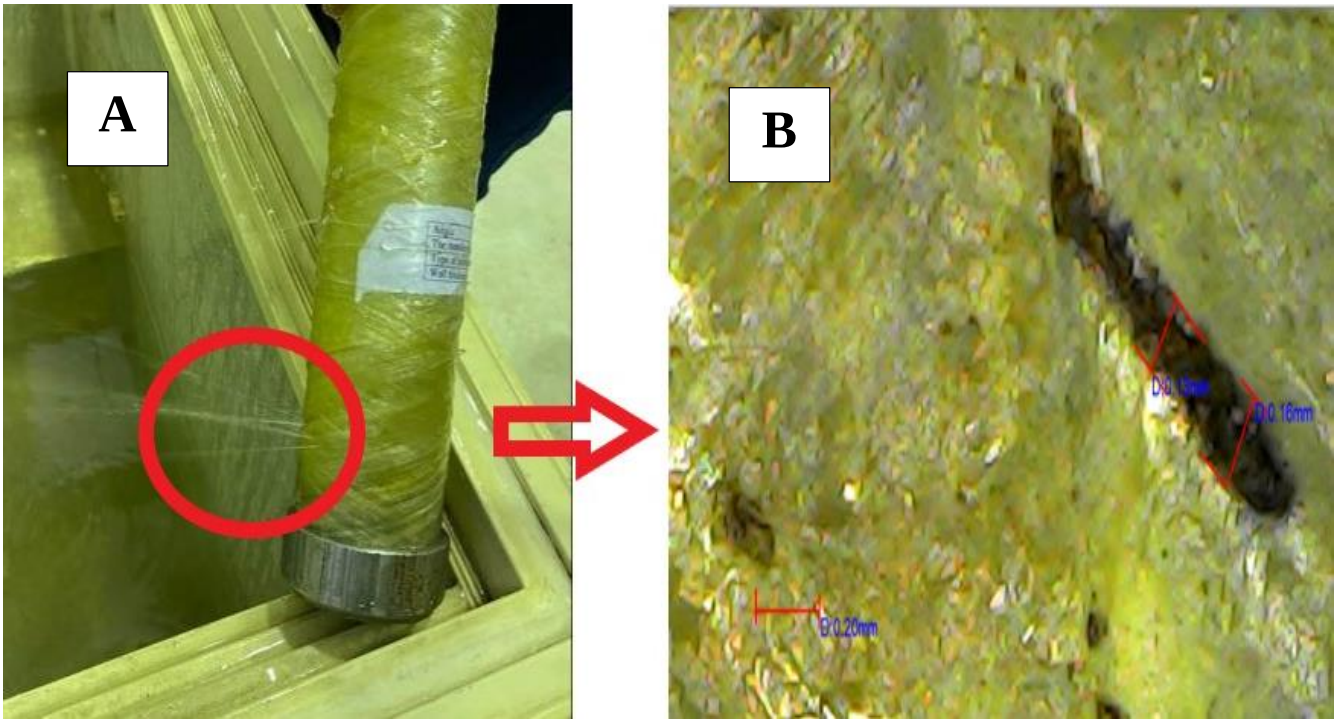

Figure 5.24: Failure of $[\pm 65°_3]$GF/epoxy laminate tube.

A) Experimental water leakage during the experimental test,

B) Digital microscope for the leakage area.

Figure 5.25 represents the $[\pm 65°_3]$ GF/epoxy laminates where show failure modes that are fiber pullout, cohesive fracture in the matrix, cohesive failure and some fiber breakage. From Figure 5.25 (a) it can be seen that smaller resin-rich zones were also formed within the composite this is can be attributed to the relocation of the glass fibers' during the curing process. Some glass fiber breakage occurred at stresses exceeding the strength of the weakest fiber. An isolated fiber break caused stress concentration on the interface around the tip of the broken fiber as shown in figure 5.25 (b).

Moreover, matrix fragments around the individual fibers referred to cohesive failure of the fiber/matrix interface as shown in figure 5.25 (b, c and d).

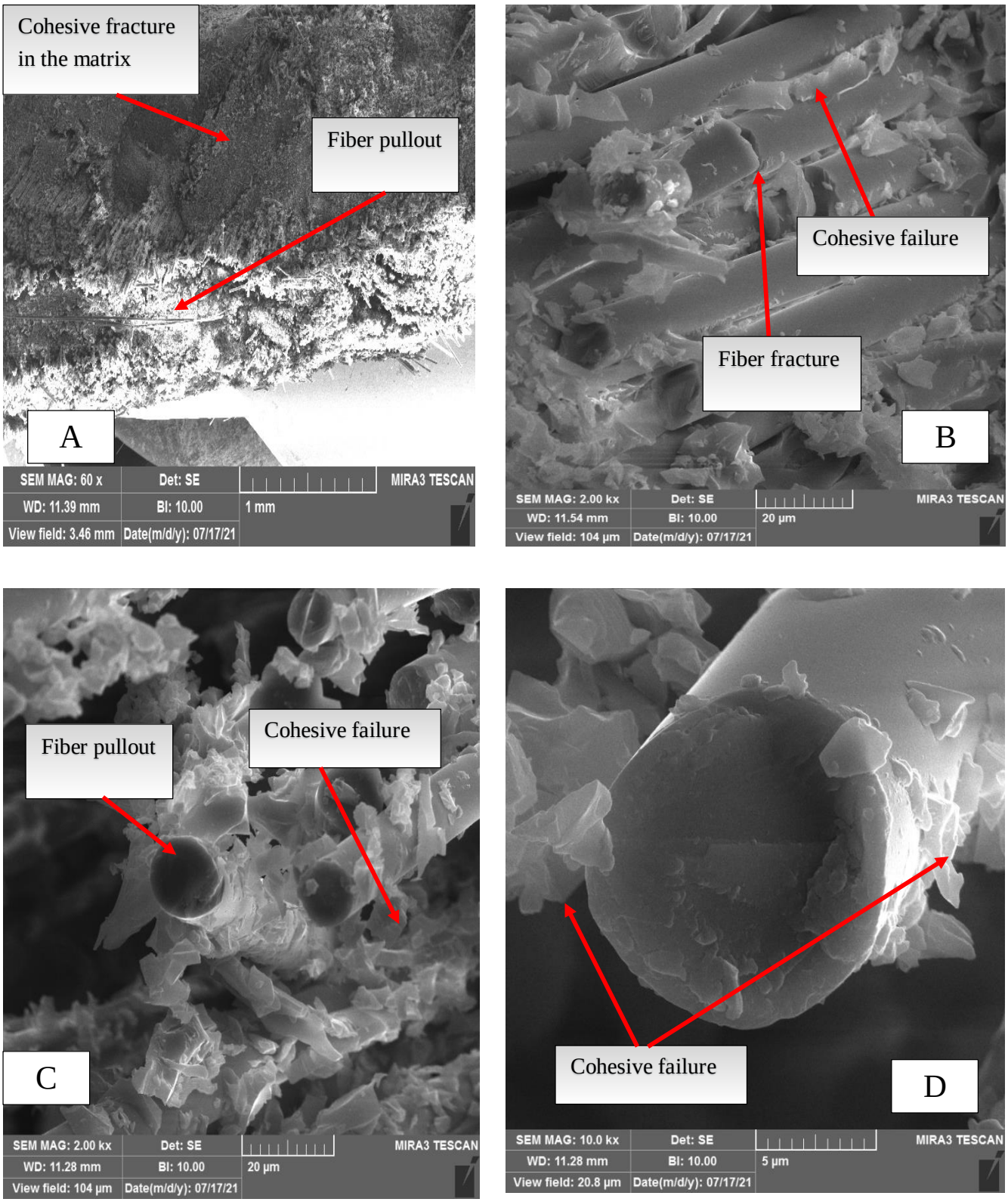

Figure 5.25: Scanning electron microscopy of $[\pm 65°_3]$ GF/epoxy laminate.

Figure 5.26 represents the water leakage $[\pm 75°_3]$ GF/epoxy during experimental burst pressure test and the digital microscope for the leakage area where it show that the surface exhibited surface burst where the initiation of the crack, crack propagation and surface burst in $[\pm 75°_3]$ GF/epoxy concentrated at a single point resulting in a stress concentration around the crack. SEM support this conclusion as shown in Figure 5.26 where large number of glass fibers experienced breakage.

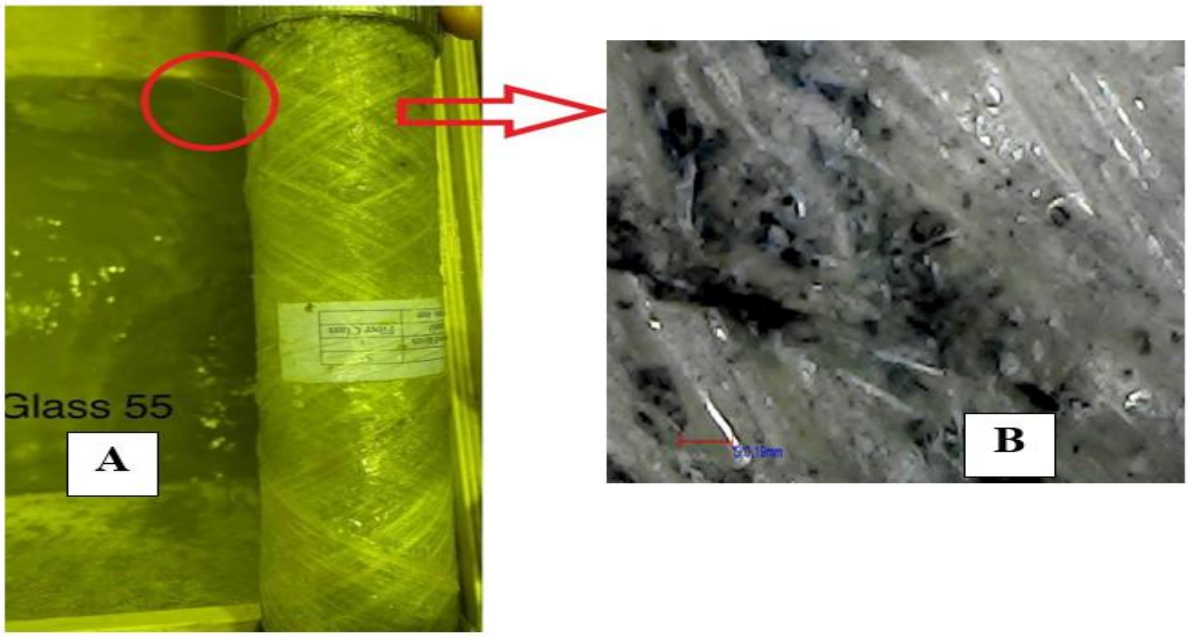

Figure 5.26: Failure of $[\pm 75°_3]$ GF/epoxy laminate tube
A) Experimental water leakage during the experimental test,
B) Digital microscope for the leakage area.

Figure 5.27 shows a SEM image of $[\pm 75°_3]$ GF/epoxy laminate which show several failure modes that are delamination, fiber pullout, cohesive failure and cohesive fracture in the matrix.

Figure 5.27 a show a delamination in two areas along the interface of the fiber/matrix that results from the pressure load exerted on composite laminate that exceeds the interlaminar strength of the laminate.

Figure 5.27 (b and c) show pullout of the fibers, fiber pullout results from fiber failure along the debonding length, so that the fiber will pull-out.

Figure (5.27 c and d) shows cohesive failure of the interface occurs due to the interface between glass fiber and epoxy is not strong enough and it can be noticed from the few pieces of matrix adhered to the fibers.

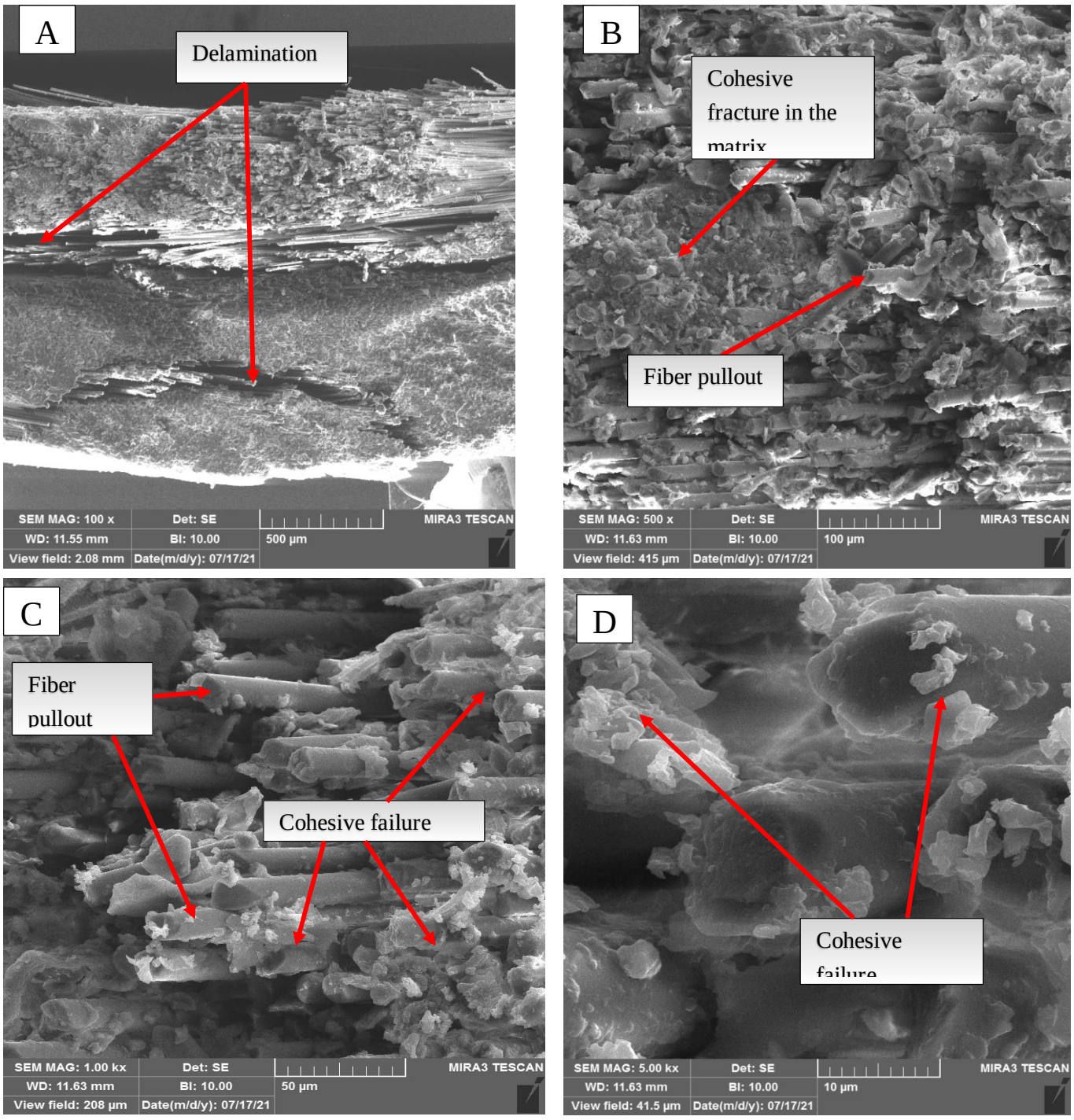

Figure 5.27: Scanning electron microscopy of $[\pm 75°_3]$ GF/epoxy laminate.

5.8 Mechanical Behavior:

5.8.1 Hardness Results:

Figure 5.28 shows the hardness property of the epoxy, CF/epoxy KF/epoxy and GF/epoxy laminates. The results show the values of hardness of epoxy increased when reinforcing with fibers because of the alignment fibers helps to distribute the load uniformly in the epoxy matrix which makes helps in controlling the load transmission from the epoxy matrix to the fibers in the interface region.

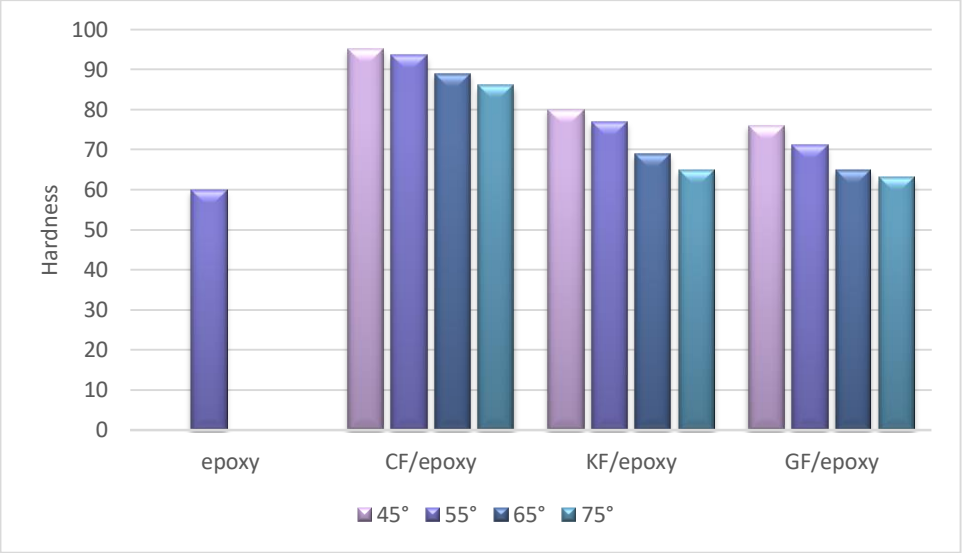

Figure 5.28: Hardness of CF/epoxy, KF/epoxy and GF/epoxy laminates.

Also it can be seen that the CF/epoxy and KF/epoxy laminates have high hardness strength owing to the high hardness values of the carbon fibers and Kevlar fibers.

Hardness of epoxy has best improvement 58.3% when reinforcing CF/epoxy with [±55°$_3$] angle orientation.

It can be said that hardness had closed values with the symmetrical stacking sequence (figure 5.29).

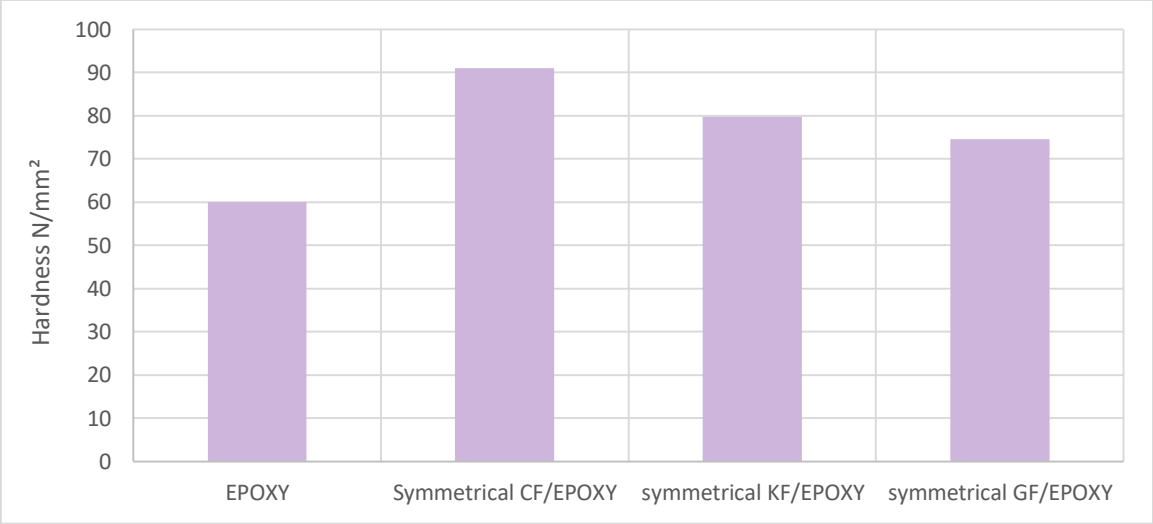

Figure 5.29: Hardness of symmetrical CF/epoxy, KF/epoxy and GF/epoxy laminates.

5.8.2 Ring Stiffness

The ring stiffness test is conducted for estimating the stiffness of epoxy, CF/epoxy, KF/epoxy and GF/epoxy laminates to analyze the effect of reinforcing fiber types, fiber orientations and symmetry. Figure 5.30 represents ring stiffness of epoxy, CF/epoxy, KF/epoxy and GF/epoxy laminates.

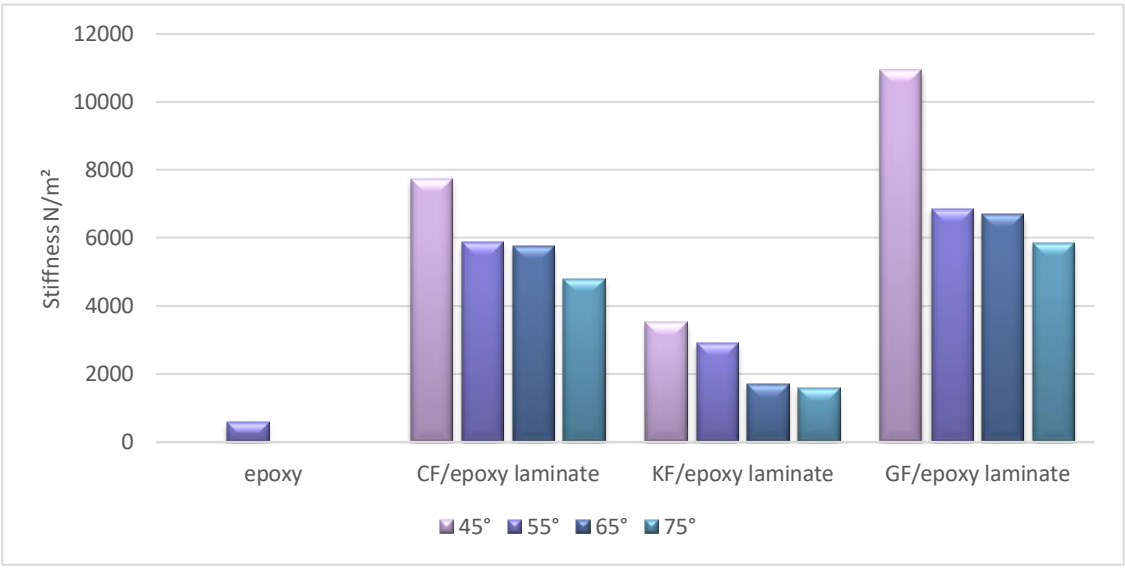

Figure 5.30: Ring stiffness of epoxy, CF/epoxy, KF/epoxy and GF/epoxy laminates.

Figure 5.30 shows variation of ring stiffness of different fiber orientation of epoxy, CF/epoxy, KF/epoxy and GF/epoxy laminates. Even the limit of compression of 3% and 15% of its original diameter, the epoxy and the composite laminates show no sign of crazing, wall cracking, wall delamination, and rupture. Instead, it absorbed all the forces, when it was completely compressed, quite interesting to note down that it regained its original shape after the load was removed.

5.8.2.1 Effect of Reinforcing Fiber Types:

It can be seen there is a difference in ring stiffness of the composite laminates. From figure 5.30 it was observed that GF/epoxy and CF/epoxy laminates exhibited the highest stiffness and peaks load when compared to the KF/epoxy laminates and they suffered less deflection. However, GF/epoxy experiment cracking sound appears during the examination due to the brittle nature of glass fibers.

The epoxy ring stiffness values has higher improvement 1768.3% with GF/epoxy with [±55°₃] angle orientation.

5.8.2.2 Effect of Fiber Orientation:

Winding angle plays a significant role in determining stiffness of the pipe as in figure 5.30. The winding angle is to be kept at intermediate levels of the range as it is seen that winding angles closer to hoop winding $[\pm 45°_3]$ and $[\pm 55°_3]$ tend to produce higher hoop strength thereby high pipe stiffness value is observed. The stiffness decreased with increasing winding angle $[\pm 65°_3]$ and$[\pm 75°_3]$.

The highest stiffness value is for GF/epoxy laminates with fiber orientations of $[\pm 45°_3]$ exhibited the highest stiffness value of 10943.9 N/m².

5.8.2.3 Effect of Symmetry:

Figure 5.31 represents the stiffness of epoxy, CF/epoxy, KF/epoxy and GF/epoxy laminates. It was very interesting to note down that during the stiffness test, there was no sign of rupture and cracking. Eventually, the symmetrical tubes regains its original shape and size.

The symmetrical laminates show higher stiffness value compared with the individual laminates. The GF/epoxy laminates show the highest value of ring stiffness 24435.16 N/m² accompanied by cracking sound during the test. CF/epoxy also show high results 11414.73 N/m² while Symmetrical KF/epoxy show the lowest ring stiffness 3253.21 N/m² and, this can be attributed to that the interfaces between the plies provide lesser number of delamination prone interfaces of symmetric laminates.

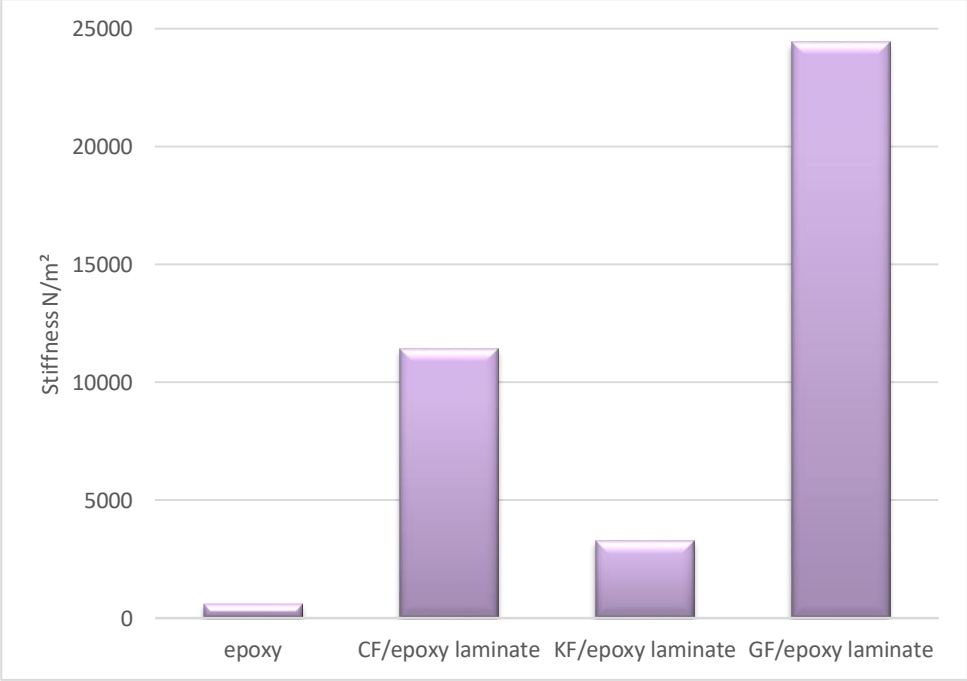

Figure 5.31: Ring stiffness of epoxy and symmetrical CF/epoxy, KF/epoxy and GF/epoxy laminates.

5.9 Failure Detection Results

5.9.1 Ultrasonic Wave Velocity:

The ultrasound wave velocity test helps in detection of cracks or defects in the internal structure. Figure 5.32 to 5.47 represents the variation of ultrasound velocity of epoxy, CF/epoxy, KF/epoxy and GF/epoxy laminates before and after the burst pressure test. The ultrasound velocity as calculated from (eq. 4.5) admits the determination and detection of deformation and cracks with different orientations.

The results of ultrasonic wave velocity of epoxy and composite laminates before burst pressure test showed that the calculated ultrasonic velocity in the longitudinal and transverse directions have close values which referring to the homogeneity in all points of the tube samples with no recording for voids or fiber-empty places. This homogeneity appears as very simple fluctuation in the wave velocity peaks so the failure could be anywhere in the tube since no recording of poor or defect region.

Distinct fluctuation in ultrasonic wave velocity can be observed after the burst pressure test where the signal weakened each time they passed through the fibers layer due to formation of cracks caused by internal pressure loading which reduced the ability to detect defects in the deeper layers.

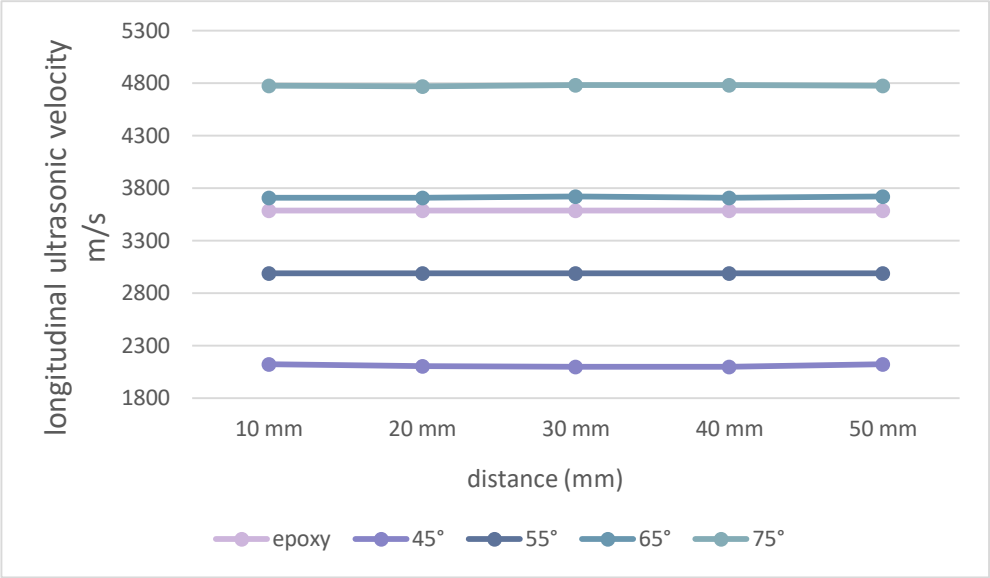

Figure 5.32: Variation of longitudinal velocity of epoxy, $[\pm 45°_3]$, $[\pm 55°_3]$, $[\pm 65°_3]$ and $[\pm 75°_3]$ CF/epoxy laminates before burst pressure.

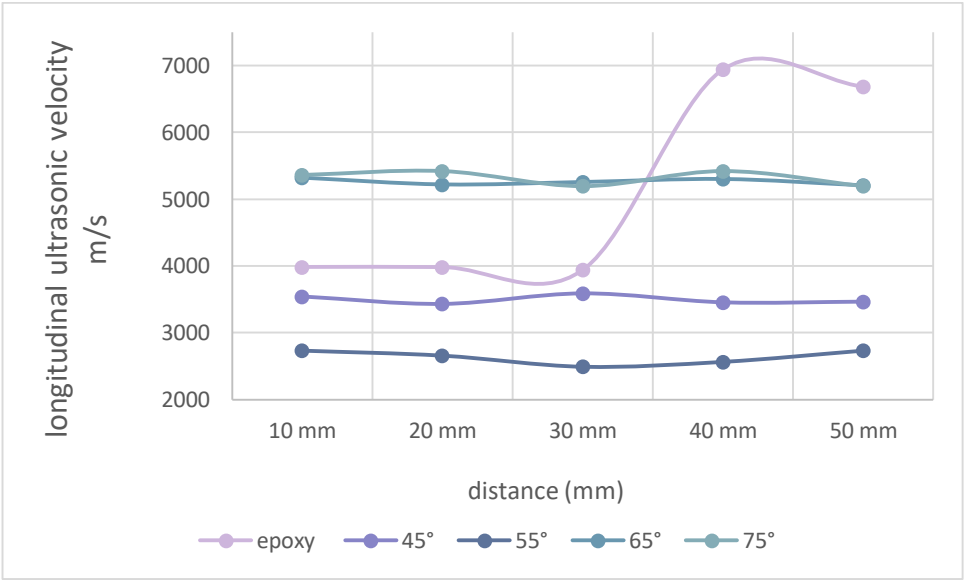

Figure 5.33: Variation of longitudinal velocity of epoxy, $[\pm 45°_3]$, $[\pm 55°_3]$, $[\pm 65°_3]$ and $[\pm 75°_3]$ CF/epoxy laminates after burst pressure.

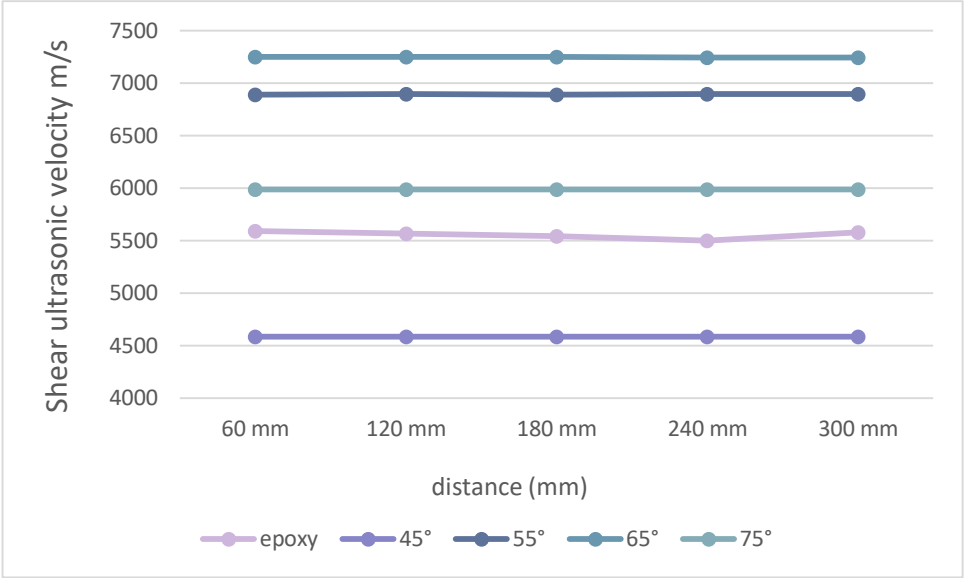

Figure 5.34: Variation of shear velocity of epoxy, $[\pm 45°_3]$, $[\pm 55°_3]$, $[\pm 65°_3]$ and $[\pm 75°_3]$ CF/epoxy laminates before burst pressure.

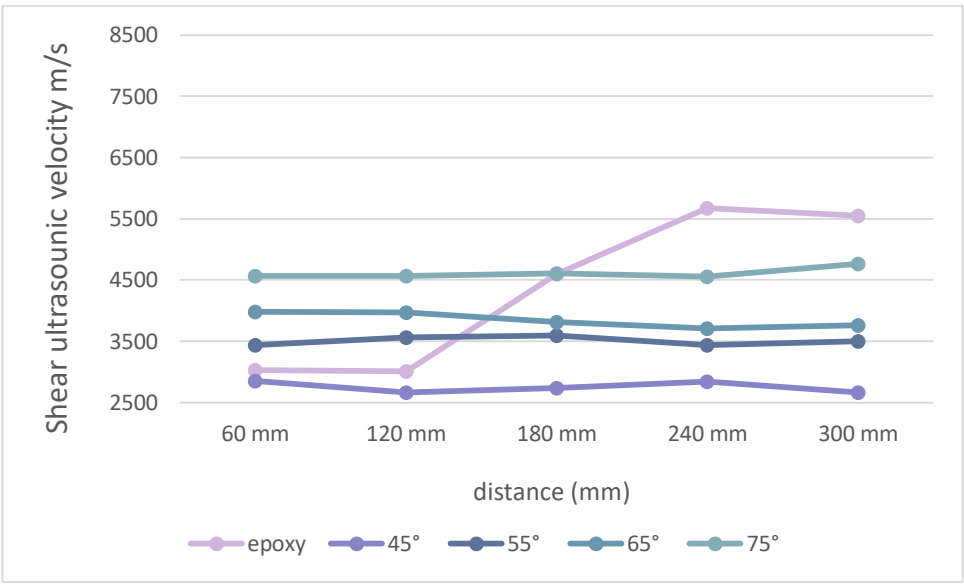

Figure 5.35: Variation of shear velocity of epoxy, $[\pm 45°_3]$, $[\pm 55°_3]$, $[\pm 65°_3]$ and $[\pm 75°_3]$ CF/epoxy laminates after burst pressure.

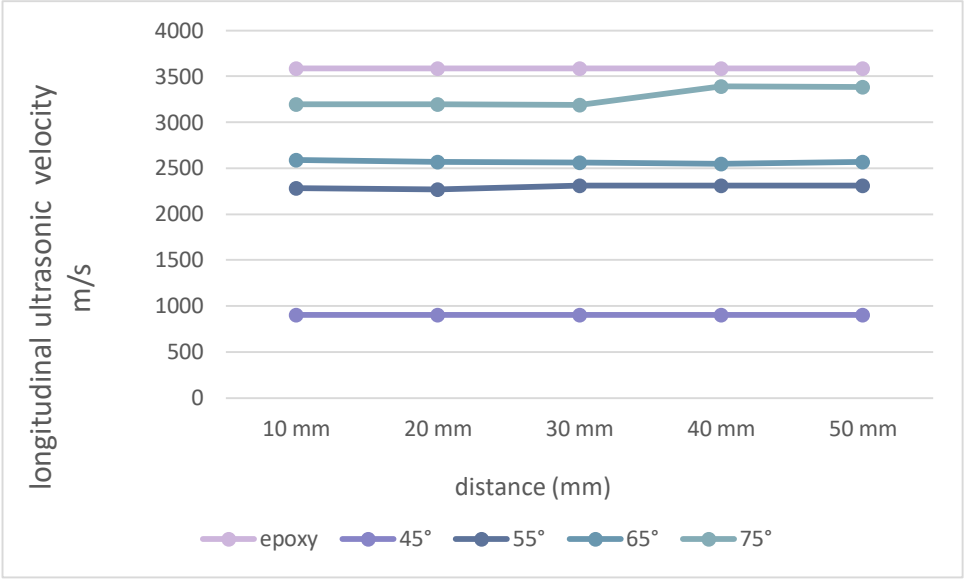

Figure 5.36: Variation of longitudinal velocity of epoxy, $[\pm 45°_3]$, $[\pm 55°_3]$, $[\pm 65°_3]$ and $[\pm 75°_3]$ KF/epoxy before burst pressure.

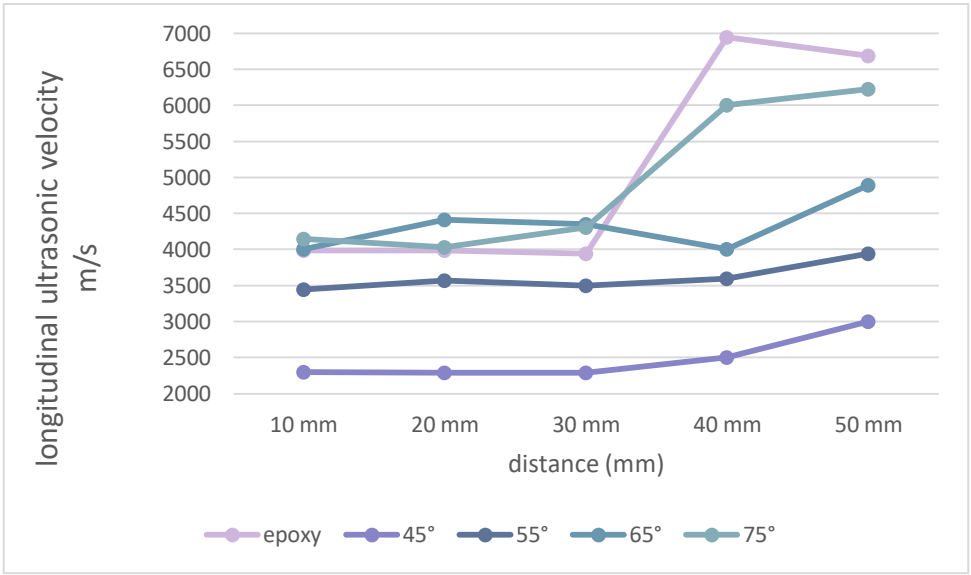

Figure 5.37: Variation of longitudinal velocity of epoxy, $[\pm 45°_3]$, $[\pm 55°_3]$, $[\pm 65°_3]$ and $[\pm 75°_3]$ KF/epoxy laminates after burst pressure.

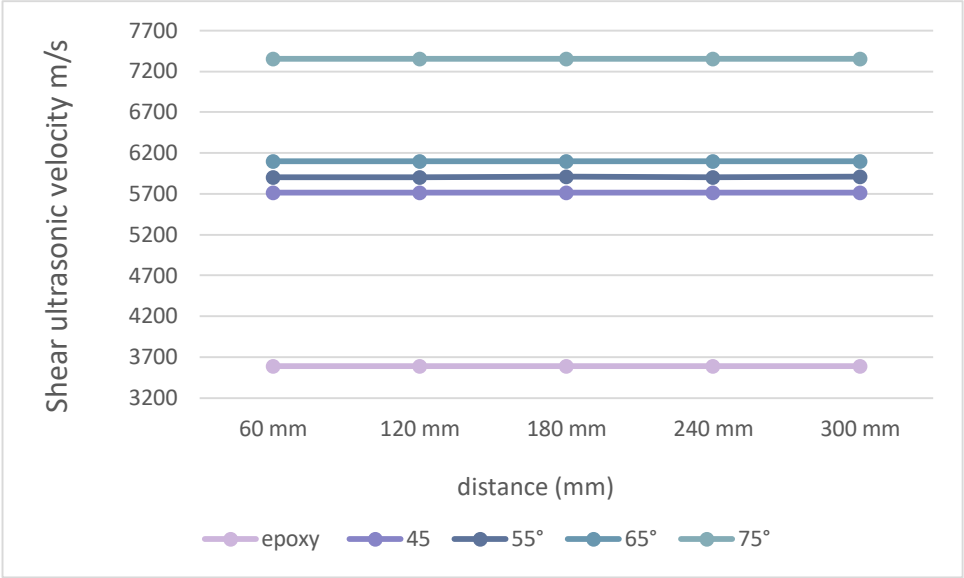

Figure 5.38: Variation of shear velocity of epoxy, $[\pm 45°_3]$, $[\pm 55°_3]$, $[\pm 65°_3]$ and $[\pm 75°_3]$ KF/epoxy laminates before burst pressure.

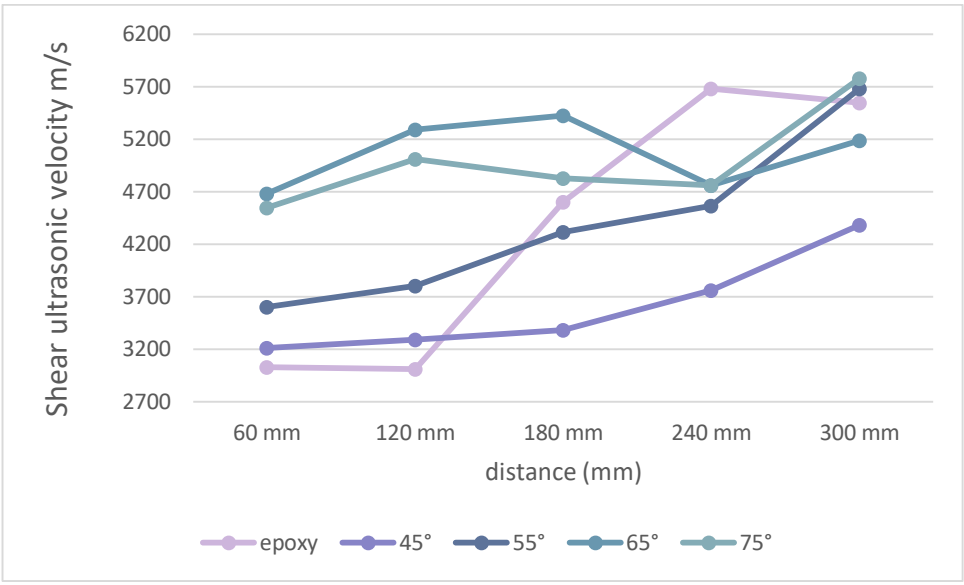

Figure 5.39: Variation of shear velocity of epoxy, $[\pm 45°_3]$, $[\pm 55°_3]$, $[\pm 65°_3]$ and $[\pm 75°_3]$ KF/epoxy laminates after burst pressure.

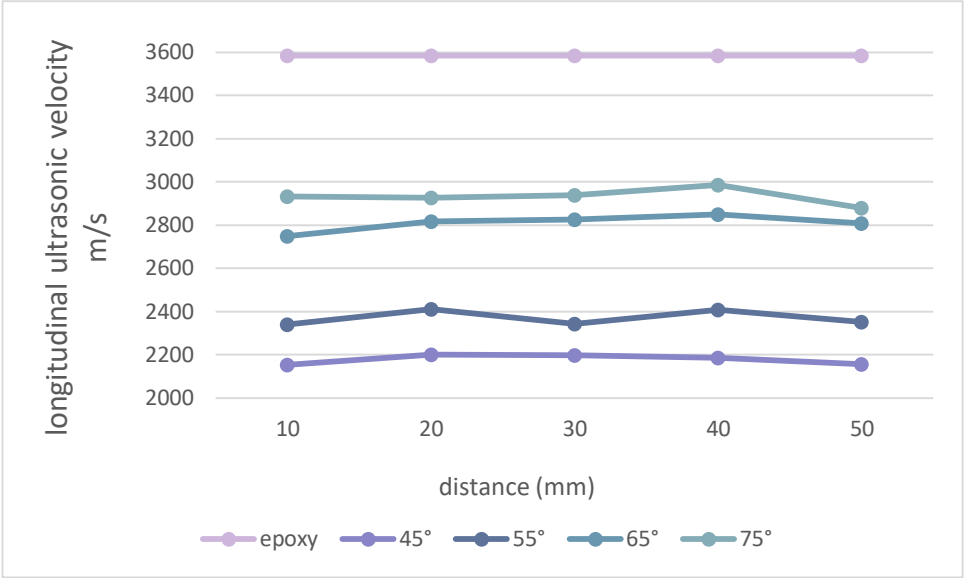

Figure 5.40: Variation of longitudinal velocity of epoxy, $[\pm 45°_3]$, $[\pm 55°_3]$, $[\pm 65°_3]$ and $[\pm 75°_3]$ GF/epoxy laminates before burst pressure.

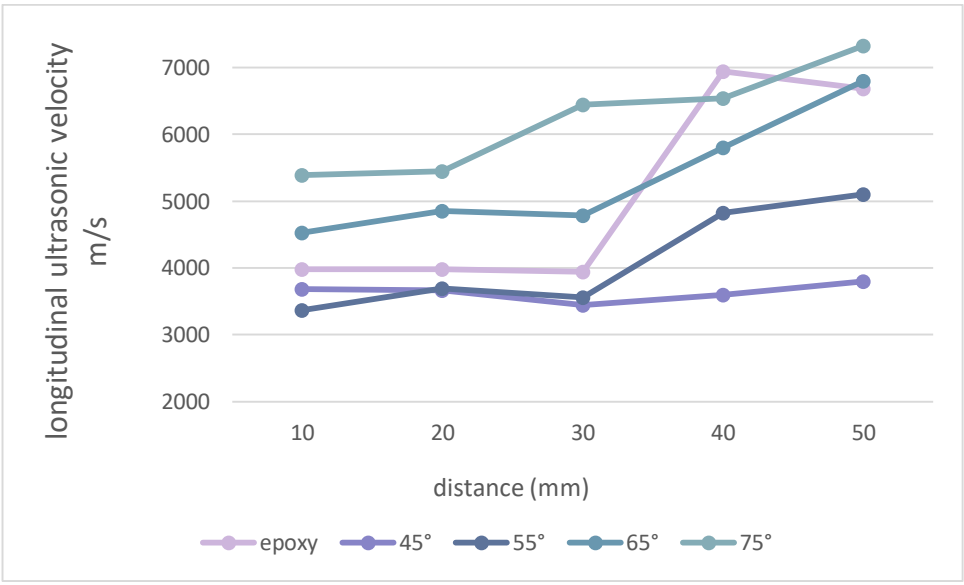

Figure 5.41: Variation of longitudinal velocity of epoxy, $[\pm 45°_3]$, $[\pm 55°_3]$, $[\pm 65°_3]$ and $[\pm 75°_3]$ GF/epoxy laminates after burst pressure.

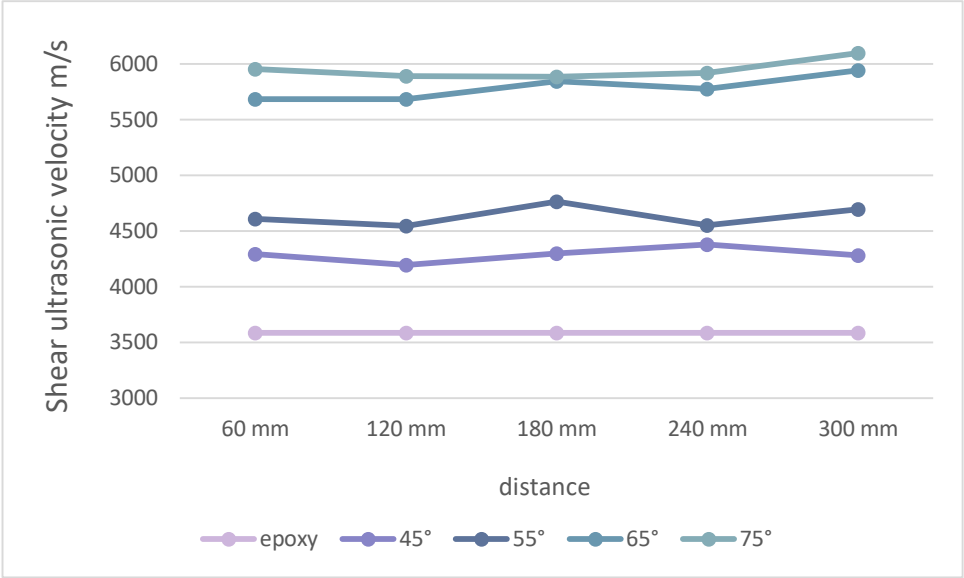

Figure 5.42: Variation of shear velocity of epoxy, $[\pm 45°_3]$, $[\pm 55°_3]$, $[\pm 65°_3]$ and $[\pm 75°_3]$ GF/epoxy laminates before burst pressure.

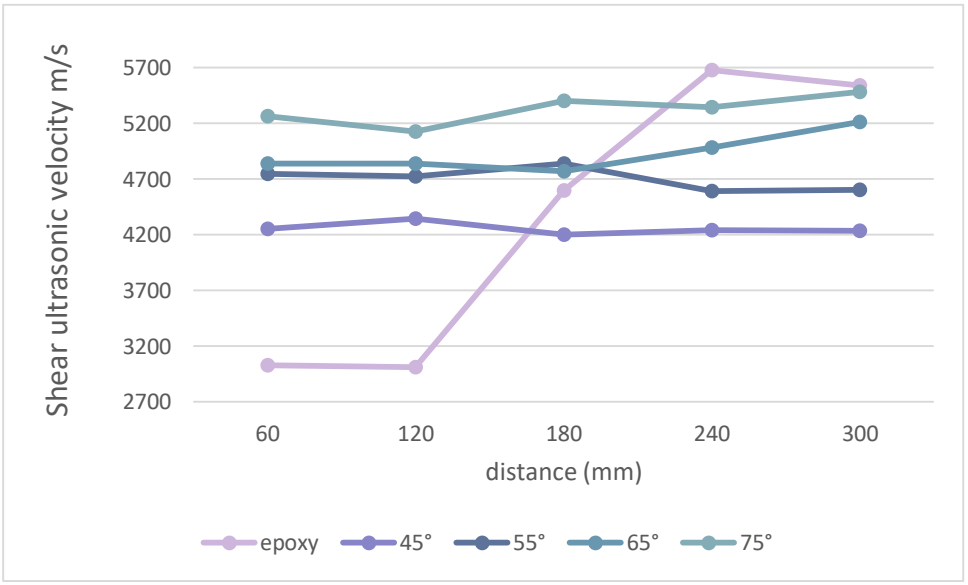

Figure 5.43: Variation of shear velocity of epoxy, $[\pm 45°_3]$, $[\pm 55°_3]$, $[\pm 65°_3]$ and $[\pm 75°_3]$ GF/epoxy laminates after burst pressure.

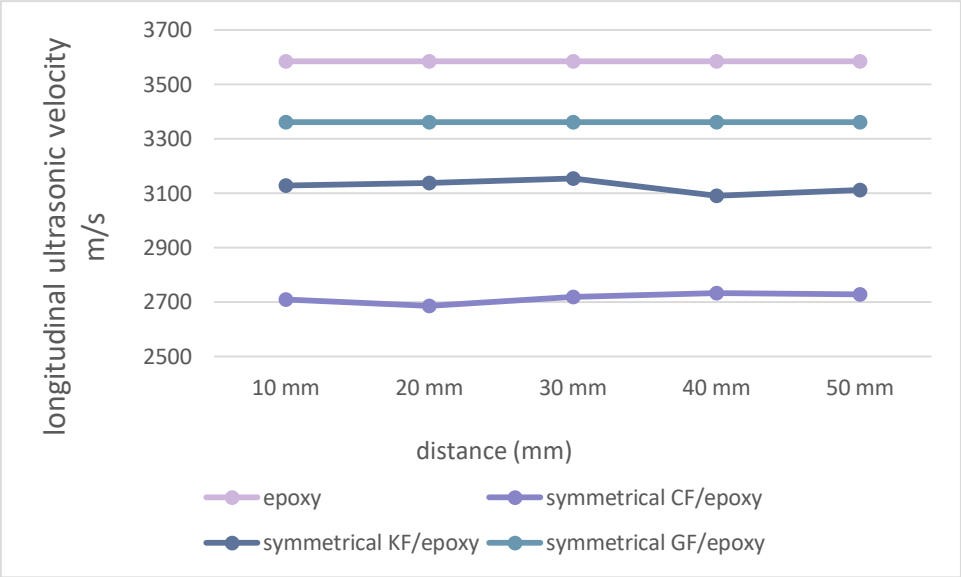

Figure 5.44: Variation of longitudinal velocity of symmetrical composite laminate before burst pressure

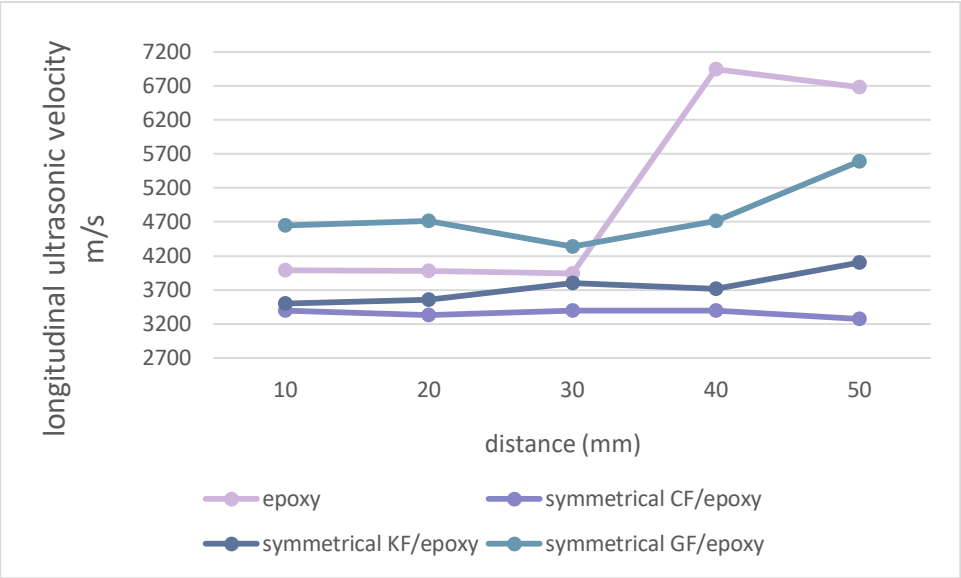

Figure 5.45: Variation of longitudinal velocity of symmetrical composite laminate after burst pressure.

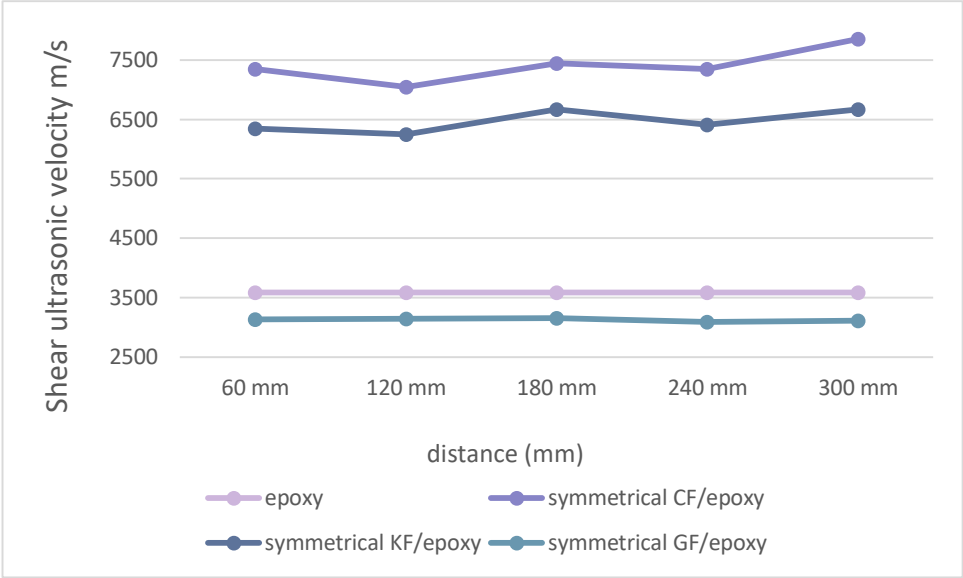

Figure 5.46: Variation of shear velocity of symmetrical composite laminate before burst pressure.

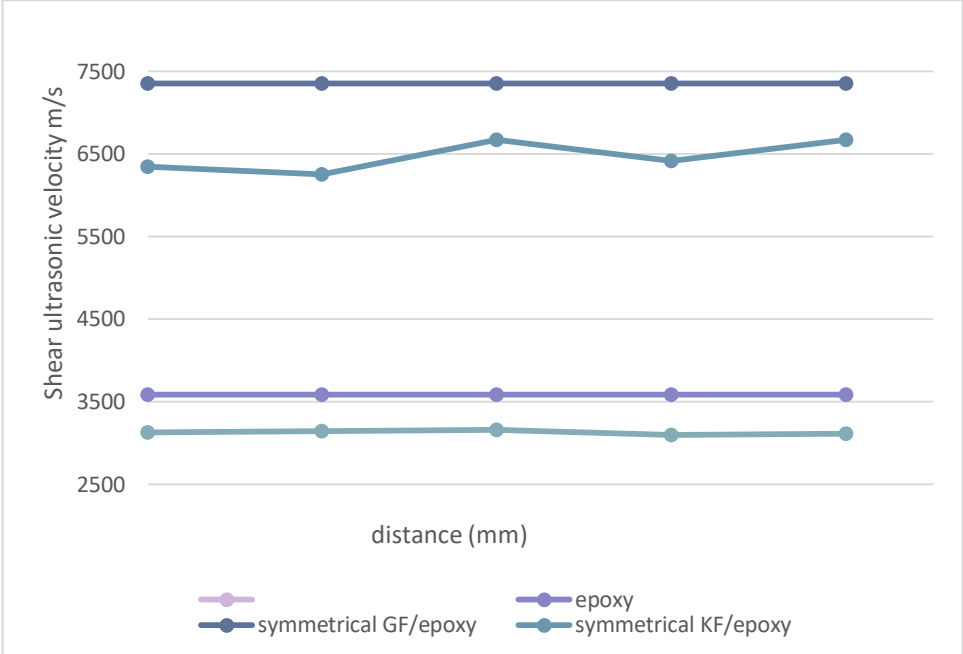

Figure 5.47: Variation of shear velocity of symmetrical composite laminate after burst pressure.

It can be noticed that the velocity increased after internal pressure loading test for epoxy, CF/epoxy, KF/epoxy and GF/epoxy laminates due to changing of density due to formation of cracks forming during burst pressure test. In addition, decreasing the travel path that demands less time for the wave to reach to the opposite probe and that's refers to existence of cracks. The crack inception appear as velocity variation of the detectable sample as shown in variation of longitudinal and shear velocity after burst pressure test.

Epoxy tube exhibited a sharp change of the wave velocity due to obvious fracture fragmentations.

Other problems arise from different combination of the layered structure since they are combination of alternating layers structure having different thickness, elastic properties and density. At each interface partial reflection and partial transmission of the constituents take place. So that the reflectivity and the transmissivity of layer's interface are affected on the ultrasonic wave response of the layered structure since multi interfaces produces large number of echoes because of multiple interference and reflections effects can be occurred.

The glass fibers have high reflectivity of the ultrasonic signal and the signal is scattered and attenuated. The glass fibers content in these samples is 75 wt. %, which produce more intense echoes since glass fiber could have some broken filaments which make variation in density along the travel path. In general, it's is more difficult to detect defects in GF/epoxy laminates due to the high reflectivity of glass fibers, this appears as fluctuation in the velocity even before internal pressure loading test.

It can be mentioned that although the ultrasonic wave velocity technique gives a remarkable information about defects existence. However, it could not determine the exact size and shape of the defects.

5.9.2 X-ray CT Scan

A medical X-ray CT scan is utilize to provide a volumetric map throughout the thickness of the specimen. Figure 5.48 represents the X-ray CT Scan of epoxy tube after burst pressure test where the fracture is distinctly appeared due to large fracture area.

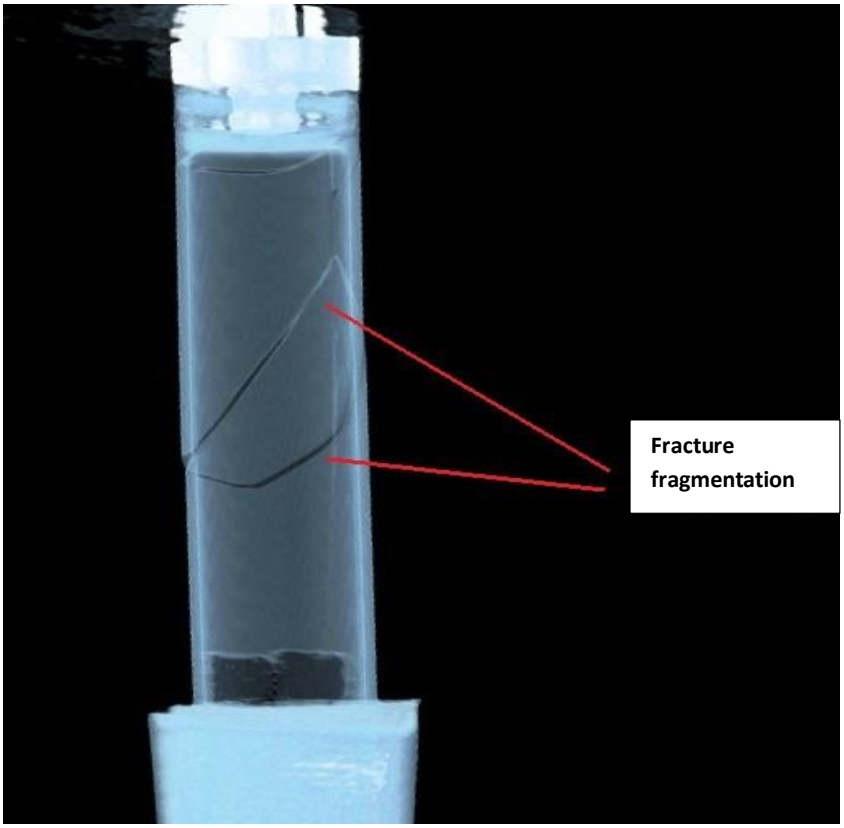

Figure 5.48: X-ray CT scan of epoxy tube.

Figure 5.49 shows the X-ray CT scan of GF/epoxy laminate with winding angle $[\pm 45°_3]$, $[\pm 55°_3]$ $[\pm 65°_3]$ and $[\pm 75°_3]$ respectively.

It can be seen that the GF/epoxy laminate have a clear scanning due to the rather large density difference between the glass fibers (1.92 g/mm^3) and the epoxy matrix (1.1 g/mm^3), the individual fibers are clearly visible in the X-ray CT scan data and can be segmented 3-dimensionally. Also it can be seen that the glass fibers appear as bright threads within the epoxy matrix. From the XCT figure it can be used to extract fiber orientation.

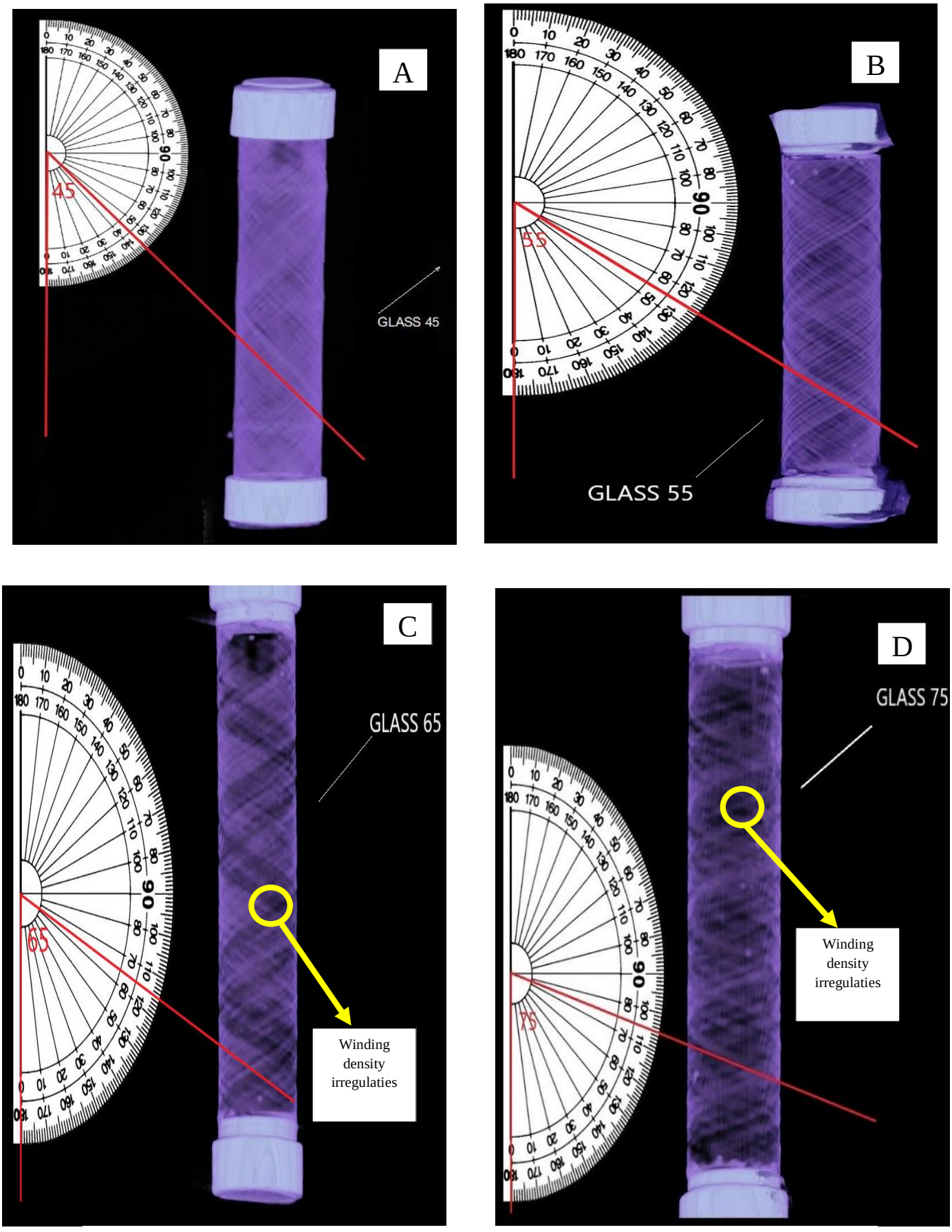

Figure 5.49: X-ray CT of GF/epoxy laminate.

A): $[\pm 45^{\circ}_3]$, B): $[\pm 55^{\circ}_3]$, C): $[\pm 65^{\circ}_3]$ and D): $[\pm 75^{\circ}_3]$

Figure 5.50 shows the X-ray CT-data three-dimensional of a CF/epoxy laminates with four different winding angles ($\pm 45°_3, \pm 55°_3$, $\pm 65°_3$ and $\pm 75°_3$).

Its worth to mention that the image contrast relies on the differences in the attenuation of X-rays paths between matrixes, fibers and damage (defects). In the case of X-ray CT, the contrast arises from the different between the linear attenuation coefficients of the constituents which related to material density, so that similar attenuation coefficients of carbon fiber and polymeric matrix make it difficult to provide sufficient information.

Some irregularities in winding density can be noticed in the filament wound composites this can be attributed to the possibility of movement of yarn guide moves slowly, some windings, rather than being merely very close to the previous ones, some windings will actually lie on top of them. The same result is obtained if the yarn guide moves fast, because initially there will be gaps left between the windings which subsequent windings fill in irregularly. These winding density irregularities can be seen in following CT scan results.

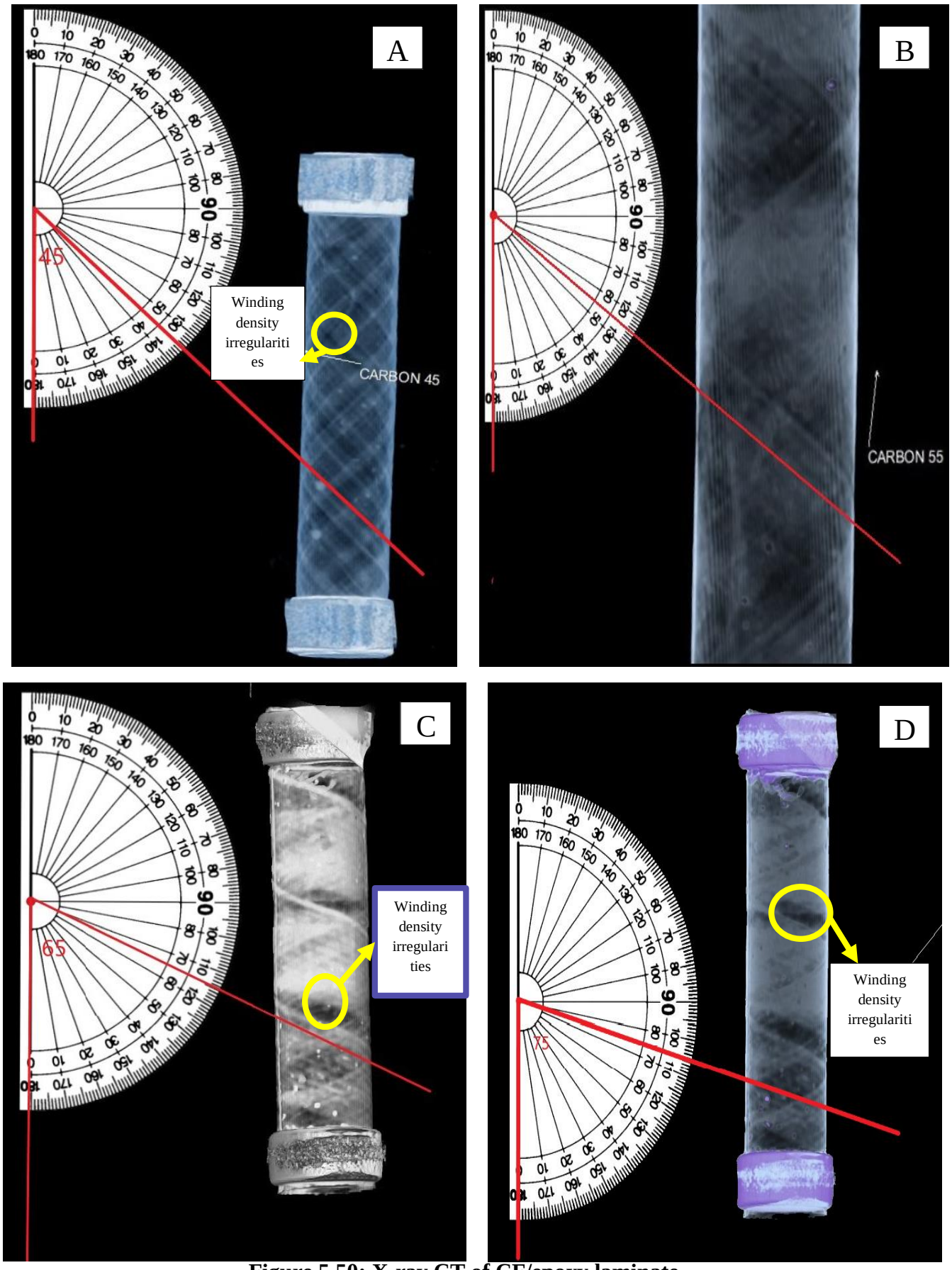

Figure 5.50: X-ray CT of CF/epoxy laminate.

A): $[\pm 45°_3]$, B): $[\pm 55°_3]$, C): $[\pm 65°_3]$ and D): $[\pm 75°_3]$

Figure 5.51 and 5.52 show the X-ray CT-data three-dimensional representation of KF/epoxy laminates with four different winding angles ($\pm 45°_3, \pm 55°_3, \pm 65°_3$ and $\pm 75°_3$). Due to the rather small density difference between the Kevlar fibers (1.44 g/cm³) and the epoxy matrix (1.1 g/cm³), the individual fibers are not clearly visible in the X-ray CT scan data. Also the high voltage of the X-ray tube reduced the contrast between the Kevlar fibers and the polymeric matrix of the scanned composites.

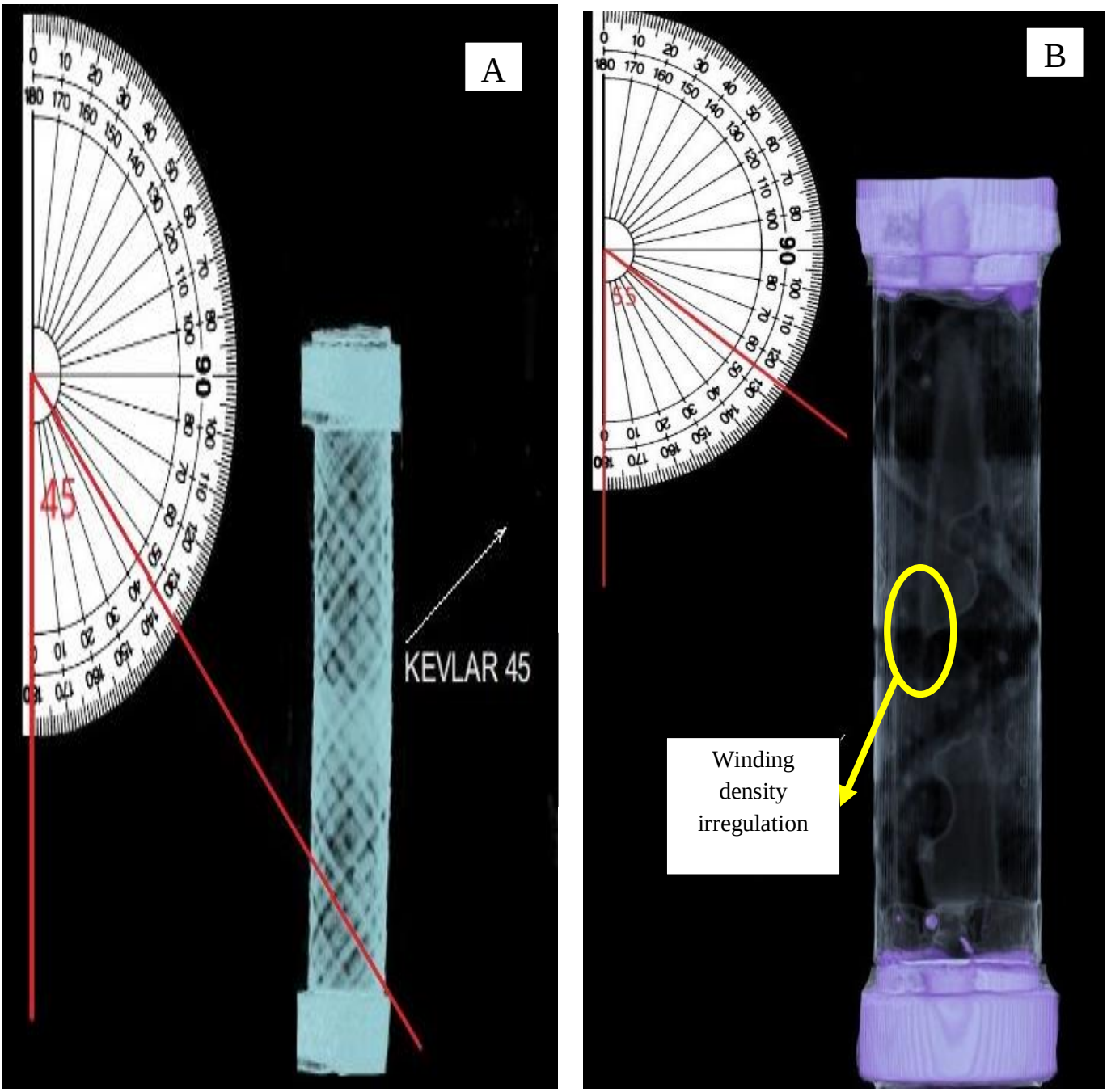

Figure 5.51: X-ray CT of A): $[\pm 45°_3]$, B): $[\pm 55°_3]$ KF/epoxy laminate.

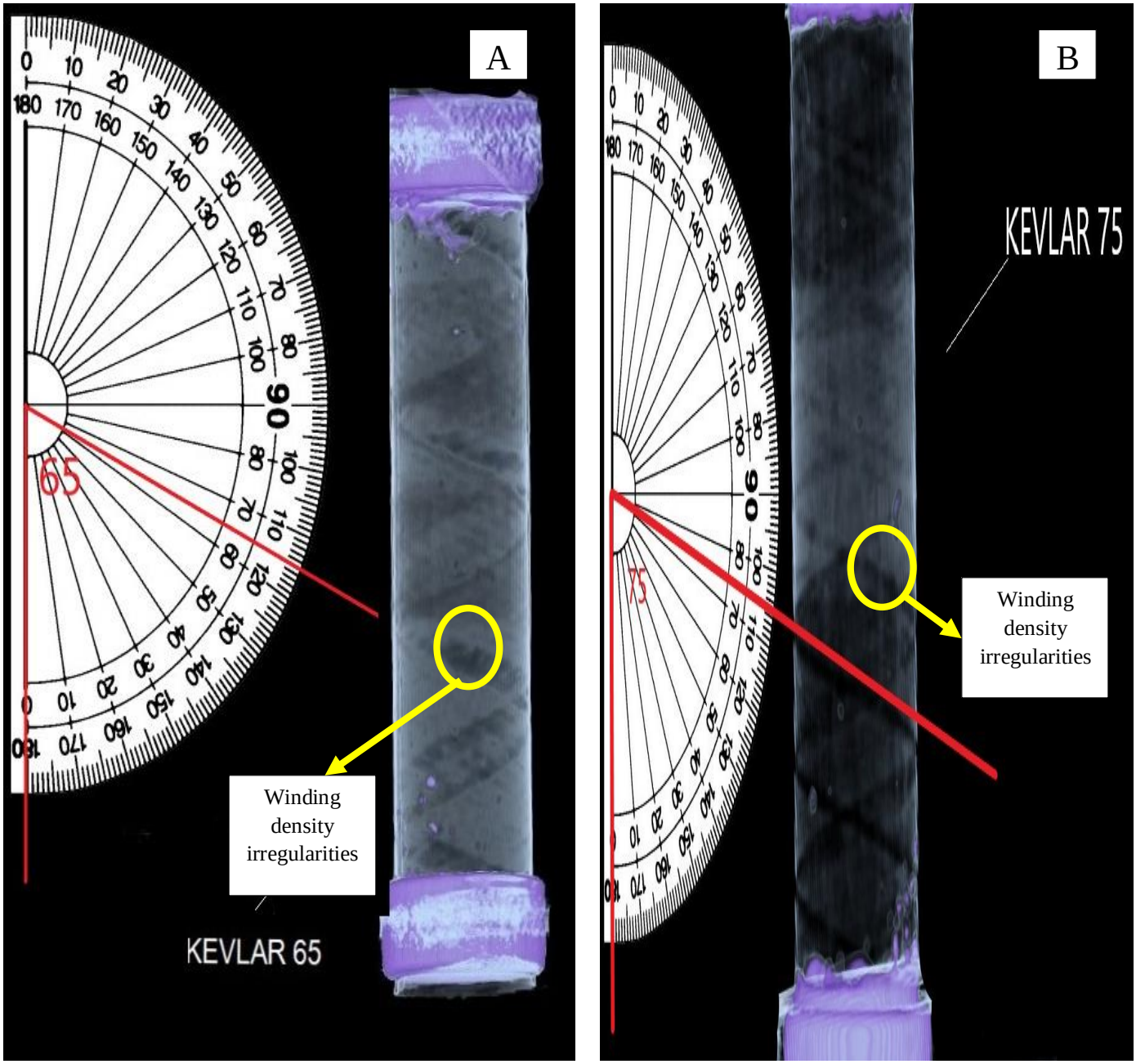

Figure 5.52: X-ray CT of A): $[\pm 65^{\circ}_{3}]$, B): $[\pm 75^{\circ}_{3}]$ KF/epoxy laminate.

It was noticed that the X-CT technique has an advantage compared to the ultrasonic wave velocity in detecting fiber orientation and misalignments due to the high attenuation and desperation of the signal of the material that is clearly detected by X-ray CT-scans. However, the X-ray CT couldn't identify objects with relatively close material densities and couldn't able to differentiate between the fiber phase and matrix phase due to their similar contrasts.

5.10 Numerical Simulation Results

The failure strength of epoxy, CF/epoxy, KF/epoxy and GF/epoxy laminates with different winding angle configuration $[\pm 45°_3], [\pm 55°_3]$, $[\pm 65°_3]$ and$[\pm 75°_3]$ are discussed in terms of deformation, Von-mises stress and Von-mises strain.

5.10.1 Total Deformation Distribution

The total deformation curves for CF/epoxy, KF/epoxy and GF/epoxy laminates with different winding angle $[\pm 45°_3], [\pm 55°_3]$, $[\pm 65°_3]$ and $[\pm 75°_3]$ as predicted by Von-mises Theory is presented in Figure 5.53 illustrate the total deformation of epoxy, CF/epoxy, KF/epoxy and GF/epoxy with different winding angle configuration.

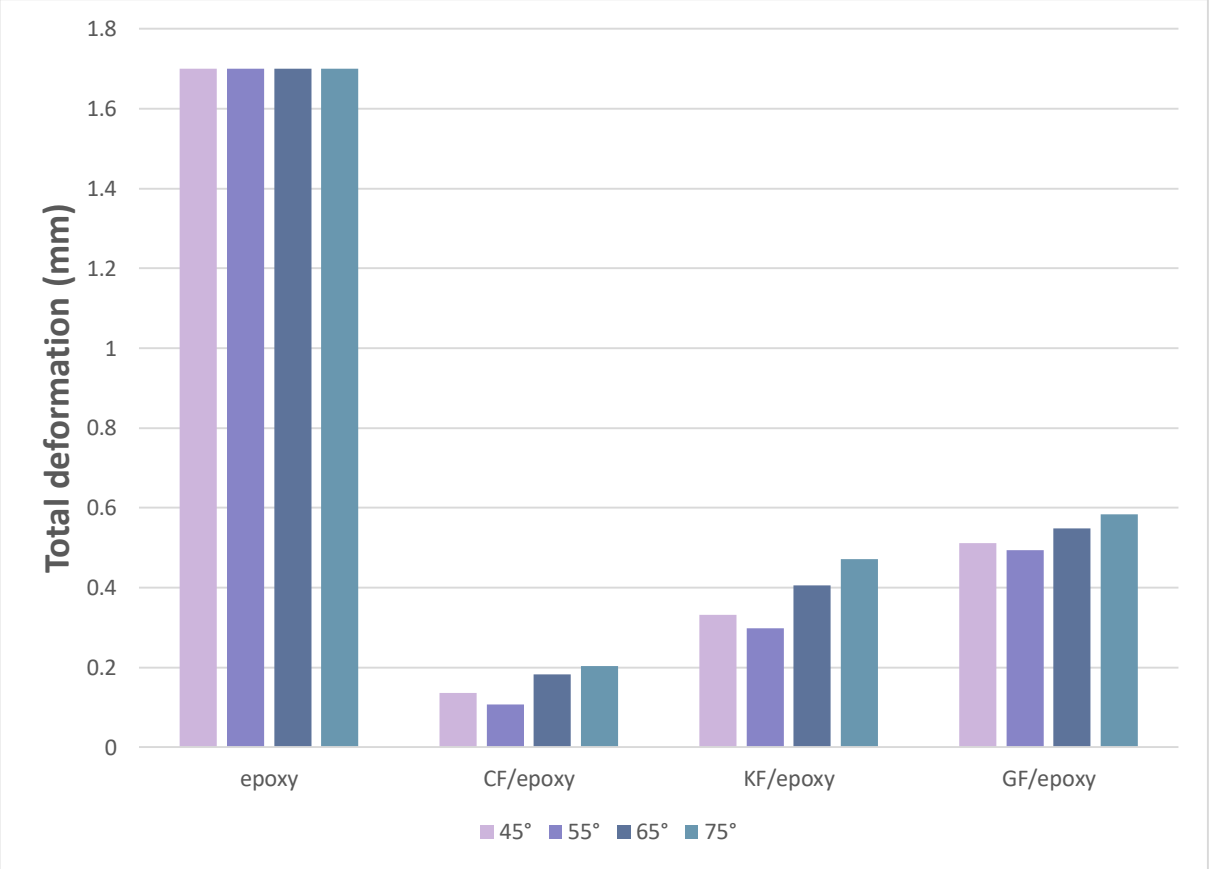

Figure 5.53: Total deformation of epoxy, CF/epoxy, KF/epoxy and GF/epoxy laminates.

5.10.1.1 Effect of Type of Reinforcing Fibers:

It can be observed from Figure 5.53 that the highest deformation is for the epoxy which show highest deformation is 1.7 mm and the deformation decreased when reinforcing by fibers where the deformation has higher decrement with CF/epoxy with winding angle [$\pm 55°_3$] where the rate of decreasing in deformation comparing with epoxy is [94.76%].

CF/epoxy laminates show lowest deformation value for all fiber composite laminates since being highly stiff and having a high elastic modulus, can sustain very high pressure before it undergoes failure. GF/epoxy laminates show the highest deformation between the composite laminate deformations.

5.10.1.2 Effect of Winding Angle:

The total deformation curve in figure 5.53 show the effect of deformation with the different winding configuration. It can be seen that the lower deformation value is for [±55°] winding angle for all composite laminates where the smallest deformation is for CF/epoxy which 0.107 mm.

However for larger winding angle the deformation increased that indicating the deformation increased with increasing the winding angle. Largest deformation is for winding angle [±75°] for all composite laminates, the highest deformation of composite laminate is for GF/epoxy which 0.584 mm. figures from 5.54 to 5.57 represents the total deformation of epoxy, CF/epoxy, KF/epoxy and GF/epoxy with different angle orientation.

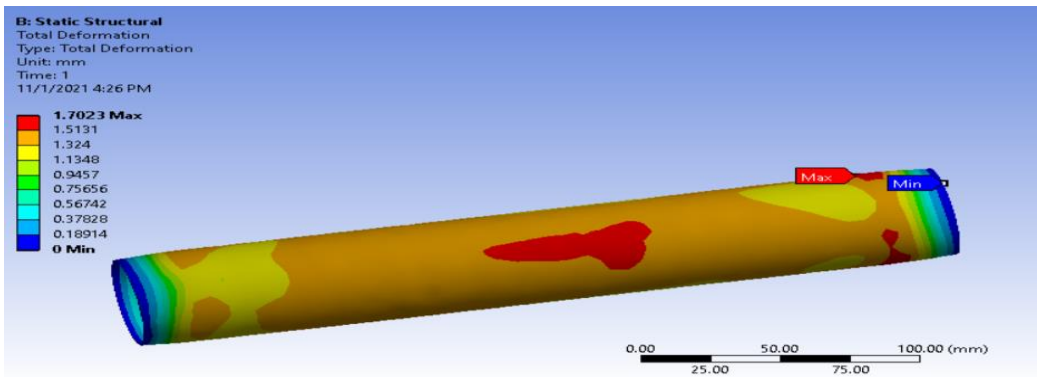

Figure 5.54: Total deformation of epoxy.

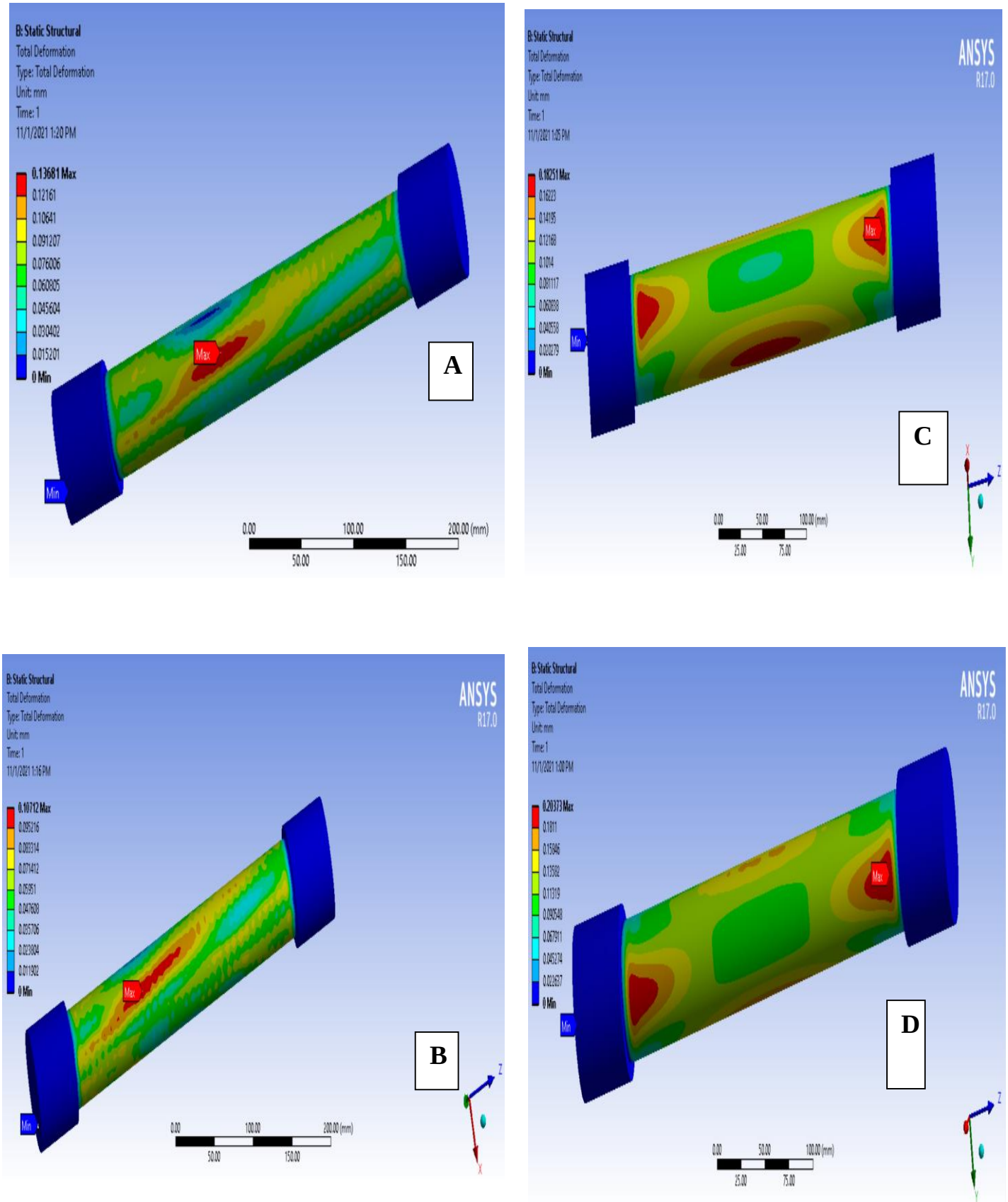

Figure 5.55: Total deformation of CF/epoxy laminate: A) [±45°], B) [±55°], C) [±65°], D) [±75°].

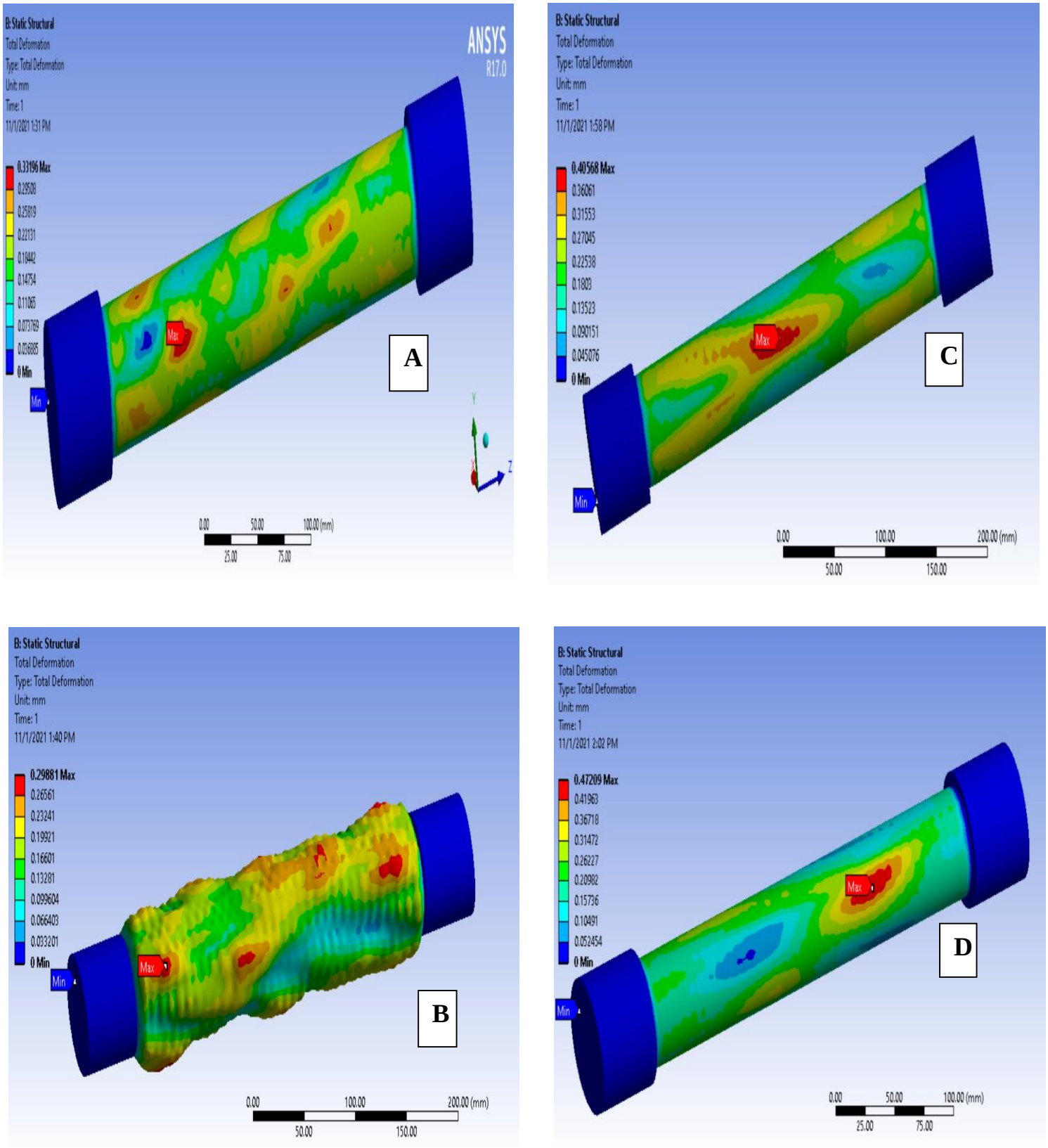

Figure 5.56: Total deformation of KF/epoxy laminate: A) [±45°], B) [±55°], C) [±65°], D) [±75°].

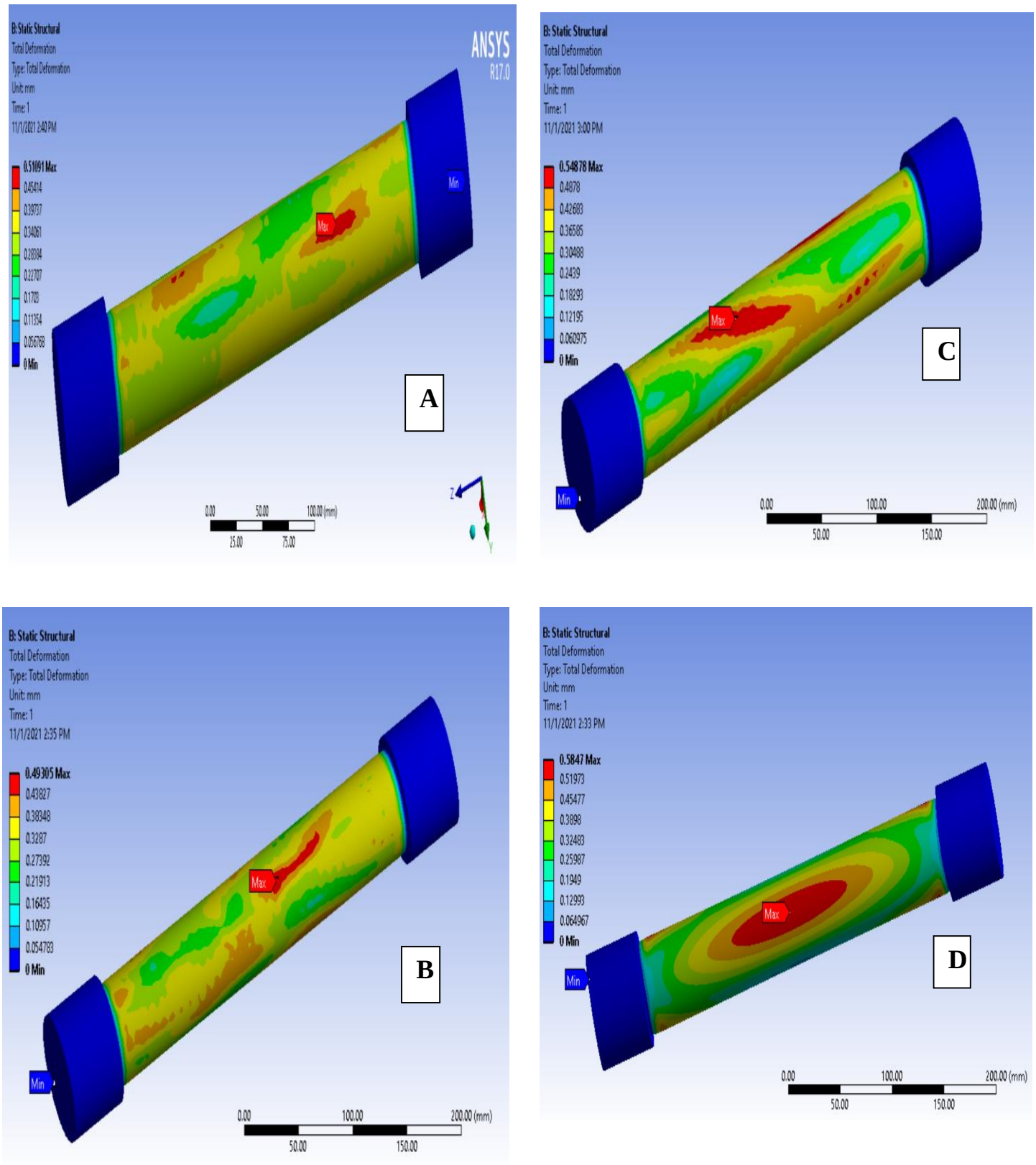

Figure 5.57: Total deformation of GF/epoxy laminate: A) [±45°], B) [±55°], C) [±65°], D) [±75°].

5.10.1.3 Effect of Ply Sequences:

The total deformation of symmetrical composite laminates with lay-up sequence $[[\pm 45°][\pm 55°]\ [\pm 65°]\ [\pm 75°]\ ]_s$ is illustrated in figure 5.58.

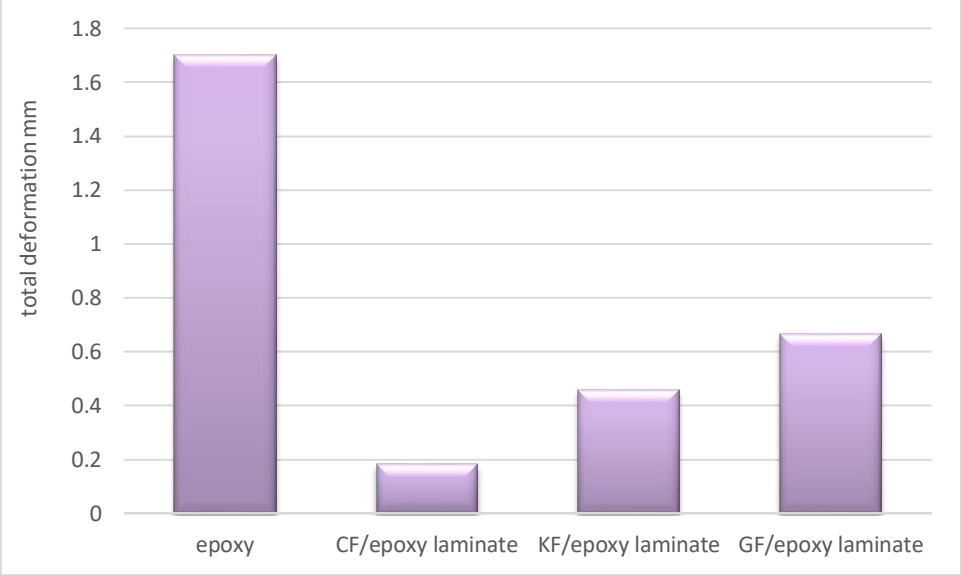

Figure 5.58: Total deformation of symmetrical composite laminates.

It can also be shown from figure 5.58 that CF/epoxy laminate has the lowest deformation is 0.182 mm which appear more resistance to the pressure load more than KF/epoxy laminates and GF/epoxy laminates. This can be attributed to the good mechanical properties of CF/epoxy while the GF/epoxy laminate exhibited the largest deformation that is 0.665 mm.

However, deformation of epoxy decreased by 89% with symmetrical CF/epoxy, by 73% with symmetrical KF/epoxy, by 60.88% with symmetrical GF/epoxy. Figure 5.59 represents the total deformation of symmetrical CF/epoxy, KF/epoxy and GF/epoxy.

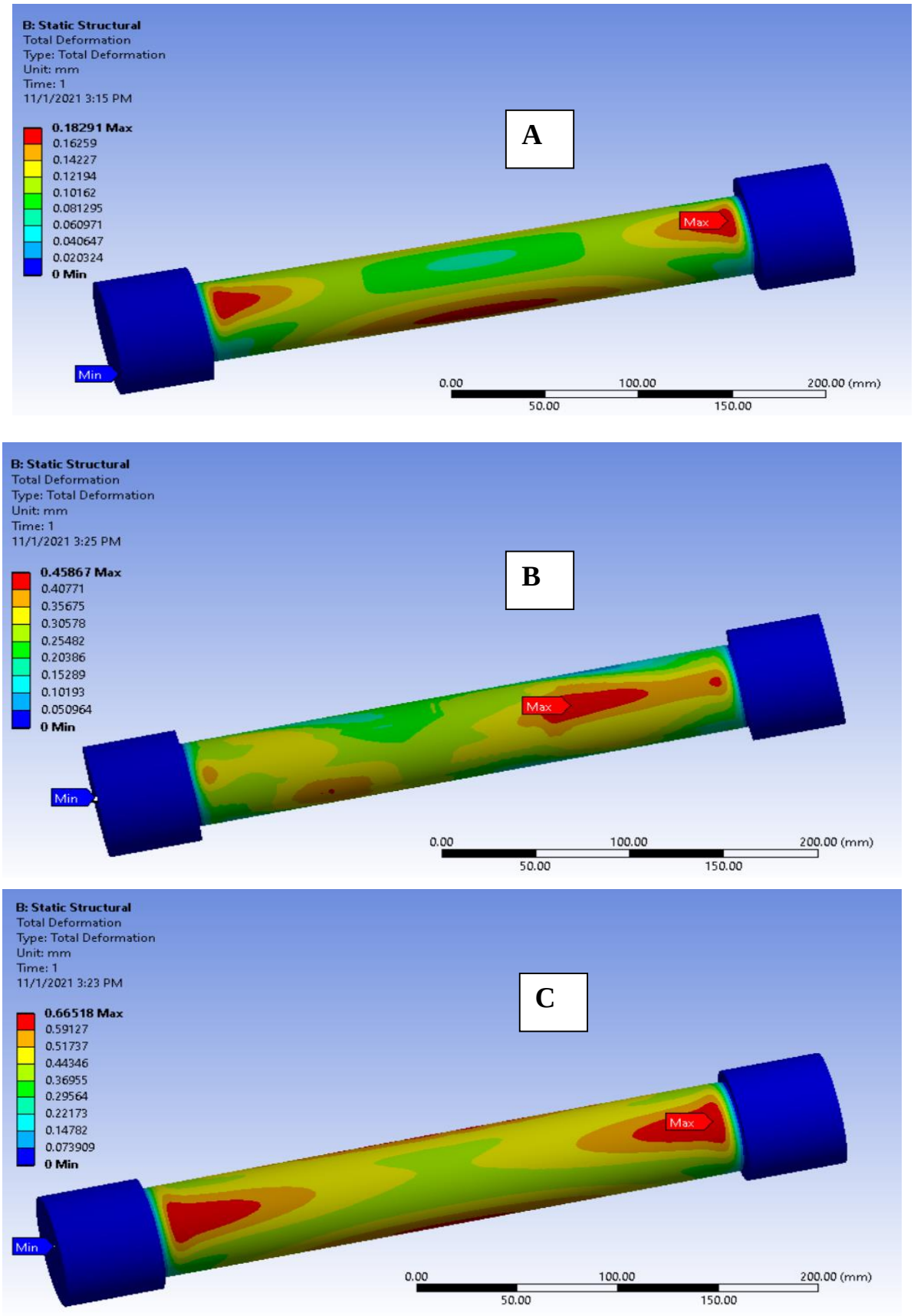

Figure 5.59: Total deformation of A: Symmetrical CF/epoxy laminate, B: Symmetrical KF/epoxy laminate and C: Symmetrical GF/epoxy laminate.

5.10.2 Equivalent Von-Mises Stress:

the results of equivalent (Von-Mises) stresses found in figure 5.60 which represents the value of Von-Mises stress of epoxy CF/epoxy laminate, KF/epoxy laminate and GF/epoxy laminates with different winding angle $[\pm 45°_3][\pm 55°_3]$, $[\pm 65°_3]$ and $[\pm 75°_3]$. The Von-Mises stress is discussed in three terms; Effect of type of reinforcing fibers, orientation and ply sequences.

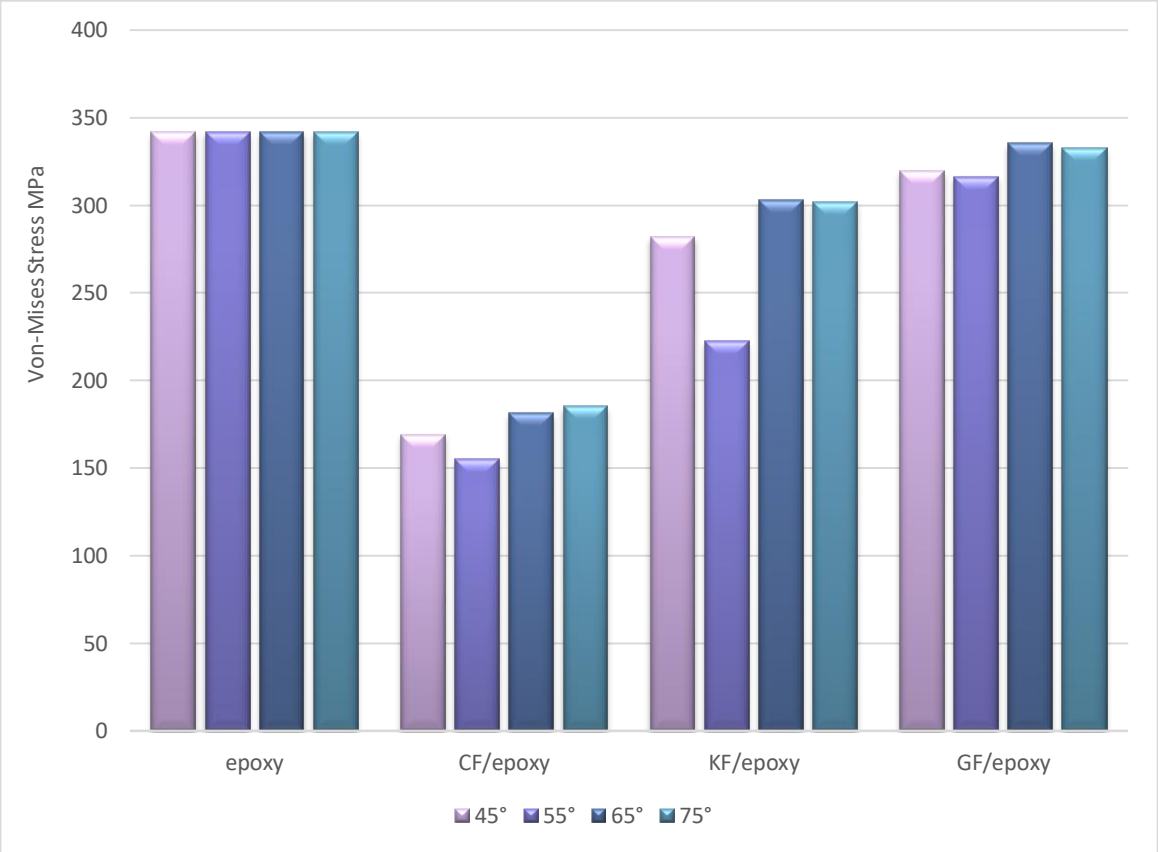

Figure 5.60: Von-Misses stresses epoxy, CF/epoxy, KF/epoxy and GF/epoxy laminates.

5.10.2.1 Effect of Type of Reinforcing Fibers:

From figure 5.60, it can be concluded that highest von-mises stress was for epoxy vessel have 342 MPa while the lowest equivalent (Von-Misses) stress values was for CF/epoxy laminates with different winding angle $[\pm 45°_3] \pm [55°_3]$, $[\pm 65°_3]$ and $[\pm 75°_3]$ are 169.13 MPa and 155.21 MPa, 181.3 MPa and 185 MPa respectively. The minimum value of Von Mises stresses refers to higher strength of the structural. From figure 5.67 can it noted be the lower value of Von-misses stress obtained with CF/epoxy laminates and this means that it has higher structural strength.

The values of von misses stress of KF/epoxy laminates of different winding angle $[\pm 45°_3][\pm 55°_3]$, $[\pm 65°_3]$ and $[\pm 75°_3]$ are 281.9 MPa, 222.5 MPa, 303 MPa and 301.8 MPa respectively, which are lower than The GF/epoxy laminates that have the higher von misses stress values with different winding angle $[\pm 45°_3][\pm 55°_3]$, $[\pm 65°_3]$ and $[\pm 75°_3]$ have values of von mises stresses that are 319.59 MPa, 316.59 MPa, 335.16 MPa and 332.59 MPa respectively.

5.10.2.2 Effect of Winding Angle:

Figures 5.61 to 5.64 shows the Von-Mises stress of epoxy and CF/epoxy, KF/epoxy and GF/epoxy laminates with the different winding configuration $[\pm 45°_3][\pm 55°_3]$, $[\pm 65°_3]$ and$[\pm 75°_3]$. It can be seen that von mises stresses decreased with increasing with winding angle where the lowest Von-Mises stress values is 155.21 MPa for CF/epoxy with $[\pm 55°_3]$ while the highest value of von-mises stress is 332.59 MPa for GF/epoxy with$[\pm 75°_3]$.

However the von-Mises stress decreased when reinforcing with fibers, where the Von-Mises stress of epoxy decreased with 54.6% when reinforcing with $[\pm 55°_3]$CF/epoxy winding orientation.

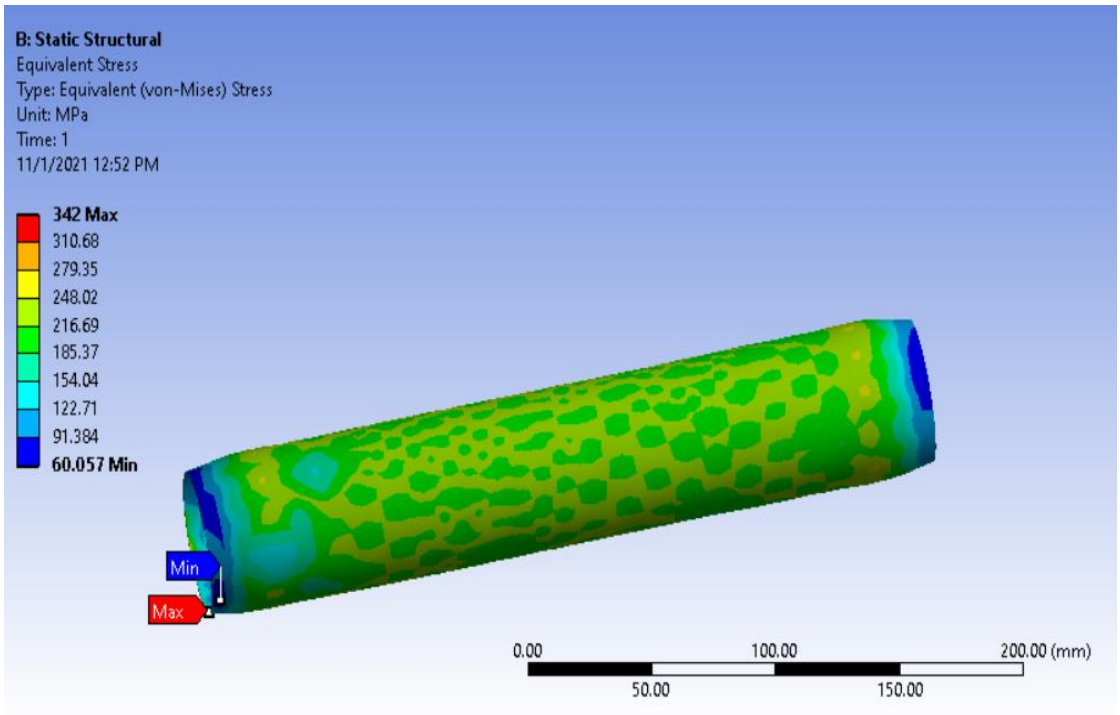

Figure 5.61: Von-Misses stress of epoxy

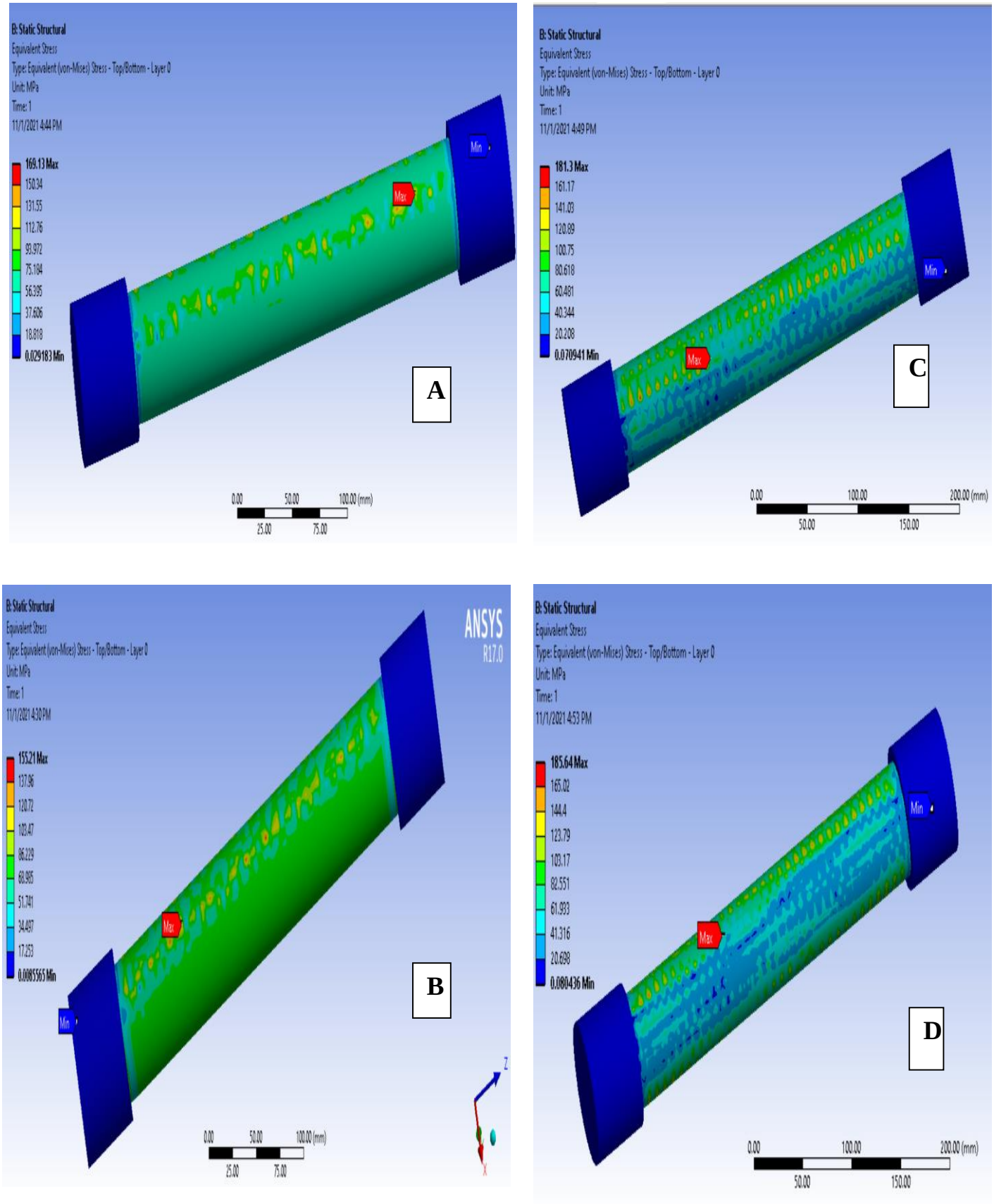

Figure 5.62: the maximum Von-Mises stress of CF/epoxy laminates A) [±45°], B) [±55°], C) [±65°], D) [±75°]

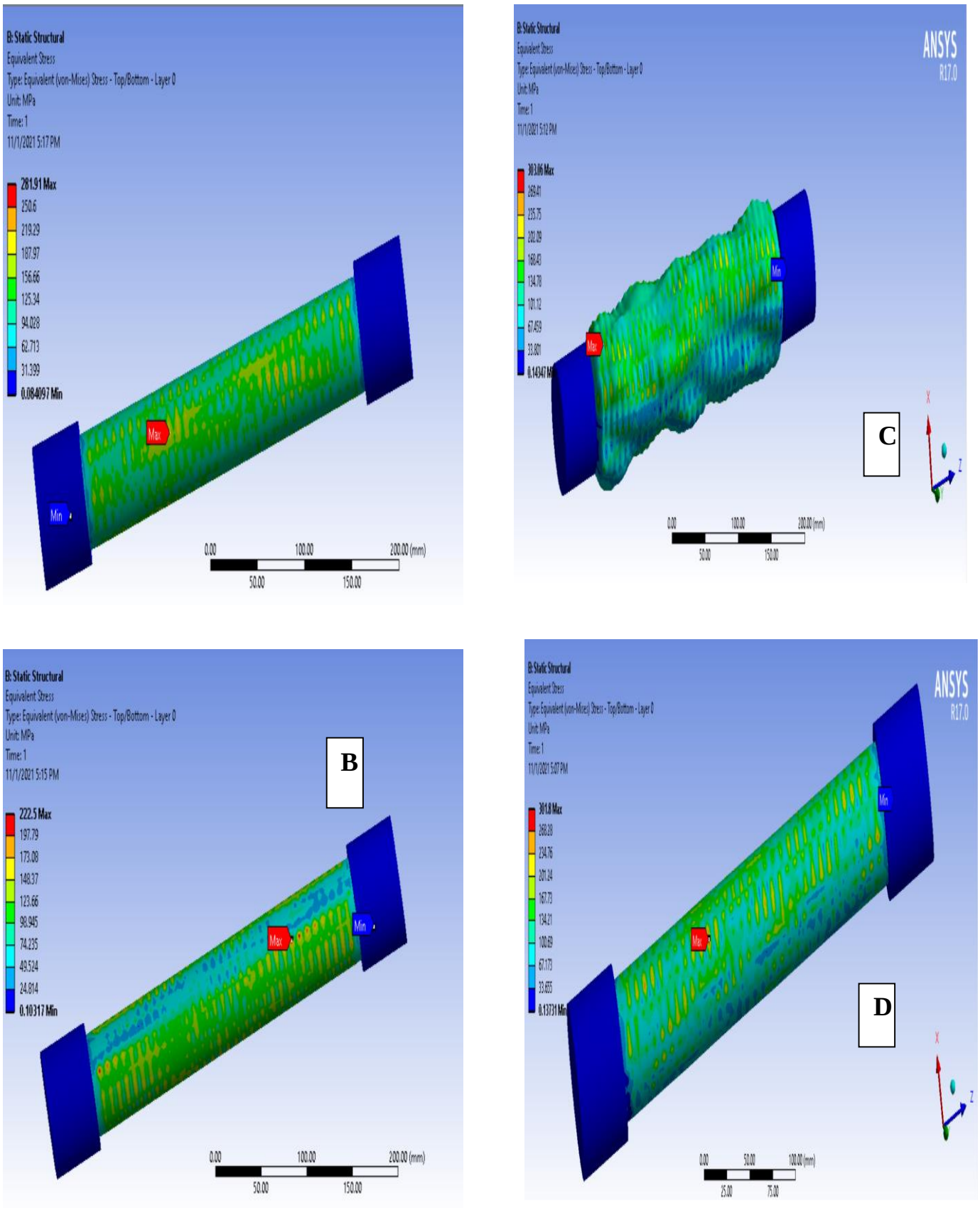

Figure 5.63: Von-Mises stress of KF/epoxy laminates: A) [±45°], B) [±55°], C) [±65°], D) [±75°].

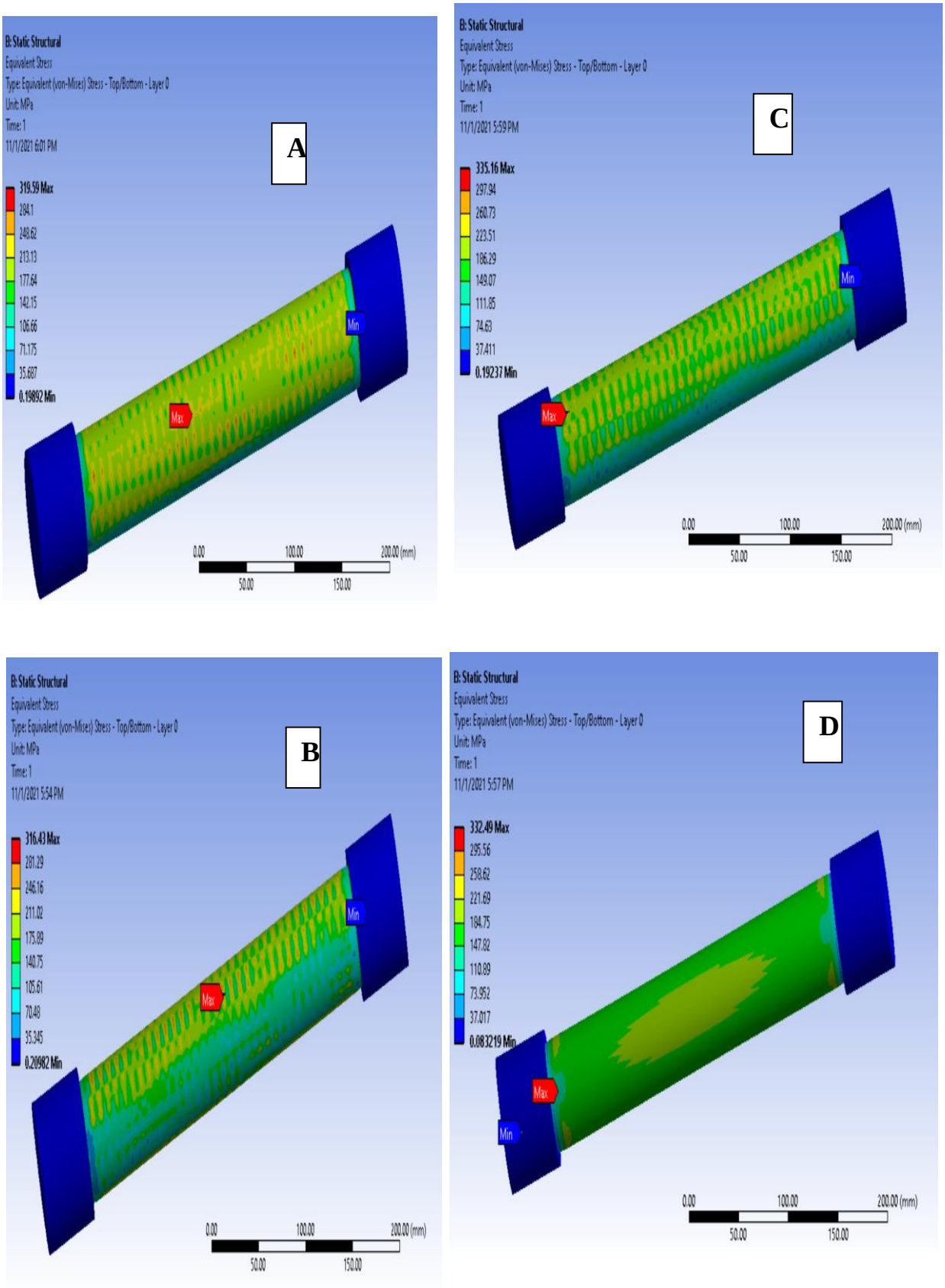

Figure 5.64: Von-Mises stress of GF/epoxy laminates A) [±45°], B) [±55°], C) [±65°], D) [±75°].

5.10.2.3 Effect of Ply Sequences:

The stacking sequence for the filament winding composite laminates is also performed. Figure 5.65 and 5.66 represent the Von-Mises stresses of symmetrical composite laminates with stacking sequence $[[\pm 45°][\pm 55°][\pm 65°][\pm 75°]]_s$

Besides providing higher burst pressures, the equivalent stress distributions for symmetric configurations have been observed to be more uniform stress distribution, allowing less stress concentration where the symmetric sequence of CF/epoxy has the lowest stress provide 255.5 MPa. KF/epoxy provide 301.26 MPa while GF/epoxy has the highest stress is 327.92 MPa means the CF/epoxy have higher strength resistance to stresses. Figure 5.88 represents the Von-Mises stress of symmetrical CF/epoxy, KF/epoxy and GF/epoxy.

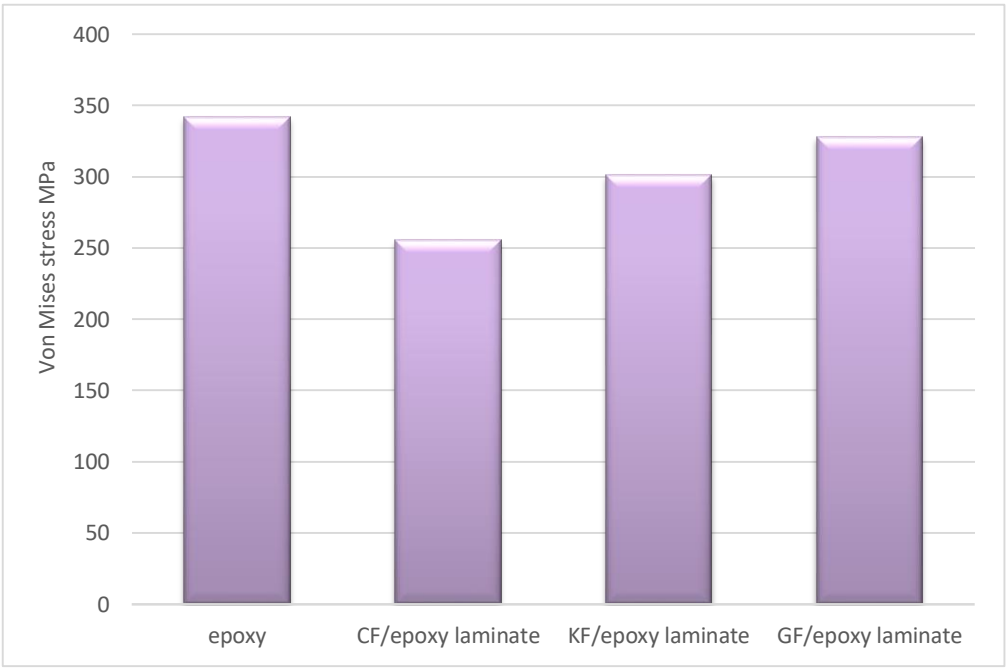

Figure 5.65: Von-Mises stress of epoxy and symmetric sequence laminates.

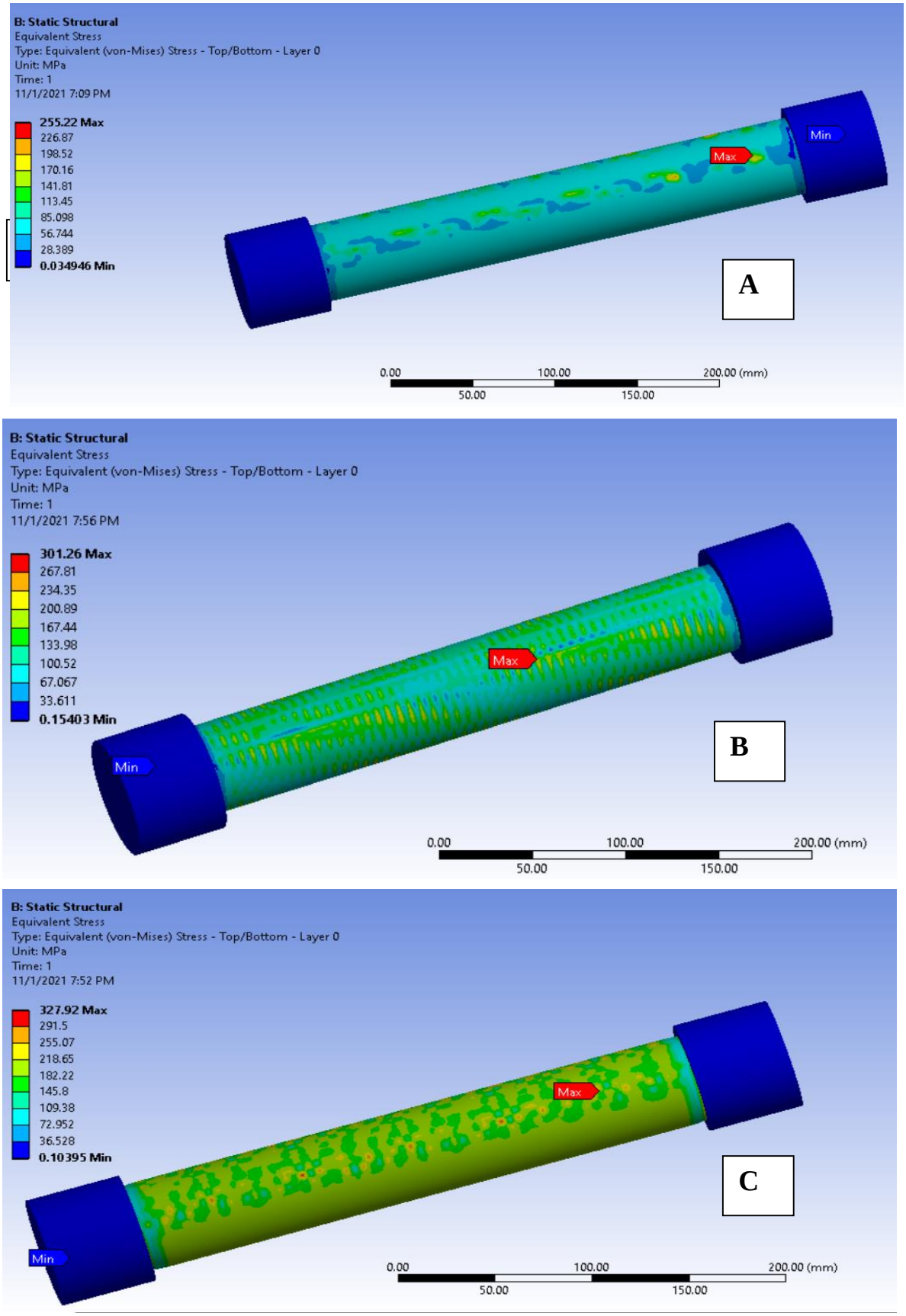

Figure 5.66: the Von-Mises stress of A: Symmetrical CF/epoxy laminate, B: Symmetrical KF/epoxy laminate and C: Symmetrical GF/epoxy laminate.

5.10.3 Equivalent Elastic Strain

The values of equivalent Von-Mises strain are found in figure 5.67 which represents the value of Von-Mises strain of epoxy, CF/epoxy laminate, KF/epoxy laminate and GF/epoxy laminates with different winding angle $[\pm 45°_3][\pm 55°_3]$, $[\pm 65°_3]$ and$[\pm 75°_3]$. The von-mises strain is discussed in three terms; Effect of type of reinforcing fibers, orientation and ply sequences.

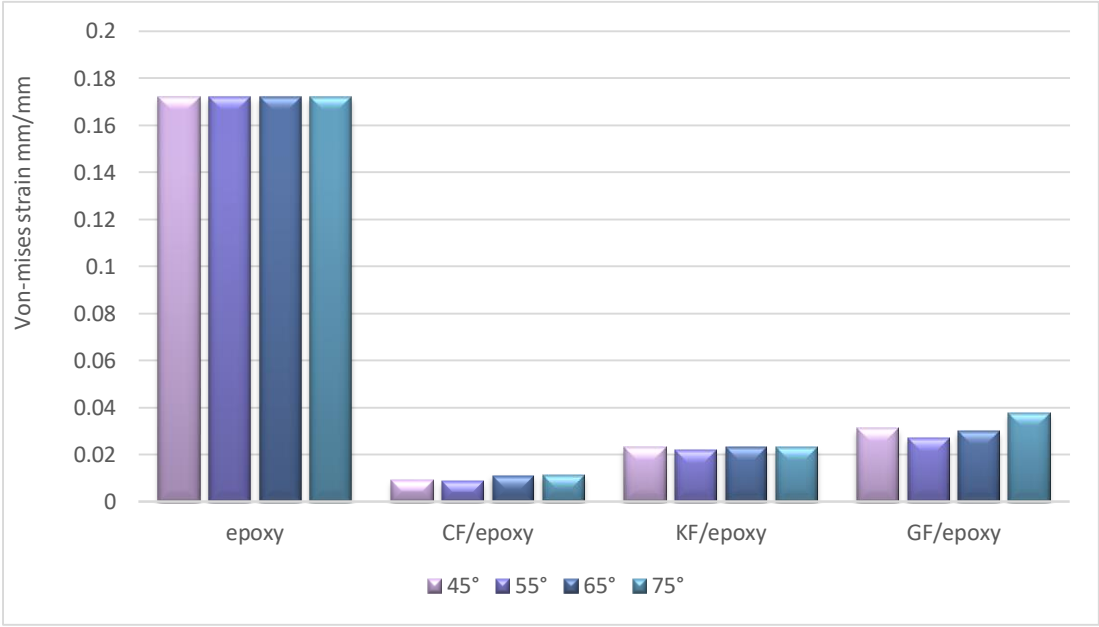

Figure 5.67: Von-Misses strain of epoxy, CF/epoxy laminates, KF/epoxy and GF/epoxy.

5.10.3.1 Effect of Type of Reinforcing Fibers:

Form figure 5.67 can be seen that the CF/epoxy laminates have the smallest strain values as compared to that of KF/epoxy laminates and the GF/epoxy laminates under the same pressure and boundary conditions. This implies that carbon fiber composite laminates has a better properties. It can be seen that the highest Von-Misses strain value is for epoxy 0.172 that decreased when reinforcing with fibers, the Von-Mises strain of epoxy has higher decrement 94.8% when reinforcing with CF/epoxy laminates.

5.10.3.2 Effect of Winding Angle:

From the structural analysis in figure 5.67 it can be seen that the $[\pm 55°_3]$ winding angle have the smallest strain values for all composite laminate, where the smallest strain value is for CF/epoxy with $[\pm 55°_3]$ is 0.0088. However the higher Von-Mises strain is 0.0378 is for GF/epoxy with $[\pm 75°_3]$ winding angle. Figures 5.68 to 5.71 show the Von-Mises strain of epoxy, CF/epoxy, KF/epoxy and GF/epoxy with different angle orientation.

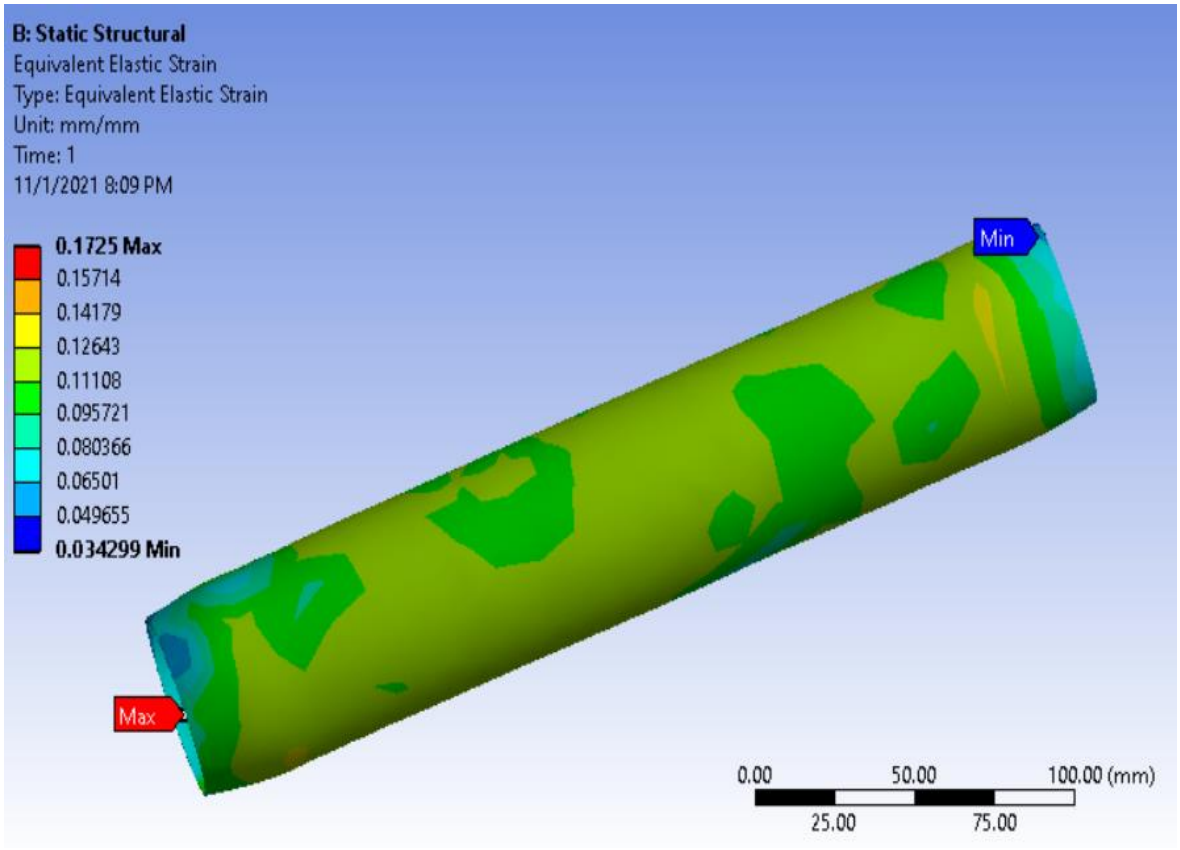

Figure 5.68: Maximum Von-Mises strain of epoxy

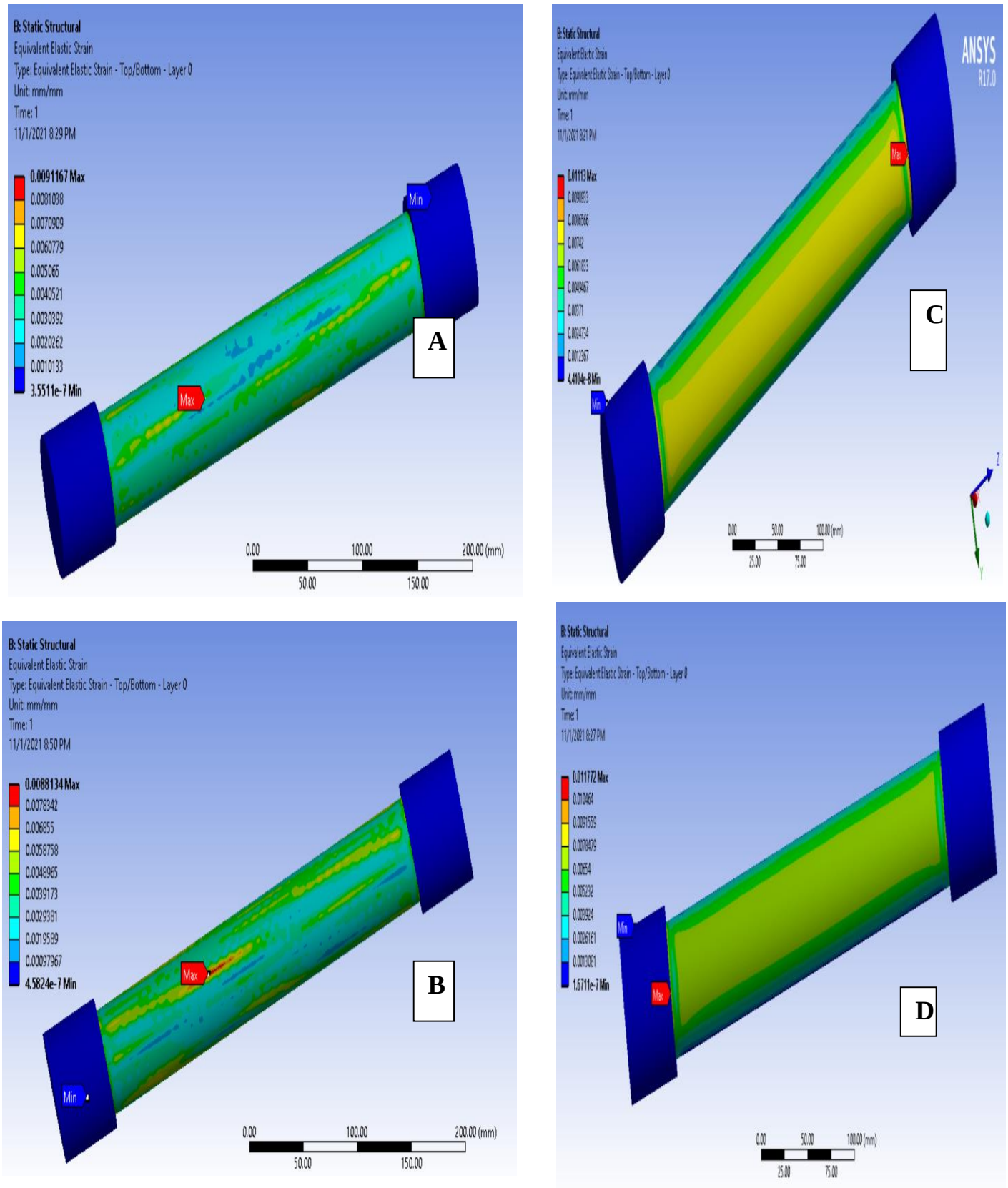

Figure 5.69: the maximum Von-mises strain of CF/epoxy laminates

A) [±45°], B) [±55°], C) [±65°], D) [±75°].

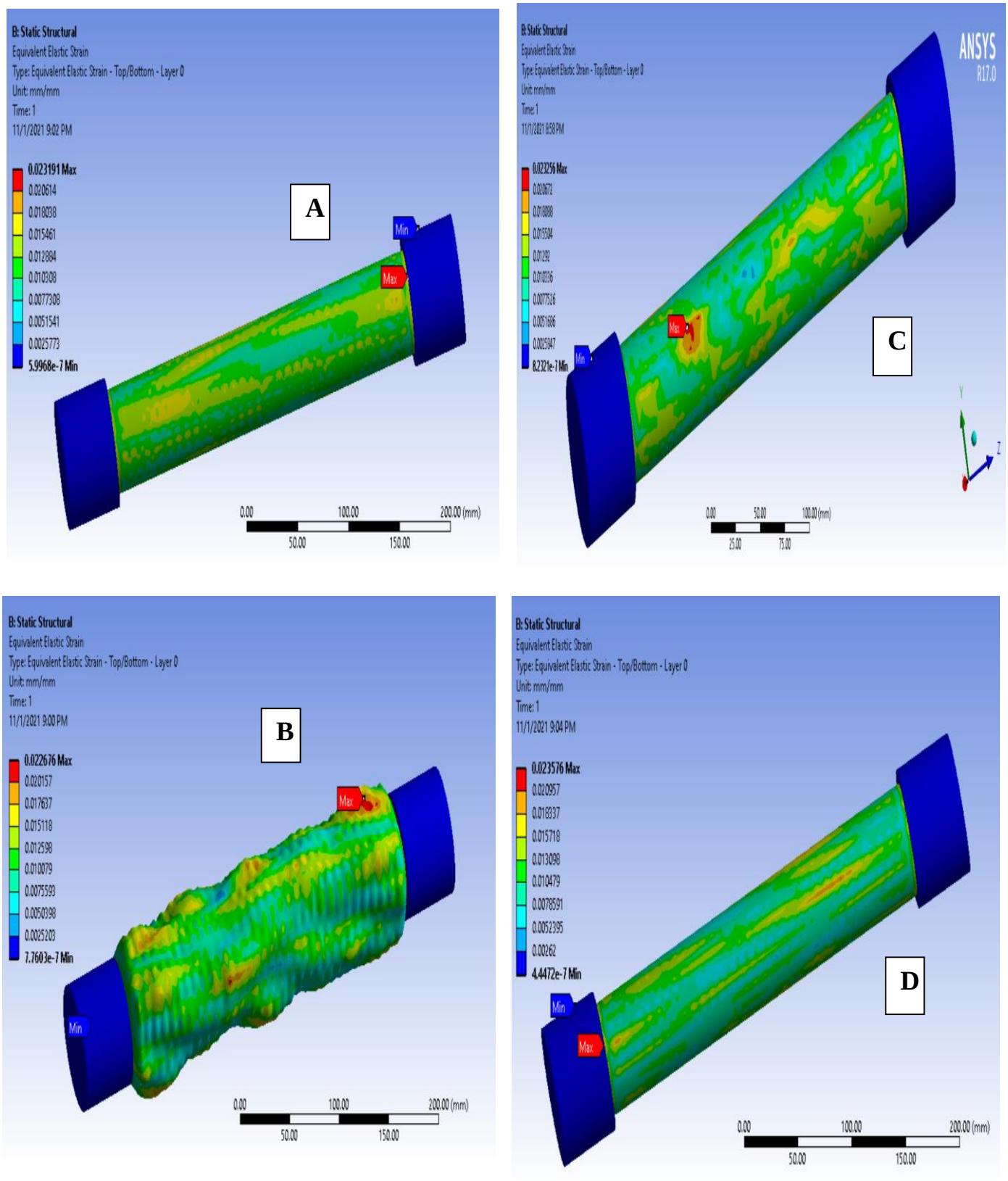

Figure 5.70: the maximum Von-mises strain of KF/epoxy laminates A) [±45°], B) [±55°], C) [±65°], D) [±75°].

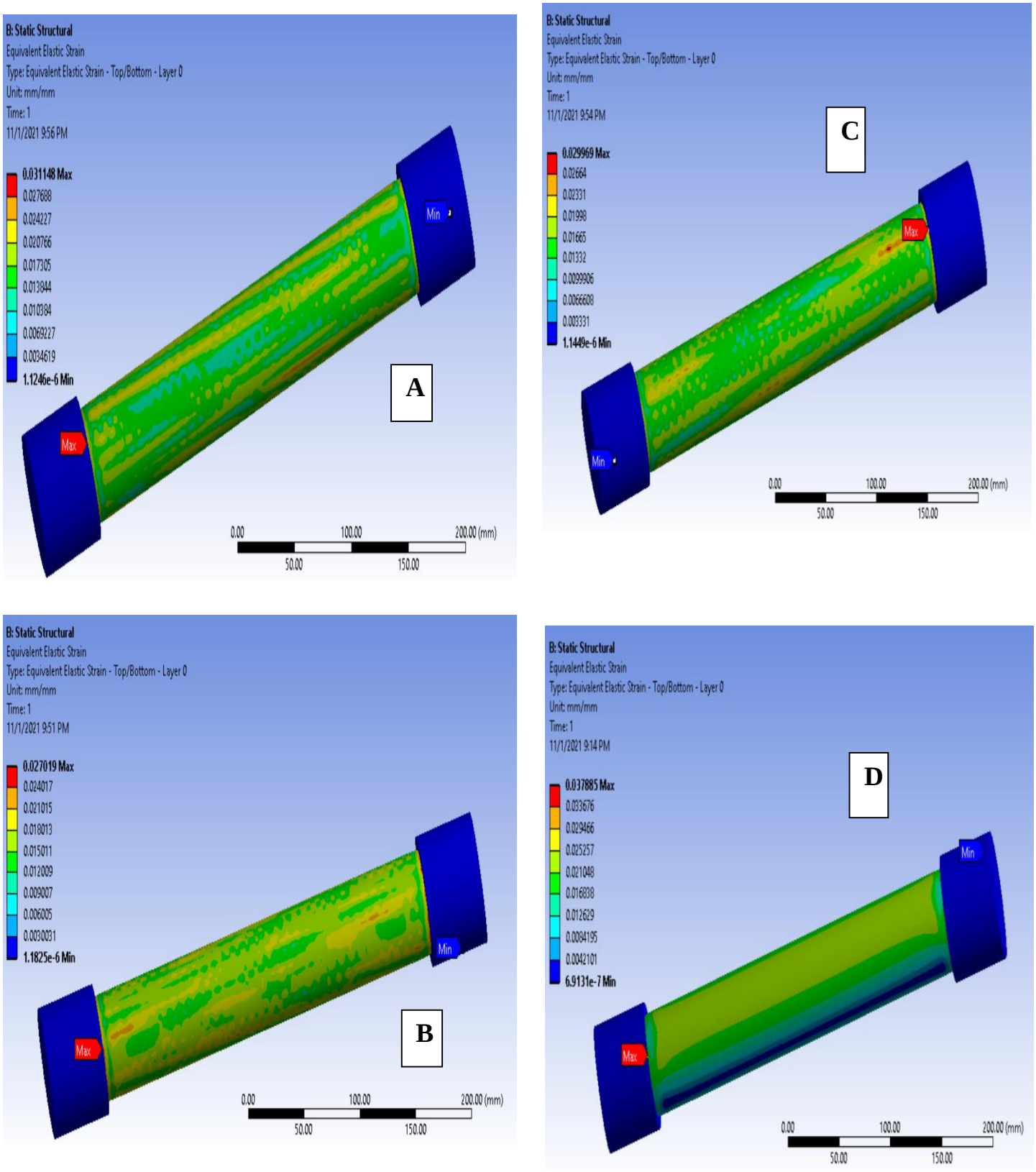

Figure 5.71: The maximum Von-Mises strain of glass GF/epoxy laminates

6 A) [±45°], B) [±55°], C) [±65°], D) [±75°].

6.1.1.1 Effect of Ply Sequences

The symmetrical stacking sequence effect of composite laminates on the Von-Mises strain are also performed as shown in Figure 5.72 and figure 5.73 which represent the Von-Misses strain of epoxy and symmetrical composite laminates with stacking sequence $[[\pm 45°][\pm 55°]\ [\pm 65°]\ [\pm 75°]\ ]_s$.The results show that the symmetric sequence of CF/epoxy laminate has the lowest strain value is 0.0097 mm/mm since carbon fibers provide higher strength to the composite while the highest strain is for GF/epoxy laminate is 0.0353 mm/mm.

However, strain decrease when reinforcing with symmetrical sequence where the strain value of epoxy decreased by 94.3% with symmetrical CF/epoxy, 83.7% with symmetrical KF/epoxy, 79.4% with symmetrical GF/epoxy.

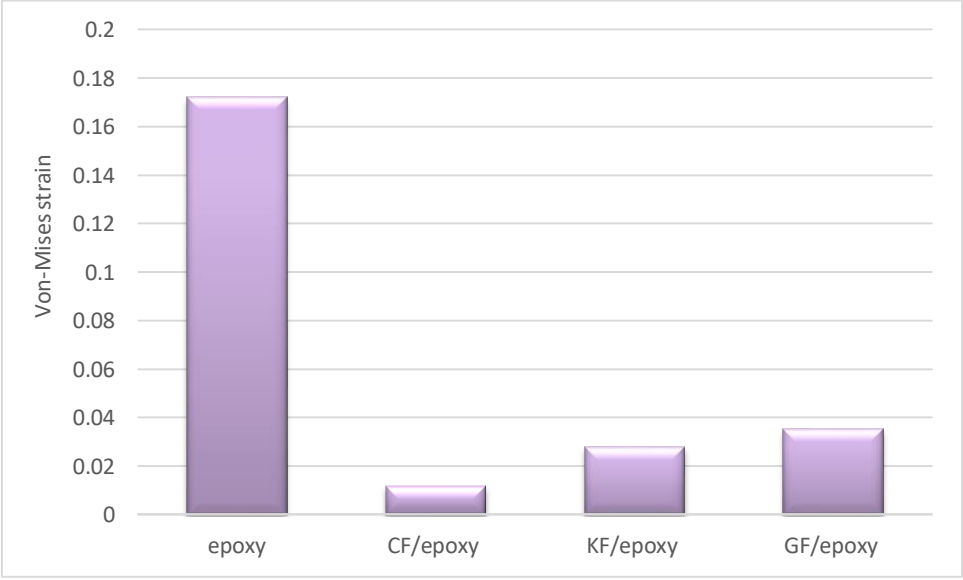

Figure 5.72: Maximum Von-misses strain of epoxy and symmetrical composite laminates.

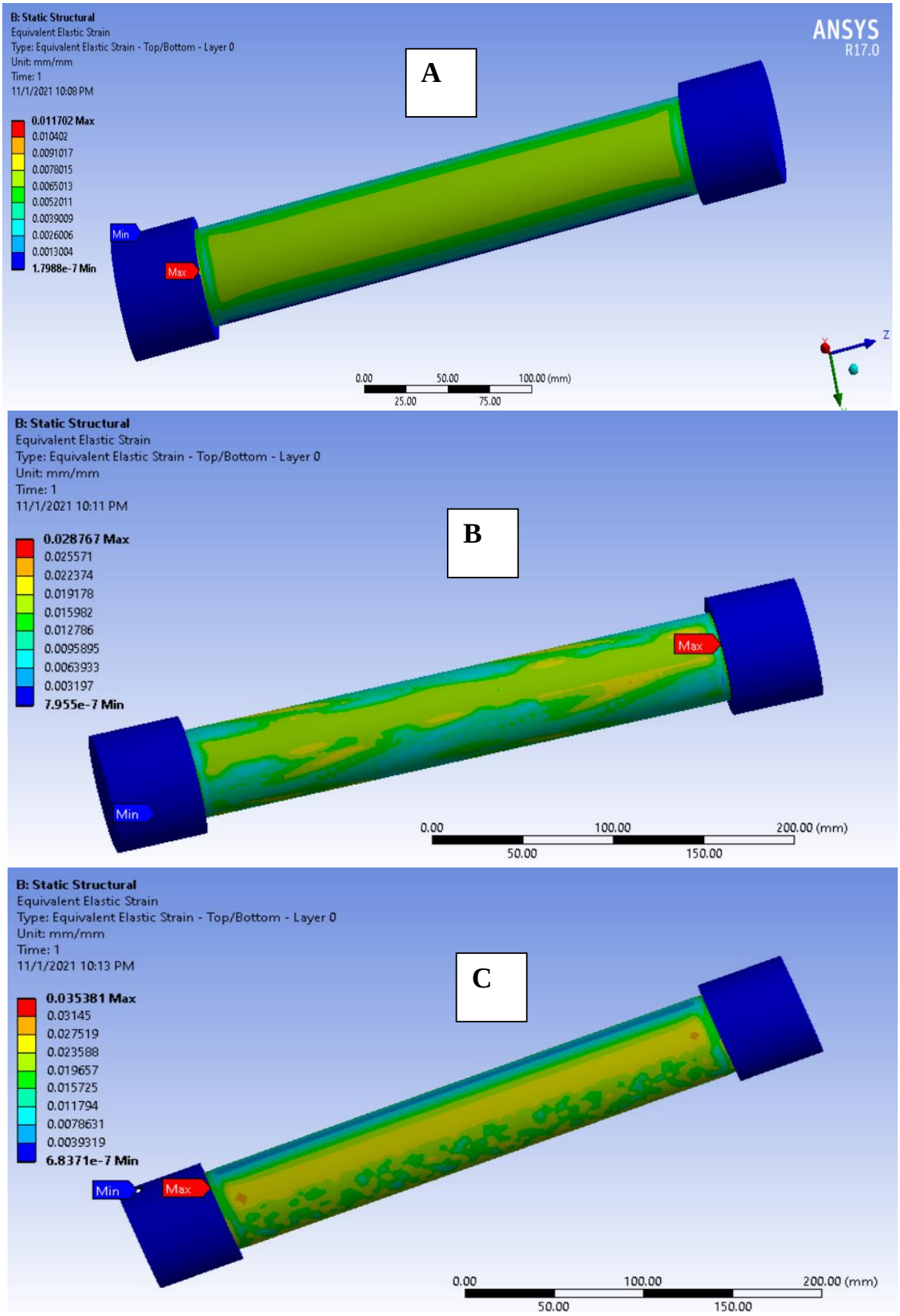

Figure 5.73: The maximum Von-misses strain of symmetrical laminates A) CF/epoxy laminate, B) KF/epoxy laminate, C) GF/epoxy laminate.

The values of Total deformation, Von misses stress and Von misses strain of epoxy and CF/epoxy, KF/epoxy, GF/epoxy laminates, symmetrical CF/epoxy, symmetrical KF/epoxy and symmetrical GF/epoxy are shown in table 5.2 and 5.3.

Table 5.2: Data of Total deformation, Von-Mises stress and Von-Mises strain of epoxy and CF/epoxy, KF/epoxy and GF/epoxy laminates.

Name of composite laminate	Total Deformation (mm)	Von-Mises Stress (MPa)	Von-Mises Strain mm/mm
Epoxy	1.7	342	0.172
$\pm 45°_3$ CF/epoxy laminate	0.136	169.13	0.0091
$\pm 55°_3$ CF/epoxy laminate	0.107	155.21	0.0088
$\pm 75°_3$ CF/epoxy laminate	0.203	185	0.01117
$\pm 45°_3$ KF/epoxy laminate	0.331	281.9	0.023
$\pm 55°_3$ KF/epoxy laminate	0.298	222.5	0.022
$\pm 65°_3$ KF/epoxy laminate	0.405	303	0.023
$\pm 75°_3$ KF/epoxy laminate	0.472	301.8	0.023
$\pm 45°_3$ GF/epoxy laminate	0.5109	319.59	0.0311
$\pm 55°_3$ GF/epoxy laminate	0.493	316.43	0.027
$\pm 65°_3$ GF/epoxy laminate	0.548	335.16	0.0299
$\pm 75°_3$ GF/epoxy laminate	0.584	332.49	0.0378

Table 5.3: Data of Total deformation, Von misses elastic stress and Von misses elastic strain of symmetrical composite laminates.

Name of composite laminate	**Total deformation (mm)**	**Von-Mises elastic stress (MPa)**	**Von-Mises elastic strain**
Symmetrical CF/epoxy	0.182	255.5	0.01173
Symmetrical KF/epoxy	0.458	301.26	0.028
Symmetrical GF/epoxy	0.665	327.92	0.0353

Chapter Six

Conclusions and Recommendations

5.1 Conclusions:

Internal pressure loading tests are carried out for epoxy and three different fiber types (carbon fibers, Kevlar fibers and glass fibers) composite laminates, and four different winding angles [±45°₃], [±55°₃], [±65°₃] and [±75°₃] as well as three symmetrical composite laminates with symmetrical sequence $[\pm 45°], [\pm 55°] [\pm 65°] [\pm 75°]_s$. Also investigated the efficiency of the ultrasonic wave velocity and X-ray CT methods for detecting defects in epoxy and fibrous composite laminates. The numerical simulation is used to evaluate their failure behavior according to the Von-Mises failure criteria at 25 MPa that can be simulated by FEM- ACP workbench 17.

From the evaluating data, it can concluded that:

1) The Ultrasonic wave velocity results confirmed that it's an effective non-destructive technique to detect defects place within 1 cm in addition to the usability for different materials types and sizes.
2) X-ray CT scan technique has the ability to detect the defects type, direction and dimension in addition to clarifying the fibers winding properties.
3) The SEM revealed the failure mode of pressure vessels where cohesive failure is the dominant failure.

4) Numerical results locate the weak areas through the maximum stress these areas confirmed with the detection techniques; Ultrasonic wave velocity and X-ray CT.
5) Composites laminates with three layers have effective results more than symmetrical laminates for shell applications
6) The burst pressure is strongly affected by the type of reinforcing fibers, symmetrical sequences and winding angle orientation.
7) The defects results from burst pressure appeared as leaks.
8) CF/epoxy laminates exhibited the best performance than the other reinforcing fibers which show no failure under 10 MPa while the GF/epoxy laminates show the lowest burst strength values.
9) The $[\pm 55°_3]$ is the best performance for all three type of reinforcing fibers which shows the maximum burst strength.
10) The winding angle $[\pm 55°_3]$ show the best hoop stress resistance, the maximum hoop stress is for CF/epoxy laminate 336.3 MPa, while the $[\pm 75°_3]$ show the lowest hoop stress is for GF/epoxy laminate 36 MPa.
11) All the composite laminates show approximate uniform wave ultrasound velocity referred to good fabrication.
12) The DSC results show that by reinforcing with carbon fibers and Kevlar fibers stabilize the thermal properties of epoxy.
13) The deformation behavior according to Von-Mises criteria for epoxy is significantly decreased with reinforcing with fibers, where the CF/epoxy laminates show the lowest deformation.
14) The Von-Mises stress show the lower Von-Mises stress is for CF/epoxy laminates that is safe under 25 MPa, while GF/epoxy laminates have the highest stress value which is yield under 25 MPa.

15) The Von-Mises strain results show that the highest decreased in von-mises strain with the CF/epoxy laminates while GF/epoxy laminates has the lowest decreased in Von-Mises strain under 25 MPa.

16) Safety factor results indicate that the CF/epoxy laminates and KF/epoxy with [±45°$_3$] and [±55°$_3$] winding angle are safe under 25 MPa while GF/epoxy and KF/epoxy with larger winding angle are unsafe under 25 MPa.

5.2 Recommendations:

1- Using higher strain rate pressure for burst pressure of carbon fiber composite laminates.

2- Using sudden burst pressure procedures to achieve complete explosion of the vessels.

3- Using developed failure analysis techniques like Acoustic emission and micro CT scan techniques.

4- Numerical analysis of another failure theories like Tsai Wu and Tsai-hill.

5- Studying the numerical analysis of first ply failure.

6- Hybridization of carbon fibers and Kevlar fibers with epoxy matrix.

7- Studying another type of mechanical failure like fatigue behavior of the composite pressure vessels.

8- Using a thermoplastic matrix.

References

[1] N. A. Yahya, O. M. Daas, N. O. F. Alboum, and A. H. Khalile,(2018) "Design of Vertical Pressure Vessel Using ASME Codes," no. September, pp. 653–664, doi: 10.21467/proceedings.4.33.

[2] D. Thomas, C. Johnson, S. Krishna, and N. S. Kumar,(2014) "Optimization Of Pressure Vessel Using A Composite Material," vol. 3, no. 3, pp. 91–96.

[3] M. M., K. H., and E.-S. E., (2015) "Design of Optimum Filament Wound Pressure Vessel with Integrated End Domes," Int. Conf. Aerosp. Sci. Aviat. Technol., vol. 16, no. AEROSPACE SCIENCES, pp. 1–15, 2015, doi: 10.21608/asat.

[4] E. E. GDOUTOS(2006) , Fracture of Nano and Engineering Materials and Structures. Springer.

[5] Y. H. Park and J. Sakai, (2020) "Optimum design of composite pressure vessel structure based on 3-dimensional failure criteria," Int. J. Mater. Form., vol. 13, no. 6, pp. 957–965, doi: 10.1007/s12289-019-01519-x.

[6] H. Y. Hong and P. D. Ridzuan,(2016) "Burst Strength Analysis of Composite Pressure Vessel using Finite Element Method," no. January.

[7] F. Heinecke and C. Willberg, (2019) "Manufacturing-induced imperfections in composite parts manufactured via automated fiber placement," J. Compos. Sci., vol. 3, no. 2, pp. 1–24, doi: 10.3390/jcs3020056.

[8] Brahim Attaf,(2011) ADVANCES IN COMPOSITE MATERIALS ECODESIGN AND ANALYSIS, ISBN:978-953-307-150-3.

[9] R. Y. K. S. .,(2012) "Composite Pressure Vessels," Int. J. Res. Eng. Technol., vol. 01, no. 04, pp. 597–618, doi: 10.15623/ijret.2012.0104011.

[10] H.-Y. Chou, (2012) "Damage analysis of composite pressure vessels using acoustic emission monitoring," no. September, p. 231.

[11] Kurt and Bittner,(2005) "MECHANICAL CHARACTERIZATION OF FILAMENT WOUND COMPOSITE TUBES BY INTERNAL PRESSURE TESTING," J. Chem. Inf. Model., vol. 12 Suppl 1, no. 9, pp. 1–29.

[12] Y. T. Shah,(2017) Chemical Energy from Natural and Synthetic Gas. Taylor & Francis Group, LLC.

[13] D. Kreculj and B. Rasuo,(2018) Impact damage modeling in laminated composite aircraft structures, no. January.

[14] S. Chattopadhyay, (2020) "Overview of pressure vessels," Press. Vessel., pp. 13–26, doi: 10.1201/9780203492468-4.

[15] C. D. Reese, (2009), Industrial Safety and Health for Goods and Materials Services. United States,CRC Press Taylor & Francis Group, 2009.

[16] M. A. Malek,(2007), Pressure Relief Devices ASME, United States, 2006: McGraw-Hill.

[17] S. Abrate, (1991) "Matrix cracking in laminated composites: A review," Compos. Eng., vol. 1, no. 6, pp. 337–353, doi: 10.1016/0961-9526(91)90039-U.

[18] EPA,(1999) "Understanding Oil Spills In Freshwater Environments," Response to Oil Spills, vol. 7, no. 3, pp. 37–44.

[19] D. S. Mannan, (2005) "Lee's Loss Prevention in the Process Industries Hazard," vol. 1, pp. 99–117.

[20] P. Akademia Baru, M. A. Khattak, A. Mukhtar, K. A. Khan, K. Pakhtoonkhwa, and M. My, (2016) "Common Root Causes of Pressure Vessel Failures: A Review," J. Adv. Res. Appl. Mech. ISSN, vol. 21, no. 1, pp. 22–37.

[21] A. Ibrahim, Y. Ryu, and M. Saidpour,(2015) "Stress Analysis of Thin-Walled Pressure Vessels,", vol. 05, no. 01, pp. 1–9, , doi: 10.4236/mme.2015.51001.

[22] F. F. Ling (2009), Mechanical Engineering Series. DOI: 10.1007/978-0-

387-49474-6.

[23] B. B. Muvdi and S. Elhouar, Mechanics of Materials with application in Excel,(2016), Taylor & Francis Group, LLC.

[24] R. Mott and J. A. Untener,(2016), Applied Strength of Materials, Sixth edit. Taylor & Francis Group, LLC.

[25] G. S. T. Sivasankaraiah,(2016), "Design, Development and Testing of Composite Pressure Tube," Int. J. Eng. Sci. Res. Technol. D, vol. 5, no. 10, pp. 131–137

[26] R. L. M. and J. A. Untener,(2018), Applied Strength of Materials, Sixth Edition SI Units Version. Taylor & Francis Group.

[27] M. Ji, J. He, and P. Ji, (2015)"Ultrasonic Testing Technology of Boiler &Pressure Vessel," Proc. 2015 Int. Conf. Manag. Educ. Inf. Control, vol. 125, no. Meici, pp. 683–686, doi: 10.2991/meici-15.2015.120.

[28] K. D. Sekaran, (2021)"Laboratory Experiment : Thin-Walled Cylinder MCEN2000 – Fundamentals of Strength of Materials Laboratory, no. May, pp. 0–11, doi: 10.13140/RG.2.2.10293.81129.

[29] G. I. Mikhasev and H. Altenbach, (2019), Thin-walled Laminated Structures, vol. 106.

[30] H. Altenbach, J. Altenbach, and W. Kissing,(2018), Mechanics of composite structural elements: Second edition, DOI: 978-981-10-8935-0

[31] B. J. G. James M. Gere, (2009), Mechanics of Materials SEVENTH, Seventh ed. Cengage Learning ALL.

[32] F. C. Campbell, (2006), Manufacturing Technology for Aerospace Structural Materials, First edit. Elsevier Ltd.

[33] S. Gopalakrishnan, (2017), WAVE PROPAGATION IN MATERIALS AND STRUCTURES, Taylor & Francis Group, LLC.

[34] D. William, J. Callister, and G. R. David,(2015) "Fundementals of Materials Science and Engineering," no. 1, pp. 2–4.

[35] M. L. Camilleri, (2010),Structural analysis. ASM International,

DOI:10.4324/9781410600745-17.

[36] M. H. Datoo,(1991) Mechanics of Fibrous Composites,DOI:10.1007/978-94-011-3670-9.

[37] V. V Vasiliev, (2007), Advanced Mechanics of Composite Materials, First edit. Elsevier Ltd.

[38] V. V Vasiliev, (2013),Advanced mechanics of composite materials and structural elements, Third edit. Elsevier Ltd.ISBN:0080982670.

[39] Fitria,(2013), LAMINAR COMPOSITES, vol. 53, no. 9. ISBN:9788578110796.

[40] Ever J. Barbero, (2011), Introduction to Composite Materials Design 2nd Edition. Taylor & Francis Group, LLC, ISBN:9781439894132.

[41] P. K. Bajpai and I. Singh,(2019), Reinforced polymer composites: Processing, characterization and post life cycle assessment. DOI:10.1002/9783527820979.

[42] P. V Marcal and N. Yamagata(2016), Design and Analysis of Reinforced Fiber Composites. DOI:10.1007/978-319-20007-1.

[43] A. Baker, S. Dutton, and D. Kelly (2004), Composite Materials for Aircraft Structures (ISBN: 1563475405).

[44] A. Güneri, Ed., (2001), Handbook of Composite Fabrication. ankara: parpa technology LTD.

[45] M. Müller, P. Valášek, and L. Tomek,(2010), "Mechanical properties of polymeric particle composites," Conf. Proceeding - 4th Int. Conf. TAE 2010 Trends Agric. Eng. 2010, pp. 454–458.

[46] Q. B. Baloch, (2017), "NON-DESTRUCTIVE EVALUATION MEASUREMENTS AND FRACTURE EFFECTS IN CARBON/EPOXY LAMINATES CONTAINING POROSITY," vol. 11, no. 1, pp. 92–105.

[47] M. G. Bader,(2012) "Handbook of composite reinforcements," Int. Mater. Rev., vol. 39, no. 3, pp. 123–124, doi:

10.1179/095066094790326130.

[48] J. Zeman, F. Rauscher, and S. Schindler, (2006), Pressure Vessel Design: The Direct Route, DOI:10.1016/B978-0-08-044950-0.X5000-8.

[49] N. L. Hancox, (2006), Engineering mechanics of composite materials, vol. 17, no. 2.

[50] R. Talreja and C. V. Singh, (2012), Damage and failure of composite materials, DOI:10.1017/CBO9781139016063.

[51] j. E. Pope, (2013), RULES OF THUMB FOR MECHANICAL ENGINEERS, vol. 53, no. 9.

[52] O. Mohammed and E. Suleiman,(2019) "A review study of delamination in composite laminated plates," no. April, doi: 10.13140/RG.2.2.12740.07041.

[53] Y. Cao, Z. Cao, Y. Zhao, D. Zuo, and T. E. Tay, (2020), "Damage progression and failure of single-lap thin-ply laminated composite bolted joints under quasi-static loading," Int. J. Mech. Sci., vol. 170, no. December, p. 105360, doi: 10.1016/j.ijmecsci.105360.

[54] D. Campbell and A. Maji, "Failure Mechanisms and Deployment Accuracy of Elastic-Memory Composites," J. Aerosp. Eng., vol. 19, no. 3, pp. 184–193, 2006, doi: 10.1061/(asce)0893-1321(2006)19:3(184).

[55] A. J. Reshma Ramesh1, (2017)"Review on Burst Pressure Analysis of Laminated Composite Pressure Vessels," Int. Res. J. Eng. Technol., vol. 4, no. 5, pp. 2738–2742.

[56] A. Zolfaghari and M. Izadi,(2020), "Burst Pressure Prediction of Cylindrical Vessels Using Artificial Neural Network," J. Press. Vessel Technol., vol. 142, no. 3, doi: 10.1115/1.4045729.

[57] R. Talreja and J. Varna, (2015), Modeling damage, fatigue and failure of composite materials. DOI:10.1016/c2013-0-16521-x

[58] J. Katz, (2008), Importance of sites of tracer administration and sampling in turnover studies, vol. 41, no. 1.

[59] J. S. Ward, I. M., (2004), An Introduction to the Mechanical Properties of Solid Polymers, Second edi. John Wiley & Sons Ltd.

[60] T. W. Huseby and S. Matsuoka, Mechanical properties of solid and liquid polymers, vol. 1, no. 6. 1967.

[61] M. Jolly, (2015), "Review of Non-destructive Testing (NDT) Techniques and their Applicability to Thick Walled Composites," Procedia CIRP, vol. 38, pp. 129–136, doi: 10.1016/j.procir.2015.07.043.

[62] I. A. and C. S. ,(2012), International Atomic Energy Agency Vienna (Austria), "Training Guidelines in Non-Destructive Testing Techniques: Leak Testing at Level 2," p. 186.

[63] International Atomic Energy Agency, (2000) "Liquid Penetrant and Magnetic Particle Testing at Level 2," no. 11, pp. 179–219.

[64] S. A. Peñaloza-Peña, C. Galvis G., and J. Quiroga M., (2019) "Failure detection in a pressure vessel using acoustic emissions technology," Rev. UIS Ing., vol. 18, no. 4, pp. 147–156, doi: 10.18273/revuin.v18n4-2019014.

[65] IAEA,(2013), "Training Course Series 54 (Manual for visual Testing Level 2)," Train. Guidel. Non-Destructive Test. Tech. Man. Vis., p. 226.

[66] M. A. Ali, R. Umer, and K. A. Khan,(2020), CT Scan Generated Material Twins for Composites Manufacturing in Industry 4.0.

[67] J. H. Kurz, F. Finck, C. U. Grosse, and H. W. Reinhardt,(2006), "Stress drop and stress redistribution in concrete quantified over time by the b-value analysis," Struct. Heal. Monit., vol. 5, no. 1, pp. 69–81, 2006, doi: 10.1177/1475921706057983.

[68] A. Carpinteri, F. Cardone, and G. Lacidogna,(2010) "Energy Emissions from Failure Phenomena: Mechanical, Electromagnetic, Nuclear," Exp. Mech., vol. 50, no. 8, pp. 1235–1243, doi: 10.1007/s11340-009-9325-7.

[69] R. Vidya Sagar, B. K. Raghu Prasad, and B. L. Karihaloo, (2010) "Verification of the applicability of lattice model to concrete fracture by

AE study," Int. J. Fract., vol. 161, no. 2, pp. 121–129, doi: 10.1007/s10704-009-9431-7.

[70] F. J. Rescalvo, I. Valverde-Palacios, E. Suarez, A. Roldán, and A. Gallego, (2018) "Monitoring of carbon fiber-reinforced old timber beams via strain and multiresonant acoustic emission sensors," Sensors (Switzerland), vol. 18, no. 4, doi: 10.3390/s18041224.

[71] F. H. Abdalla,(2007) "Design and fabrication of low cost filament winding machine," Mater. Des., vol. 28, no. 1, pp. 234–239, doi: 10.1016/j.matdes.2005.06.015.

[72] T. Hasiotis, E. Badogiannis, and N. G. Tsouvalis,(2011) "Application of ultrasonic C-scan techniques for tracing defects in laminated composite materials," Stroj. Vestnik/Journal Mech. Eng., vol. 57, no. 3, pp. 192–203, doi: 10.5545/sv-jme.2010.170.

[73] N. Kumar, (2011)"Optimization of Shell- Thickness in Multilayer Pressure Vessel and Study on Effect of Number of Shells on," vol. 3, no. 4, pp. 2693–2700.

[74] S. Mutasher, N. Mir-nasiri, and L. E. E. C. Lin, (2012) "SMALL-SCALE FILAMENT WINDING MACHINE FOR PRODUCING FIBER COMPOSITE PRODUCTS 2 . Mechanical and Electrical Setup of Winding Machine," vol. 7, no. 2, pp. 156–168.

[75] S. Sulaiman, S. Borazjani, and S. H. Tang, (2013) "Finite element analysis of filament-wound composite pressure vessel under internal pressure," IOP Conf. Ser. Mater. Sci. Eng., vol. 50, no. 1, doi: 10.1088/1757-899X/50/1/012061.

[76] I. Journal and C. Science, (2013)"Issn 2278-3091 Abstract : Design and Analysis of Cfrp Composite Multilayer High Pressure Vessels and Burst Pressure Analysis for Various Fiber," vol. 2, no. 1, pp. 602–607.

[77] J. H. S. Almeida, M. L. Ribeiro, V. Tita, H. Faria, A. T. Marques, and S. C. Amico, (2015) "Progressive failure analysis of filament wound

composite tubes under internal pressure," ICCM Int. Conf. Compos. Mater., vol. 2015-July, no. September.

[78] J. S. Park, W. H. Hong, W. Lee, J. H. Park, and S. J. Yoon, (2014) "Pipe stiffness prediction of buried GFRP flexible pipe," Polym. Polym. Compos., vol. 22, no. 1, pp. 17–24, doi: 10.1177/096739111402200103.

[79] A. A. Hassen, A. Poudel, T. P. Chu, M. Yester, and U. K. Vaidya,(2015) "Tracing Defects in Glass Fiber / Polypropylene Composites Using Ultrasonic C- Scan and X-Ray Computed Tomography Methods Tracing Defects in Glass Fiber / Polypropylene Composites Using Ultrasonic C-Scan and X-Ray Computed Tomography Methods," ASNT Annu. Conf., no. June, doi: 10.13140/RG.2.1.2385.5202.

[80] J. H. S. Almeida Júnior, M. L. P. Tonatto, H. Faria, A. T. Marques, and S. C. Amico,(2014) "Effect of environmental conditioning on burst pressure of carbon/epoxy filament wound composite pipes," 16th Eur. Conf. Compos. Mater. ECCM 2014.

[81] A. Hawa, M. S. Abdul Majid, M. Afendi, M. Haslan, K. Pranesh, and N. A. M. Amin, (2015) "Burst Strength of Glass Fibre/Epoxy Composite Pipes Subjected to Impact Loading," Appl. Mech. Mater., vol. 786, no. March, pp. 121–125, doi: 10.4028/www.scientific.net/amm.786.121.

[82] S. D. Urade,(2015) "Stress Analysis of Multilayer Pressure Vessel," J. Appl. Mech. Eng., vol. 04, no. 02, pp. 34–43, doi: 10.4172/2168-9873.1000157.

[83] B. G. Sumana, H. N. V. Sagar, K. V. Sharma, and M. Krishna, (2015) "Numerical Analysis of Stresses on Layer-by-Layer Basis in FML Composite Cylinder Subjected to External Hydrostatic Loading," Mater. Sci. Appl., vol. 06, no. 06, pp. 489–499, doi: 10.4236/msa.2015.66052.

[84] V. Srebrenkoska, S. Zhezhova, and S. Naseva, (2015) "Hoop Tensile Properties of Filament Wound Pipes," XII. Int. Mach. Technol. Mater. Congr., vol. 1, pp. 103–105.

[85] G. Suresh and L. S. Jayakumari, (2016) "Analyzing the mechanical behavior of E-glass fibre-reinforced interpenetrating polymer network composite pipe," J. Compos. Mater., vol. 50, no. 22, pp. 3053–3061, doi: 10.1177/0021998315615408.

[86] A. Wagdy, A.- Ghany, and S. Ebeid, (2016) "Failure Prediction of Fiber Reinforced Polymer Pipes using FEA Rapid Prototyping of Functionalized Polymer Composites View project Review researches View project," Artic. Int. J. Eng. Tech. Res., no. February.

[87] Y. Ma, Y. Yang, T. Sugahara, and H. Hamada, (2016) "Review article A study on the failure behavior and mechanical properties of unidirectional fi ber reinforced thermosetting and thermoplastic composites," Compos. Part B, vol. 99, pp. 162–172, doi: 10.1016/j.compositesb.2016.06.005.

[88] N. O. Dowd and T. A.Sebaey,(2018) "Design of Composite Pipes with Different Fiber Orientations Evaluation of the Internal Pressure Capacity," no. April, pp. 1–5, doi: 10.15224/978-1-63248-163-4-13.

[89] R. J. de Medeiros, S. H. S. da Nóbrega, and E. M. F. De Aquino, (2019) "Failure theories on carbon/Kevlar hybrid fabric based composite laminate: Notch and anisotropy effects," Mater. Res., vol. 22, no. 3,doi: 10.1590/1980-5373-MR-2018-0099.

[90] Ö. ÖZBEK, A. KILIÇ, and Ö. Y. BOZKURT,(2020) "Development of Filament Winding Machine for Producing Round Shapes with Different Fiber Reinforcements," Gümüşhane Üniversitesi Fen Bilim. Enstitüsü Derg., vol. 10, pp. 552–558, doi: 10.17714/gumusfenbil.687600.

[91] M. Gargol, T. Klepka, and Ł. Klapiszewski,(2021) "Synthesis and Thermo-Mechanical Study of Epoxy Resin-Based Composites with Waste Fibers of Hemp as an Eco-Friendly Filler," pp. 1–17.

[92] ANSYS Inc., (2013) "ANSYS Composite PrepPost User's Guide," ANSYS Man., vol. 15317, no. November, pp. 724–746.

[93] M. Barschke, D. Uribe, and O. E. Ruiz,(2009) "Finite Element Modeling

of Composite Materials using Kinematic Constraints," Ing. y Cienc., vol. 5, no. 10, pp. 133–153.

[94] N. Griya, K. C. Nithin Kumar, D. P. Singh, and A. Shaikh, (2019) "Finite element analysis of UD carbon-epoxy laminate under in-plane load," Mater. Today Proc., vol. 26, pp. 756–759, doi: 10.1016/j.matpr.2020.01.020.

[95] S. Paver (2005), "The Laminator Classical Analysis of Composite Laminates." pp. 11–13.

[96] B. A. E. A. A. Hassan, M. Abo-Elkhier,(2020) "EVALUATION OF OPTIMUM CONFIGURATIONS FOR COMPOSITE OILFIELD THREE-PHASE SEPARATOR PRESSURE VESSEL Piping stress analysis engineer , Engineering for the Petroleum, Menoufia University , Faculty of Engineering , Production Assistant Professor ," vol. 43, no. 1, pp. 23–39.

[97] C. Oucif and L. M. Mauludin,(2019) "Numerical modeling of high velocity impact applied to reinforced concrete panel," Undergr. Sp., vol. 4, no. 1, pp. 1–9, doi: 10.1016/j.undsp.2018.04.007.

[98] P. Data,(2015) "Sikadur ® -52 LP (IN)," pp. 2–4.

[99] Z. Wei,(2016) "Mechanical and Microstructural Characteristics of the Fiber-Reinforced Composite Materials," no. August, pp. 6–7, doi: 10.20944/preprints201608.0220.v1.

[100] S. Test, "Standard Test Method for Resistance to Wetting of Garment-Type Leathers," Test, vol. i, no. 152 mm, pp. 7–9, 1913, doi: 10.1520/D1599-14E01.2.

[101] Annual Book of ASTM Standard, (2003), "Standard Test Method for Plastics Properties-Durometer Hardness", D 2240-03, PP. (1-12).

[102] "Glass reinforced plastics (GRP) pipes, joints and fittings for use for water supply or sewerage.," vol. 5, 1990.

[103] S. Kimura, K. Kitayama, H. Takahashi, K. Kimoto, K. Kawamura, and

H. Kikura, (2018) “Longitudinal and Shear Wave Velocities Measurement in Compacted Bentonite for Water Content,” E3S Web Conf., vol. 43, pp. 4–9, doi: 10.1051/e3sconf/20184301016.

[104] F. Al-Sulaiman, Z. Khan, N. Merah, M. A. Kounain, and M. Mehdi, (2011) “Effects of weathering on failure pressure of filament-wound GFRP thermoset pipes,” J. Compos. Mater., vol. 45, no. 6, pp. 645–655, doi: 10.1177/0021998310377933.

[105] A. Hawa, M. S. Abdul Majid, M. Afendi, M. Haslan, K. Pranesh, and N. A. M. Amin,(2015) “Burst Strength of Glass Fibre/Epoxy Composite Pipes Subjected to Impact Loading,” Appl. Mech. Mater., vol. 786, pp. 121–125, doi: 10.4028/www.scientific.net/amm.786.121.